An Experimental Study of the Interaction of Water With Granitic Melt

Thesis by

Phillip Dean Ihinger

In Partial Fulfillment of the Requirements
for the Degree of
Doctor of Philosophy

California Institute of Technology
Pasadena, California

1991

(Submitted May 24, 1991)

Acknowledgements

This work was completed only as a result of the patience and good-will of my thesis advisor, Ed Stolper. It is impossible to properly acknowledge his contribution to my development as a scientist. More importantly, I thank him for his friendship and his guidance; I can not imagine a greater man to have as a mentor.

Sam Epstein taught me everything I know about stable isotopes and how to analyze them. I thank him for sharing his wisdom and his lab. George Rossman continually provided expertise on spectroscopic techniques. His open door, his generosity, and his unequaled enthusiasm serves as a great role-model for any young scientist. The experimental equipment was forged out of the laboratory of Peter Wyllie. The sometimes obscure, Rube Goldbergian alterations made to his equipment were always met with his support and generosity.

Six years on the third floor of Arms has brought me into contact with a great number of people who have had a positive impact on my work. Specifically, I wish to acknowledge the advice and friendship of Gerry Fine, Roger Aines, Mike Baker, David Bell, Mike Carroll, Pat Dobson, Andy Gaynor, Dana Johnston, Sven Maaløe, Stephanie Mattson, Sally Newman, Lynn Silver, Laurie Watson, and Youxue Zhang. In addition, lively interaction with John Beckett, Jen Blank, Lori Chamberlin, Jackie Dixon, Yigal Erel, Carey Gazis, Gunther Haehn, Louis Johnson, Tom Johnson, Hans Keppler, Diane Knott, Glenn Mattiole, Greg Miller, David Pyle, Paula Rossner, Jack Sheng, Danny Sykes, Sieger van der Laan, and Dimitri Vlassopoulos made it all worthwhile.

This thesis would not be complete without acknowledging the many house mates who put up with my unusual time-schedules and idiosyncrasies. I thank the residents of 109 S. Chester (including Huw Davies, Mark Fahnestock, David Pickett, David Scott, Mike Wolf, Bruce Worden, and, of course, Gloria) and those of 635 S. Mentor (including

Carmen Corredera, Laura Fente, Jim Kendall, Elizabeth Nagy, Rob Ripperdan, and, oh yeah, Apchu!).

I wish to thank Lauren Stolper for introducing me to Caltech. I will always cherish her friendship.

Thanks, too, to Michele, for making the last six months so special.

I dedicate this thesis to my family; Marilyn, Bob, Bev, Irv, Rob, Lance, Shannon, and Erika, for encouraging me to accept the challenge of Caltech and for their strong support throughout my tenure.

Abstract

The nature of water in granitic melt is investigated through a variety of experimental and analytical techniques. The knowledge of the presence of two dissolved melt species (hydroxyl and molecular water groups), and the precise determination of their concentrations with infrared spectroscopy, is used in conjunction with vacuum extraction and hydrogen isotopic techniques to determine, (1) the solubility of water in granitic melts as a function of pressure at 850°C, (2) the speciation of water in granitic melt as a function of temperature, and (3) the fractionation factors which govern the partitioning of hydrogen isotopes between water vapor and granitic melt.

Natural obsidian starting materials were held at 850°C and pressures ranging from 200 to 1600 bars in the presence of excess vapor. Samples were rapidly quenched to glasses and their water contents were determined using vacuum manometry and infrared spectroscopy. The results of these experiments demonstrate a progressive increase in solubility with pressure, but suggest that increasing dissolution of water has no influence on the total volume of the melt (the partial molar volume of water in these low pressure melts is near zero). The solubility measurements can be used to model shallow level eruptive cycles which involve crystal fractionation, volatile saturation, onset of eruption, and influx of new magma to repeat the cycle. Preliminary experiments on the temperature dependence of water solubility suggest a dependence as high as 1 wt % per 200°C at 1600 bars. This result supports the suggestion that mafic intrusion into silicic magma chambers induces supersaturation of the felsic liquid and subsequent explosive eruption.

Hydrated obsidian chips were held at temperatures ranging from 450 to 600°C to determine the equilibrium speciation of water in the melt. These data show distinct non-ideal behavior, ln K_{eq} decreases with increasing water content (K_{eq} = the equilibrium constant for the reaction involving dissolved water species). Relaxation analyses are used to demonstrate that these rapidly-quenched glasses preserve their high-temperature

speciation. This analysis has been used to demonstrate that melts held at 850°C do not preserve their equilibrium speciation on quench. Intersection of the equilibrium isotherms with the fictive temperature curve recorded by the 850°C samples provides identification of the last-equilibrated temperature for the quenched glasses. This information, coupled with the speciation recorded in glasses quenched at a slower rate, is used to extract the viscosity of hydrous rhyolitic liquids as a function of temperature. This formulation is compared to empirical methods for determining melt viscosities. The equilibrium speciation data is used to formulate a regular solution model to determine the speciation of water in rhyolitic melts at any temperature and water content.

The hydrogen isotopic composition of water evolved from quenched granitic melts is compared to the isotopic composition of their equilibrium vapors. The bulk partitioning of hydrogen isotopes between melt and vapor varies as a regular function of the total dissolved water content, suggesting that two independent fractionation factors control their equilibrium. The fractionation factor between vapor and hydroxyl groups ($\approx 1.040 \pm 0.05$ ‰) is significantly greater than the fractionation between vapor and the molecular water species ($\approx 1.00 \pm 0.10$ ‰). These fractionation factors can be used to explain the degassing trends measured in natural igneous environments. The magma chamber beneath Mono Craters, CA may have experienced a significant amount of closed system degassing before undergoing open system degassing late in its history.

Table of Contents:

List of Tables

List of Illustrations

Introduction:

Water is arguably the most important chemical component in the geologic environment. In sedimentary environments, water acts as the primary transport medium from which nearly all deposits form. In metamorphic environments, water serves as the primary component of most crustal fluids, thus having profound controls on the chemical and thermal transport which govern the evolution of a region. Though perhaps less appreciated, water holds an equally important role in igneous environments. The amount of water determines the melting temperature of source regions and the crystallization temperature of magmas. Just a few weight percent water can change the viscosity of a melt by over five orders of magnitude, thus playing a critical role in evolutionary processes including rate of migration, degree of assimilation and fractionation, and approach to equilibrium. Exsolving aqueous fluids are essential for the development of magmatic pegmatites and the generation of many ore bodies. In addition, the volatile content of a shallow magma chamber directly controls its eruptive style, varying from passive extrusion to violent explosions.

Given the important role of water in igneous petrogenesis, it is surprising how poorly we understand the interaction of water with silicate melts. Goranson (1931) accurately determined the solubility of water in several melts of geologic interest. Tuttle and Bowen's monumental work (1958) firmly established the overriding importance of water on the phase relations in granitic systems. Burnham (1975a; 1979) developed a thermodynamic model that described the interaction of water in silicate melts, but based this description on the assumption that only one species of dissolved water exists in a hydrous melt. It is now well established that hydrogen exists as both hydroxyl and molecular groups within the silicate framework of melts of geologic composition (Stolper, 1982a,b). Silver and Stolper (1985; 1989) have developed a rigorous thermodynamic model to describe the equilibrium of the dissolved species. Careful experimental examination of the interaction of water with natural geologic compositions under relevant crustal pressures and

temperatures, however, is still lacking. What is not well established is precise knowledge of the dependence of the concentration of dissolved water species on temperature and melt composition.

In this thesis, I describe a simple set of experiments from which I determine the precise dependence of the concentration of dissolved water species on temperature and melt composition. In addition, I present a series of experimental results which describe the solubility of water in rhyolitic melt. Thirdly, I describe the first set of experiments which describe the fractionation factors which govern the partitioning of hydrogen isotopes between hydrous rhyolitic melt and an exsolving aqueous phase. But why should we care about the precise concentrations of dissolved water species? What new insights can we gain once we have this information? I have mentioned the important role water exerts on the behavior of magmas. By precisely understanding how water is interacting with the melt structure, we can seek out correlations of melt structure with macroscopic melt properties, such as viscosity, density, and mineral stabilities. By building a deep understanding of microscopic structure, we can begin to predict its effect on the behavior of magmas in complex changing environments. Not only will we be able to observe the changes in magmatic properties, but we will have a fundamental understanding of why they are taking place. It is this understanding that is so valuable in both modelling and tracing the evolution of igneous systems in natural settings.

This thesis is an experimental study of the interaction of water with rhyolitic melt. Natural obsidian starting materials are held under carefully controlled temperatures and pressures to observe the change in solubility, speciation, and the partitioning of hydrogen isotopes in the saturated silicate melt. The experimental methods, results, and geologic applications of each of these aspects of melt-water interaction are discussed in respective chapters.

It was necessary to design and construct a rapid-quench experimental apparatus to properly investigate the temperature dependence of water speciation in the melt. The design and operational characteristics of this apparatus are presented in an appendix. The results of earlier investigations on the dependence of water speciation on the bulk melt composition are presented in a second appendix. Finally, the preliminary results of experiments bearing on the reaction rate of dissolved melt species are presented in a third appendix.

Chapter 1:

The Solubility of Water in Granitic Melt

Introduction:

Knowledge of the solubility of water in silicate magmas under geologic conditions is extremely useful. The amount of water incorporated into the structure of a melt determines such important properties as the viscosity, the density, the diffusivity of all constituent elements, and the kinetic behavior of many melt-crystal and melt-vapor reactions (e.g., Shaw, 1963; Bottinga and Weill, 1970; Zhang and Walker, 1990; London, 1988). Solubility data are used to estimate phase diagrams which help to determine the physical conditions of crystallization of natural granites (e.g., Whitney, 1975; Maaløe and Wyllie, 1975; Day and Fenn, 1982). Water solubility also determines the conditions under which water-rich magmas begin to degas, thus influencing the generation of many ore-forming fluids as well as the ultimate eruptive style of the magma (e.g., Prestwich, 1885; Taylor, 1988; Newman et al., 1988; Tait et al., 1989). All of these issues have dominated the thinking of igneous petrologists since Bowen's monumental publication of *The Evolution of the Igneous Rocks* (1928) and remain important topics of research today.

This chapter explores a recently developed method for determining the solubility of water in a silicate melt. Building upon the exploratory work of Keller and Pickett (1954), petrologists can now reproducibly measure the water content of a glass to within 0.1 weight percent using the technique of infrared spectroscopy (Stolper, 1982a; Newman et al., 1986). Infrared spectra of hydrous silicate glasses show the presence of absorption bands at 5200 cm^{-1} and 4500 cm^{-1}, demonstrating that water is present in these glasses as both an H_2O molecular species and an OH hydroxyl species. In Chapter 2 of this thesis, I describe how the concentrations of these two species are dependent on the quench rate of glass formation, demonstrating both the rapidity of the equilibrium reaction between the species in the melt as well as the temperature dependence of the equilibrium species concentrations. Though the distribution of the two species does change as a function of

quench rate, I will show that the dissolution of water into the melt is clearly not dependent on the quench rates that are used in my experiments. Thus, the water content of a melt saturated with pure water vapor will not change in cooling a sample from melt temperature to room temperature. The total water content of the melt can thus be determined by measuring the peak heights of the characteristic absorption bands generated by the excitation of the respective species.

However, the degree of accuracy with which we can determine the concentration of each species is dependent on the accuracy of our calibration of the extinction coefficients associated with each absorption in the near infrared region. Thus, another independent method for determining the water contents of hydrous glasses is needed to calibrate the infrared spectroscopic technique. In this chapter, I outline a series of experiments in which I have accurately calibrated the extinction coefficients for the two absorption bands using extraction manometry similar to the methods described in Newman et al. (1986). I then discuss the results of solubility measurements made on glasses synthesized at 850°C and compare my results to previous measurements. The implications of these results on modelling the evolution of rhyolitic magmas is discussed.

Previous Work:

The experimental methods described in this study represent a unique combination of many of the methods that have been applied to solubility studies in the past. This study provides a complete investigation of the distribution of hydrogen atoms between each of the various environments they may occupy in the melt-vapor system. Two independent determinations are made on the water content of the vapor phase as well as the water content in the melt, thus providing the most thorough assessment of the factors controlling the dissolution of water into a silicate melt.

The range of experimental techniques that have been employed in determining the solubility of water in silicate melts is as varied as the personalities which have initiated them. Goranson (1931; 1936) studied the solubility of water in both natural (Stone Mountain granite, Mt. Kiamis rhyolite) and synthetic (albite, orthoclase, orthoclase-silica) melts using a weight-loss on ignition technique. He equilibrated finely powdered starting materials at pressures up to 4 kbars and temperatures up to 1200°C before quenching to ambient conditions. After removing excess vapor by piercing and heating charges to 110°C, he combusted the entire hydrous assemblage at high temperature and atmospheric pressure. The total amount of water dissolved in solution at the temperature of the experiment was assumed to be the difference in weight before and after the combustion process, with a minor correction made for some diffusive loss of indigenous water during the 110°C heating step.

Several groups have modified Goranson's original weight-loss technique. Kennedy et al. (1950), on measuring the solubility of water in pure silica, measured only the amount of water released during the 110°C heating step. By knowing the amount of water loaded into the charge before the experiment, the concentration of silica in the vapor phase before quench, the amount of water the colloidal silica scavenged from the vapor upon precipitation, and the total anhydrous weight of the silica starting material, they calculated the total water content of the glass by evaporative weight difference. Hamilton et al. (1964) applied the same technique to melts of basaltic and andesitic composition. They ignored the solute correction but applied a new correction to account for the loss of H_2 through the platinum capsule walls generated by the oxidation of ferrous to ferric iron in the melt during the experiment. A simplified version of this weight-loss technique (ignoring both corrections) was adopted by Hamilton and Oxtoby (1978) and Oxtoby and Hamilton (1978) for solubility determinations on synthetic albite and orthoclase glass. Yoder, Stewart, and Smith (1956) tried a more ingenious weight-difference technique; water

solubilities of feldspathic melts were determined by completely crystallizing hydrated glasses and measuring the difference in the weight between their anhydrous crystalline products and their hydrous glassy experimental run products.

Khitarov et al. (1959) applied another modification to Goranson's technique; rather than assuming that all weight lost on ignition was due to water released from the glass, they measured the quantity of water actually released on ignition by absorbing the released water in "anhydrone" contained within weighable "Pregl" tubes. Their results on the El'Dzurtinskii granite at 900°C were significantly different from Goranson's results on the Stone Mountain Granite (up to 2.0 weight percent under identical conditions). Dingwell et al. (1984) modified the technique of Khitarov et al. by heating their hydrous glasses in vacuum, rather than in air, and cryogenically separating other volatiles evolved on heating to 1200°C. They measured the total amount of water released from hydrated glasses of haplogranitic composition using a manometer attached to their extraction line. Pichavant (1981) also used a vacuum extraction technique, but determined the volatile composition evolved from a haplogranitic melt using a gas chromatograph that was attached to the vacuum line.

Burnham and Jahns (1962) applied a simple visual criterion to determine the solubility of water in melts of pegmatitic composition. By running a series of isothermal and isobaric experiments with progressively increased total water in the charge, they interpreted the onset of dimples in the capsule walls to signify the establishment of a free vapor phase. Stern and Wyllie (1973) applied a similar approach using phase equilibria techniques. Location of the three-phase invariant point (crystals + liquid + vapor) in T-X space defines the solubility of water at the wet solidus. Stern and Wyllie measured the solubility in rhyolitic melts by locating this point at 25 and 35 kbar (22.5 and 27 wt % water, respectively). This approach was adopted by Hodges (1974; on the solubility of

water in anorthitic and forsteritic melts) and Egglar and Burnham (1984; on the solubility of water in diopsidic melts).

Several microbeam techniques have also been employed in determining the solubility of water in silicate melts. Using an ion microprobe, Karsten et al. (1982) measured the $H/^{16}O$ ratio at the edge of rhyolitic glass plates in a diffusion study and, applying various calibrations, determined the solubility of water at 650°C, 750°C, and 850°C at 700 bars. Orlova (1964) used the microbeam technique of infrared spectroscopy to study the solubility of water in albitic melts. This technique has proven to be the most effective method for the determination of the water content of silicate glasses. The analysis is reproducible, fast, and non-destructive. It is surprising that this technique has been ignored in solubility determinations over the past 27 years.

Given the enormous influence of water on the chemical and physical properties of magmas, it is essential that we develop a deep understanding of the factors controlling the dissolution behavior of water in silicate melts. The variable and scattered results presented in the studies described above necessitate a re-investigation of the solubility of water in silicate melts. Each study is limited by its own set of problems, some of which have been hotly debated in the literature (e.g., see Dingwell et al., 1984; Hamilton and Oxtoby, 1986). The list of short-comings for the techniques mentioned above is just too long to describe in this discussion. The study presented in this thesis is in some ways a combination of many of the methods described above. The study is unique in that it is the first investigation to carefully account for the partitioning of all hydrogen atoms in the melt-vapor system throughout each stage of analysis. Microbeam analyses (infrared spectroscopy) are used in conjunction with manometric measurements on both the vapor and the dissolved species to independently determine the solubility of water in rhyolitic melt. The superior accuracy and reproducibility of the techniques used in this study will be demonstrated in the following sections.

Experimental Methods:

Natural rhyolitic chips were loaded into platinum capsules with a sufficient amount of triply distilled water to insure saturation of the melt with a pure aqueous phase. A series of charges were equilibrated at a range of pressures and temperatures in the experimental apparatus described in Appendix 1. At the conclusion of the experiment, water contents of the quenched glasses were measured using both infrared spectroscopy and manometric analysis on a vacuum extraction line.

The manometric technique allows for accurate measurement of the water content of the glass as well as complete extraction and measurement of the fluid phase. Hence the technique provides a good check of the total yield of each experiment. In addition, the manometric analyses provide an excellent calibration of the infrared technique. The degree of accuracy with which we determine the total amount of water in the glass on the extraction line determines the degree of accuracy with which we can calculate the total water content of a hydrous glass using the absorption peak heights from an infrared spectrum. The details of the calibration of the extinction coefficients for the relevant infrared absorption peaks are described below.

Sample preparation: An aphyric rhyolite from Glass Buttes, Oregon, (see Table 1.1) was used as the starting material in all experiments. This natural obsidian was ideal for making controlled measurements on the solubility of water in melts of rhyolitic composition because of its lack of phenocrysts, which potentially complicate both the infrared and manometric determinations of water content. Cylindrical glass cores 0.100 in. in diameter were extracted from a single hand sample and sealed in platinum capsules 0.150 in. OD with triply distilled water. Welded capsules were attached to elevator rods and

loaded into rapid-quench cold-seal pressure vessels (see Appendix 1). Water was used as the pressure medium in these experiments to prevent significant loss of hydrogen through the capsule walls. The oxygen fugacity of the fluid within the pressure vessel and the experimental charge is fixed at the Ni-NiO buffer by the reaction of the nickel-rich vessel walls with the pressurizing medium (Kerrick, 1987).

The glass cores were smoothed by sanding off sharp edges to prevent the rigid glass starting material from tearing the platinum capsule while pressurizing the bomb. Weighing the capsules after quenching determined whether the charges were leak-tight throughout the experiment. The cylindrical cores allowed for convenient measurement of water diffusion profiles into the glass. The approach to equilibrium could easily be traced by the flattening of these profiles into the center of the core. Equilibrium times significantly greater than several weeks were observed for samples held at 750°C, in agreement with the diffusion data of Zhang et al. (1991). To reduce the diffusion distance required for equilibrium, smaller glass chips were used in place of the cylindrical cores. These chips were prepared by crushing and sieving the obsidian to fragments between 1.2 and 2.0 millimeters large. The angular fragments were then rounded by abrasion in a SPEX mill lined with 40 micron grit, aluminum-oxide microfinishing film (3M). Shaking times of five hours were required for several gram aliquots. The rounded chips were then ultrasonically cleaned in water to remove the abraded glass powder and the alumina contamination from the polishing paper. The smaller-sized rounded chips allowed for much shorter diffusion distances and hence quicker equilibration times. Experiments at 750°C were run for 2 to 6 weeks and shown to be homogeneous in water content.

Manometry: Water content analyses of experimental charges were performed in a vacuum extraction line, as shown in Fig. 1.1. The vacuum line consists of an input port, a vacuum gauge, a copper-oxide furnace, a cryogenic trap, a uranium furnace, a manometer,

a Toepler pump, and an exit port (see Fig. 1.1). A two-stage extraction procedure was necessary to analyze the hydrogen content of both the fluid and the melt phase. During rapid cooling of an experiment, the fluid phase condensed to liquid water, and the melt quenched to a glass. The first stage of extraction involved piercing the capsule and extracting the liquid water at room temperature with no concurrent loss of dissolved water. The second stage involved heating the glass chips in a radio-frequency induction furnace to temperatures around 1200°C for complete extraction of all dissolved water.

Sealed run products were loaded in a vacuum-tight, capsule-piercing device and attached to the input port. The piercing device was designed by modifying a NUPRO bellows valve (SS-4BK). A conical point was machined out of tool steel and attached to the valve "seal" such that upon turning the valve, the pointed end pierced the platinum charge. I found that piercing capsules while exposed to liquid nitrogen temperatures resulted in the formation of ice inside the capsule. The potential loss of diffusing molecular water from the glass precluded heating the sample to quickly sublimate the metastable ice phase. Thus, extraordinarily long extraction times were necessary to achieve complete yields. Formation of this ice was prevented by piercing the capsule under vacuum not exposed to liquid nitrogen temperatures. Two valves were inserted between the capsule piercer and the cryogenic trap. Aliquots of evaporated water were expanded into the volume between these valves. This volume was then sealed from the piercer and exposed to the cold trap. Alternating cycles of expansion and condensation were performed without exposure of the sample to the liquid nitrogen temperatures. About ten aliquots for each capsule were necessary to prevent ice formation and thus to allow for expedient extraction. I also found that small amounts of water ($\approx$ 1-10 μmoles) continued to seep out of the capsule for up to eight hours, and I found it necessary to leave the piercer attached to vacuum overnight to achieve complete fluid extraction.

A small fraction (< 1 μmole) of non-condensible gas at liquid nitrogen temperature was always observed after piercing the capsule. This gas was primarily composed of the air which fills the volume in the capsule after welding. After pumping away this non-condensible fraction, the frozen sample was purified by sequentially pumping away evolved fractions of gas at higher trap temperatures. CO_2 was released by bathing the trap in a dry-ice, M-17 slurry. This fraction was passed through the Toepler pump into a calibrated volume for manometric analysis. The sample remaining in the trap was pure water. This water was converted to H_2 by expanding over hot (750°C) uranium using the procedure of Bigeleisen et al. (1952) and transferred into the manometer. A small analytical uncertainty of the manometric measurement is associated with reading the height of the column of mercury and is estimated to be less than one percent of the volume of the sample.

Enough glass was loaded into each capsule such that two aliquots of the glassy run product could be separated for high temperature extraction without worry of a significant blank contribution. After removing the platinum capsule, several hydrated chips were separated for subsequent infrared and microscopic analysis. The remainder of the chips were crushed with an agate mortar and pestle, and the fragments less than 150 microns were removed by sieving. Particles greater than 150 microns do not supply a detectable contribution of adsorbed water to extraction analyses (Newman et al., 1986). For most experimental products, two extraction aliquots were separated and weighed on a Cahn 29 electrobalance. Each sample was added to a platinum crucible, loaded into an extraction vessel as illustrated in Fig. 1.2, and attached to the vacuum line illustrated in Fig. 1.1. After pumping away the volume of air which filled the extraction vessel, the heating coil of the induction furnace was centered around the crucible. An oscillating current applied to the copper coils creates an oscillating magnetic field. This changing field induces movement of the free electrons in the platinum metal. The oscillating electrons generate

heat within the crucible which is transferred to the sample via conduction and radiation. This process allows for efficient extraction at high temperatures (>1200°C) for long durations.

Fig. 1.3 shows the release rate of water from a rhyolitic glass with 1.2 wt % water as a function of the temperature of extraction (Sally Newman, unpublished data). The details of the release rate of water from each glass will vary from sample to sample, depending upon the water content and the size of the chips. However, the general release trend shown in Fig. 1.3 was observed for all water content samples in this study; water is released from hydrous glasses in a bimodal fashion. A significant amount of water is released at ~300°C. Zhang et al. (1991) report that at these temperatures, the diffusion rate of the molecular species is at least fifty times greater than that for the hydroxyl species ($D_{OH} < 0.02\, D_{H2O,molecular}$). Thus, the peak at lower temperature represents the release of the molecular water fraction in the glass. A second peak of evolved water occurs at ~800°C and corresponds to the release of the hydroxyl component of dissolved water in the glass. Because of the possibility of interconversion of the two species at these temperatures, it was impossible to conveniently separate the two dissolved species during extraction (see Chapter 3).

I found it necessary to completely extract the molecular water fraction of dissolved water at temperatures less than ~450°C to prevent the nucleation of tiny bubbles within the glass. The bubbles serve as storage sites for diffusing hydroxyl species at higher temperatures. The viscosity of the molten sample was sufficiently high to maintain the integrity of the bubbles and thus prevent the escape of exsolving water to the vacuum line. Care was taken to slowly extract the dissolved water; extraction times greater than 40 hours were needed to completely extract the water from water-rich samples. Table 1.2 shows a typical heating step needed to successfully prevent the formation of bubbles during the extraction procedure.

Blanks: Characterization of the blank contribution to the extraction procedure was essential for accurate manometric analysis of the hydrous glasses. The long extraction times outlined in Table 1.2 exacerbated the problem of the blank contribution from the extraction procedure to the total yield. Table 1.3 shows the results of several experiments performed at variable temperature intervals to resolve the blank contribution of water to the yield. An initial set of extractions was performed in platinum crucibles which had been soaked in hot hydrofluoric (HF) acid for up to five hours to dissolve the silicate residue which remained after previous high temperature extractions. These soaked crucibles were pre-heated on the extraction line at 1250°C for 1-3 hours to remove any HF associated with the crucible. As seen in Fig. 1.4, blank extractions (after pre-heating) at several durations illustrate an unacceptable time-dependent contribution of hydrogen released from these HF-treated crucibles. A constant release rate of 1 μmole/hour is illustrated in Fig. 1.4 and matches the available data fairly well. Theoretically, the release rate of H_2 from an HF-bearing crucible should level off with time. The actual release rate will depend upon several factors, including the duration of HF-soaking, the time of pre-heating (clearly a factor as seen from blank-1), the rate of temperature increase, and the size of the platinum crucible. The variability of these factors may explain the scatter observed in Fig. 1.4. The point of concern is the unacceptable variability (over 7 μmoles) of the blank at similar heating durations.

I found, however, that bypassing the acid treatment allowed for much smaller blanks. Careful picking of quenched silicate from the bottom of the crucible removed over 95% of the total extracted sample. Pre-heating the crucible at 1250°C for 1-3 hours removed most of the trace hydrogen still present in the residual glass, and subsequent blanks had consistently low yields only slightly dependent on time. Table 1.3 shows the results of blank extractions from several hand-picked crucibles. The evolution of water

while heating these crucibles is a mixture of three components; 1) the fraction exsolved from the residual glassy fragments, 2) the blank inherent to the line, and 3) the component of adsorbed water onto the crucible and vessel walls.

Three samples of glass recovered after extraction have been analyzed by IR spectroscopy to determine their residual water content. The water content of these chips is ≈ 250 ppm based upon the absorption of the fundamental O-H stretching vibration at 3550 cm-1 (ε_{3550} = 88 l/mol-cm; Dobson et al., 1989) The weight of the residual glass is estimated to be less than 10 milligrams. Thus, the contribution of water derived from the residual glass to subsequent extractions will typically be less than 0.2 μmoles, which we can neglect as a significant contribution to the blank. The large yields in blanks 6-9 (see Table 1.3) are then a mixture of components 2 and 3. No detailed efforts have been performed in this study to distinguish between these two sources of blank, and they will be treated as a single "adsorbed" component in this discussion. I note again that water adsorbed onto the glass chips used in the extractions (greater than 150 microns in diameter) is a negligible contributor to the total blank (Newman et al., 1986).

The component of adsorbed water: Several blanks were run on hand-picked crucibles to determine the contribution of adsorbed water to the blank. Table 1.3 illustrates a consistent release of 6.0 ± 3.0 μmoles of H_2O and 2.0 ± 1.0 μmoles of CO_2 in blank extractions from crucibles not pre-treated with HF acid and run for durations from 1-50 hours. This blank is suspected to be an adsorbed component from the atmosphere onto the crucible and vessel walls, in addition to the inherent blank of the line, and is considered to be a base level for any blank assigned to any extraction. Blank 8 (Table 1.3) illustrates that the baseline blank is released in at least two temperature steps. Previous workers (e.g., Richet et al., 1986) have tried to eliminate the adsorbed component simply by holding the sample at less than 200°C and subsequently pumping away the released vapor. I will

discuss the results of a set of experiments which suggest that complete separation of adsorbed water from water indigenous to a sample by heating at low temperatures is not possible without the use of a dry-box. However, removal of the low temperature fraction leaves a remarkably consistent high temperature component that can be quantitatively accounted for in high temperature extractions.

Table 1.4 outlines a series of experiments which demonstrate the reproducibility of the high temperature component of the baseline blank. These experiments were performed on three nominally anhydrous minerals collected and prepared by David Bell. These include 1) orthopyroxenes from Kilbourne Hole, New Mexico, 2) a diopside megacryst from the Premier kimberlite pipe, Republic of South Africa (RSA), and 3) a garnet megacryst from the Monastery pipe, RSA. Infrared spectroscopy on these mantle samples depict sizable absorptions around 3500 wavenumbers (e.g., see Fig. 1.6), demonstrating the presence of structurally-bound water in these minerals. These samples were carefully cleaned and polished into millimeter-sized slabs such that no visible contamination of adjacent minerals remained. Three different weight fractions of each mineral (two for the garnet) were analyzed on the extraction line. Each sample was brought to 200°C and held for three hours. The water and CO_2 released at this temperature was collected and measured (see Table 1.4). The sample was then brought to ~800°C, such that the sample did not melt and held at this temperature until no further hydrogen was released. Melting the samples resulted in homogenization of the crushed slabs and lengthened the diffusion distance required for release and collection of volatiles.

Results from the high temperature extraction of these minerals are listed in Table 1.4 and shown in Fig. 1.5. For a given weight fraction, the clinopyroxene releases more water than the orthopyroxene, which in turn releases more water than the garnet sample. Infrared analyses on the extracted pyroxene chips demonstrate that over 98% of the water was released during extraction. The garnet spectrum illustrated in Fig. 1.6 shows a small

shoulder at 3510 cm^{-1}, which still remained after extraction. The hydroxyl generating the absorption at this frequency is clearly more difficult to remove than the hydroxyl generating the dominant absorption at 3550 cm^{-1}. A second extraction was performed on these chips to remove the water associated with this absorption. Though an observable peak still remained after the second extraction, the decrease in the absorption (over 70% of the peak height) corresponding to the extraction yield of 1 μmole indicates that essentially all of the water has been released from these mineral chips.

The different weight fractions of all three minerals point to a 0.0 mg (blank) contribution of 2.95 ± 0.20 μmoles (see Fig. 1.5). This is in agreement with the high-temperature contribution of blank 8 (see Table 1.3) of 2.97 μmoles. The consistent high-temperature blank contribution of 2.95 ± 0.2 μmoles is convenient for making accurate water-content measurements on samples with small amounts of dissolved water. The data illustrated in Fig. 1.5 can be used to calibrate the extinction coefficients for the infrared absorption peaks for each of these minerals. Knowledge of these extinction coefficients has allowed for the accurate determination of the partitioning of water between various mantle minerals and the nature of possible water reservoirs in the mantle (Bell, unpublished Ph.D. thesis).

The variability of the total blank (low + high-temperature) in blanks 1-9 is therefore due to the low-temperature contribution of the blank. Several explanations can account for these observations. It may be that the low-temperature fraction represents the adsorbed water onto the crucible, and the high-temperature blank is released from the vessel walls when the radiative heat from the hot platinum crucible excites the water molecules off the vessel walls and into the gas phase (see Fig. 1.2 for a schematic of the extraction vessel). It is also possible that the high-temperature blank represents the first layer of adsorbed water onto the platinum crucible. The low-temperature component may represent loosely bound water adhering to the initial layer. The variability in the amount of loosely bound

water may be the result of the dependence of subsequent adsorbed layers on the temperature and water pressure in the room at the time the crucible is loaded onto the extraction line. Alternatively, adsorbed water onto the crucible may be released at low temperatures, and hydrogen occluded within the crucible is expelled while heating at high temperature; that is, the platinum metal acts as a sponge and absorbs water at room temperature, only to release this occluded component at temperatures greater than 400°C. This phenomenon was first noticed in the late nineteenth century (Graham, 1876; Mond, et al., 1895) when it was observed that up to 0.5 wt percent water could be occluded in platinum metal at room temperature, which was not released until the metal was brought to a red heat.

Infrared Spectroscopy: Two glass chips (approximately 2 millimeters in diameter) were separated from each experiment for spectroscopic analysis. The chips were mounted in dental resin (L. D. Caulk Co.) and polished by grinding on alumina grit micropolishing paper (3M). Final polishing was accomplished using 0.3 micron alumina powder in distilled water on polishing cloth (3M). The singly-polished samples were glued to glass slides with epoxy (Crystalbond 509, Aremco Products, Inc.), and samples were ground to thicknesses varying from 200 to 800 microns. The final thickness for each sample was fixed such that infrared analyses could be made through both the edge and the center of the sample to check for inhomogeneity in water content. These doubly-polished sections were soaked in acetone to remove traces of epoxy and rinsed in toluene to remove any acetone residue. Samples were positioned over apertures varying from 50 to 1000 microns in diameter. All infrared analyses were performed on a Nicolet 60SX Fourier transform infrared spectrophotometer (FTIR) using a W tungsten source, CaF_2 beamsplitter, and an InSb detector with a resolution of 2 cm^{-1}, a mirror velocity of 1.57

cm/sec and 1024-2048 scans. A background spectrum was taken before each series of analyses and subtracted from each sample to yield the absorption spectrum of the glass.

The Beer-Lambert Law (or Beer's Law) states that within a matrix, the amount of absorption in an energy spectrum is proportional to the number of absorbers. For dissolved water species in a silicate glass, we can express the number of absorbers as the product of the species concentration (C) in the glass, the thickness (d) of the glass, and the density (ρ) of the glass;

# of absorbers = $C*d*\rho$.

Thus, the absorbance of an infrared band (Abs) will be proportional to the concentration of the dissolved species such that :

$$\text{concentration} = \frac{\text{Abs}}{d * \rho * \varepsilon} \qquad (1)$$

where ε is the constant of proportionality or the extinction coefficient from Beer's Law. In this study, I use the molar absorptivity as described by Newman et al. (1986), such that units of concentration are in weight percent, d is in cm, ρ is in grams/cm^3, and the right-hand-side of eq. 1 is multiplied by 18.015 grams/mole. The validity of Beer's Law in hydrous silicate glasses has been demonstrated by Newman et al. (1986, Fig. 7) and Silver (1988, Fig. 7).

Fig. 1.7 shows an absorption spectrum of a water-rich (5.2 wt %) glass in the near infrared region between 7500 cm^{-1} and 3500 cm^{-1}. Absorption peaks at 7075 cm^{-1}, 5235 cm^{-1}, 4501 cm^{-1}, and 3900 cm^{-1} are observed. Following Stolper (1982a), the peaks at 7075 cm^{-1} and 3900 cm^{-1} are correlated with the total water content of the glass and correspond, respectively, to the fundamental overtone of the O-H stretching vibration at 3550 cm^{-1} and some combination of the fundamental O-H stretch with a low energy silicate framework vibration. The peaks at 5235 cm^{-1} and 4500 cm^{-1} have been assigned to the combination stretching and bending mode of H-O-H molecular water (Scholze 1960), and

X-O-H hydroxyl species (Harrison 1947), respectively. Thus, the relative concentrations of H_2O molecular groups and OH hydroxyl groups can be distinguished simply by measuring the absorption peak heights in the near infrared region, provided an accurate ε value is known for each respective absorption band.

Results:

The results of experiments bearing on the solubility of water in natural rhyolitic melts at 850°C are presented in Tables 1.5 - 1.7. The water contents of samples equilibrated at pressures ranging between 200 and 1600 bars have been determined by both extraction manometry and infrared spectroscopy.

Results from manometry: The results of manometric analyses using the vacuum extraction technique on hydrated glasses are presented in Tables 1.5 and 1.6. An initial set of experiments (GB 7-21) involved extraction of water from a single aliquot of sample. Subsequent experiments (GB 25-76) included extraction analyses on two aliquots of the available sample. For each experiment, the temperature, pressure, and run duration are presented with extraction analyses on both the quenched vapor and melt phases. In addition, Table 1.6 presents the results of infrared analyses on glasses from the same experiments (see Table 1.7) for comparison with the manometric measurements.

The vapor phase: The measured quantity of water released from the aqueous vapor phase as determined by hydrogen manometry is given in column 5 of Table 1.5. This value is compared to the weight-loss measurement (column 6) determined by weighing the capsule before and after piercing under vacuum. The weight-loss measurement is typically 2-5 μmoles (assuming weight-loss as H_2O) greater than the manometric determination of

extracted water vapor. This value is consistent with a small yield of non-hydrous volatiles (dominantly non-condensible gas at liquid nitrogen temperatures) observed in all vapor extractions. In several experiments, re-piercing at the opposite end of the capsule released an additional quantity of vapor. Collapse of the platinum capsule around the porous sample (rounded chips several millimeters in diameter) at high pressures may isolate pockets of vapor from vacuum upon piercing. Vapor extractions varying by more than 10 μmoles from the weight-loss determination are interpreted as incomplete extractions, and the weight-loss determination for these experiments was used in subsequent bulk yield analyses.

Dissolved water: The amount of water and carbon dioxide measured from each glass extraction is presented in columns 7 and 8 in Table 1.5. There are several ways of assigning the blank contribution to these measurements. The simplest and most straightforward assignment is to assume a constant blank independent of extraction duration or pre-history of the platinum crucible (e.g., see Newman et al., 1986 (2 ± 1 μmoles) and Dobson et al., 1989 (7 ± 2 μmoles)). Our results on extractions for the long durations outlined in Table 1.2 suggest that this simple assignment is not accurate. In fact, HF-soaked crucibles can yield blanks up to 11.6 μmoles (see blank-2 in Table 1.3). However, a relatively steady value of 7 ± 3 μmoles (including the low and high temperature steps) was observed in blank extractions for durations ranging from 1 to 50 hours on crucibles which had not been pre-treated with HF. This value could well be assigned to extractions not performed in HF-soaked crucibles (GB 71-76). An alternative blank assignment to the extractions performed in crucibles soaked in HF (GB 7-65) is to assign a time dependent value similar to that shown in Fig. 1.3; i.e., hydrogen that was absorbed in the platinum metal during the hot HF-treatment was released at ≈ 1 μmole/hour at high temperatures in the vacuum line.

There is another alternative and more informative assignment of a blank that can be consistently applied to all extractions. CO_2 can be used as a tracer of contaminant throughout the extraction process in the experiments described in this thesis. The starting materials contain no detectable CO_2 (<3 μmoles; Jen Blank, personal communication). The only other potential source of CO_2 in the experiment comes from the small volume of air trapped in the capsule on welding. An approximate value of 1% CO_2 in the 0.1 cc volume yields a trivial amount of CO_2 available for dissolution from the vapor into the melt. Clearly, any measured CO_2 from my extractions must have been added as a contaminant. I have chosen to assign a blank to each yield based upon the amount of CO_2 recovered in each extraction. The various sources of blank can be characterized by their relative concentrations of H_2O and CO_2. An understanding of the relative proportions of each source of blank allows for an accurate quantitative determination of extraneous water added to each individual extraction.

The possible sources of contaminant have been described in the *blank* section above; these include adsorbed CO_2 from the atmosphere (+ CO_2 added as a characteristic blank of the extraction line) and CO_2 added in the HF-soaking procedure. As discussed previously, the characteristic blank of the line has not been distinguished from the adsorbed (or occluded) blank component. This source of blank has an H_2O / (H_2O + CO_2) value (%.H_2O_{bl}) of 0.71 ± 0.10 (see blanks 7-10). From the total yield of CO_2 in each extraction, the amount of extraneous water can be calculated. This is the characteristic composition of the adsorbed blank component and is removed from the total yield to determine the total amount of recovered water from the glass chips (column 10 of Table 1.5).

The %.H_2O_{bl} value for HF-treated crucibles must be determined independently, as extractions performed in these crucibles contain a mixture of the HF-blank component as well as the adsorbed component. The two blanks performed on HF-treated crucibles (with

measured CO_2 yields) have a $\%.H_2O_{bl}$ value of 0.91 ± 0.10 (see blanks 2 and 3). The composition of the blank component is enriched in H_2O relative to the $\%.H_2O_{bl}$ value for just the adsorbed component. In fact, the total CO_2 yields are identical to those recovered in blank extractions from crucibles not soaked in HF. It is reasonable to assume that the $\%.H_2O_{bl}$ value of the HF component is 1.0; i.e., no CO_2 is added to the crucible in the HF-soaking procedure. Thus, the blank contribution to extractions performed in pre-soaked crucibles contain the same adsorbed component as in the non-soaked crucibles (determined from the CO_2 content via the $\%.H_2O_{bl}$ value of 0.71) as well as an additional time-dependent release of H_2 evolved as a result of the HF-treatment. I have assigned an average release rate of 0.005 μmoles/min, which is the best-fit release rate observed in Fig. 1.4 after assigning an initial base-line adsorbed blank of 4.1 μmoles determined from blank-8 (see Table 1.3).

Water solubility in rhyolitic melt: The amount of water extracted from each sample (blank corrected) is shown in columns 12 and 13, and the weight of each extraction aliquot is given in column 15 of Table 1.5. The amount of water remaining in the glass chips after extraction have been measured by IR spectroscopy on three post-extraction products. Based upon the best-fit molar absorptivity of 88 l/mol-cm for the fundamental stretching vibration of O-H at 3550 cm-1 (from Dobson et al., 1989), these values are 403, 253, and 101 ppm. An average value of 250 ppm is added to the extraction yields in Table 1.5 to give the total concentration of dissolved water in the glass chips prior to extraction. The calculated concentration of water in the glasses is given in column 16 and shown as a function of the pressure of the experiment in Fig. 1.9. The X symbols represent the results from extractions GB 7-65 (extracted from HF-soaked platinum crucibles) and the O symbols represent the results from extractions GB 71-76 (extracted from hand-picked

crucibles). These measurements define the solubility relationships of water in a rhyolitic melt saturated with pure water vapor.

Yield analyses: The accounting of water molecules in the melt-vapor system is useful in many respects. Independent measurements of both the vapor and dissolved water components provide a check on the accuracy of each technique. Table 1.6 presents such an accounting of the water yields from each experiment. The total amount of dissolved water is calculated by applying the measured concentration of water to the total anhydrous weight of the glass loaded into the capsule. Thus the total amount of dissolved water in the experiment can be determined without having to extract water from the chips used for infrared analyses or the fine-grained fraction removed by sieving. By including the amount of water recovered from the vapor phase (the value determined by the weight-loss measurement), all of the water in the system at the conclusion of the experiment can be accounted for. This value is compared to the total amount of water loaded into the experiment in columns 13 and 14 of Table 1.6 and displayed graphically in Fig. 1.10. In general, the yield analyses are satisfactory; i.e., a 1:1 correlation exists for most of the experiments. Unusual results become obvious. For example, Sample GB-71.1 **and** 71.2 both give an excess of 145 μmoles. This value is consistent with the weight the capsule gained during the experiment in the pressure vessel (this was the only sample analyzed in the data set which experienced a weight change during the experiment). In addition, an unusual excess (≈115 μmoles) was observed for sample GB-65. This excess is most likely due to the loss of a glass chip in transportation after piercing and before the weight-loss determination. A more accurate assessment of the yield of this experiment incorporates the actual amount of water recovered on extraction ($\Delta_{yield} < 15$ μmoles). These examples are the exception rather than the rule; recovery of water from sample GB3-

11 came within 1% (less than three μmoles) of the total amount of water loaded into the experiment, demonstrating the quality of the technique.

Results from infrared spectroscopy: The results of infrared analyses performed on glasses recovered from the experiments described in Table 1.5 are listed in Table 1.7. Each experiment in Table 1.5 has been analyzed using the IR technique through the center of a doubly polished wafer as described above (labeled with a (.c) in Table 1.7). Where possible, infrared spectra have also been taken through the edges of the wafers to measure the water content of the melt in close proximity to the vapor phase and provide a check for homogeneity within the charge (labeled with an (.e) in Table 1.7). The measured absorptions of the 5200 cm^{-1} and 4500 cm^{-1} bands are listed in columns 4 and 5. To determine the absolute concentrations of each species, accurate knowledge of the density and thickness of each glass chip is required along with the molar absorptivities of the respective bands. The thicknesses of the glasses at the location of the position of the apertures have been measured using a Mitutoyo digimatic micrometer and is reproducible to within 3 microns. The densities of a series of hydrous rhyolitic glasses have been measured with a Berman balance by weighing in air and in toluene at a known temperature and are displayed in Fig. 18a of Silver et al. (1990; Appendix 2). The observed linear trend of density with total dissolved water content implies that the hydroxyl and molecular water components have similar molar volumes in these glasses (see discussion below). The proportional relationship enables an easy calculation of the density for each of the glasses measured in this study; the density is calculated iteratively in Table 1.7 using the measured relative concentrations of hydroxyl and molecular water. Knowledge of the extinction coefficients for each of the absorption bands is needed to calculate the absolute concentrations of the dissolved water species. Using previously published ε values (ε_{5235} cm^{-1} = 1.61 l/mol-cm and ε_{4500} cm^{-1} = 1.73 l/mol-cm; Newman et al., 1986), I have

calculated the total water contents of each of the glasses listed in Table 1.7 by summing the respective concentrations of the two species. These results are compared to the results of the manometric determinations of total water content performed on glasses from the same experiments in Fig. 1.11. The total water as determined by the infrared measurements generally fall short of the manometric determinations. A new calibration of the extinction coefficients is required to match the manometric results with the IR results.

Calibration of absorption band extinction coefficients: Newman et al. (1986) have measured the water contents by both vacuum manometry and IR spectroscopy on 29 natural rhyolitic glasses, ranging from 0.07 to 2.64 wt % total dissolved water. Their best-fit ε values for the 5235 cm^{-1} and 4500 cm^{-1} band are 1.61 l/mol-cm and 1.73 l/mol-cm, respectively. Because of the nature of the blank correction (up to 10 per cent of the total sample), the length of their run durations (generally two hours and less), and the lack of samples more water-rich than 2.4 wt %, I have recalibrated the extinction coefficients for the characteristic absorption bands of the two water species using the data listed in Tables 1.5 and 1.7. In this study, I have measured the water content of glasses with up to 6 weight percent water. The extinction coefficients have been fit by two regressions of an equation of the form;

$$\frac{\rho * d * H_2O_{tot}}{18.015} = \frac{\text{Abs } (5200\ cm^{-1})}{(\varepsilon_{5200cm^{-1}})} + \frac{\text{Abs } (4500\ cm^{-1})}{(\varepsilon_{4500cm^{-1}})} \qquad \text{(a)}$$

where Abs (i) = absorbance at wavenumber i, ε = extinction coefficient of i (g/mol-l), ρ = iterated density (g/l), d = thickness (cm), and 18.015 = the molecular weight of H_2O. A simple least squares regression incorporating the best data from Newman et al. (1986; 19 samples), Dobson et al. (1989; 3 samples), and this study (19 samples; labeled with an asterisk in Table 1.6) gives best-fit values of $\varepsilon_{5235\ cm^{-1}} = 1.51 \pm 0.09$ l/mol-cm, and $\varepsilon_{4500\ cm^{-1}} = 1.73 \pm 0.14$ l/mol-cm. A second regression was performed using a weighted

errors routine (Alberede and Provost, 1977). The errors in the manometric measurements have been applied based on the relative percentage of the blank to the total amount of recovered sample. Errors in the absorbances are based on the quality of individual spectra and are generally between 1 and 5% of the total absorbance. The results are similar to the simple least squares regression; ε_{5235} cm^{-1} = 1.40 ± 0.06 l/mol-cm, and ε_{4500} cm^{-1} = 1.95 ± 0.13 l/mol-cm. Because the error assignments to the results in the previous studies are relatively arbitrary, I have applied the ε values fit by the non-weighted least-squares regression to the spectroscopic data in Table 1.7.

Fig. 1.11 shows the results of infrared measurements from the center of glass chips as well as their edges. The agreement of the water contents in these two regions are within the error of the measurements, which are roughly the size of the symbols. The results of the water content analyses from infrared spectroscopic measurements are shown in Fig. 1.12 as a function of the pressure of equilibrium. The solubility curve is identical to that of water in rhyolites from Mono Craters, CA illustrated in Fig.13a of Appendix 2, demonstrating the reproducibility of the technique on similar bulk compositions. The yield analyses based on total dissolved water determined by IR measurements are shown in column 14 of Table 1.6 and illustrated in Fig. 1.13. As with the manometric technique, Fig. 1.13 demonstrates the ability of this technique to account for all the water loaded into the experiments.

Discussion:

Eruption triggering: The solubility relations of water in silicate melt exert an enormous influence on the timing of volcanic eruptions. The energy generated by the PΔV (and VΔP) of exsolution drives the explosive activity observed in volatile-rich magmatic eruptions. We can apply our solubility measurements to two completely different styles of

eruptive activity. In the first case, I consider an undersaturated magma evolving in a shallow chamber. In the second case, I consider the rapid explosive eruption caused by the mixing of two compositionally distinct magmas.

"Passive" evolution of shallow magma chambers: Periodicity in volcanic systems has been observed throughout the world in a variety of tectonic environments, including the Mono Craters, Ca. (Taylor et al., 1983) and the Coso Range, Ca. (Bacon, 1982) rhyolitic eruptions, the subduction-related Mt. St. Helens dacites, (Anderson and Fink, 1989) the Hawaiian hot-spot basalts, (e.g., Wadge, 1980), the east African rift carbonatites (Pyle, 1991), and many others. We can envision a very simple mechanism to generate the eruptive cycles of volcanoes. A simple description of, for example, the chamber beneath Mono Craters in California is as follows; a) pooling of rhyolite magma with 3 wt. % water at 2 kilometers depth, b) crystallization of plagioclase removing anhydrous components from the melt, thus driving the water content of the magma to saturation (around 3.5 wt. % at 700 bars), c) the growth of bubbles drives the pressure in the chamber up until d) the pressure in the chamber exceeds the yield strength of the overlying rock and initiates an eruption, e) continued extrusion of volatile-poor magma through the ruptured roof rock, f) sealing of the magma pathways with continued cooling, and g) repeating the cycle with new influx of lava from below. The model is rather simple as presented. A full description of the system incorporating the timing of the periodicity must include, 1) precise knowledge of the initial volatile content of the magma (including CO_2, S species, halides, etc.), 2) the solubility of these volatiles in the magma as a function of pressure, temperature, and vapor composition, 3) the capacity for the transferal of heat away from the surrounding wallrock (including the heat conductivity, porosity, and vigor of meteoric water circulation through the rock) and hence the crystallization rate of the magma, 4) the volume change on crystallization, 5) the rigidity of the surrounding wall rock, and 6) the

recharge rate of new magma to the chamber. Full understanding of all these factors is necessary for accurate modelling of the eruptive periodicity of volcanoes, and such a description is beyond the scope of this thesis (see Pyle, 1991 for new insights). Tait et al. (1989) present a model of eruption periodicity and claim that the solubility relations of water in the melt represent the most important factor controlling eruptive cycles. The measurements presented in this thesis quantitatively provide the solubility relations of water in rhyolites and can be used as a good approximation for the behavior of volatile exsolution in the silica-rich end-members of the Cascade Range, as well as the water-rich rhyolites of California.

magma mixing: The intimate association of basalt with more silicic magmas has been documented in many different tectonic environments. For example, Sparks et al. (1977) describe mafic bands and clots in acid pumice from Askja, Iceland and Santorini, Greece; Smith (1979) documents mixed pumices in ash flows from the the Valley of Ten Thousand Smokes, Alaska; Gerlach and Grove (1982) found zoned olivine phenocrysts varying from Fo_{81} to Fo_{64} over a 50 micron traverse in basaltic andesites at Medicine Lake Highland in northern California; Bacon (1986) observed andesitic inclusions in silicic andesites at Crater Lake, as well as high-silica rhyolite hosting mafic andesite in the Coso volcanic field.

The textural association of the basaltic fragments within the erupted rhyolite imply that the eruption proceeded shortly after intrusion of the basalt into the silicic host, and Sparks et al. (1977) suggested that the mixing of mafic magmas into silicic chambers actually triggers the eruption process. In their landmark paper, they presented three mechanisms for supersaturation of the silicic magma on intrusion by basalt, (a) the hot dense basalt intruding the chamber remains gravitationally stable at the bottom of the chamber and rapidly heats the overlying silicic lava. The super-heated deep silicic lava

becomes less dense than the overlying cooler lava, and density instabilities cause parcels of magma to rise. Rising blobs become super-saturated at lower pressures and generate eruption, b) superheating of the silicic lava lowers the solubility of the melt to super-saturation and generates eruption, and c) the volume increase due to the intruding basalt causes fracturing of the chamber walls, causing pressure release, supersaturation, and eruption.

Several models have been developed to quantitatively model the mixing and eruption triggering process (e.g., Huppert and Sparks, 1980; Rice, 1981; Sparks and Marshall, 1986; Oldenburg et al., 1989; Russell, 1990). However, these treatments have ignored mechanism (b) of Sparks et al. (1977). For example, Russell (1990) has modeled the mixing of two water-saturated magmas. Although the thermodynamics of the water component are included in the heat and entropy of mixing terms, the temperature dependence of the solubility is ignored. Rather, he ascribes vesiculation on mixing to be the result of the super-saturation of the resultant magma after complete hybridization of the two end-member magmas. Such thermodynamic treatments of magma mixing are no doubt extremely important in modelling natural phenomena, as there are many examples of complete hybridization of magmas occurring before eruption (e.g., Anderson, 1976; Eichelberger, 1978; Sakuyama, 1981; Bacon, 1986). However, such complete mixing and supersaturation is not likely to generate the explosive eruptions cited earlier.

The preliminary data in Table 1.5 on the temperature dependence of the solubility of water in melt suggest that little mixing will occur before supersaturation drives an eruption. Thermal diffusion rates are 3 to 5 orders of magnitude greater than chemical diffusion rates (e.g., Sparks and Marshall, 1986). Consider the intrusion of a basalt ($\approx$ 1150°C) into an undersaturated rhyolitic magma chamber at 750°C (5.5 wt. % water at 4 kilometers depth). The temperature of the rhyolite in contact with the basalt will instantly rise to 950°C. From my preliminary data in Table 1.5, the solubility of water in a melt at 1.5 kbars decreases

from 6.1 to 5.6 wt. % on heating from 750°C to 850°C. If we assume a similar change on heating to 950°C, the solubility of water in rhyolite will decrease to ≈ 5.1 wt. %. Thus, our 5.5 wt % magma rapidly becomes super-saturated, and the exsolution of vapor may quickly drive an eruption. A more thorough investigation of the temperature dependence of the solubility of water is required before this process can be more accurately modelled. Clearly, this is an important field of study and experiments are currently being performed to better understand the effect of temperature on solubility. The discussion is presented to emphasize the importance of the solubility relations to natural phenomena.

Application of solubility measurements to the thermodynamics of melt-vapor systems:

The goal of this thesis is to develop a deeper understanding of the nature of the interaction of water with silicate melt. Thermodynamics provide an accessible, quantitative framework in which to study hydrous melts. Knowledge of the thermodynamic properties of wet melts is essential for modelling magmatic processes under varying geologic conditions. In addition, knowledge of thermodynamic properties yield insights into the structural characteristics of the melt. More complete understanding of the thermodynamic properties of the individual components in hydrous melt systems can shed light on important phenomena including; (1) the energy ($P\Delta V$ work) associated with the exsolution of water vapor from a melt, which may be the primary driving force for explosive eruptions, (2) the heat of reaction involved in vapor exsolution, which exerts a significant control on the heat budget of evolving saturated magmas in open systems, (3) The molar volume of the components in the melt, whose variability as a function of pressure controls the crystal-melt phase boundaries in P-T-X space. The molar volume of the magma components also affect the density of the melt, which exerts a dominant role on the ascent

rate of the magma, thus influencing the amount of time the melt will remain in the source region before ascent, as well as the amount of time available for crystallization and assimilation while migrating upward through surrounding country rock. The density of the melt is also an important property in determining whether a magma chamber will convect, either via thermally- or compositionally-induced instabilities. This section describes how my solubility measurements are used to set constraints on important thermodynamic properties including the heat of mixing water molecules in the vapor with water molecules in the melt, and the partial molar volume of water species in the melt.

Demonstration of Henry's Law : Knowledge of the structure of microscopic systems may be used in conjunction with thermodynamic descriptions to yield constructive insights into the nature of microscopic processes. For example, the application of Henry's Law is a simple and useful thermodynamic description of the mixture of a dilute substance in a solvent. Henry's Law states;

$$a^{m}_{solute} \alpha X^{m}_{solute} \qquad (4)$$

where a^{m}_{solute} is the activity of the dilute component in a solvent, m, and X^{m}_{solute} is the mole fraction of the solute in m. If Henry's Law is valid and the constant of proportionality is known, the activity of the solute in the mixture can be calculated if the concentration of the solute species is known.

A Henrian relationship has long been observed in hydrous silicate glasses quenched from low pressure experiments (e.g., Tomlinson, 1956; Russell, 1957; Kurkjian and Russell, 1958; Moulson and Roberts, 1960; Uys and King, 1963). By noting a linear relationship between the fugacity of water (f_{H_2O}) and the square of the mole fraction of total dissolved water (X^{m}_{w}), researchers have concluded that the dissolution mechanism for water is primarily through the reaction;

$$H_2O^{vapor} + O^{melt} \rightarrow 2\ OH^{melt} \quad (5)$$

Burnham and Davis (1974) observed that the linear relationship holds in albitic glasses with compositions as water-rich as $(X_w^m) = 0.5$. They invoke a new mechanism for water dissolution to account for the non-linear behavior observed at higher water contents. Burnham (1975) proposed an initial cation exchange reaction of H^+ with Na^+ until all Na^+ ions are exhausted; with further dissolution, water enters the melt in hydroxyl form without the exchange of proton for cation.

The infrared measurements presented in Table 1.7 suggest that a different mechanism is needed to describe the dissolution of water into silicate melts. Stolper (1982a) has shown that the linear relationship between f_{H_2O} and $(X_w^m)^2$ does not require that the reaction in eq. 5 be the only mechanism for water dissolution into the melt. He demonstrates that such a linear relationship is compatible with the dissolution of two water species in the melt. Homogeneous equilibrium in a saturated silicate melt can be described by the following two reactions;

$$(H_2O)^{vapor} \Leftrightarrow (H_2O,_{molecular})^{melt} \quad (6)$$

$$(H_2O,_{molecular})^{melt} + O^{melt} \Leftrightarrow 2OH^{melt} \quad (7)$$

In Chapter 2 of this thesis, I demonstrate that the concentrations of the dissolved water species measured on hydrous glasses (listed in Table 1.7) do not represent the corresponding concentrations of the species in the melt from which they were quenched. However, I will present a series of experiments which allow for calculation of the concentration of the molecular water species in the melt at any temperature using a simple regular solution model (please see discussion in Chapter 2). The appropriate application of Henry's Law, (according to Guggenheim, 1952), is to the relationship of the dissolved molecular species with H_2O in the vapor.

Following Silver and Stolper (1985), I treat the molecular H_2O species in the melt as a solute in rhyolitic melt. The experiments outlined in Table 1.5 have all been performed under water saturated conditions. At saturation,

$$\mu_{H_2O}^{vapor} = \mu_{H_2O}^{melt} \tag{8}$$

where $\mu_{H_2O}^{vapor}$ = the chemical potential of water in the vapor and $\mu_{H_2O}^{melt}$ = the chemical potential of water in the melt. Further, in pure water vapor, $\mu_{H_2O}^{vapor}$ can be calculated at any pressure and temperature given an appropriate equation of state. We can derive an expression for the activity of water in the melt;

$$a_{H_2O}^{m}(P_2,T_2) = a_{H_2O}^{m}(P_1,T_1)\,\frac{f_{H_2O}^{o}(P_2,T_2)}{f_{H_2O}^{o}(P_1,T_1)}\,\exp\left\{-\int_{P_1}^{P_2}\frac{V_{H_2O}^{o,m}(P,T_2)}{RT_2}dP + \int_{T_1}^{T_2}\frac{\Delta H_{H_2O}^{o}(P_1,T)}{RT^2}dT\right\} \tag{9}$$

where $(P_i\,,\,T_i)$ represent two conditions of vapor saturation; $a_{H_2O}^{m}(P_i,T_i)$ is the activity of water in the melt at P_i and T_i; $f_{H_2O}^{o}(P_i,T_i)$ is the fugacity of pure water vapor at P_i and T_i; $V_{H_2O}^{o,m}(P,T)$ is the molar volume of water in the melt in its standard state; and $\Delta H_{H_2O}^{o}$ is the standard state enthalpy change for dissolution of water vapor into the melt.

Whenever $P_2 - P_1$ is small, the first integral in the exponential term reduces to a negligible value. We can therefore express the activity of water in the melt as;

$$a_{H_2O}^{m}(P_2,T_2) = k\, f_{H_2O}^{o}(P_2,T_2) \tag{10}$$

$$\text{where } k = \frac{a_{H_2O}^{m}(P_1,T_1)}{f_{H_2O}^{o}(P_1,T_1)}\,\exp\left\{\int_{T_1}^{T_2}\frac{\Delta H_{H_2O}^{o}(P_1,T)}{RT^2}dT\right\}. \tag{11}$$

Thus, for a series of water saturated melts under isothermal conditions, k will be constant, and the fugacity of water vapor in equilibrium with the melt will by proportional to the activity of water in the melt. The validity of Henry's Law is thus easily demonstrated if a

proportional relationship between the mole fraction of molecular water and the fugacity of water in the vapor exists. Table 1.6 lists the calculated mole fraction of molecular water ($X^m_{H_2O}$) in the melts at 850°C (determined by the regular solution model presented in Chapter 2). Table 1.6 also lists the fugacity of water for each experiment calculated from the modified Redlich-Kwong equation of state (Holloway, 1977). $X^m_{H_2O}$ is plotted as a function of the fugacity of water in the vapor in Fig. 1.14. The clear linear relationship observed in these experiments demonstrates the applicability of Henry's Law to hydrous silicate melt systems at low pressures. The slope of the line determines the Henry's Law constant for water in rhyolitic melt.

The usefulness of this simple thermodynamic description is apparent. The knowledge of the total water concentration and temperature of a melt (and hence the concentration of the molecular water species) allows for a determination of the activity of water in the system and, under saturated conditions, the fugacity of water in the vapor in equilibrium with the melt. Conversely, knowledge of the fugacity of water in the system can lead to the determination of the water content of a magma. For example, Wones and Eugster (1965), and Wones (1972) present a technique for estimating the water fugacity in crystallizing rhyolitic magmas. If independent determinations of oxygen fugacity and pressure are known, the composition of biotite in equilibrium with magnetite and alkali feldspar will uniquely give an estimate of the water fugacity. Application of the Henry's Law constant determined in this study determines the molecular water content of the crystallizing magma. Such detailed knowledge of the conditions of crystallization for natural magmas yields extremely useful insights into the properties of evolving magmas.

Determination of ΔH: Equations (6) and (7) describe the interaction of water with silicate melt. The change of heat associated with each of these reactions can give us insights into the temperature dependence of the equilibria. The ΔH for the reaction between

the two dissolved species will be discussed in Chapter 2. The change in enthalpy associated with the dissolution of water molecules from the vapor phase into the melt describes the temperature dependence of solubility. There are not enough data in this study to accurately constrain this dependence. However, a preliminary treatment is now given. Equations (10) and (11) allow for the determination of the heat of mixing if the activity and fugacity of water are known for a series of melts equilibrated at a constant pressure. That is;

$$\ln \frac{a_{H_2O}^{melt}}{fug_{H_2O}^{melt}} = \ln \frac{a_{H_2O}^{o}}{fug_{H_2O}^{o}} - \frac{\Delta H}{R}\left(\frac{1}{T} - \frac{1}{T^o}\right) \qquad (12)$$

This equation expresses a linear relationship between $\ln \frac{a_{H_2O}^{melt}}{fug_{H_2O}^{melt}}$ and 1/T. Using the activity composition relationship described earlier, a simple linear regression on a series of isobaric experiments will allow for the determination of $\Delta H^{melt\text{-}vapor}$ associated with reaction (6).

Determination of ΔV: The partial molar volume of molecular water in the melt can also be determined by our measurements. The dissolution of water vapor into the melt is expressed by eq. (6). At saturation with aqueous vapor for a variety of melts equilibrated at constant temperature, we can write;

$$\ln \frac{a_{H_2O}^{melt}}{fug_{H_2O}^{melt}} = \ln \frac{a_{H_2O}^{o}}{fug_{H_2O}^{o}} - \frac{V^o}{RT}\left(P - P_o\right) \qquad (13)$$

This equation is analogous to eq. (12) but expresses $\ln \frac{a_{H_2O}^{melt}}{fug_{H_2O}^{melt}}$ as a linear function of pressure for a series of isothermal melts. Given experimental data on the mole fraction of

molecular water in equilibrium with melts at a range of pressures (at constant temperature), a simple linear relationship will provide the molar volume of molecular water in the melt. This analysis is shown in Fig. 1.15, and a slope of 0 is observed.

This result is significant. If the partial molar volume of molecular water in the melt is actually zero, we expect the total volume of the melt-vapor system to decrease with the dissolution of water. Further, this result implies that water dissolution will cause an actual increase in the density of the melt. If enough water is driven into the melt such that the molar volume of the melt is actually smaller than the crystals in equilibrium on the liquidus, we expect the liquidus of natural wet magmas to have negative slopes. This implies that at greater depths, the onset of crystallization occurs at lower temperatures than in shallow magma chambers. Likewise, in considering the progressive batch melting of granitic source regions, the temperature at which the system is completely molten is significantly lower than if the dissolved water had increased the total volume of the system. Though such negative slopes might seem contrary to our intuition (e.g., see Burnham, 1975, Fig. 9), the available data on the phase equilibria of natural granites (Whitney et al., 1975) support my results. Fig. 1.16 (adapted from Day and Fenn, 1982, Fig. 8) illustrates the results of Whitney et al. (1975) on the phase relations of the wet granite system. Schematic undersaturated liquidi have been drawn in to match the disappearance of feldspar on the liquidus of their granitic composition. The dry liquidus has a positive slope indicating a positive change of volume and entropy on melting of the liquidus phase; i.e., from the Clausius-Clapeyron equation;

$$\frac{\Delta P}{\Delta T} = \frac{\Delta S}{\Delta V} \qquad (16)$$

Figure 1.16, however, illustrates progressively decreasing slopes (decreased ΔV) of undersaturated liquidi with increasing total water content. Thus, with the addition of water to the melt, the relative difference in volume between the crystalline plagioclase phase

and the hydrous melt phase becomes smaller. Addition of water must be decreasing the molar volume of the melt. The liquidi in Fig. 1.16 actually become negative at water contents of 4 weight % and greater. Thus, from Fig. 1.16, the volume of the hydrous melt is identical to the plagioclase phase at around 3 wt % water. Given the molar volume per oxygen of the plagioclase phase at 850°C at 8.3 kbar (12.5 cc/mol is calculated for $Ab_{56}An_{44}$: 1 atm molar volume from Robie et al., 1978; thermal expansion and compressibility data from Clark, 1966; compare to pure albite at 12.38 cc/mol) and an approximate volume for the anhydrous melt of 13.8 cc/mol (the value experimentally determined by Arndt and Haberle, 1973), we can calculate the molar volume of water in the melt. AT 3 wt % total dissolved water corresponds to roughly 31 mole % water in the melt. A partial molar volume of water of 4.26 cc/mol accounts for the observed decrease in the total volume per oxygen in the melt from 13.8 cc/mol (with 0 % H_2O) to 12.4 cc/mol (at 3 wt % H_2O). To conclude, available experimental phase equilibria data support the contention that the addition of water to a melt lowers the total molar volume per oxygen of that melt.

This conclusion is consistent with a host of data available on hydrous glasses. McMillan and Chlebik (1980) have measured the density of hydrous sodium silicate glasses. They observed an increase in density with water dissolution suggesting a very low (and possibly negative) partial molar volume of water (water as hydroxyl). Their results on the density of low water content glasses is consistent with the suggestion of Boulos and Kreidl (1972) that hydroxyl dissolution results in the collapse of the silicate framework of the glass. Thus, there exists good evidence for a low partial molar volume of hydroxyl in silicate melts. Silver et al. (1990; see Appendix 2) have measured the density of hydrous rhyolitic glasses and determined a decrease in the molar volume of oxygens in the melt from 13.8 cc/mol (< 0.5 wt % water) to 13.5 cc/mol (> 8.5 wt % water). These water-rich glasses have a significant proportion of molecular water (up to

75% of the total dissolved water). Thus, the partial molar volume of molecular water is also smaller than the molar volume of the anhydrous silicate glass. A positive partial molar volume of water in rhyolitic **glass** ($\overline{V}^{glass}_{H_2O,\,tot} = 12.0$), must be reconciled with my experimental results for the partial molar volume of water in **melt** of ($\overline{V}^{melt}_{H_2O,\,tot} = 0$). Nevertheless, both studies indicate a decrease in the partial molar volume of the total melt with the dissolution of water.

This conclusion is strikingly different from the results of Burnham and Davis (1974) and Silver et al. (1990; Appendix 2) on hydrous melts of similar composition. The results of Burnham and Davis suggest a partial molar volume of water ≈ 15 cc/mol for albite melt at 8.3 kbar and ≈ 17 cc/mol at 10.2 kbar at 1100°C. Hodges (1974) also observed a high (≈ 16.5 cc/mol) partial molar volume for water in diopside melt at 20 kbar. Figures 15, 16b, and 17b of Appendix 2 demonstrate that the best-fit partial molar volumes of water in orthoclasic, albitic, and Ca-Al silicate melts are also greater than the partial molar volumes of their anhydrous components. A more careful inspection of these results reveals distinct linear trends of $\overline{V}^{melt}_{H_2O,\,tot}$ vs. f_{H_2O} at pressures below 2 kbar. Perhaps a change in the influence of water on dissolution in the melt occurs at high water contents. Water may initially be incorporated into the structure of the melt by filling holes. At around 2 kbars (and/or at 6 wt. % total water, the limit of my experiments), these holes are all occupied, and additional incorporation of water molecules must be accompanied with expansion of the melt volume. An alternative explanation may be found in considering the compressibility of the melt; increasing pressure may squeeze the "holes" into which the water molecules reside such that their occupation influences the total melt volume. The onset of this new "mechanism" of water dissolution may change the solubility relations at high pressures and hold importance in modelling the behavior of very water-rich magmas, but such magmas are rare in problems of crustal evolution.

Conclusions

The solubility of water in rhyolitic melt has been determined as a function of pressure at 850°C using the most accurate methods available. The water content of glasses has been determined using both extraction manometry and infrared spectroscopy to provide the most complete description of the partitioning of water molecules in the rhyolitic melt-aqueous vapor system. These data show a regular increase in the solubility of water with increasing pressure, and can be used to model the degassing histories of evolving silica-rich magmas. Preliminary results on the temperature dependence of solubility suggest that supersaturation of silicic chambers upon intrusion of hotter mafic magmas is a viable mechanism for the triggering of violent eruptions.

Knowledge of the speciation of water within these liquids has led to the determination of the partial molar volume of water at pressures < 1600 bars. My results suggest that the dissolution of water has no influence on the total volume of the melt (the partial molar volume of water is near zero). This result is consistent with other studies on rhyolitic glasses and using phase equilibria in the granite-water system to 8 kbars, but inconsistent with numerous studies of water solubility in other silicate melts at higher pressures.

	GB (1)	GB-A (2)	GB-B (2)
SiO2	77.61	77.7	77.3
TiO2	0.06	0.1	0.06
Al2O3	12.92	12.97	12.97
FeO	0.36	0.71	0.75
MnO	0.03	0.03	0.03
MgO	0.04	0.05	0.05
CaO	0.52	0.53	0.52
Na2O	4.18	4.06	4.11
K2O	4.17	4.18	4.16

Table 1.1 Glass Buttes rhyolite microprobe analyses
(1) analyses done at Caltech
(2) analyses done at Bayreuth, FRG

~Temperature	(Variac Setting)		Duration
110°C	(11)	for	10 minutes
150°C	(13)	for	20 minutes
200°C	(15)	for	10 hours
350°C	(17)	for	12 hours
500°C	(20)	for	1 hour
650°C	(25)	for	30 minutes
800°C	(30)	for	5 hours
850°C	(33)	for	3 hours
900°C	(35)	for	1-5 hours
1000°C	(40)	for	30 minutes
1100°C	(45)	for	30 minutes
1200°C	(51)	for	2 1/2 hours
Total			36 - 40 hours

Table 1.2: Bakeout procedure for water-rich silicate glasses used to prevent formation of bubbles at high temperatures on extraction line.

Sample	min lowT	H2O low T	CO2 low T	min mid T	H2O mid T	min high T	H2O high T	CO2 high T	min total	umoles total H2O	umoles total CO2	%H2O	∂D	preheat time	HF treatment?
Blank-1				51	0.11	215	2.93		266	3.04	NSOA	NA	NA	121 min	HF soaking
Blank-2	54	2.43	0.30	95	1.05	326	8.12	*0.3	475	11.60	*0.6	95.08	NA	76 min	HF soaking
Blank-3	68	1.15	0.10	117	0.80	291	5.46	*1.0	476	7.41	*1.1	87.07	NA	79 min	HF soaking
Blank-4	63	0.33				373	2.74		436	3.07	NA	NA	NA	123 min	no HF soaking
Blank-5									438	7.10	NSOA	NA	NA	70 min	HF soaking
Blank-6									655	4.49	NSOA	NA	-130.0	195 min	no HF soaking
Blank-7									2931	6.58	3.06	68.26	-120.0	ads+time	no HF soaking
Blank-8	152	1.13	0.25			326	2.97	1.70	277	4.10	1.95	67.77	-111.0	pure ads	no HF soaking
Blank-9									1969	8.50	1.94	81.42	-117.2	ads+time	no HF soaking
Blank-10	open to air after Bl-9								48	4.68	1.07	81.39	NA	pure ads	no HF soaking
D-Blank	90	0.70				726	7.10		816	7.80					HF soaking
D-Blank	90	1.60				372	6.50		462	8.10					HF soaking
D-Blank	90	0.80				378	4.50		468	5.30					HF soaking

Table 1.3: Blank extractions for platinum crucibles both soaked and not soaked in hot HF acid (see text).
na = CO2 separated from water yield but not measured; NSOA = CO2 not separated from water yield
* = CO2 yield determined by calibrated deflection of gauge
D-Blank; results from Dobson et al., 1989

Sample	Extrct wt (mgrams)	µmoles H2O obs LT	µmoles CO2 obs LT	µmoles H2O obs HT	µmoles CO2 obs HT
blank - 8	0	1.13	0.25	2.97	1.7
diopside					
PMR.53.500	500	3.1	0.15	10.44	1.88
PMR.53.1000	1000	4.02	*.4	18.03	2.92
PMR.53.200	200	1.38	0.26	5.43	1.67
orthopyroxene					
KBH-1.1300	1300	4.12	0.54	16.38	2.9
KBH-1.650	650	3	0.39	9.76	2.05
KBH-1.200	200	1.64	0.3	5.06	1.55
garnet					
MON-9.1000	1000	4.48	0.44	6.95	2.66
MON-9.3000	3000	4.3	0.54	12.16	4.29

Table 1.4 Water extraction from nominally anhydrous mantle minerals: Diopside megacryst from the Premier kimberlite, RSA; garnet megacryst from Monastery kimberlite, RSA; orthopyroxenes from Kilbourne Hole, NM

Sample	Temp	Pressure	time	umoles vapor	umoles wt loss	umoles H2O, total	umoles CO2	minutes Hi Temp	blank assignment	notes	umoles extracted	mgrams extracted	mgrams remaining	Extrctd smp wt	Wt % H2O
GB3-7	850	202	84	113.50	139.88	80.38	8.50	479	22.54	HF	57.84	1.042	0.023	93.732	1.14
GB3-8	850	409	84	141.55	147.70	129.91	11.7	312	29.29	HF	100.62	1.813	0.022	87.304	2.10
GB3-9	850	1206	84	164.92	171.52	207.10	2.90	252	8.13	HF	198.97	3.584	0.021	84.787	4.25
GB3-11	850	635	216	116.60	116.60	130.62	5.8	311	15.30	HF	115.32	2.077	0.018	71.135	2.95
GB3-12	850	1066	216	140.37	144.90	170.61	3.50	431	10.45	HF	160.16	2.885	0.018	71.027	4.09
GB3-13	850	1362	216	159.81	171.52	183.94	6.53	329	17.12	HF	166.82	3.005	0.016	65.186	4.64
GB3-18	850	501	117	135.66	146.00	114.70	7.30	376	19.18	HF	95.52	1.721	0.018	73.908	2.35
GB3-19	850	498	117	184.84	195.40	111.13	4.68	345	12.82	HF	98.31	1.771	0.020	79.478	2.25
GB3-20	850	795	117	127.46	132.67	176.96	5.25	295	13.92	HF	163.04	2.937	0.022	89.204	3.32
GB3-21	850	775	117	159.55	170.41	138.93	5.05	322	13.58	HF	125.35	2.258	0.018	70.018	3.25
GB3-25.1	850	500	312	138.60	169.30	107.80	4.20	435	12.13	HF	95.67	1.724	0.016	62.778	2.77
GB3-25.2	850	500	312	138.60	169.30	112.83	1.65	391	5.87	HF	106.96	1.927	0.015	61.892	3.14
GB3-26.2	850	498	243	154.93	158.20	95.52	1.45	385	5.36	HF	90.16	1.624	0.014	55.274	2.96
GB3-43.1	850	546	185	155.86	160.98	73.12	2.24	420	7.41	HF	65.71	1.184	0.018	45.690	2.63
GB3-43.2	850	546	185	155.86	160.98	99.02	1.95	467	6.96	HF	92.06	1.659	0.024	59.701	2.82
GB3-44.1	850	518	185	163.13	162.64	104.76	8.50	513	22.71	HF Ar	82.05	1.478	0.012	46.877	3.18
GB3-44.2	850	518	185	163.13	162.64	84.36	4.23	417	12.11	HF Ar	72.25	1.302	0.012	44.391	2.96
GB3-45	850	486	185	161.47	163.20	146.14	NSOA	463	14.17	HF	131.98	2.378	0.008	83.396	2.86
GB4-52.1	850	1590	504	220.49	223.70	104.29	2.00	1486	4.74	no HF	99.55	1.793	0.008	32.026	5.62
GB4-52.2	850	1590	504	220.49	223.70	82.81	16.91	3360	40.08	other	42.73	0.770	0.003	13.520	5.72
GB4-64.1	850	501	234	122.29	128.23	102.65	15.79	1103	42.94	HF	59.71	1.849	0.012	49.870	3.73
GB4-64.2	850	501	234	122.29	128.23	81.38	2.63	940	10.93	HF	70.45	1.466	0.012	47.225	3.13
GB4-65.1	850	501	234	164.90	263.10	96.35	2.88	370	8.68	HF	87.67	1.736	0.014	54.036	3.24
GB4-65.2	850	501	234	164.90	263.10	71.71	3.60	351	10.29	HF	61.42	1.292	0.010	40.790	3.19
GB4-71.1	850	1204	345	272.88	284.76	114.55	NSOA	1024	11.85	other	102.70	1.850	0.010	41.006	4.54
GB4-71.2	850	1204	345	272.88	284.76	94.47	5.26	1509	12.47	no HF	82.00	1.477	0.008	32.934	4.51
GB4-73.1	850	1410	597	4.70	na	138.73	2.66	2543	6.30	no HF	132.43	2.386	0.012	46.172	5.19
GB4-73.2	850	1410	597	4.70	na	143.56	3.89	1656	9.22	no HF	134.34	2.420	0.012	49.076	4.96
GB4-74.1	850	806	596	136.63	145.99	100.63	5.75	2802	13.63	no HF	87.00	1.567	0.011	45.343	3.48
GB4-74.2	850	806	596	136.63	145.99	131.46	3.00	1945	7.11	no HF	124.35	2.240	0.015	60.253	3.74
GB4-75.1	850	1207	596	120.32	121.9	144.24	13.21	1287	31.31	no HF	112.93	2.034	0.013	51.923	3.94
GB4-75.2	850	1207	596	120.32	121.9	168.24	7.60	2981	18.01	no HF	150.23	2.706	0.015	60.701	4.48
GB4-76.1	850	1002	596	148.00	151.54	128.58	9.20		21.80	no HF	106.78	1.924	0.013	51.221	3.78
GB4-76.2	850	1002	596	148.00	151.54	122.76	10.34		24.51	no HF	98.25	1.770	0.012	47.225	3.77
GB4-68.1	750	1669	453	185.90	195.00	192.43	10.11		20.70	CO2	171.73	3.094	0.013	51.168	6.07
GB4-68.2	750	1669	453	185.90	195.00	148.26	2.60		7.09	CO2	141.17	2.543	0.011	42.007	6.08

Table 1.5: Experiments on the solubility of water in granitic melt; results from manometry
na = CO2 separated from water yield but not measured; NSOA = CO2 not separated from water yield
HF = crucible cleaned by soaking in hot HF acid; CO2 yield determined by calibrated deflection of gauge
no HF = crucible cleaned by hand-picking; CO2 yield determined by manometry
other = sample opened to air during extraction to check for melting; Ar = argon pressure medium

Sample	IR wt % center	IRwt% edge		anhydrs smp wt	umoles man smpl	rcvrd man systm	loaded system	umoles IR smpl	rcvrd IR systm	rcvrd wtl man systm	rcvrd wtl IR systm	µmole yield rcvrd	µmole yield IR
GB3-7	1.01	1.25	*	114.96	73.37	186.87	206.49	65.27	178.77	213.25	205.15	6.76	-1.34
GB3-8	2.31		*	109.00	129.87	271.42	291.00	143.03	284.58	277.57	290.73	-13.43	-0.27
GB3-9	4.46		*	101.10	249.25	414.17	425.38	261.75	426.67	420.77	433.27	-4.61	7.89
GB3-11	2.97			91.55	154.23	270.83	273.60	155.49	272.09	270.83	272.09	-2.77	-1.51
GB3-12	3.94		*	79.51	188.08	328.45	330.90	181.20	321.57	332.98	326.10	2.08	-4.80
GB3-13	4.90	4.58	*	69.22	186.76	346.57	353.95	197.76	357.57	358.28	369.28	4.33	15.33
GB3-18	2.35	2.44	*	95.48	127.73	263.39	284.19	127.79	263.45	273.73	273.79	-10.46	-10.40
GB3-19	2.40	2.38	*	103.59	132.56	317.40	329.12	141.68	326.52	327.96	337.08	-1.16	7.96
GB3-20	3.45	3.45	*	100.12	190.71	318.17	327.56	198.51	325.97	323.38	331.18	-4.18	3.62
GB3-21	3.43		*	84.86	158.24	317.79	328.29	167.14	326.69	328.65	337.55	0.36	9.26
GB3-25.1	2.83	2.78	* *	145.81	230.62	369.22	471.32	235.59	374.19	399.92	404.89	-71.40	-66.43
GB3-25.2	2.83	2.78	* *	145.81	262.25	400.85	471.32	235.59	374.19	431.55	404.89	-39.77	-66.43
GB3-26.2	2.78		* *	135.70	230.04	384.97	391.70	215.18	370.11	388.24	373.38	-3.46	-18.32
GB3-43.1	2.27	2.42	*	129.61	194.40	350.26	365.35	167.11	322.97	355.38	328.09	-9.97	-37.26
GB3-43.2	2.34	2.49	*	129.61	208.63	364.49	365.35	172.14	328.00	369.61	333.12	4.26	-32.23
GB3-44.1	2.95			130.26	237.47	400.60	383.75	219.73	382.86	400.11	382.37	16.36	-1.38
GB3-44.2	2.95		*	130.26	220.45	383.58	383.75	219.73	382.86	383.09	382.37	-0.66	-1.38
GB3-45	2.64	2.51		132.10	215.97	377.44	366.24	198.80	360.27	379.17	362.00	12.93	-4.24
GB4-52.1	5.15	5.16	*	114.29	378.11	598.60	565.92	344.56	565.05	601.81	568.26	35.89	2.34
GB4-52.2	5.15	5.16	*	114.29	384.84	605.33	565.92	344.56	565.05	608.54	568.26	42.62	2.34
GB4-64.1	2.74			117.75	253.47	375.76	316.03	184.04	306.33	381.70	312.27	65.67	-3.76
GB4-64.2	2.74			117.75	211.15	333.44	316.03	184.04	306.33	339.38	312.27	23.35	-3.76
GB4-65.1	2.79			120.07	222.98	387.88	367.40	191.01	355.91	486.08	454.11	118.68	86.71
GB4-65.2	2.79			120.07	219.77	384.67	367.40	191.01	355.91	482.87	454.11	115.47	86.71
GB4-71.1	4.48			123.34	325.38	598.26	463.88	320.81	593.69	610.14	605.57	146.26	141.69
GB4-71.2	4.48		*	123.34	323.41	596.29	463.88	320.81	593.69	608.17	605.57	144.29	141.69
GB4-73.1	5.11	5.09	*	121.75	370.10	na	495.86	363.73	368.43				
GB4-73.2	5.11	5.09	*	121.75	352.44	na	495.86	363.73	368.43				
GB4-74.1				116.97	234.22	370.85	386.98			380.21	145.99	-6.77	-240.99
GB4-74.2				116.97	252.48	389.11	386.98			398.47	145.99	11.49	-240.99
GB4-75.1				129	293.96	414.28	466.87			415.86	121.90	-51.01	-344.97
GB4-75.2				129	336.12	456.44	466.87			458.02	121.90	-8.85	-344.97
GB4-76.1	4.24	4.27	*	120.84	263.54	411.54	421.36	297.30	445.30	415.08	448.84	-6.28	27.48
GB4-76.2	4.24	4.27	*	120.84	263.02	411.02	421.36	297.30	445.30	414.56	448.84	-6.80	27.48
GB4-68.1	5.92	5.71	* *	119.73	429.59	615.49	628.81	418.16	604.06	624.59	613.16	-4.22	-15.65
GB4-68.2	5.92	5.71	* *	119.73	430.19	616.09	628.81	418.16	604.06	625.19	613.16	-3.62	-15.65

Table 1.6: Experiments on the solubility of water in granitic melt: yield comparisons for IR and manometric techniques; rcvrd wtl = measurement of total yield based on weight loss determination for vapor
* = sample used in regression for new epsilon calibration; ** = run product contained bubbles

Sample	Pressure	density	H2O,mol-abs	OH-abs	thickness	H2O,mol-wt%	OH	H2O,tot	X(B)	X(H2O)	X(OH)	X(O)	ln(Ks)	
GB3-7c	202	2341	0.0171	0.0724	4.04E-04	0.2157	0.7968	1.0125	0.0181	0.0039	0.0285	0.9676	-1.5250	
GB3-8	409	2324	0.0813	0.1197	4.13E-04	1.0106	1.2987	2.3094	0.0409	0.0179	0.0460	0.9361	-2.0693	
GB3-9	1206	2296	0.1347	0.0953	2.54E-04	2.7548	1.7015	4.4563	0.0776	0.0480	0.0593	0.8928	-2.5012	
GB3-12	1066	2303	0.0677	0.0567	1.54E-04	2.2786	1.6650	3.9436	0.0689	0.0398	0.0582	0.9020	-2.3611	
GB3-13	1362	2291	0.1270	0.0806	2.10E-04	3.1493	1.7457	4.8950	0.0849	0.0546	0.0606	0.8848	-2.5782	
GB3-18	501	2323	0.0426	0.0573	2.02E-04	1.0837	1.2705	2.3543	0.0417	0.0192	0.0450	0.9358	-2.1831	
GB3-19	498	2323	0.0732	0.1022	3.47E-04	1.0836	1.3210	2.4046	0.0425	0.0192	0.0467	0.9341	-2.1036	
GB3-20a c	795	2309	0.0983	0.0946	2.71E-04	1.8737	1.5749	3.4486	0.0605	0.0329	0.0553	0.9118	-2.2838	
GB3-20a e	795	2309	0.0988	0.0924	2.69E-04	1.8984	1.5490	3.4475	0.0605	0.0333	0.0544	0.9123	-2.3305	
GB3-20b c	795	2307	0.1014	0.0938	2.62E-04	2.0007	1.6160	3.6168	0.0634	0.0351	0.0566	0.9083	-2.2951	
GB3-20b e	795	2308	0.0983	0.0916	2.61E-04	1.9464	1.5827	3.5291	0.0619	0.0341	0.0555	0.9103	-2.3109	
GB3-21 e	775	2309	0.1221	0.1185	3.40E-04	1.8552	1.5716	3.4268	0.0601	0.0326	0.0552	0.9123	-2.2784	
GB4-43 c	546	2323	0.0915	0.1251	4.41E-04	1.0654	1.2713	2.3367	0.0414	0.0189	0.0450	0.9361	-2.1649	
GB4-43 e	546	2321	0.0950	0.1318	4.33E-04	1.1280	1.3658	2.4938	0.0441	0.0199	0.0483	0.9318	-2.0753	
GB4-45 c	486	2320	0.0585	0.0794	2.49E-04	1.2084	1.4312	2.6396	0.0466	0.0213	0.0506	0.9281	-2.0478	
GB4-45 e	486	2321	0.0534	0.0786	2.50E-04	1.0978	1.4104	2.5082	0.0443	0.0194	0.0499	0.9307	-1.9829	
GB3-25.c	500	2317	0.11488	0.12768	4.12E-04	1.4357	1.3927	2.8284	0.0499	0.0253	0.0491	0.9256	-2.2734	bubbles
GB3-25.e	500	2318	0.11232	0.12224	4.05E-04	1.4276	1.3561	2.7837	0.0491	0.0252	0.0478	0.9270	-2.3222	bubbles
GB3-26.c	498	2318	0.10912	0.13152	4.15E-04	1.3535	1.4238	2.7773	0.0490	0.0239	0.0502	0.9259	-2.1702	bubbles
GB3-44.c	518	2316	0.10764	0.10621	3.50E-04	1.5846	1.3647	2.9493	0.0520	0.0279	0.0481	0.9240	-2.4120	
GB4-52.c	1590	2287	0.5286	0.3132	8.12E-04	3.3954	1.7560	5.1513	0.0892	0.0588	0.0608	0.8804	-2.6387	
GB4-52.e	1590	2287	0.5304	0.3168	8.16E-04	3.3904	1.7675	5.1579	0.0893	0.0587	0.0612	0.8801	-2.6238	
GB4-64.c	501	2318	0.13902	0.17178	5.43E-04	1.3176	1.4210	2.7386	0.0483	0.0233	0.0502	0.9266	-2.1477	
GB4-65.c	501	2318	0.11448	0.13734	4.33E-04	1.3610	1.4251	2.7861	0.0491	0.0240	0.0503	0.9257	-2.1738	
GB4-71.c	1204	2296	0.2288	0.15236	4.20E-04	2.8308	1.6453	4.4761	0.0779	0.0493	0.0573	0.8934	-2.5965	
GB4-73.c	1410	2288	0.2484	0.14742	3.85E-04	3.3644	1.7428	5.1071	0.0885	0.0583	0.0604	0.8813	-2.6453	
GB4-73.e	1410	2288	0.24592	0.14848	3.85E-04	3.3304	1.7551	5.0855	0.0881	0.0577	0.0608	0.8815	-2.6211	
GB4-76.c	1002	2299	0.20352	0.15192	4.11E-04	2.5698	1.6743	4.2441	0.0740	0.0448	0.0584	0.8968	-2.4667	
GB4-76.e	1002	2299	0.20654	0.15226	4.13E-04	2.5956	1.6701	4.2658	0.0744	0.0453	0.0582	0.8965	-2.4816	
GB4-68.c	750°C/1669	2278	0.4032	0.2178	5.25E-04	4.0227	1.8966	5.9193	0.1019	0.0693	0.0653	0.8654	-2.6429	bubbles
GB4-68.e	750°C/1669	2280	0.3906	0.21465	5.30E-04	3.8557	1.8494	5.7051	0.0984	0.0665	0.0638	0.8697	-2.6542	bubbles
post-45	extraction	2350		0.0611	4.90E-04		0.0109	0.0109						8 hours

Table 1.7: Infrared spectroscopic measurements using best-fit epsilons as discussed in text;
(e5200 = 1.51 l/mol-cm; e4500 = 1.73 l/mol-cm; e3550 =88 l/mol-cm)
mole fractions of individual species determined as following;
X(B) = mole fraction of total dissolved water; (wt%H2O/18) / ((wt%H2O/18) + (100-wt%H2O)/32.49)
X(H2O) = mole fraction of molecular water; (wt%H2O,mol/18) / ((wt%H2O/18) + (100-wt%H2O)/32.49)
X(OH) = mole fraction of hydroxyl species; 2(X(B)-X(H2O,mol))
ln (Ks) = ln {X(OH)^2 / (X(O)*X(H2O))}

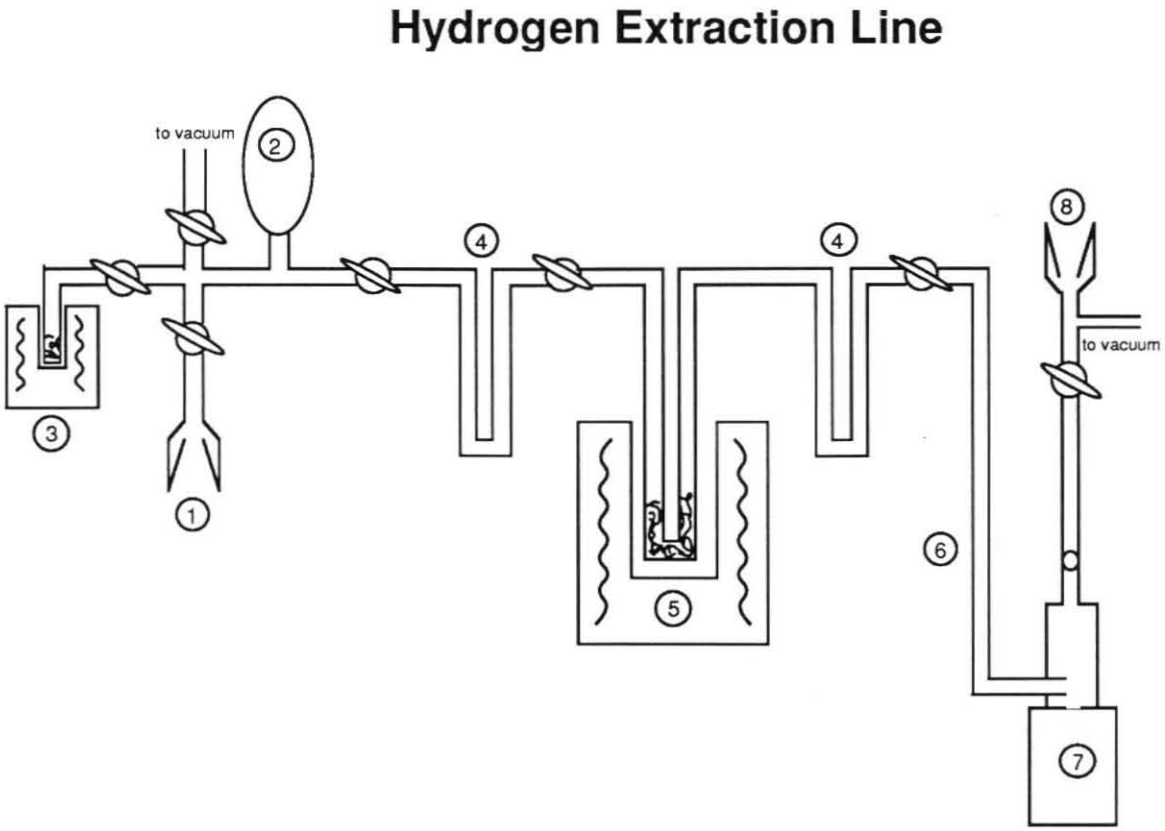

Figure 1.1: Schematic diagram of the vacuum extraction line; 1) input port for extraction vessel, capsule piercer, and septum, 2) vacuum gauge, 3) copper-oxide furnace, 4) cryogenic trap, 5) uranium furnace, 6) manometer, 7) Toepler pump, and 8) exit port.

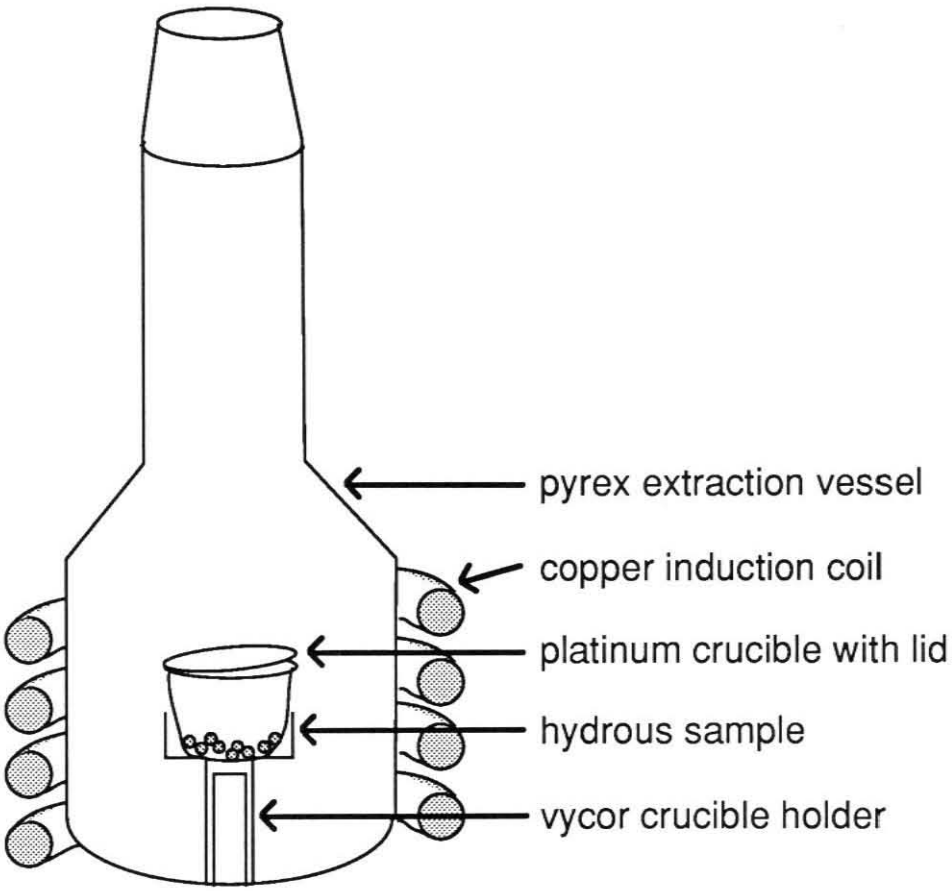

Figure 1.2: Extraction vessel in RF induction furnace

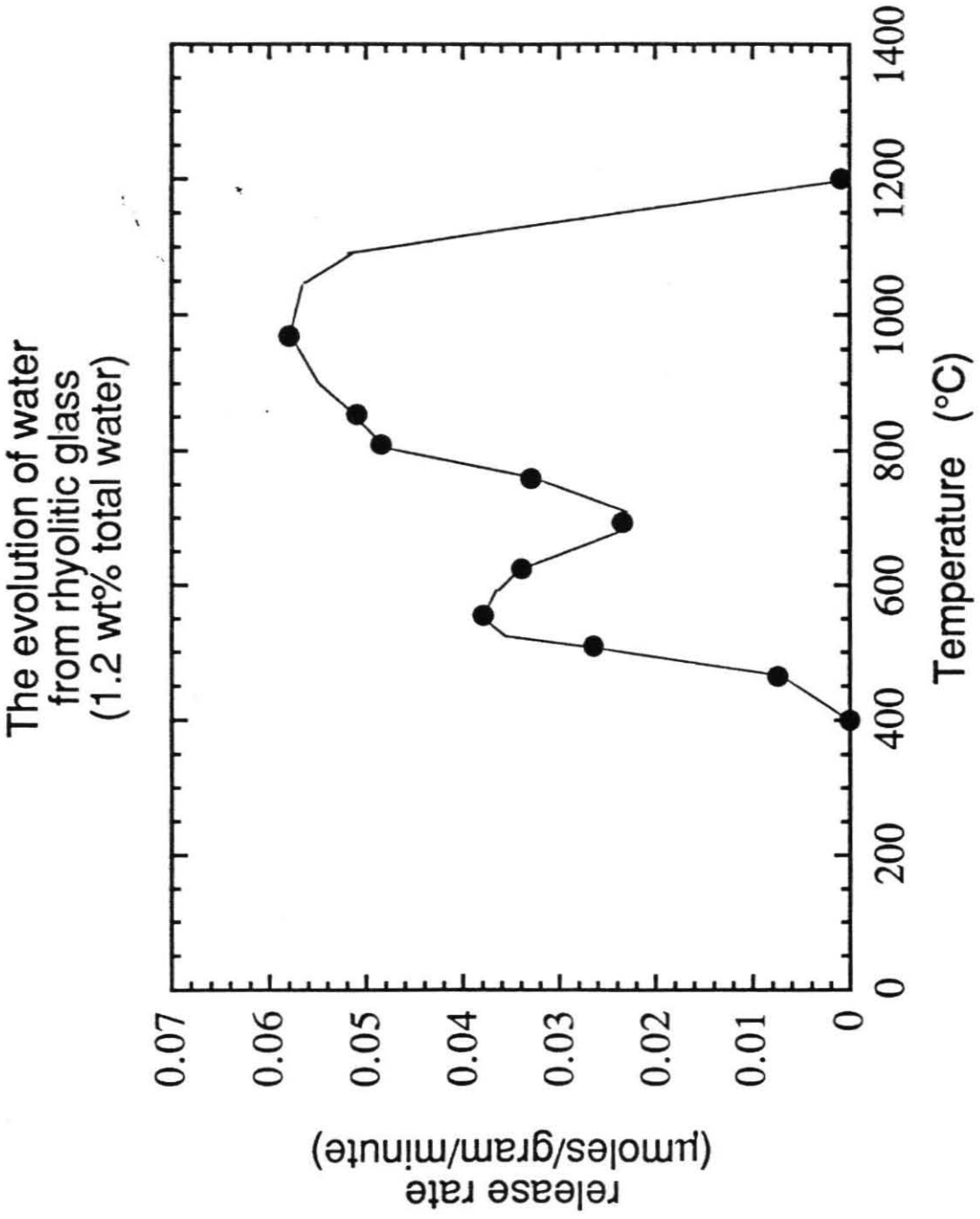

Figure 1.3: The release rate of water from a hydrous rhyolitic glass (1.2 wt % total dissolved water. The peak at ≈ 500°C represents the evolution of water molecules from the glass. The peak at ≈ 900°C represents the release of hydroxyl species (see text). Unpublished data courtesy of Dr. S. Newman.

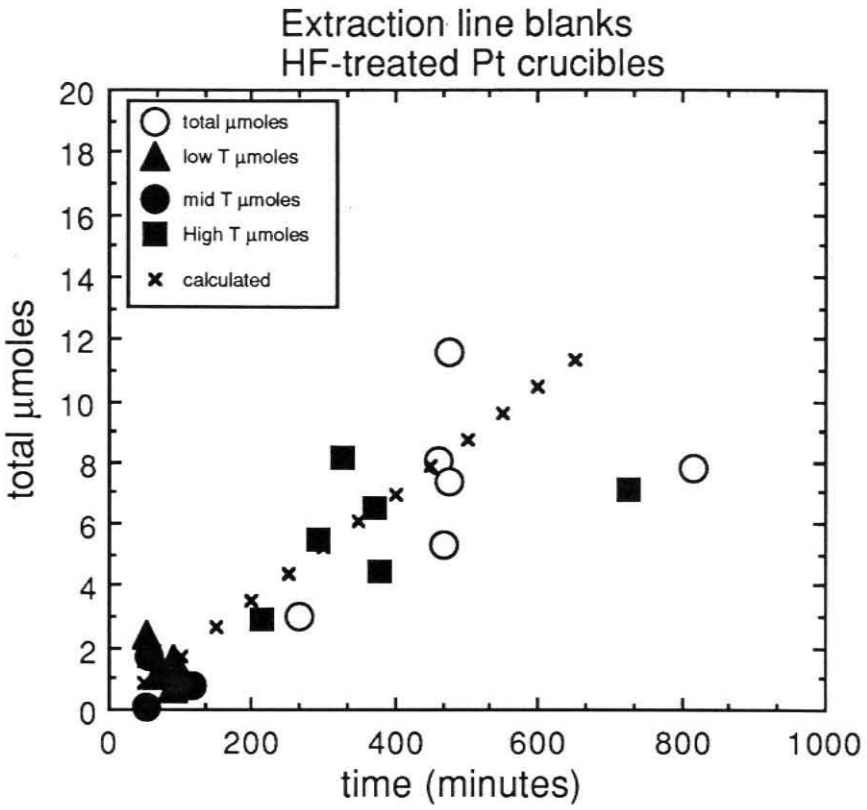

Figure 1.4: Manometric analyses of blank extractions for variable durations using platinum crucibles soaked in hot HF and pre-heated to 1200°C for 1-3 hours. Filled circles are low temperature (<250°C) blanks, filled triangles are mid-temperature (250°C<T<700°C) blanks, filled squares are high temperature (>700°C) blanks, and hollow circles are the total yields for six blank extractions. The Xs represent a constant release rate of 1µmole H_2/hr. Actual release rate will depend upon time of HF-soaking, time of pre-heating, rate of temperature increase, crucible size, and should theoretically level off with time.

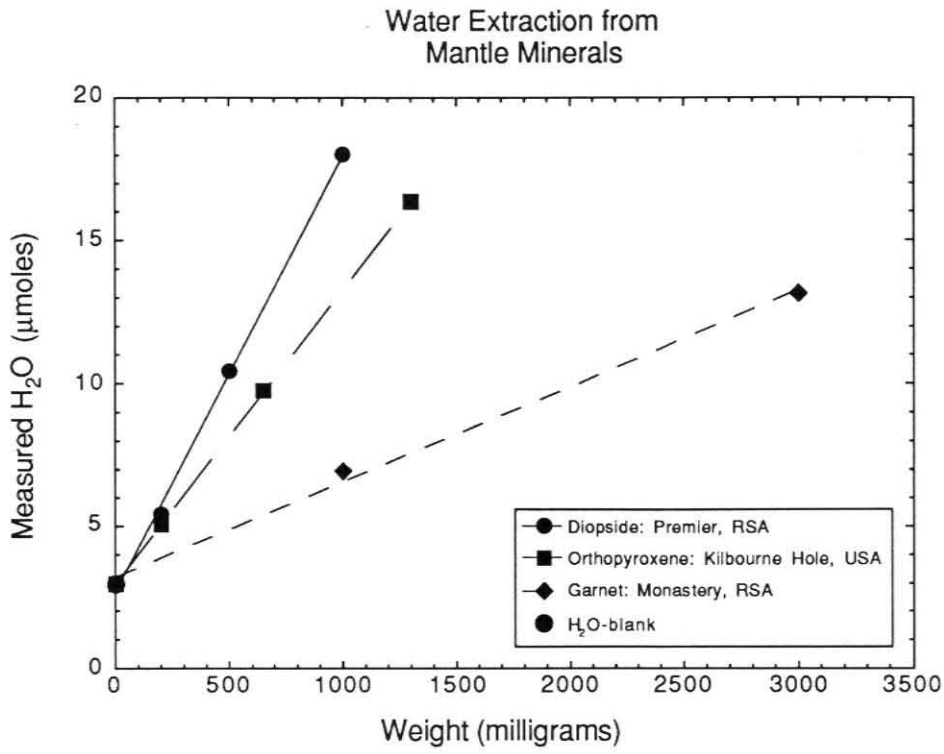

Figure 1.5: The quantity of water extracted from three different mantle minerals as a function of aliquot size. All extractions were performed at ≈ 800°C for 5 hours after removing all water evolved at ≈ 200°C for 1.5 hours. These results demonstrate the consistency of the high temperature blank.

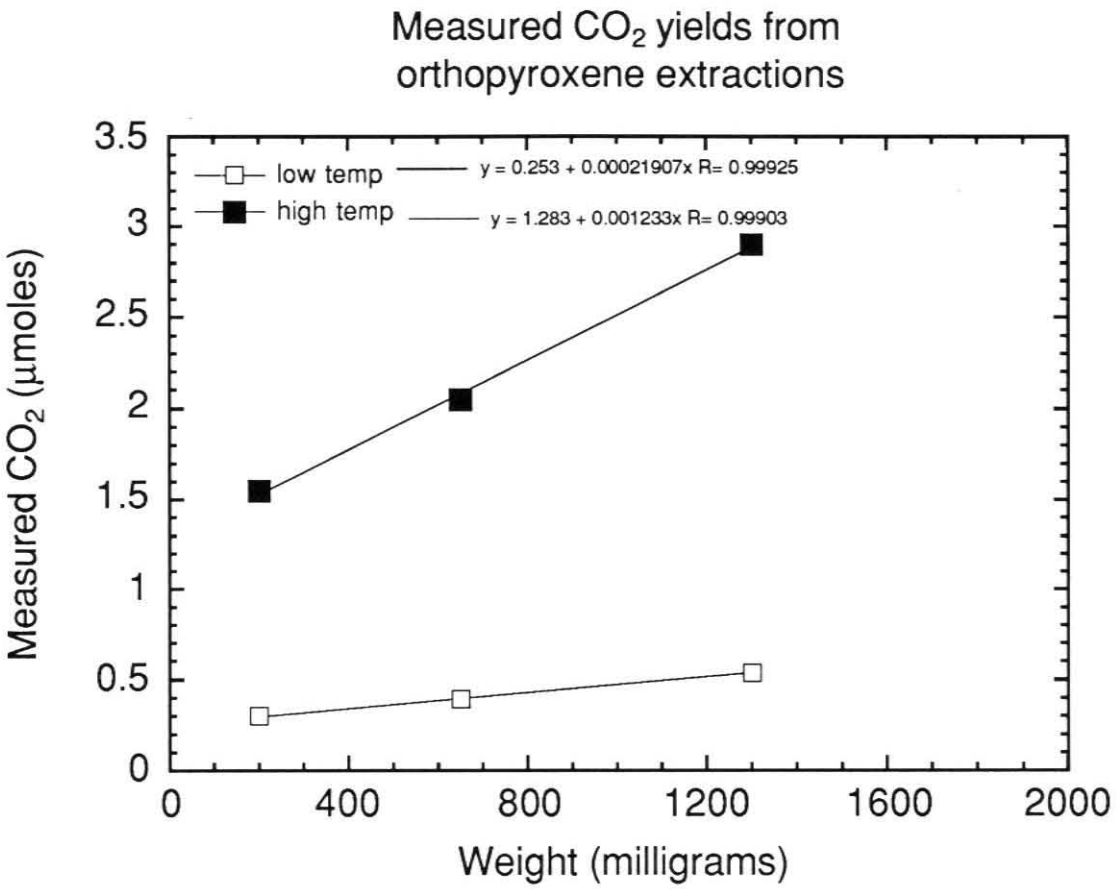

Figure 1.6: The measured amount of CO_2 released from a nominally CO_2-free orthopyroxene crystal as a function of mass of crystal extracted. The hollow squares represent CO_2 evolved at low temperatures. The solid squares represent the quantity of CO_2 evolved at high temperatures (>250°C) after removal of the low temperature fraction. The best-fit y-intercepts are shown in the least-squares regression analyses and demonstrate the reproducibility of the blank contribution of CO_2 at each temperature step.

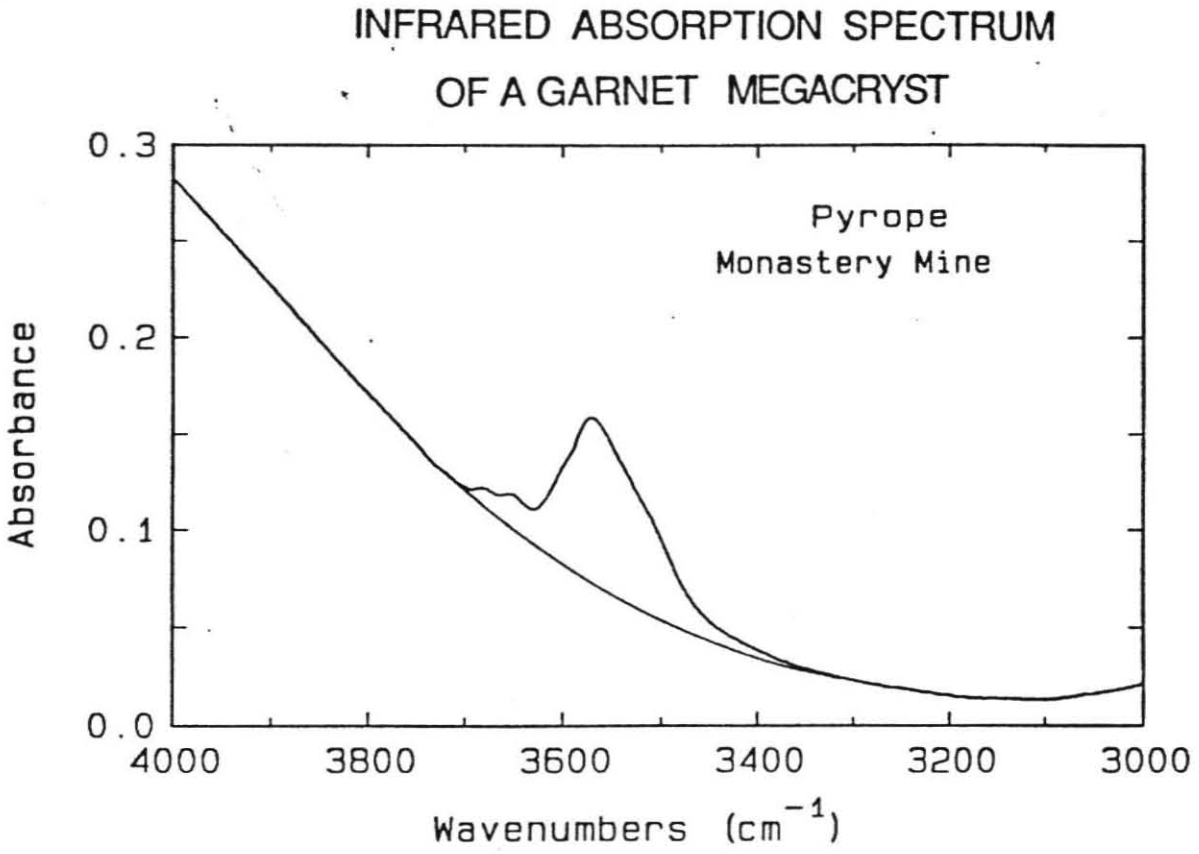

Figure 1.7: The infrared absorption spectrum of a garnet megacryst from the Monastery kimberlite pope, RSA. The peak at 3550 cm^{-1} is due to the fundamental O-H stretching indicating the presence of structurally-bound hydrogen in this nominally anhydrous mineral. Figure from David Bell, unpublished PhD thesis.

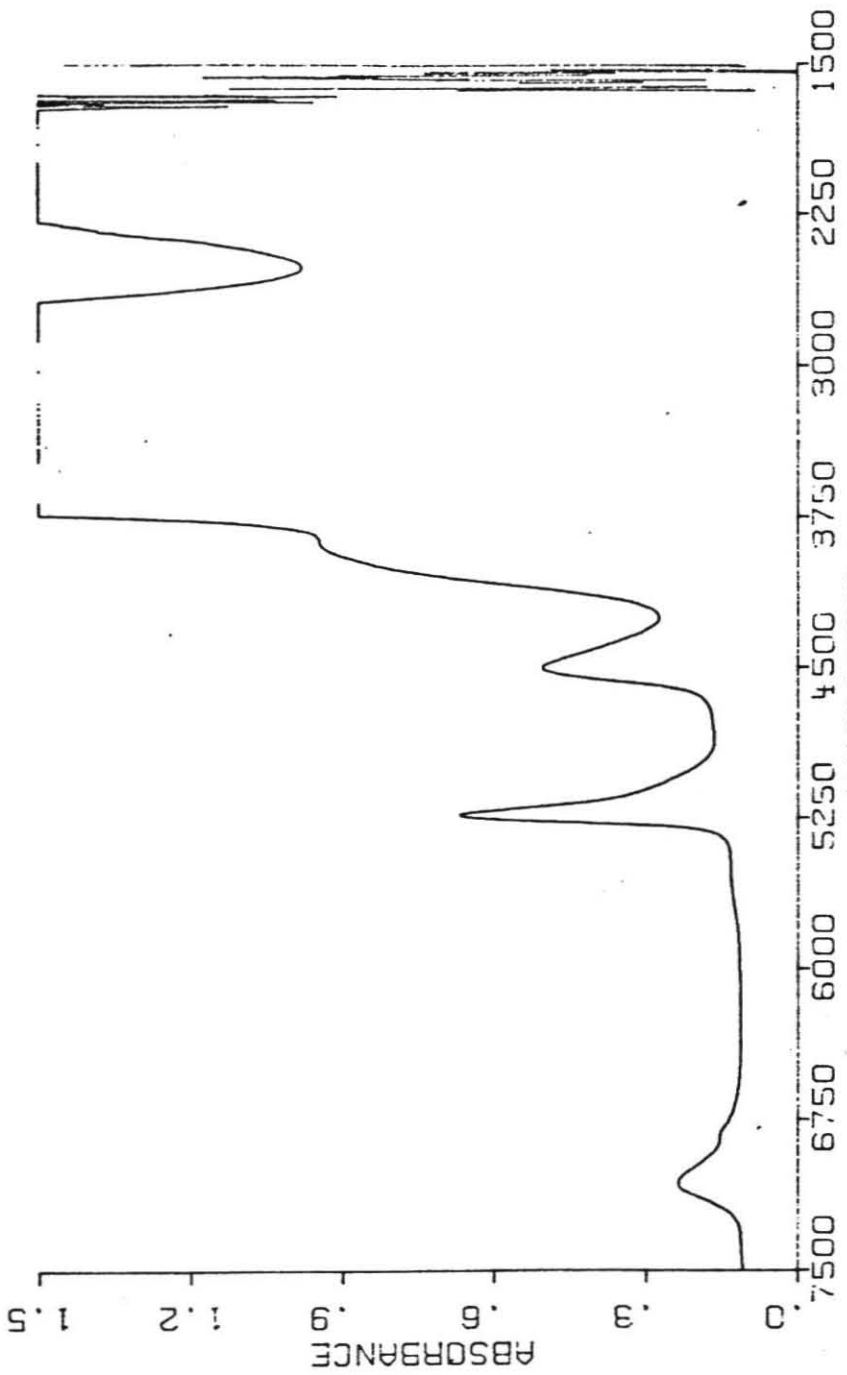

Figure 1.8: The infrared absorption spectrum of a hydrous rhyolitic glass, showing the prominent absorptions at 7100 cm^{-1}, 5200 cm^{-1}, 4500 cm^{-1}, and 3500 cm^{-1}. The peaks at 5200 cm^{-1} and 4500 cm^{-1} are proportional to the concentrations of molecular water and hydroxyl species, respectively. See discussion in the text.

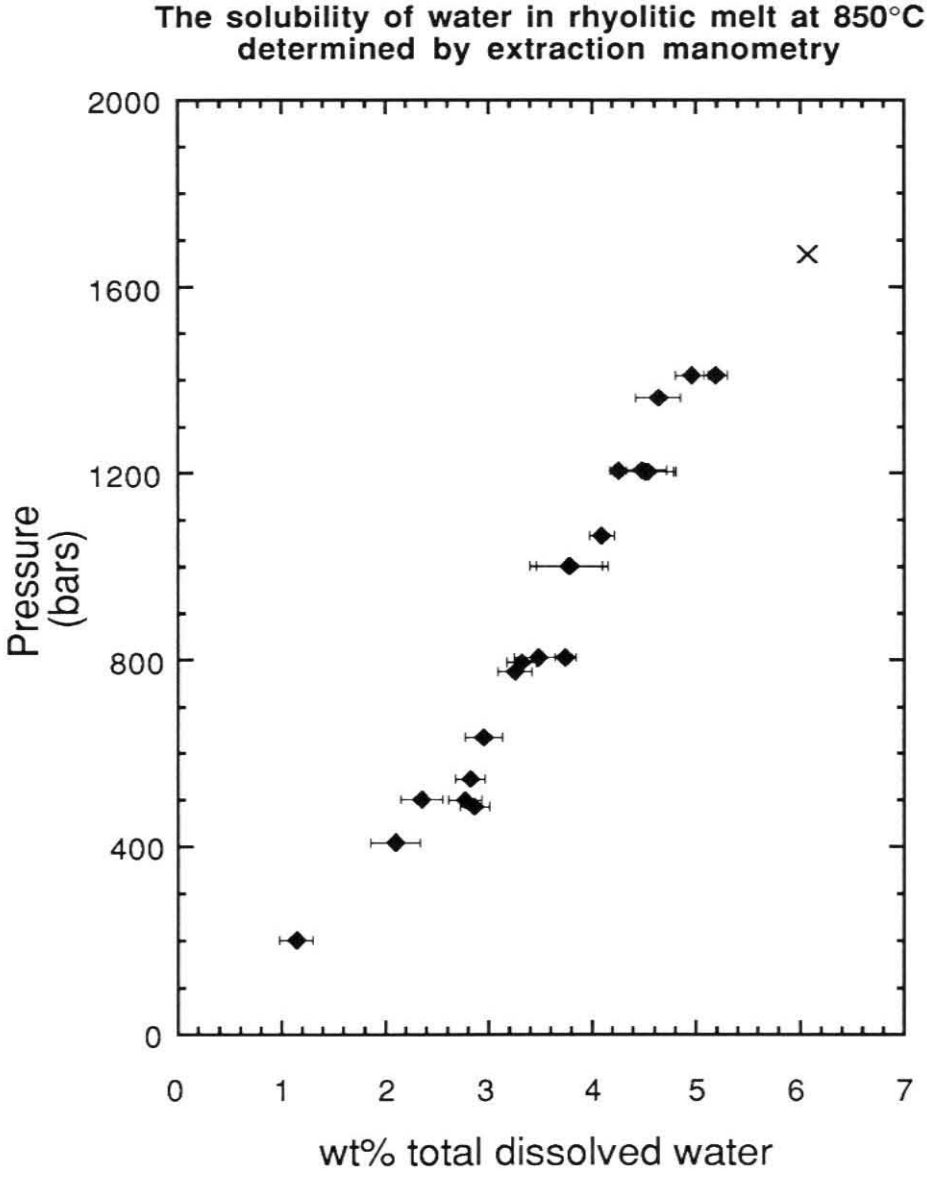

Figure 1.9: The solubility of water in rhyolitic melt as a function of pressure at 850°C as determined by extraction manometry on quenched glasses. Error bars are assigned based on the percentage of blank contributed to the total yield. The Xs represent two extractions on glasses quenched from 750°C.

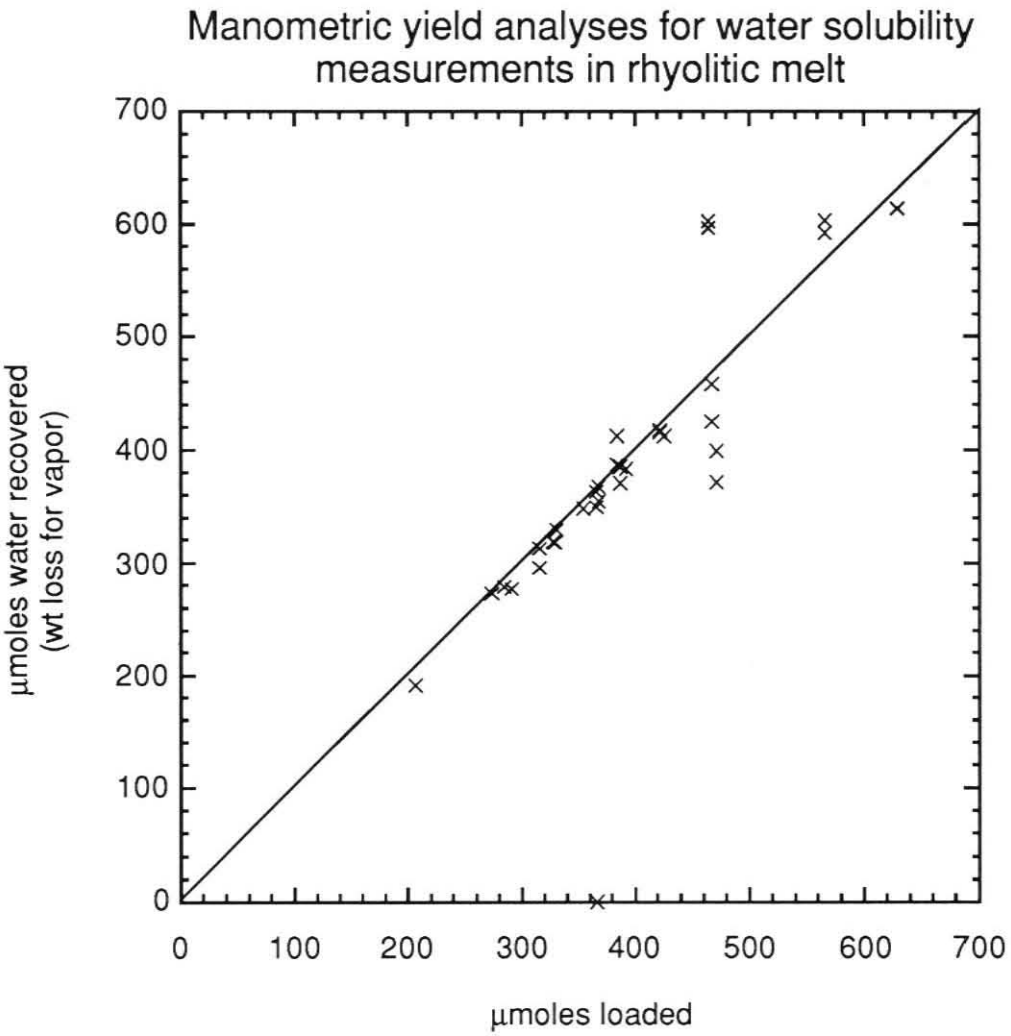

Figure 1.10: The quantity of water recovered in the extraction line (amount of water dissolved in rhyolitic glass chips + total amount of water in vapor) as a function of total water loaded into solubility experiments of Table 1.5 (blanks assigned by quantity of recovered CO_2 (see text). The 45° line represents a 1:1 correspondence, i.e., a perfect yield.

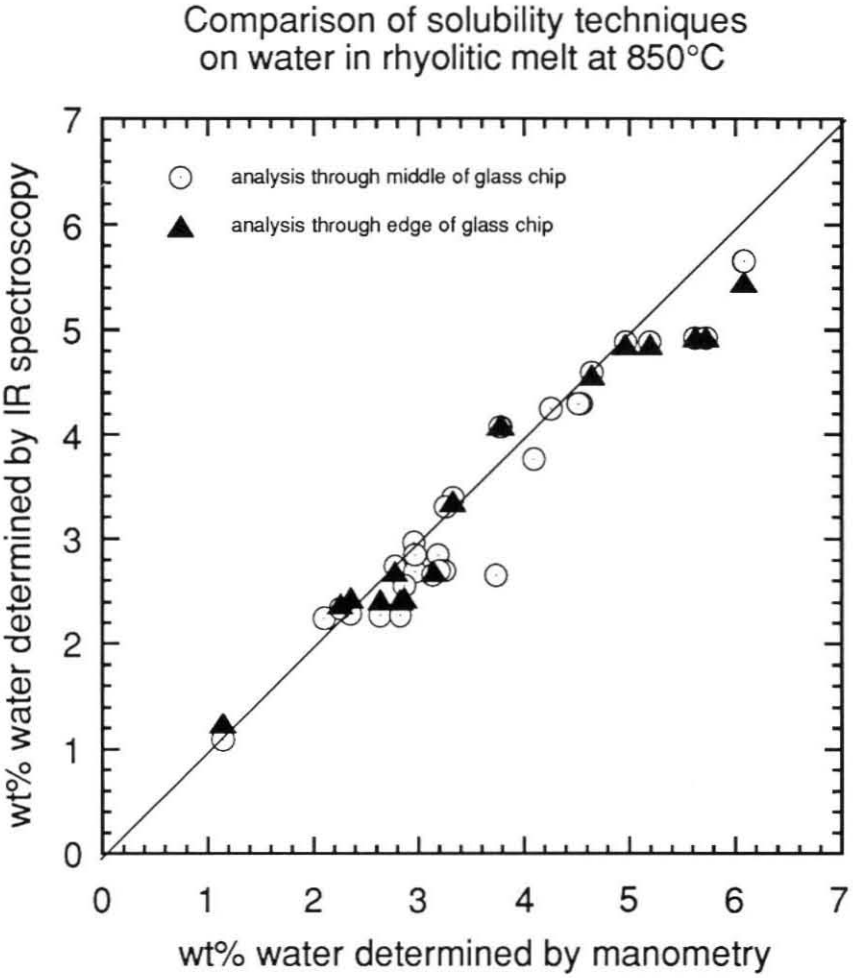

Figure 1.11: Comparison of the solubility determinations of water in rhyolitic melt at 850°C. The spectroscopic value is based upon previously published epsilons for the 5200 cm^{-1} (ε = 1.61 l/mol-cm) and 4500 cm^{-1} (ε = 1.73 l/mol-cm) determined on low water-content glasses (< 2.0 wt % ; Newman et al., 1986). The line represents a perfect correspondence between the two techniques. The comparison of the two techniques on these high water-content glasses suggests a re-calibration of the respective epsilons is needed. The hollow circles represent analyses through the middle of the glass wafers; the filled triangles are results through the edges of the wafers. Agreement is always within experimental error (the size of the symbols) and demonstrate homogeneity in the run products.

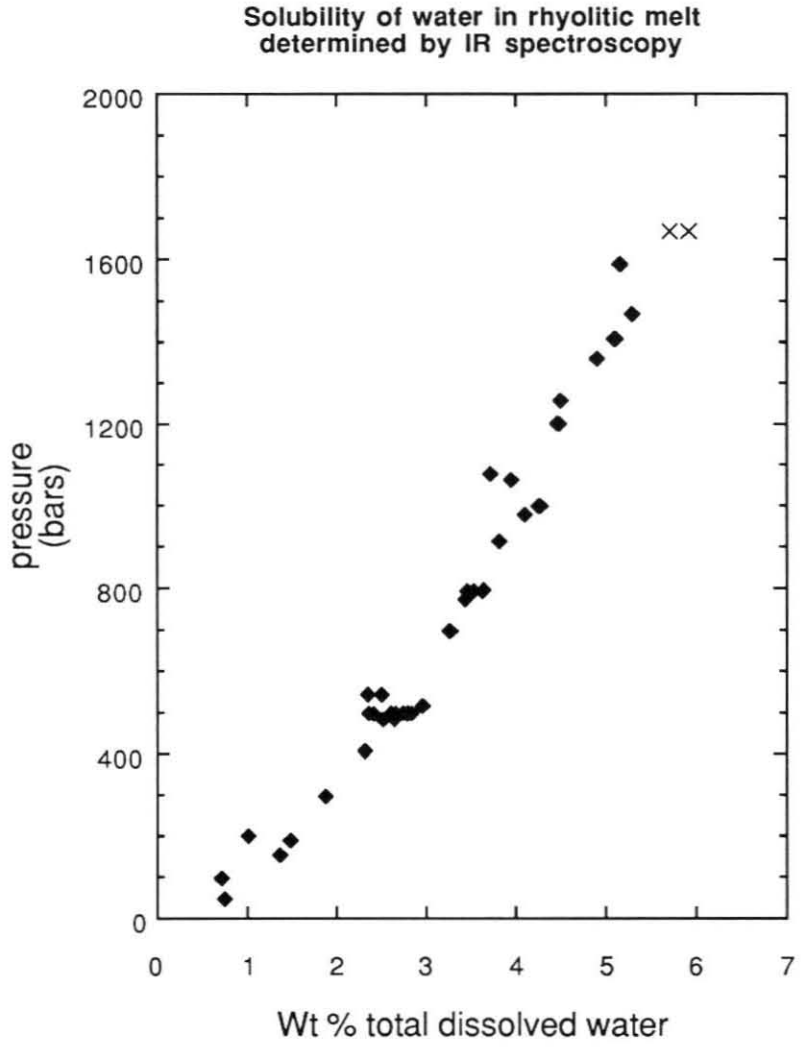

Figure 1.12: The solubility of water in rhyolitic melt as a function of pressure as determined by infrared spectroscopy on quenched glasses. Extinction coefficients used are calibrated in this study (ε_{5200} cm^{-1} = 1.51 l/mol-cm and ε_{4500} cm^{-1} = 1.73 l/mol-cm). The two Xs represent the results of extractions on glasses which were equilibrated at 750°C.

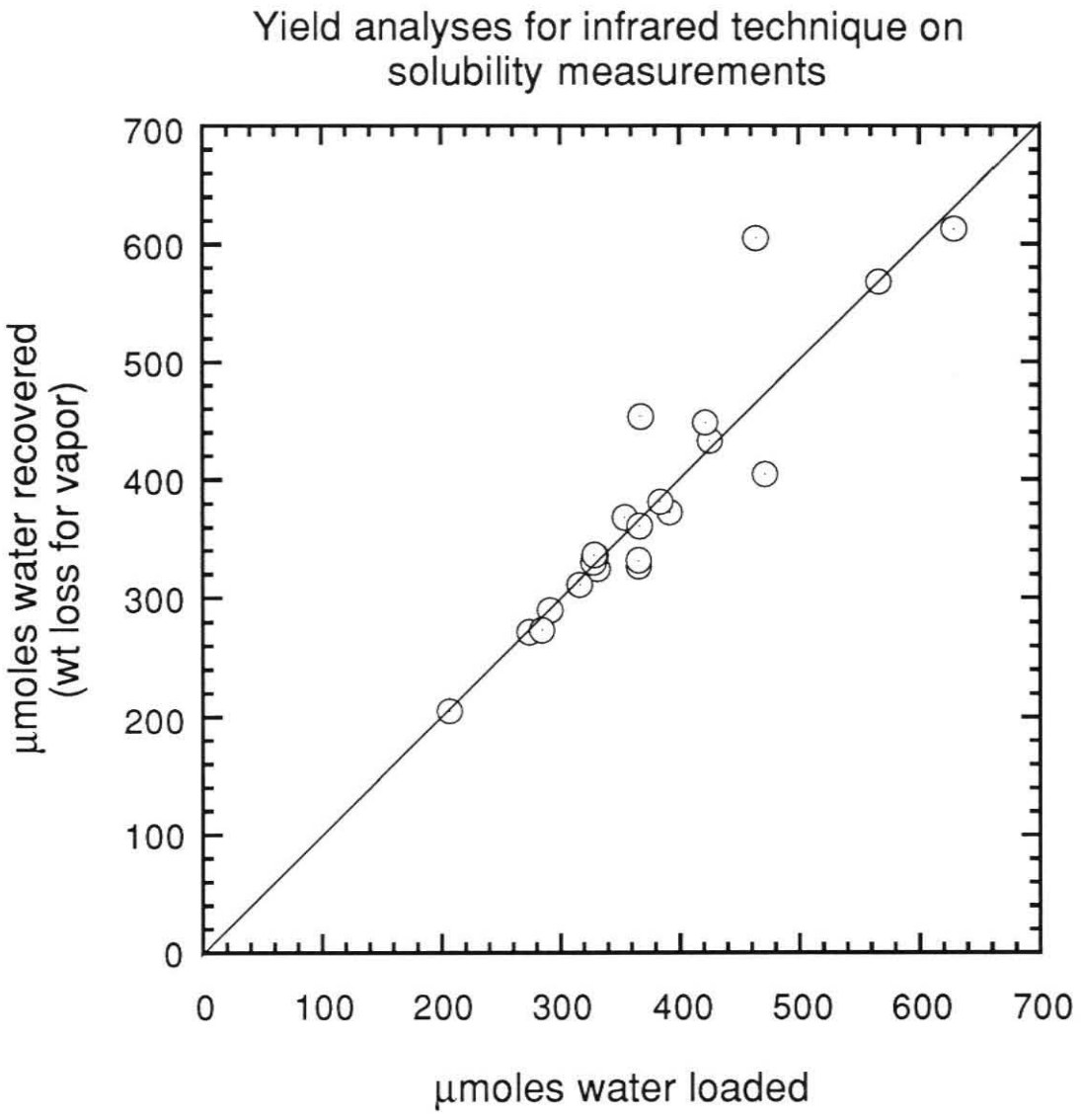

Figure 1.13: Comparison of total water loaded and total water recovered from water-saturated rhyolitic glasses. Recovery is based on water concentrations in glass determined by measuring the absorption peak heights in the infrared (ε_{5200} cm^{-1} = 1.51 l/mol-cm and ε_{4500} cm^{-1} = 1.73 l/mol-cm) and water concentrations in vapor determined by weight-loss on piercing in vacuum. The IR analyses were made by placing a 200 micron aperture over the center of the glass chips. The line represents complete recovery of water.

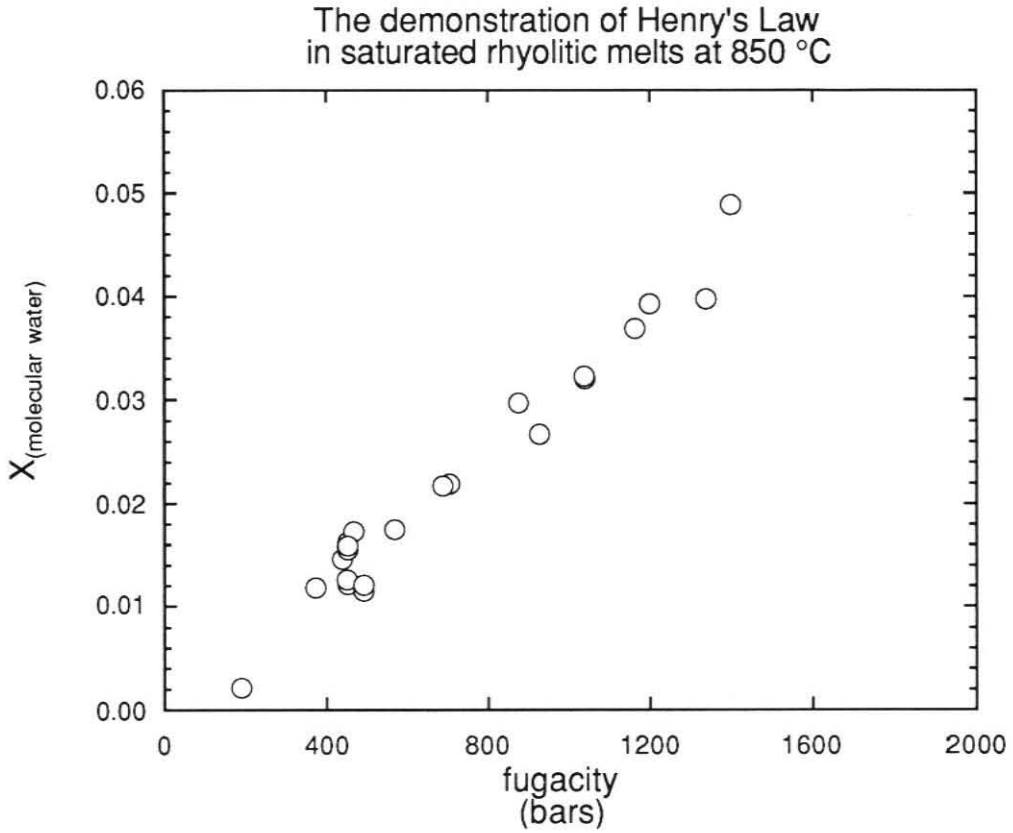

Figure 1.14: The mole fraction of molecular water plotted as a function of water fugacity in rhyolitic melt at 850°C. $X_{H_2O,\,molecular}$ was calculated from the regular solution model presented in Chapter 2. Total water was determined by IR measurements; the fugacity was calculated using the modified Redlich-Kwong equation of state for pure water vapor (Holloway, 1977). The linear relationship demonstrates the applicability of Henry's Law to wet silicate melts at these pressures.

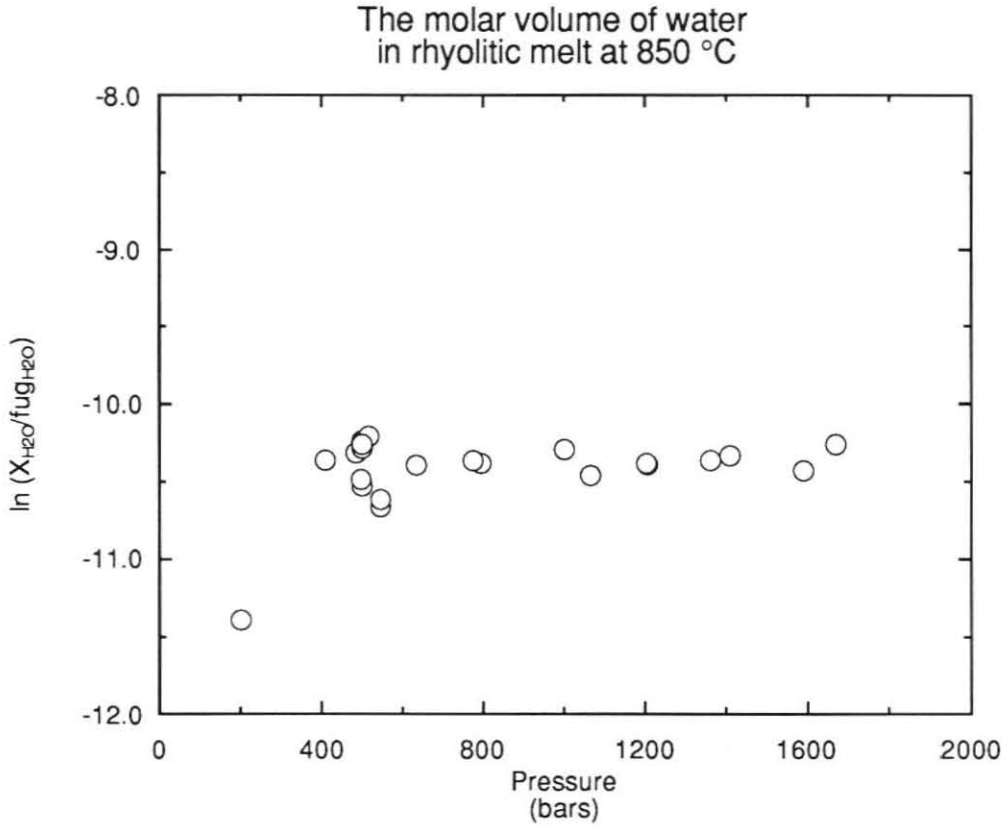

Figure 1.15: The logarithm of the ratio of the mole fraction of molecular water to the fugacity of water in the melt as a function of the total pressure of equilibrium. $X_{H_2O,\,molecular}$ was calculated from the regular solution model presented in Chapter 2; the fugacity was calculated using the modified Redlich-Kwong equation of state for pure water vapor (Holloway, 1977). A slope of 0 implies a partial molar volume of 0 for water in rhyolitic melts. Implications are discussed in the text.

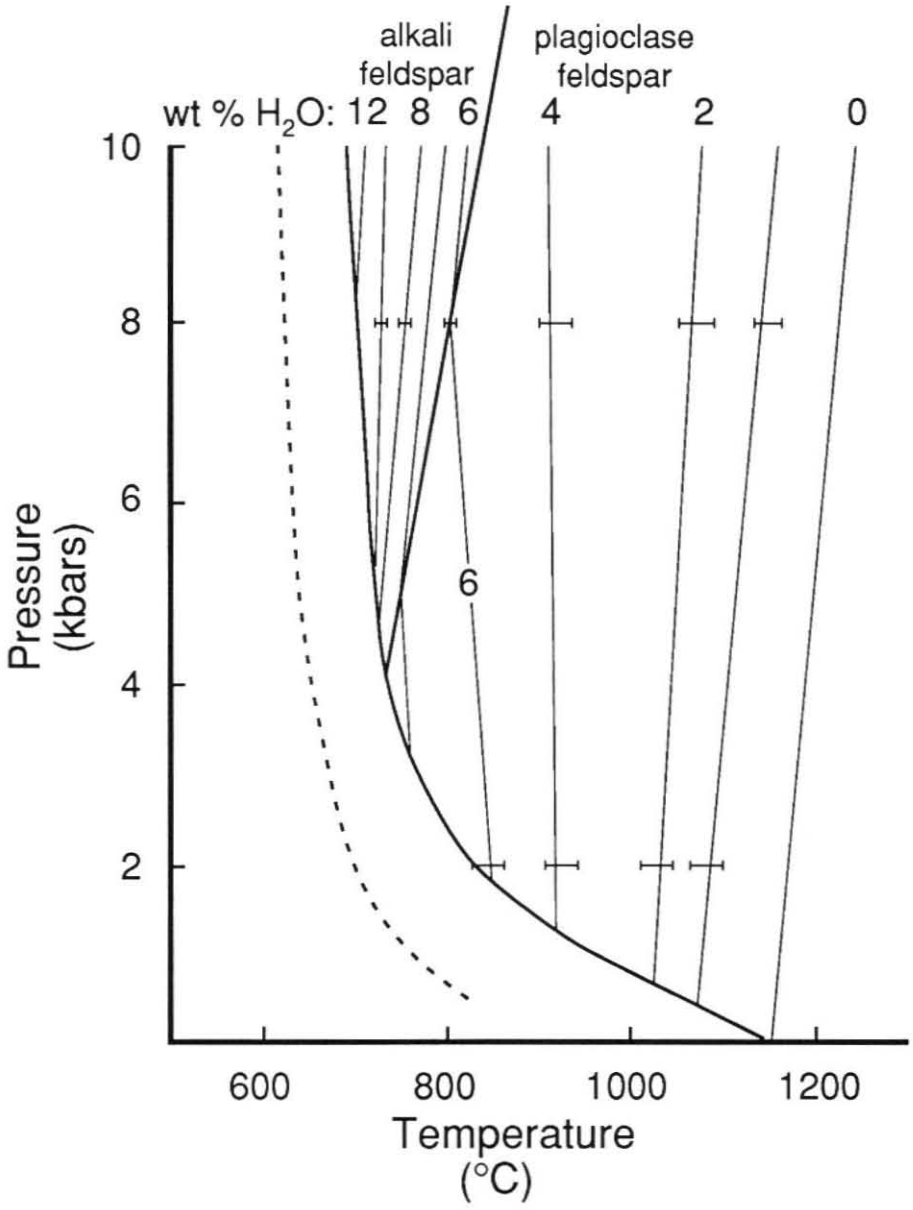

Figure 1.16: Schematic phase diagram for granite + water; data from Whitney et al. (1975). Figure adapted from Day and Fenn (1982). Undersaturated liquidi are schematically drawn in to fit experimental data at 2 and 8 kbar. Progressive increase in slope occurs with increasing water content, until, at three wt % total dissolved water, the liquidus slope becomes negative. A change in slope may occur with appearance of alkali feldspar on the liquidus at high water contents. Dotted line is the granite wet solidus. These data may constrain the partial molar volume of water in granitic melt (see text).

Chapter 2:

The Speciation of Water in Granitic Melt

Introduction:

The nature of water in silicate melt has long been a topic of considerable interest to geologists. The introduction of water into a silicate melt can cause dramatic changes to its structure and hence affect its physical and chemical behavior. A few weight percent dissolved water can change the viscosity of a granitic magma by over five orders of magnitude (e.g., Shaw, 1963a). The viscosity of the magma strongly influences both its ability to migrate away from its source region and its residence time in surrounding environments as it migrates through the crust. The diffusivity of crystal-forming elements is also strongly affected by a small amount of dissolved water in the melt (e.g., Watson, 1979). Given the important role of water in igneous processes, it is not surprising that much effort has been applied to understanding exactly how water reacts with the melt structure. By understanding the interaction between melt and water on a molecular level, we can correlate changes in microscopic structure with changes in macroscopic properties such as viscosity and density. Full understanding of melt-water interaction will allow us to set constraints in predicting the influence of water on the behavior of evolving magmas.

There has been considerable debate about the nature of water speciation in silicate melts over the last ten years. Because of the linear relationship of the square of the concentration of total dissolved water to water fugacity, glass scientists and igneous petrologists believed for years that water dissolved almost exclusively as a network-breaking hydroxyl species, X-O-H, where X is some cation other than H^+ (e.g., Tomlinson, 1956; Kurkjian and Russell, 1958; Burnham and Davis, 1974; Burnham, 1975b). This thinking was in contrast to the results of infrared and near-infrared spectroscopic measurements made on hydrous silicate glasses which quantitatively demonstrated the presence of both hydroxyl and molecular water (H-O-H) species (Keller and Pickett, 1954; Orlova, 1962; Ernsberger, 1977). Because of the lack of a significant absorption near 1630 cm^{-1}, Raman spectroscopic data (Mysen et al., 1980; Mysen and

Virgo, 1980, 1986) have been cited to support the hypothesis that little or no molecular water is stable in the melt. However, the growing body of spectroscopic data, both from nuclear magnetic resonance techniques (Bartholomew and Schreurs, 1980; Eckert et al., 1987; Farnham et al., 1987; Watson et al., 1990) and infrared techniques (Bartholomew, et al.,1980, Stolper 1982a,b, 1989; Newman et al., 1986; Silver and Stolper, 1989; Silver et al., 1990), conclusively demonstrates the presence of molecular water in hydrous glasses. Because molecular water is not expected to be an efficient Raman scatterer (e.g., Stone and Walrafen, 1982), the conclusions reached by the Mysen group have largely been discounted (e.g., McMillan et al., 1983; Silver et al., 1990), and it is now generally recognized that at least two independent water species are present in hydrous silicate glass.

The question still remains, however, whether the relative species concentrations measured in a glass at room temperature represent the same concentrations of species that exist in the melt at high temperature. Molecular water in a silicate glass may be the result of a quench phenomenon (e.g., Mysen and Virgo, 1986; Dingwell and Webb, 1990). The most straightforward way to address this issue is to measure the speciation of water in the melt at the temperature of interest *in situ*. A preliminary investigation (Aines et al., 1983) demonstrates absorption phenomena due to molecular species at temperatures to 850°C. However, this technique is not yet quantitative due to a variety of experimental difficulties. The extinction coefficients for the dissolved species in the melt are expected to change as the vibration of the framework lattice changes with increasing temperature. Calibration of these extinction coefficients will be difficult, if not impossible. An additional complication results from the blackbody radiation emitted by the hot melt in the energy range of interest. At present, we must be content to determine the structural relationship of water in silicate melts by studying quenched glassy products.

The nature of hydrogen in silicate melt:

The presence of volatiles in crystal cavities was firmly established by the pioneering work of Sir Humphrey Davy (1824), Sir David Brewster (1826) and Sorby and Butler (1869). Their definitive conclusions about the structural state of gases in minerals led Tilden (1896), in the first systematic study of the release of volatiles from natural rocks (five samples including a granite and a gabbro), to suggest that volatiles evolved on heating were "wholly inclosed in cavities..." Chamberlin (1908) analyzed 112 natural rocks (including fresh volcanic rocks) and concluded, contrary to Tilden, that the water released upon heating rock powders *in vacuo* represents magmatic water that is not associated with gas cavities. Rather, the hydrogen he measured (evolved at high temperatures) was either chemically bonded to the solids (including glass) or physically "occluded" in the molecular state. Goranson's (1931) measurements of the solubility of water in granitic melts represent the first accurate determination of the water contents of synthetic hydrous glasses. He made no assumption about the dissolution mechanism involved in the reaction of the melt with water vapor and determined the total water evolved from his experiments by a weight-loss method. Shepherd (1938) used the technique of Goranson to accurately determine the water content of a number of natural obsidians collected from around the world, but again, no distinguishing characteristics emerged between the possible structural species of water in the glasses he analyzed.

Wasserburg (1957) postulated that water may exist within a silicate melt as three possible species: 1) discrete molecules residing in small pockets or in positions hydrating non-tetrahedral cations, 2) hydroxyl species formed on depolymerization of the silicate framework, and/or 3) hydroxyl species formed on reaction with oxygens associated with network modifying cations. He concluded that the oxygens associated with species 1 and 3 are indistinguishable and modeled the dissolution of water in silicate melt as an ideal mixture of two species. This treatment accurately predicted Goranson's (1936; 1938)

experimental solubility data. Kennedy et al. (1962) presented a series of experimental data bearing on the freezing point depression due to water dissolution into a pure silica melt, and concluded that Wasserburg's ideal solution model was not capable of describing their data. Shaw (1963b) extended Wasserburg's ideal treatment by including entropy and heat of mixing terms that arise from the potential clustering of water molecules. This treatment matched the available experimental data on silicate-water systems including $NaAlSi_3O_8$-H_2O (Goranson, 1938), $NaAlSi_3O_8$-SiO_2-H_2O (Tuttle and Bowen, 1958), $KAlSi_3O_8$-H_2O (Goranson, 1938; Spengler and Burnham, 1961), $KAlSi_3O_8$-SiO_2-H_2O (Schairer and Bowen, 1955; Shaw, 1963c), and $CaAl_2Si_2O_8$-SiO_2-H_2O (Schairer and Bowen , 1947; Stewart, 1958), but also failed in estimating the freezing point depression in the SiO_2-H_2O system.

Burnham and Davis (1974) and Burnham (1975a,b) ignored the considerations of Wasserburg and Shaw, and emphasized the linear relationship between the square of the concentration of dissolved water in the melt to the activity of water in the melt and assumed that all dissolved water existed as hydroxyl groups. Burnham (1975b) proposed a cation exchange reaction for the initial dissolution mechanism of water in albitic melt. At $X_{H_2O} >$ 0.5 (and the complete exhaustion of Na^+ ions), he proposed further hydroxyl dissolution not associated with cation exchange. Hodges (1974) proposed the onset of a new dissolution mechanism at high pressures (> 20 kbar) involving molecules of water based on the dramatic increase in water solubility in pure forsterite, enstatite, and anorthite melts. He, too, felt that the dominant mechanism for water dissolution at $X_{H_2O} < 0.5$ was the near exclusive formation of hydroxyl groups.

Spectroscopic techniques provide the most insightful analyses on the dissolution behavior of water into a melt structure. For example, Mysen et al. (1980) and McMillan et al. (1983) have used Raman spectroscopy to look at water-rich glasses and have noted the ability of the technique to quantitatively determine the concentration of hydroxyl species within a silicate glass. Bartholomew and Shreurs (1980), Eckert et al. (1987;1988),

Farnan et al. (1987), and Leshin et al. (1990) have investigated the chemical environments of proton sites in hydrous silica-rich glasses using a variety of nuclear magnetic resonance (NMR) techniques. These techniques are useful for gaining insights into the bonding environments of dissolved water. Further work on these spectroscopic techniques are needed, however, before quantitative distinction of all hydrogen species existing within a glass can be made.

The presence of a molecular water species in volcanic glasses was first detected by Keller and Pickett (1954), who observed a significant absorption at 1630 cm^{-1} in the infrared spectrum. This absorption was observed only in water-rich perlitic glasses. Although their water-rich perlites were believed to have been formed by low temperature hydration of originally water-poor obsidians, they considered the presence of the molecular species as a fundamental feature of high water content silicate glasses. Evidence for the presence of molecular water in a silicate melt was first observed by Orlova (1962), who applied an infrared spectroscopic technique to albitic melts quenched to hydrous glasses. She noted the presence of an absorption at 1600 cm^{-1} indicative of the molecular water, H-O-H species as well as the hydroxyl species associated with X-O-H vibration at 4500 cm^{-1}. Ostrovskiy et al. (1964) used this technique to investigate the influence of cation size on the solubility of water in alkali melts. They distinguished two hydrous species and observed Henrian behavior for the molecular species based on their experimental results at 2 and 4 kbars.

Stolper (1982a,b) applied the infrared technique to glasses of geologic composition and he and his colleagues carefully began to characterize the infrared technique (e.g., Stolper et al, 1983; Newman et al., 1986; Silver and Stolper, 1989). They observed the following distinctive pattern in all glass compositions: at low total water contents hydroxyl species are the dominant hydrogen-bearing species, but with increasing water dissolution, the proportion of molecular water species increases. Thus, in water-rich glasses, molecular species become the dominant form of dissolved water.

Silver and Stolper (1985) developed a thermodynamic model for hydrous silicate melts using their spectroscopic measurements as a basis for their model. They assumed ideal mixing of three oxygen species; hydroxyl groups, H_2O molecules, and bridging oxygens within the silicate melt framework. They treated the reaction of dissolved species as independent of temperature, pressure, and total water content, but fit the available phase equilibria data, including the SiO_2-H_2O freezing point depression of Kennedy et al. (1962).

There remains, however, a noticeable lack of experimental data bearing on the relationship of species concentrations with temperature, pressure, total water content, and bulk melt composition. Silver and Stolper (1989) and Silver et al. (1990) present a series of experimental results exploring the relationship of hydrogen speciation to total dissolved water content and bulk melt composition (see Appendix 2). Again the regular increase in the proportion of molecular water with increasing total dissolved water was observed and a detailed thermodynamic analysis was presented with implications for hydrous melt behavior. The effect of temperature on the equilibrium of the two species in the melt was discussed but not fully investigated. This chapter presents a series of experimental results in which the equilibrium speciation of water in a melt is determined as a function of temperature, water content, and melt composition. I show that the equilibrium concentration of the two species is a strong function of temperature and that the time to reach equilibrium at high temperatures and high water contents is faster than the time it takes to quench an experiment, even using the fastest quench rates attainable in conventional experimental apparatus. Nevertheless, the equilibrium speciation of a glass can be preserved in water-poor samples and, at low temperatures, in water-rich samples. Results from these experiments are used to model the equilibrium speciation of water in rhyolitic melts at all temperatures.

Experimental methods:

Three experimental methods are presented for the investigation of water speciation in rhyolitic melts. The first method involves equilibration of natural obsidians with pure water vapor at melt temperatures before rapidly quenching to glasses at room temperature. The results of these experiments are compared to similar experiments carried out on rhyolitic melts that were quenched at slower rates in slow-quench cold-seal and internally-heated pressure vessels. A second set of experiments was performed on previously hydrated glasses held at temperatures varying from 450°C to 600°C for durations sufficiently long to reach internal species equilibrium. These experiments are used to formulate a regular solution model to predict the speciation of water in rhyolitic samples held at any temperature and pressure. A third set of experiments was carried out to more thoroughly investigate the effect of quench rate on the speciation of water in glasses of rhyolitic composition.

Starting materials: A rhyolite collected from Glass Buttes, Oregon was used for most of the experiments in this study (see Table 1.1). This obsidian locality was recommended by Robert Smith of the USGS as the driest, crystal-poor, natural rhyolite in North America. The samples I collected are indeed aphyric with the exception of rare feldspar grains (<500 microns) and the presence of ubiquitous opaque oxides (<200 microns). The water content of this glass is homogeneous from hand-sample to hand-sample. Infrared analyses on various chips yield values of 0.024 ± 0.010 wt % H_2O (see Table 1.1). In addition, water-poor obsidians from Mono Craters, California, the Coso Range extrusive domes, and the Los Pasos volcanic field are also used in this study (see Table 1.1). These glasses are also relatively aphyric but contain many tiny opaque oxides.

Experiments quenched rapidly from 850°C: The first set of experiments is described in detail in Chapter 1 of this thesis. Briefly, rhyolitic chips were crushed to less than 2 millimeters in diameter and abraded in a SPEX mill shaker for up to five hours. The rounded chips were sealed in platinum capsules with triply distilled water and loaded in the modified rapid-quench cold-seal pressure vessels described in Appendix 1. Sufficient water was loaded into the capsules to insure saturation with a pure aqueous vapor. Equilibration times exceeding several days were necessary to achieve homogeneous run products. Quenching was accomplished by dropping the sample from the hot portion of the apparatus to the chilled portion positioned outside the furnace. Quenching to room temperature is believed to occur in less than 2 seconds (see Appendix 1).

Experiments quenched slowly from 850°C: The results of a similar set of experiments on rhyolitic glasses are presented by Silver et al. (1990; see Appendix 3). In these experiments, cores of obsidian glass were held for durations ranging from 1-3 weeks in cold-seal and internally-heated pressure vessels. The cold-seals used in these experiments are made of René alloy bombs with a wall thickness of 3/8 in. Quenching was achieved by pulling the bomb out of the furnace and blasting compressed air over the exterior of the vessel. Thus, the cooling rate of the sample was limited by the rate of heat conduction out of the thick bomb walls. Cooling rates were monitored with internal thermocouples and are estimated at $\approx$ 200°C per minute. Experiments in internally-heated pressure vessels were quenched by switching off power to the apparatus (while maintaining run pressure) providing similar cooling rates ($\approx$ 200°C per minute) to those experiments performed in the slow-quench cold-seal apparatus.

Equilibrium speciation at lower temperatures: A second set of experiments was performed on previously hydrated rhyolitic glasses and held at a range of temperatures and pressures in modified rapid-quench cold-seal pressure vessels (see

Appendix 1) for durations long enough for the dissolved species to reach equilibrium concentrations. These hydrated glasses were then re-loaded in capsules without any addition of water. The experimental design outlined in Appendix 1 is ideal for investigating the speciation of water in glasses for two reasons. Exsolution of water from water-rich glasses held at temperatures above 400°C and at 1 atm pressure occurs at time-scales faster than that required for internal species equilibrium (Stolper, 1989). The modified cold-seal pressure vessels allow for long durations at high temperatures without the complications of exsolution. To avoid the potential exsolution of water, these experiments were held at pressures ranging from 500 to 1000 bars. Secondly, the precise durations necessary for a time series of experiments can be controlled with the use of the elevator rod, which is capable of bringing a run from room temperature to run temperature and vice versa within seconds. Thus, time-dependent data are collected on water-rich samples held at high pressures that would otherwise bubble and rapidly exsolve water in low pressure experiments. These data on rhyolitic glasses are then compared to the results on low water content samples described elsewhere (Stolper, 1989; Zhang et al., 1991).

An additional set of preliminary experiments were performed on silica and albite glasses synthesized in Professor D. Hamilton's laboratory at the University of Manchester, UK. These samples were prepared by mixing pure reagent grade powders, melting at high temperatures, and quenching to a dry glassy product. Single glass cores were loaded in platinum capsules with distilled water. Experimental charges were held at 1100°C for 2-4 days at pressures ranging from 500 to 3000 bars in internally-heated pressure vessels with argon as the pressure medium. Additional details of the experiments are given in Tables 2.5 and 2.6.

The effect of quench rate on speciation: An additional set of experiments was performed in the laboratory at Bayreuth, Germany, by Professor M. Carroll to investigate the effect of quench rate on the speciation of water recorded in hydrous glasses.

Rhyolitic glass chips (see Table 1.1) were hydrated in slow-quench cold-seal vessels. Sample B-16 was cooled by blasting compressed air over the cold-seal vessel with an associated quench rate estimated between 100°C/min and 200°C/min. Sample B-18 was cooled by turning off the power to the furnace. The slow quench rate is estimated to be around 4°C/min based on a chart-recorder measurement. These hydrated samples were used as starting materials for experiments run in piston-cylinder apparatus. All experiments were performed in 3/4 in. piston cylinders and held at 1200°C for one hour before isobaric quenching to room temperature at quench rates varying from 2400°C/min to 0.17°C/min. Quench rates were controlled by ramping down temperature using a programmable Eurotherm controller. Additional details of these experiments are given in Table 2.7.

Infrared Spectroscopy: Doubly-polished sections of all run products were prepared and analyzed on an FTIR Nicolet 60SX spectrometer as described in Chapter 1. Care was taken to polish the edges of the glass wafers, where the potential for diffusive loss of molecular water may have taken place (Zhang et al., 1991). The intensities of the absorbance bands at 5200 cm^{-1} and 4500 cm^{-1} were measured and converted to concentrations using the molar absorptivities calibrated in Chapter 1 (ε_{5200} = 1.51 l/mol-cm; ε_{4500} = 1.73 l/mol-cm). The densities of the glass compositions were calculated using an iterative technique described in Silver et al. (1990; see Appendix 2). The anhydrous molecular weight per mole of oxygen for each composition is 32.49 g/mol for rhyolite, 32.78 g/mol for albite, and 30.04 g/mol for silica glass.

Errors associated with the infrared measurements are estimated based on the quality of individual spectra. In general, most samples are of high quality and uncertainties are estimated to be $\approx$1 % of the total absorbance. There is an additional source of error associated with fitting a background to the spectra; care was taken to apply a consistent background shape to each spectrum. The silica peaks present an additional complication; there are two visible components associated with both the 5200 cm^{-1} and 4500 cm^{-1}

absorbance bands. Their close proximity makes it difficult to resolve the height of each component, and molar absorptivities for the integrated absorbances is perhaps a more precise assessment for determining species concentrations (e.g., see Langer and Flörke, 1974). However, to maintain consistency in this study, I have used previously established molar absorptivities for the respective peak-heights at each absorbance (see below).

Results and Discussion

Experiments equilibrated at high temperatures: The species concentrations of water-saturated glasses quenched slowly from 850°C (Silver et al., 1990; Appendix 2) are presented in Table 2.1. The concentration of the molecular species has been adjusted by applying the best-fit epsilon of 1.51 l/mol-cm to the absorbance at 5200 cm^{-1} as described in Chapter 1. The concentration of the individual species is plotted versus the total water content of the glass in Fig. 2.1. The hollow circles represent the concentration of the hydroxyl species and the hollow squares represent the concentration of the molecular water species. As observed in natural samples (e.g., Stolper, 1982b; Newman et al., 1988), the glasses show a distinctive variation of species concentration with water content. Dissolved water is primarily present as hydroxyl species at low total water contents. With increasing water content, the molecular species becomes more concentrated. At a total water content of around 3 wt %, the hydroxyl concentration no longer increases, and all additional dissolved water is present in the glass as a molecular species. In fact, the relative concentrations of the two species with water content in these controlled experiments are similar to the relative concentrations in natural obsidians (compare to data of Newman et al., 1988). The similarity of the speciation of water in these samples suggest that they have undergone similar thermal histories (see, e.g., Stolper, 1989).

The results of experiments held at 850°C (and three experiments held at 750°C) and rapidly-quenched to ambient conditions (in ≈ 2 seconds) are shown in Table 2.2. These

results (shown as filled symbols) are compared to the species concentrations of glasses quenched slowly from 850°C in Fig. 2.1. Both sets of experiments were performed under water-saturated conditions. As two sets of experiments with different quench rates give identical total water contents at each pressure of equilibration, we reasonably conclude that the time required for exsolution or dissolution of water into the glass at high pressures is sufficiently long such that melt does not react with the vapor on quenching. This result is different from the effect of quench rate on speciation. Although the same trends in the variation of species content with total water are similar, the difference in the relative concentrations of the two species at similar total water contents is apparent. The concentration of hydroxyl groups at a given total water content is noticeably higher in the rapidly-quenched glasses (see also Fig. 2.2). Thus, the dissolved water has continued to react during the slow cooling of the melt such that an increase in the concentration of the molecular species is observed; i.e., the relative concentrations of the two dissolved species changes from their original concentrations in the melt on cooling. Not only is the reaction associated with the equilibrium between the two dissolved species sensitive to temperature, but the rate of reaction is sufficiently fast so as to be observable in the five minutes required to cool the slow-quenched samples to room temperature. It is reasonable to question whether the rapid quench rate of my modified cold-seal pressure-vessel is rapid enough to preserve the equilibrium species concentrations in melts quenched from high temperatures.

I will present a series of experiments which show that the species concentrations observed in glasses rapidly quenched from melt temperatures are, indeed, not preserved in the short time-scales necessary to cool them to room temperature. But first, I wish to develop a simple way of expressing the relative species concentrations without having to refer to the cumbersome plots of Fig. 2.1. One such formulation is illustrated in Fig. 2.2. The relative species concentrations are expressed as a single parameter; the relative percent of the total dissolved water present as hydroxyl species. Thus, in Fig. 2.2 the trends

observed in both sets of experiments suggest that at very low total water contents, all water dissolves as O-H species, (wt % OH / wt% total water = 1.0).

There is a more informative species parameter that I have adopted for this work. Within the melt we can express the homogeneous equilibrium between the dissolved species as:

$$OH^{melt} + O^{melt} = H_2O^{melt} \quad (1)$$

where OH^{melt} is a hydroxyl group, O^{melt} is a bridging oxygen in the melt, and H_2O^{melt} is a molecular species dissolved in the melt. The equilibrium constant associated with this reaction is expressed as follows:

$$K_{eq.} = \frac{(aOH^{melt})^2}{(aO^{melt}) * (aH_2O^{melt})} \quad (2)$$

where aOH^{melt} is the activity of the hydroxyl species in the melt; aO^{melt} is the activity of bridging oxygens in the melt; and aH_2O^{melt} is the activity of the molecular species in the melt. If the melt were an ideal mixture of these three species, we could replace the activity terms with the concentrations of the species; i.e.,

$$K_{eq.} = \frac{(XOH^{melt})^2}{(XO^{melt}) * (XH_2O^{melt})} \quad (3)$$

where X_i is the mole fraction of species i in the melt. Thus, K_{eq} will be constant with variable total water content if the mixture is truly ideal. I adopt the parameter, K_s as follows:

$$K_s = \frac{(X_mOH^{melt})^2}{(X_mO^{melt}) * (X_mH_2O^{melt})} \quad (4)$$

where K_S is defined as the "simple" equilibrium constant determined by the relationship of the X_m^i s; the measured concentrations of the respective species in the glassy product as determined by infrared spectroscopy (see, e.g., Zhang et al., 1991; Appendix 3). The speciation of water in the glasses listed in Tables 2.1 and 2.2 are illustrated in Fig. 2.3; the natural logarithm of the K_S parameter is plotted as a function of the total water content of the glass. In this expression, a higher value of $\ln(K_S)$ indicates a greater concentration of O-H. The observed curvature in the trend of rapidly-quenched glasses indicates that if the speciation were preserved on quenching (i.e., if $K_{eq} = K_S$), the oxygen species would not be mixing ideally at 850°C.

Knowledge of K_{eq} provides insights into the nature of the equilibrium of the hydrous species. An understanding of the temperature dependence of K_{eq} will yield insights into the energetics associated with the reaction of water with silicate melt. Thus, it is of importance in the study of hydrous melts to describe the relationship of K_S to K_{eq}. The observation in Fig. 2.3 of variable species concentration with quench rate indicates that the speciation recorded by K_S may reflect some intermediate melt condition frozen in at the "glass transition" of the cooling liquid (Dingwell and Webb, 1990). The "glass transition" is actually a confusing and often mis-used concept. The "transition" temperature is brought on by the inability of the liquid structure at low temperatures to accommodate the motions necessary to behave in equilibrium fashion. Scherer (1984) notes that molten samples have a unique "closure temperature" (or fictive temperature) associated with every property (including heat capacity, viscosity, thermal expansion, etc.) and with every reaction (involving all melt species) that may take place in the liquid state. Its presence is marked by a gradual change in the response indicative of the property (or reaction rate) of the melt to that which is characteristic of the glass; i.e., it does not occur at a distinct temperature. Furthermore, these closure temperatures are observed to depend on the thermal history of the sample (e.g., Scherer, 1986). Thus, reaction (1), involving hydrous species in silicate melt, will continue to react with decreasing temperature until the motions of the lattice

framework are too sluggish to accommodate the speciation reaction. The conditions of this closure temperature will vary with initial temperature, quench rate, total water content, and bulk melt composition.

Though the preceding discussion presents a dim prospect for the possibility of knowing the actual temperature of melt equilibration, I will now present a series of experiments from which the speciation has not changed in falling from run temperature to room temperature; i.e., the quench rate is sufficiently fast that the structural motions of the liquid do not have time to respond the the changing conditions during the quench. These experiments allow us to predict the true speciation of water in rhyolitic melts at all temperatures.

Experiments equilibrated at low temperatures: Stolper (1989) investigated the temperature dependence of the species concentrations of water in hydrous glasses by equilibrating natural obsidians at atmospheric pressure and temperatures between 400°C and 900°C. Because of the problems associated with wafer deformation and bubble growth at high temperatures, his study was limited to glasses with less than 2.0 wt % total water. He observed a regular increase of hydroxyl species with increasing temperature. By using the rapid-quench data at 850°C of Silver et al. (1990; Table 2.2) to fix a reference point, he developed a regular solution model to describe the temperature dependence of the equilibrium of dissolved water species. Zhang et al. (1990) have determined the diffusion rate of water as a function of temperature. They, too, observed the increase in the proportion of hydroxyl to molecular species with increasing temperature in glasses which they observed to have reached species equilibrium.

I have picked the highest quality experiments (53) of Stolper (1989) as well as the experiments known to have reached equilibrium by Zhang et al. (1990) and recalculated their species contents in Table 2.3 using the best-fit epsilon for the 5200 cm^{-1} peak described in Chapter 1. These data are displayed graphically in Fig. 2.4. The results,

though rather scattered, show an observable decrease in $\ln(K_S)$ with increasing total water content at each temperature. The important question remains, however, as to whether the observed variation in speciation with water content is a fundamental feature of equilibrium in hydrous glasses, or is simply an artifact of quenching.

Zhang et al. (1990; see Appendix 3) have performed a series of experiments to determine the rate of reaction between the dissolved water species in rhyolitic glasses. Fig. 2.5 summarizes the results of these experiments and demonstrates the amount of time required to reach equilibrium at a variety of temperatures. In these experiments, a series of glasses were held at temperature in 1 atm. furnaces for variable run durations. Glass wafers were pulled out of the furnace and dropped into water for rapid quenches approaching 1 second. The speciation recorded in these experiments are reversible in that the same speciation is approached whether the initial glass composition has a higher or lower $\ln(K_S)$ value. Fig. 2.5 shows that at higher temperatures and at higher water contents, the reaction rate between the two species is much faster than at low temperatures and in low water content glasses. Thus, a glass with 1 wt % water takes about 150 minutes to reach equilibrium at a temperature of 500° C. We should expect that the rapid quenches of $\approx$ 1 second recorded in the modified hydrothermal apparatus are sufficient to preserve the equilibrium speciation in these low total water content glasses at these low temperatures. On the other hand, extrapolation of the 600°C equilibration curve to time-scales approaching that of the rapid quench suggests that higher water content glasses (>3 wt %) may undergo re-equilibration on cooling.

Dingwell and Webb (1990) present an interesting analysis for determining whether quenching an experiment will preserve the high temperature melt structure. In their analysis, they envision a relaxation curve (the τ-curve) characteristic of the melt-glass transition which traverses time-temperature space (log (time) is plotted as a function of inverse temperature; see Fig. 2.6). At a given temperature, the material will respond as a liquid if a disturbance occurs on a time-scale longer than that defined by the relaxation

boundary curve (i.e., at a time-scale plotting above the τ-curve in Fig. 2.6). If the disturbance occurs at a shorter (i.e., faster) time-scale than that defined by the τ-curve, the material will not respond in equilibrium fashion and will behave as a glass. Thus a melt held at high temperature (the dwell temperature) for a long period of time will plot in the upper right-hand quadrant of Fig. 2.6. In their treatment, the quench rate of the experiment is represented as a horizontal line, i.e., independent of temperature. The intersection of the τ-curve with the quench-rate line (the q-curve) defines the "fictive" temperature of the experiment, and the equilibrium properties of the melt at this temperature will be recorded in the quenched product if the melt was quenched from some higher temperature. Thus, true equilibrium at run temperatures is only observed in experiments whose dwell temperatures are less than their fictive temperatures (see Fig. 2.6).

Dingwell and Webb (1990) assume that the viscous response of a silicate liquid directly correlates with the reaction rate of the internal species. They further assume the equivalence of mechanical and enthalpic relaxation and calculate the viscosity of the hydrous silicate at the glass transition using the relation;

$$\log_{10} \eta^* = \log_{10} \tau_q + \log_{10} G_\infty \qquad (5)$$

where η^* is the viscosity at the glass transition (in Pascal-seconds), τ_q is the equilibration time determined by the quench rate (in seconds), and G_∞ is the shear modulus at infinite frequency ($\approx 10 \pm 0.5$ Pascals). Thus, knowledge of the relationship of viscosity to temperature allows them to use the linear relationship of viscosity to relaxation time and calculate relaxation curves in a time vs 1/T plot. They have applied the empirical algorithm for the viscosity of wet rhyolites developed by Shaw (1972) and calculated the various τ-curves for hydrous rhyolites at 1, 3, and 5 wt % total dissolved water. Though this is obviously an approximate treatment, it might serve well as a first check on the feasibility of preserving the equilibrium speciation under my experimental conditions.

Fig. 2.7 shows the calculated τ-curves for rhyolites with 1, 3, and 5 wt % water (adapted from Dingwell and Webb (1990), Fig. 12). Also shown in Fig. 2.7 are the representative quench rates for the two sets of experiments listed in Tables 2.1, 2.2, and 2.3. From the analysis of Dingwell and Webb (1990), a glass held above and to the right (at lower temperatures) of the intersection between the τ-curve and the q-curve will accurately record the equilibrium speciation of the dwell temperature. Thus, a rhyolite with 5 wt % water will quench without reaction if equilibrated below ≈ 550°C. The intersection of the rapid-quench q-curve with the respective τ-curves defines the approximate limit of accurately recording the speciation at the "dwell" temperature in the quenched product. For rhyolites with 1 and 3 wt % water, dwell temperatures above 790°C, 620°C, respectively, will re-equilibrate on cooling. The data illustrated in Fig. 2.4 all fall below these predicted upper limits and should record the speciation at their respective dwell temperatures.

This treatment must be used with extreme caution. For instance, Dingwell and Webb (1990) have erroneously used this analysis with the assumption of ideal mixing of species (i.e., K_{eq} is constant for variable water content) to calculate the temperature dependence of reaction (1). This treatment should not be used as a predictive tool for the fine details of melt structure, as it is based on several assumptions. For example, the quench rate of the experiment is a complicated function of several factors as discussed above. Though q is a single value at the fictive temperature (assuming one can define a specific temperature as the fictive temperature!), its estimation at this critical stage in the cooling history will only be approximate. The viscosity calculations must also be treated with caution. They are based on an empirical relationship of the total water with viscosity. The viscosity is most influenced by the concentration of hydroxyl species (that is, the breaking of the bridging oxygens to create the network modifying O-H bonds). In a study where the variation of the relative concentrations of the two species are highly sensitive to temperature, water content, and bulk composition, Shaw's simple approximation should not be taken literally.

Although the theoretical treatment described above is a dangerous predictive tool, it may be used in conjunction with experimental data to evaluate the assumptions used to develop the treatment. For example, the data in Fig. 2.3 delineate the fictive temperatures for hydrous rhyolites synthesized at two quench rates. Knowledge of the true temperature dependence of the speciation with total water content will allow for the identification of the actual fictive temperature in the re-equilibrated melt; i.e., the respective intersections of the true isotherms with the fictive temperature curve in Fig. 2.3 provide the fictive temperatures of each experiment. This information can then be used to determine the τ-curves for hydrous rhyolites and thus set constraints on the actual viscosity of the melts.

Based on the results outlined in Fig. 2.5, the measured speciation in glasses illustrated in Fig. 2.4 are recording the equilibrium speciation at the temperatures from which they were quenched. Thus, the temperature dependence data of Stolper (1989) are essentially accurate. His assignment of the 850°C speciation from the rapid-quench data as a reference point for his model, however, needs revision. Further, an accurate model treating the speciation of water in rhyolite with greater than 2 wt % water should have experimental data at higher water contents to better constrain this variable. I now describe the results of set of experiments which, in conjunction with the low water content data, allow for the complete calculation of the temperature dependence of the speciation of water in glasses and melts with variable water content.

To determine the equilibrium speciation in glasses with higher water contents, sufficient pressure must be applied to prevent the rapid exsolution of water, i.e., the formation of bubbles. The modified rapid-quench cold-seals described in Appendix 2 is suited for such experiments. Table 2.4 lists the experiments of a series of hydrous glasses ranging from 1 to 5 wt % water and held at temperatures ranging from 450°C to 650°C. Fig. 2.8 shows the measured values of $\ln(K_S)$ as a function of temperature and water content. Also plotted in Fig. 2.8 are the results of Zhang et al. (1990; Appendix 3). The data define an approximately linear trend in $\ln(K_S)$ for each series of isothermal experiments

to water contents as high as 5.2 wt % total dissolved water. I have sketched in isotherms in Fig. 2.8 for clarity and to highlight the dependence of speciation on the water content of the samples. These trends are continuous until the trend of the rapid-quench 850°C "dwell isotherm" (or rapid-quench fictive temperature curve) is approached. Intersection of the isotherms with the fictive temperature curve delineates the temperature limit at which rapidly-quenched glasses of a given total water content will reflect the equilibrium speciation of their dwell temperature. That is, the speciation in rhyolitic glasses is preserved from ≈2 second quenches provided the water contents and run temperatures are lower than those which outline the trend of the 850°C data in Figs. 2.3 and 2.8. Note that the experiments held at 600°C fall off the linear tend at water contents greater than 3.0 wt % total water. In these water-rich glasses, the speciation is altered during the quench, and the speciation they record is the equilibrium speciation at the characteristic fictive temperature, which can be determined by the lower temperature isotherms.

The data in Fig. 2.8 indicate that K_S (and hence K_{eq}) is not constant with variable water content. Either the three species are not mixing ideally, or there are more than three distinguishable oxygen species in the melt. A possible explanation is that the hydroxyls associated with Na-O-H, Al-O-H , and/or Si-O-H have different molar absorptivities associated with the 4500 cm^{-1} band; i.e., the measured values in Tables 2.1, 2.2, and 2.3 are not reflecting the true concentration of hydroxyl groups. In fact, Zhang et al.(1990) have observed an increase in the apparent total water contents of glass wafers held at different temperatures. This observed variation is reversible in that samples held at low temperature appear to lose water, but when they are brought back to the same higher temperatures, they appear to recover their lost water. This would result if two distinguishable hydroxyls are present and their relative concentrations are sensitive to temperature changes. Another possible explanation to account for the apparent non-ideality is that a third species (e.g., an hydronium H_3O^+ ion), not detected in our infrared measurements, is present in the glass. The hydronium ion is expected to absorb around ≈

2200 cm-1 (George Rossman, personal communication). Though absorption phenomena are often present is this region, silicate lattice combination absorption modes obscure the possible identification of this hydrous species. Though I believe that several hydroxyl species will be distinguished in future experiments, I will model the melt as a regular solution and account for the possible interaction parameters associated with mixing of three distinguishable species. This model is based on the model at constant temperature outlined in Appendix 2, and is presented with the form:

$$-\ln\left(\frac{X_{OH}^{m\,2}}{X_{H2O}^{m} * X_{O}^{m}}\right) = A + \frac{1000}{T}\left(B + CX_{H2O}^{m} + DX_{OH}^{m}\right) \qquad (6)$$

where A, B, C, and D are constants to be determined and T is the temperature in °K. Using the data marked with an X in Table 2.4 and the best data of Zhang et al. (1990) (see Table 2.3), I have calculated the best-fit parameters; A = -1.187, B = 2.696, C = 4.676, and D = 0.835, with a correlation coefficient of .971). This model is used to predict the speciation of water in rhyolitic melt at any temperature with any water content. In Fig. 2.8, I show the predicted speciation in the melt at 850°C before quenching to a glass. The importance of this model should be re-emphasized. For the first time, we can now correlate the changes in melt properties such as density and viscosity with the microscopic structural changes occurring within the melt. Direct measurements of these properties at melt conditions can now be compared to the species measurements determined in this study.

The theoretical treatment outlined by Dingwell and Webb (1990) allow us to calculate the viscosity of hydrous rhyolitic liquids. To the extent that the treatment is theoretically sound, and of our ability to estimate the quench rate of the experiment, we can extract the viscosity of rhyolitic liquids as a function of both water content and temperature from my experimental data. The water content of the melt at the intersection of the true isotherm with the rapid-quench dwell isotherm defines the fictive temperature for that melt.

Knowledge of the fictive temperature coupled with the quench rate fixes a point on the τ-curve of the melt. The intersection of the true isotherm with the dwell isotherm associated with the slower quench rate provides a second point on the τ-curve. The two points for water contents up to 5 wt % water provide an approximate τ-curve for hydrous rhyolites and are compared to Shaw's 1972 empirical calculations in Fig. 2.7. The reasonable comparison of the viscosity values leads some credence to the approach of Dingwell and Webb (1990) for investigating quench phenomena, but again I wish to stress the limitations of its applicability. In this discussion, I have taken a series of well-constrained experiments and used them to test the assumptions behind the theory. To the degree that the theory is valid, I can say something fundamental about the viscosity of rhyolite.

Preliminary experiments on the effect of melt composition: A preliminary set of experiments similar to those described in Table 2.4 on rhyolitic samples was performed on glasses of pure silicic and albitic glasses to explore the effect of bulk composition on equilibrium speciation in silicate melt. The starting materials were prepared in internally-heated pressure-vessels by Professor D. Hamilton of the University of Manchester, UK.

Knowledge of the extinction coefficients for the respective bulk compositions is necessary to determine the respective species concentrations. The associated epsilon values for albite glass have been determined by Silver and Stolper (1989; ε_{5200} = 1.67 l/mol cm and ε_{4500} = 1.13 l/mol cm). There is much variation in the calibrated molar absorptivities of the 5200 cm^{-1} and 4500 cm^{-1} absorption bands in silica glass, however. For example, Dodd and Fraser (1966) have determined a value of 1.7 l/mol cm for the absorbance at 4500 cm^{-1} in a fused silica sample. Blank, Silver, and Stolper (unpublished data) have determined best-fit values of ε_{5200} = 1.5 l/mol cm and ε_{4500} = 4.3 l/mol cm. These values were determined by comparing the measured intensities of the characteristic absorption bands of undersaturated glasses with the known amount of water loaded into their

experiments. A similar calibration on the saturated glasses used in this study (corrected for weight-loss at 110°C, durations ranging from 0.02 to 2 days) yield best-fit epsilons of $\varepsilon_{5200} = 1.20 \pm 0.08$ l/mol cm and $\varepsilon_{4500} = 6.0 \pm 1.6$ l/mol cm. Because of the inhomogeneity of the samples (up to 13% total water; see Table 2.5) used in this calibration, the values determined by Blank et al. are preferred and adopted for this study.

The results for silicic samples held at 550°C and 600°C are plotted and compared to their initial speciation in Fig. 2.9. The infrared analyses of each of the starting materials reveal substantial inhomogeneity, which probably accounts for their scatter in Fig. 2.9. The speciation of water recorded in samples held at both temperatures is essentially identical to the scattered initial values. Either the 2 and 5 minute durations were not long enough for the dissolved species to react, or there is not a temperature dependence associated with water speciation in silica glass (rather unlikely). Further work on the kinetics of the reaction of the dissolved species in silica glass is underway to address this issue.

The results on albitic glasses are more informative. The results of samples held under the same conditions described for the silicic glasses are presented in Table 2.6 and shown in Fig. 2.10. All of the samples have re-equilibrated to higher hydroxyl contents. A hypothetical isotherm is drawn through the 550°C data to highlight this change. Clearly, the 2 minute durations at 600°C were not sufficient for the albitic glasses to reach equilibrium. More experimental work is necessary to demonstrate that equilibrium was reached in the 550°C experiments. It is interesting to note that the silicic and albitic glasses with identical water contents, at identical temperatures, and for identical run durations (the experiments were performed at the same time in the same vessel) behave differently; the albitic samples reacted in the short duration at high temperature, but the pure silica glass did not. As both samples are fully polymerized, this result reflects a variation in reaction kinetics due to sample chemistry. This may be the result of the influence of the Na^+ ion in the structure or that the reaction:

$$H_2O^{melt} + (Na+)\ Al\text{-}O\text{-}X^{melt} = (Na+)\ Al\text{-}O\text{-}H^{melt} + X\text{-}O\text{-}H^{melt} \quad (7)$$

is faster than the reaction:

$$H_2O^{melt} + Si\text{-}O\text{-}Si^{melt} = 2\ Si\text{-}O\text{-}H^{melt} \quad (8)$$

where (Na+) Al-O-X^{melt} is a bridging oxygen associated with an aluminum tetrahedron and X is either Al^{3+} or Si^{4+}. Again, more work is needed on these compositions to set very interesting and useful constraints on our understanding of the fundamental nature of the interaction of water with silicate melt.

Preliminary experiments on the speciation of water as a function of quench rate: A third set of experiments was performed to more thoroughly investigate the effect of quench-rate on the speciation of water in melt. These experiments were performed in a piston-cylinder apparatus, where precise cooling rates have been applied using a programmable temperature controller. Table 2.7 lists the results of experiments which were held at 1200°C for 1 hour and cooled at quench rates varying from 2400°C/min to 0.17°C/min. The results of these experiments are plotted in Fig. 2.11 and compared to the rapid- and slow-quench data listed in Tables 2.1 and 2.2. The final water contents vary from 3.8 to 5.3 wt % water; thus, relaxation analyses similar to that described for the rapid- and slow- quench rate data are difficult to perform. However, I have sketched in the estimated dependence of the dwell isotherms for each quench rate noting the parallelism of the rapid and slow quench dwell isotherms observed in Fig. 2.3. With the exception of the slowest quench rate and the poorly estimated cold-seal quench of QR-B18, the results show predictable behavior; slower quenches are recording equilibrium speciation at lower fictive temperatures. The true curvature observed in both fictive isotherms in Fig. 2.3 complicate the extrapolation of the quench effect to rhyolites of all water contents, but future work may help to constrain the τ-curves and hence help in calculating the viscosities

of rhyolites as discussed earlier. The disparity in the results of the speciation of water in samples with identical water contents and similar estimated quench rates (from the cold-seal and the piston-cylinder apparatus) highlights the problem of estimating the actual quench rate occurring at the onset of glassy behavior. Nevertheless, wet rhyolites may be used to calibrate experimental quench rates, once an accurate scale has been determined.

Conclusions

The speciation of water in rhyolitic liquids has been experimentally determined as a function of temperature and water content. Relaxation analyses have demonstrated the ability of rapid-quench apparatus to quench in the equilibrium speciation of some hydrous rhyolitic samples held at and below 600°C. These results are used to formulate a regular solution model to describe the speciation of rhyolitic melts at any pressure and temperature. It has previously been shown that the rapid-quench apparatus can not preserve the equilibrium speciation in samples quenched from 850°C. Rather, they preserve the speciation at the fictive temperature of the glass. The speciation at the fictive temperature of re-equilibrated samples quenched at variable rates can be used to extract the viscosity of hydrous rhyolitic liquids at any temperature and water content. The viscosities predicted by this analysis are somewhat different from previous empirical determinations of the viscosity of hydrous liquids, especially at low temperatures.

Preliminary experiments have been performed on melts of end-member compositions to determine the effect of the anhydrous melt composition on the speciation of water in silicate melt. These results are inconclusive at present, but indicate that much can be learned from analyses similar to those performed on the rhyolitic compositions. We can now determine the effect of cation chemistry and size on speciation and melt viscosity, address the nature of Al-O-H vs Si-O-H species, and evaluate the possible presence of other hydroxyl species, such as Na-O-H. The analytical methods developed in this study

will address important issues in melt chemistry that have associated applications to igneous petrology.

Sample	Pressure	Temp	H2O,mol	OH	H2O,tot	X(B)	X(H2O)	X(OH)	X(O)	ln (Ks)
KS-100	118	850	0.38	0.77	1.15	0.0206	0.007	0.028	0.966	-2.17
KS-200	223	850	0.65	0.95	1.60	0.0285	0.012	0.034	0.955	-2.27
KS-300	357	850	1.15	1.12	2.27	0.0402	0.020	0.040	0.940	-2.50
KS-400	482	850	1.40	1.17	2.57	0.0454	0.025	0.041	0.934	-2.60
KS-500	522	846	1.55	1.20	2.75	0.0485	0.027	0.042	0.930	-2.65
KS-500X	500	850	1.58	1.13	2.71	0.0478	0.028	0.040	0.932	-2.79
KS-600	717	850	2.03	1.28	3.31	0.0581	0.036	0.045	0.919	-2.78
KS-800	793	850	2.06	1.31	3.37	0.0592	0.036	0.046	0.918	-2.75
KS-900	1044	850	1.87	1.26	3.13	0.0550	0.033	0.044	0.923	-2.73
KS-310	232	850	0.78	0.98	1.76	0.0313	0.014	0.035	0.951	-2.38
KS-311	113	850	0.38	0.83	1.21	0.0217	0.007	0.030	0.963	-2.02
KS-530	366	850	1.26	1.14	2.40	0.0424	0.022	0.040	0.937	-2.55
KS-640	452	850	1.54	1.23	2.77	0.0488	0.027	0.043	0.929	-2.59
KS-650	548	850	1.79	1.26	3.05	0.0537	0.032	0.044	0.924	-2.69
KS-800.2	800	850	2.4097	1.37	3.78	0.0662	0.042	0.048	0.910	-2.81
KSR-800	800	850	2.4736	1.34	3.81	0.0668	0.043	0.047	0.910	-2.88
KS_950	945	850	2.6229	1.35	3.97	0.0695	0.046	0.047	0.907	-2.93
KS-960	960	850	2.4097	1.34	3.75	0.0657	0.042	0.047	0.911	-2.86
KS-1000	1000	850	3.2733	1.45	4.72	0.0821	0.057	0.050	0.893	-3.00
DOBS-152	500	850	1.8126	1.16	2.97	0.0524	0.032	0.041	0.927	-2.87
DOBS-153	1000	850	3.22	1.29	4.51	0.0785	0.056	0.045	0.899	-3.22
DOBS-154	2000	850	4.0303	1.3	5.33	0.0922	0.070	0.045	0.885	-3.42

Table 2.1: The speciation of water in slowly-quenched rhyolitic glasses (composition KS).
Data recast from Silver, 1988 using recalibrated epsilons;
e5200 cm-1 = 1.51 l/mol-cm and e4500 cm-1 = 1.73 l/mol-cm
see chapter 1 for details of calibration
see Table 1.5 for mole fraction calculations

Sample	Pressure	H2O,mol	OH	H2O,tot	X(B)	X(H2O)	X(OH)	X(O)	ln(Ks)
-KS									
PDI07	49	0.110	0.627	0.74	0.013	0.002	0.022	0.976	-1.33
PDI08	156	0.396	0.959	1.36	0.024	0.007	0.034	0.959	-1.75
PDI10	190	0.465	1.019	1.48	0.026	0.008	0.036	0.955	-1.79
PDI05	299	0.714	1.157	1.87	0.033	0.013	0.041	0.946	-1.96
PDI01	500	1.252	1.396	2.65	0.047	0.022	0.049	0.929	-2.13
PDI02	500	1.212	1.384	2.60	0.046	0.021	0.049	0.930	-2.12
PDI04	699	1.782	1.482	3.26	0.057	0.031	0.052	0.917	-2.36
PDI14	799	2.033	1.596	3.63	0.064	0.036	0.056	0.908	-2.34
PDI03	917	2.215	1.593	3.81	0.067	0.039	0.056	0.905	-2.42
PDI15	980	2.385	1.708	4.09	0.071	0.042	0.060	0.899	-2.35
PDI11	1470	3.517	1.774	5.29	0.092	0.061	0.061	0.878	-2.65
PDI13	1260	2.823	1.671	4.49	0.078	0.049	0.058	0.893	-2.56
PDI09	98	0.097	0.617	0.71	0.013	0.002	0.022	0.976	-1.24
PDI06	1080	2.192	1.562	3.75	0.066	0.038	0.055	0.907	-2.45
PDI10.3-c	190	0.430	1.000	1.43	0.026	0.008	0.036	0.957	-1.75
-GB									
GB3-7c	202	0.216	0.7968	1.0125	0.018	0.004	0.029	0.968	-1.52
GB3-8	409	1.011	1.2987	2.3094	0.041	0.018	0.046	0.936	-2.07
GB3-9	1206	2.755	1.7015	4.4563	0.078	0.048	0.059	0.893	-2.50
GB3-12	1066	2.279	1.6650	3.9436	0.069	0.040	0.058	0.902	-2.36
GB3-13	1362	3.149	1.7457	4.8950	0.085	0.055	0.061	0.885	-2.58
GB3-18	501	1.084	1.2705	2.3543	0.042	0.019	0.045	0.936	-2.18
GB3-19	498	1.084	1.3210	2.4046	0.043	0.019	0.047	0.934	-2.10
GB3-20a c	795	1.874	1.5749	3.4486	0.061	0.033	0.055	0.912	-2.28
GB3-20a e	795	1.898	1.5490	3.4475	0.060	0.033	0.054	0.912	-2.33
GB3-20b c	795	2.001	1.6160	3.6168	0.063	0.035	0.057	0.908	-2.30
GB3-20b e	795	1.946	1.5827	3.5291	0.062	0.034	0.056	0.910	-2.31
GB3-21 e	775	1.855	1.5716	3.4268	0.060	0.033	0.055	0.912	-2.28
GB4-43 c	546	1.065	1.2713	2.3367	0.041	0.019	0.045	0.936	-2.16
GB4-43 e	546	1.128	1.3658	2.4938	0.044	0.020	0.048	0.932	-2.08
GB4-45 c	486	1.208	1.4312	2.6396	0.047	0.021	0.051	0.928	-2.05
GB4-45 e	486	1.098	1.4104	2.5082	0.044	0.019	0.050	0.931	-1.98
GB3-25.c	500	1.436	1.3927	2.8284	0.050	0.025	0.049	0.926	-2.27
GB3-25.e	500	1.428	1.3561	2.7837	0.049	0.025	0.048	0.927	-2.32
GB3-26.c	498	1.353	1.4238	2.7773	0.049	0.024	0.050	0.926	-2.17
GB3-44.c	518	1.585	1.3647	2.9493	0.052	0.028	0.048	0.924	-2.41
GB4-52.c	1590	3.395	1.7560	5.1513	0.089	0.059	0.061	0.880	-2.64
GB4-52.e	1590	3.390	1.7675	5.1579	0.089	0.059	0.061	0.880	-2.62
GB4-64.c	501	1.318	1.4210	2.7386	0.048	0.023	0.050	0.927	-2.15
GB4-65.c	501	1.361	1.4251	2.7861	0.049	0.024	0.050	0.926	-2.17
GB4-71.c	1204	2.831	1.6453	4.4761	0.078	0.049	0.057	0.893	-2.60
GB4-73.c	1410	3.364	1.7428	5.1071	0.088	0.058	0.060	0.881	-2.65
GB4-73.e	1410	3.330	1.7551	5.0855	0.088	0.058	0.061	0.881	-2.62
GB4-76.c	1002	2.570	1.6743	4.2441	0.074	0.045	0.058	0.897	-2.47
GB4-76.e	1002	2.596	1.6701	4.2658	0.074	0.045	0.058	0.896	-2.48

Table 2.2: The speciation of water in rapidly-quenched rhyolitic glasses (compositions KS & GB)
Water contents determined using e5200 cm-1 = 1.51 l/mol-cm and
e4500 cm-1 = 1.73 l/mol-cm (see chapter 1 for details of calibration)
see Table 1.5 for mole fraction calculations

Sample	Temperature (C)	H2O,mol	OH	H2O,tot	X(B)	X(H2O)	X(OH)	X(O)	ln (Ks)
Stolper data									
LT-26	400	0.78	0.75	1.53	0.0272	0.0139	0.0267	0.9594	-2.924
LT-27	400	0.67	0.7	1.37	0.0245	0.0120	0.0250	0.9630	-2.918
LT-28	400	0.60	0.68	1.28	0.0228	0.0107	0.0243	0.9651	-2.859
LT-33	400	0.30	0.59	0.89	0.0159	0.0053	0.0211	0.9735	-2.456
LT-34	400	0.30	0.59	0.89	0.0159	0.0053	0.0211	0.9735	-2.456
LT-35	400	0.30	0.57	0.87	0.0156	0.0053	0.0204	0.9742	-2.525
LT-45	400	0.30	0.58	0.88	0.0157	0.0053	0.0208	0.9739	-2.490
LT-51	400	0.27	0.54	0.81	0.0145	0.0048	0.0194	0.9759	-2.521
LT-52	420	0.26	0.53	0.79	0.0141	0.0046	0.0190	0.9764	-2.518
LT-50	430	0.26	0.57	0.83	0.0148	0.0046	0.0204	0.9750	-2.371
LT-53	431	0.26	0.52	0.78	0.0139	0.0046	0.0186	0.9768	-2.556
LT-29	450	0.78	0.85	1.63	0.0290	0.0139	0.0303	0.9559	-2.671
LT-31	450	0.81	0.87	1.68	0.0299	0.0144	0.0310	0.9546	-2.664
LT-32	450	0.83	0.88	1.71	0.0305	0.0148	0.0313	0.9539	-2.667
LT-22	455	0.83	0.89	1.72	0.0306	0.0148	0.0317	0.9535	-2.644
LT-36	485	0.26	0.55	0.81	0.0144	0.0046	0.0197	0.9757	-2.443
LT-38	487	0.25	0.58	0.83	0.0148	0.0044	0.0208	0.9748	-2.294
LT-46	487	0.27	0.59	0.86	0.0153	0.0048	0.0211	0.9741	-2.343
LT-16	496	0.49	0.76	1.25	0.0223	0.0088	0.0271	0.9641	-2.439
LT-13	497	0.50	0.79	1.29	0.0231	0.0089	0.0282	0.9628	-2.382
LT-20	500	0.85	0.87	1.72	0.0307	0.0152	0.0310	0.9539	-2.715
LT-30	500	0.75	0.93	1.68	0.0298	0.0133	0.0331	0.9536	-2.447
LT-23	502	0.70	0.9	1.60	0.0286	0.0125	0.0321	0.9554	-2.455
LT-14	507	0.52	0.8	1.32	0.0236	0.0093	0.0286	0.9621	-2.398
LT-25	512	0.22	0.64	0.86	0.0155	0.0040	0.0229	0.9731	-2.004
LT-37	529	0.22	0.58	0.80	0.0144	0.0040	0.0208	0.9752	-2.203
LT-40	530	0.21	0.58	0.79	0.0142	0.0038	0.0208	0.9754	-2.154
LT-47	530	0.23	0.6	0.83	0.0150	0.0042	0.0215	0.9743	-2.181
LT-15	539	0.44	0.8	1.24	0.0221	0.0078	0.0286	0.9636	-2.220
LT-17	543	0.44	0.8	1.24	0.0221	0.0078	0.0286	0.9636	-2.220
LT-1	547	0.35	0.72	1.07	0.0192	0.0063	0.0258	0.9680	-2.217
LT-4	547	0.53	0.88	1.41	0.0252	0.0095	0.0314	0.9591	-2.225
LT-6	547	0.48	0.82	1.30	0.0232	0.0086	0.0293	0.9622	-2.263
LT-8	547	0.48	0.84	1.32	0.0236	0.0086	0.0300	0.9614	-2.214
LT-10	547	0.18	0.55	0.73	0.0131	0.0033	0.0197	0.9770	-2.099
LT-24	549	0.59	0.87	1.46	0.0260	0.0105	0.0310	0.9585	-2.343
LT-39	580	0.19	0.61	0.80	0.0144	0.0034	0.0219	0.9747	-1.948
LT-42	580	0.18	0.59	0.77	0.0138	0.0032	0.0212	0.9756	-1.958
LT-48	580	0.20	0.62	0.82	0.0147	0.0036	0.0222	0.9741	-1.969
LT-18	595	0.35	0.8	1.15	0.0206	0.0063	0.0286	0.9651	-2.004
LT-2	597	0.33	0.73	1.06	0.0190	0.0059	0.0261	0.9680	-2.127
LT-5	597	0.06	0.38	0.44	0.0080	0.0012	0.0137	0.9852	-1.803
LT-7	597	0.53	0.90	1.43	0.0256	0.0095	0.0321	0.9584	-2.179
LT-9	597	0.39	0.80	1.19	0.0213	0.0070	0.0286	0.9644	-2.118
LT-11	597	0.16	0.57	0.73	0.0131	0.0029	0.0204	0.9767	-1.902
LT-41	620	0.17	0.6	0.77	0.0138	0.0031	0.0215	0.9754	-1.863
LT-44	621	0.16	0.61	0.77	0.0138	0.0029	0.0219	0.9753	-1.766
LT-49	621	0.18	0.62	0.80	0.0144	0.0032	0.0222	0.9745	-1.858
LT-3	642	0.32	0.74	1.06	0.0190	0.0057	0.0265	0.9678	-2.067
LT-12	642	0.15	0.58	0.73	0.0131	0.0027	0.0208	0.9765	-1.798
LT-43	660	0.15	0.6	0.75	0.0134	0.0027	0.0215	0.9758	-1.730
LT-19	700	0.74	1.05	1.79	0.0318	0.0131	0.0373	0.9496	-2.187
LT-21	900	0.82	1.12	1.94	0.0345	0.0146	0.0398	0.9456	-2.165

Table 2.3a: The speciation of water in rhyolitic glasses equilibrated at 1 atm
Data recast from Stolper, 1989 using recalibrated epsilons;
e5200 cm-1 = 1.51 l/mol-cm and e4500 cm-1 = 1.73 l/mol-cm
see chapter 1 for details of calibration
see Table 1.5 for mole fraction calculations

Sample	Temperature (C)	H2O,mol	OH	H2O,tot	X(B)	X(H2O)	X(OH)	X(O)	ln (Ks)
Zhang data									
3a-D1a1	600	1.04	1.30	2.34	0.0415	0.0185	0.0460	0.9355	-2.100
3a-D2c	600	1.07	1.27	2.34	0.0414	0.0189	0.0450	0.9361	-2.168
3b-D6a	600	0.51	0.93	1.44	0.0256	0.0091	0.0331	0.9578	-2.077
POB10-D1c	600	0.32	0.75	1.06	0.0190	0.0057	0.0267	0.9676	-2.038
POB1-D2a	600	0.22	0.65	0.87	0.0156	0.0040	0.0232	0.9728	-1.979
Ka-D2	590	0.17	0.55	0.71	0.0128	0.0030	0.0196	0.9774	-2.025
3a-D2c	550	1.15	1.20	2.35	0.0416	0.0204	0.0425	0.9371	-2.359
3b-D6a	550	0.58	0.89	1.47	0.0262	0.0104	0.0317	0.9579	-2.292
3b-D1b1	550	0.88	0.46	1.34	0.0240	0.0158	0.0163	0.9679	-4.051
3b-D1b2	550	0.50	0.84	1.34	0.0238	0.0088	0.0300	0.9612	-2.247
3b-D1b3	550	0.49	0.83	1.32	0.0236	0.0087	0.0297	0.9616	-2.256
3b-D1b4	550	0.48	0.82	1.30	0.0232	0.0086	0.0292	0.9622	-2.270
KS-D4b.1	550	0.22	0.59	0.81	0.0146	0.0040	0.0210	0.9749	-2.184
KS-D4b.2	550	0.21	0.57	0.77	0.0139	0.0037	0.0203	0.9759	-2.175
Ka-D1a	550	0.21	0.57	0.78	0.0140	0.0038	0.0204	0.9758	-2.184
3b-D5dif	550	0.08	0.37	0.45	0.0082	0.0015	0.0133	0.9852	-2.114
3b-D3	530	0.42	0.75	1.16	0.0208	0.0075	0.0266	0.9659	-2.320
KS-D2	530	0.25	0.60	0.85	0.0153	0.0045	0.0215	0.9740	-2.251
3a-D2d.P	500	1.42	1.23	2.65	0.0468	0.0250	0.0435	0.9315	-2.514
3b-D1b.1P	500	0.57	0.81	1.38	0.0245	0.0101	0.0289	0.9610	-2.451
3b-D1b.3P	500	0.55	0.80	1.35	0.0241	0.0098	0.0286	0.9616	-2.447
3a-D1b.P	500	0.55	0.80	1.35	0.0241	0.0098	0.0285	0.9617	-2.456
POB10-D2a	500	0.40	0.68	1.08	0.0193	0.0071	0.0244	0.9685	-2.452
6b-D1.1	500	0.32	0.63	0.95	0.0170	0.0057	0.0225	0.9718	-2.405
6b-D1.2	500	0.36	0.66	1.03	0.0184	0.0065	0.0237	0.9698	-2.420
POB1-D1a	500	0.30	0.62	0.91	0.0163	0.0053	0.0220	0.9726	-2.368
KS-D3b	500	0.26	0.58	0.84	0.0150	0.0047	0.0207	0.9747	-2.363
3b-D1	490	0.58	0.78	1.36	0.0242	0.0103	0.0278	0.9619	-2.546
POB10-D3	490	0.43	0.69	1.12	0.0200	0.0076	0.0247	0.9676	-2.487
KS-D3	490	0.27	0.57	0.84	0.0150	0.0048	0.0204	0.9748	-2.423
POB1-D3	482	0.31	0.59	0.90	0.0161	0.0056	0.0210	0.9734	-2.514
3b-D1c	450	0.56	0.70	1.26	0.0226	0.0100	0.0251	0.9649	-2.734
POB10-D1c	450	0.50	0.67	1.16	0.0208	0.0089	0.0238	0.9673	-2.721
KS-D5a	450	0.32	0.54	0.86	0.0154	0.0058	0.0192	0.9750	-2.721
Mn-D1a	450	0.28	0.51	0.78	0.0140	0.0049	0.0182	0.9769	-2.676

Table 2.3b: The speciation of water in rhyolitic glasses equilibrated at 1 atm
Data recast from Zhang et al., 1990 using recalibrated epsilons;
e5200 cm-1 = 1.51 l/mol-cm and e4500 cm-1 = 1.73 l/mol-cm
see chapter 1 for details of calibration
see Table 1.5 for mole fraction calculations

SAMPLE	Pressure (bars)	Temp (C)	time (hrs)	density	H2O,mol abs/cm	OH abs/cm	thickness	H2O,mol	OH	H2O,tot	X(B)	X(H2O)	X(OH)	X(O)	ln(Ks)	used in regr?
500°C																
LPR1.411	994	500°C	60m	2304	0.308	0.224	6.75E-04	2.36	1.50	3.86	0.067	0.041	0.052	0.906	-2.62	X
LPR2.411	994	500°C	60m	2291	0.366	0.215	5.94E-04	3.21	1.64	4.85	0.084	0.056	0.057	0.887	-2.73	X
LPR3.411	994	500°C	60m	2300	0.322	0.220	6.36E-04	2.63	1.57	4.19	0.073	0.046	0.055	0.900	-2.63	X
MC84.211	994	500°C	60m	2336	0.082	0.134	7.33E-04	0.57	0.81	1.39	0.025	0.010	0.029	0.961	-2.45	X
GB45.211	994	500°C	60m	2318	0.083	0.081	2.88E-04	1.49	1.26	2.75	0.049	0.026	0.045	0.929	-2.51	X
Q8.211	994	500°C	60m	2311	0.264	0.220	7.08E-04	1.93	1.40	3.33	0.058	0.034	0.049	0.917	-2.56	X
gran min	994	500°C	60m	2310	0.210	0.182	5.62E-04	1.93	1.46	3.39	0.059	0.034	0.051	0.915	-2.48	X
475°C																
MC84.311		475°C	7	2354	0.051	0.075	4.22E-04	0.61	0.78	1.40	0.025	0.011	0.028	0.961	-2.61	X
GB45.311		475°C	7	2336	0.118	0.106	3.96E-04	1.52	1.19	2.71	0.048	0.027	0.042	0.931	-2.65	X
Q3.311		475°C	7	2319	0.219	0.171	5.35E-04	2.11	1.44	3.54	0.062	0.037	0.050	0.913	-2.59	
530°C																
LPR1.111e	744	530°C	10m	2303	0.577	0.430	1.25E-03	2.39	1.56	3.95	0.069	0.042	0.054	0.904	-2.55	X
LPR2.111	744	530°C	10m	2293	0.738	0.465	1.26E-03	3.05	1.68	4.73	0.082	0.053	0.058	0.889	-2.63	X
LPR3.111	744	530°C	10m	2298	0.654	0.450	1.27E-03	2.68	1.61	4.30	0.075	0.047	0.056	0.897	-2.59	X
LPR3.112	744	530°C	10m	2298	0.650	0.449	1.26E-03	2.68	1.61	4.29	0.075	0.047	0.056	0.897	-2.59	
650°C																
LPR1.311	1036	650°C	15m	2300	0.612	0.443	1.24E-03	2.55	1.61	4.16	0.073	0.045	0.056	0.899	-2.54	
LPR1.312	1036	650°C	15m	2301	0.606	0.430	1.25E-03	2.52	1.56	4.08	0.071	0.044	0.054	0.902	-2.60	
LPR3.311	1036	650°C	15m	2296	0.686	0.450	1.26E-03	2.84	1.62	4.47	0.078	0.049	0.056	0.894	-2.63	
LPR3.312	1036	650°C	15m	2295	0.712	0.453	1.26E-03	2.93	1.63	4.56	0.079	0.051	0.056	0.892	-2.66	
LPR3.313	1036	650°C	15m	2295	0.695	0.456	1.26E-03	2.88	1.65	4.53	0.079	0.050	0.057	0.893	-2.61	
600°C																
LPR1.221	1005	600°C	2m	2303	0.399	0.272	8.37E-04	2.47	1.47	3.94	0.069	0.043	0.051	0.906	-2.70	
LPR2.222	1005	600°C	2m	2289	0.500	0.278	7.69E-04	3.39	1.65	5.04	0.087	0.059	0.057	0.884	-2.78	
LPR3.222	1005	600°C	2m	2297	0.380	0.229	6.84E-04	2.88	1.52	4.40	0.077	0.050	0.053	0.897	-2.78	
MC84.411	1005	600°C	2m	2336	0.054	0.106	5.51E-04	0.50	0.86	1.36	0.024	0.009	0.030	0.961	-2.22	
GB45.411	1005	600°C	2m	2318	0.184	0.167	6.17E-04	1.53	1.22	2.75	0.048	0.027	0.043	0.930	-2.61	
gran min	1005	600°C	2m	2309	0.152	0.111	3.69E-04	2.12	1.35	3.48	0.061	0.037	0.047	0.915	-2.72	
Q8.411	1005	600°C	2m	2312	0.201	0.156	5.35E-04	1.94	1.31	3.25	0.057	0.034	0.046	0.920	-2.70	
new 600°C																
LPR1.231	1002	600°C	20m	2303	0.125	0.104	2.82E-04	2.29	1.67	3.96	0.069	0.040	0.058	0.902	-2.37	
LPR2.231	1002	600°C	20m	2289	0.178	0.112	2.87E-04	3.24	1.78	5.02	0.087	0.056	0.061	0.882	-2.58	
LPR3.231	1002	600°C	20m	2298	0.109	0.082	2.18E-04	2.59	1.70	4.29	0.075	0.045	0.059	0.896	-2.45	
MC84.421	1002	600°C	20m	2337	0.014	0.031	1.60E-04	0.44	0.87	1.30	0.023	0.008	0.031	0.961	-2.06	X
GB45.421	1002	600°C	20m	2320	0.090	0.112	3.68E-04	1.25	1.36	2.62	0.046	0.022	0.048	0.930	-2.19	X
Q8.421	1002	600°C	20m	2312	0.155	0.158	4.72E-04	1.69	1.51	3.20	0.056	0.030	0.053	0.917	-2.27	X
450°C																
LPR1.211	551	450°C	130m	2304	0.587	0.377	1.24E-03	2.45	1.37	3.82	0.067	0.043	0.048	0.909	-2.83	X
LPR2.211	551	450°C	130m	2287	0.884	0.430	1.26E-03	3.67	1.56	5.22	0.090	0.063	0.054	0.883	-2.97	X

Table 2.4: The speciation of water in rapidly-quenched rhyolitic glasses
Water contents determined using ε5200 cm-1 = 1.51 l/mol-cm and ε4500 cm-1 = 1.73 l/mol-cm (see chapter 1 for details of calibration)
see Table 1.5 for mole fraction calculations

SAMPLE	Starting material	Pressure (bars)	Temp (C)	time (hrs)	H2O Hmltn	H2O,mol	OH	H2O,tot	X(B)	X(H2O)	X(OH)	X(O)	ln(Ks)	Comments	110°C
Starting Mtl															
CT-18.001	center	1400	1300	18hr	2.13	1.26	0.98	2.24	0.040	0.021	0.039	0.941	-2.568	hot saturated	2 days
CT-18.002	edge	1400	1300	18hr	2.13	1.22	0.94	2.16	0.039	0.020	0.037	0.943	-2.616		
CT-19.001	center	1400	1300	18hr	2.41	1.32	0.99	2.31	0.041	0.022	0.039	0.939	-2.594	just sat	1 day
CT-19.002	edge	1400	1300	18hr	2.41	1.15	0.93	2.08	0.037	0.019	0.037	0.944	-2.587		
CT-16.001	center	2000	1250	23hr	3.20	1.83	1.09	2.92	0.052	0.030	0.044	0.926	-2.661	hot saturated	2 days
CT-16.002	NW	2000	1250	23hr	3.20	2.01	1.08	3.09	0.055	0.033	0.044	0.923	-2.749		
CT-16.003	NE	2000	1250	23hr	3.20	1.96	1.09	3.05	0.054	0.032	0.044	0.924	-2.716		
CT-16.004	SW	2000	1250	23hr	3.20	1.95	1.08	3.02	0.054	0.032	0.044	0.924	-2.730		
CT-13.001	center	2000	1250	23hr	3.60	2.10	1.08	3.18	0.056	0.034	0.044	0.921	-2.788	sat	2 days
CT-13.002	NW	2000	1250	23hr	3.60	2.56	1.05	3.61	0.064	0.042	0.044	0.914	-2.975	sat	
CT-13.003	NE	2000	1250	23hr	3.60	2.57	1.09	3.65	0.065	0.042	0.046	0.913	-2.911	sat	
CT-13.004	SE	2000	1250	23hr	3.60	2.54	1.06	3.60	0.064	0.041	0.045	0.914	-2.944	sat	
CT-15.001	center	2000	1250	23 hr	4.10	2.63	1.03	3.66	0.065	0.043	0.044	0.913	-3.017	sat	2 days
CT-15.002	NW	2000	1250	23 hr	4.10	2.57	1.05	3.62	0.064	0.042	0.044	0.914	-2.970	sat	
CT-15.003	SW	2000	1250	23 hr	4.10	2.54	1.07	3.61	0.064	0.041	0.045	0.914	-2.933	sat	
CT-15.004	SE	2000	1250	23 hr	4.10	2.50	1.02	3.52	0.062	0.041	0.043	0.916	-3.007	sat	
CT-09.002	edge	3000	1250	24 hr	5.00	2.97	1.12	4.09	0.072	0.048	0.048	0.904	-2.953	sat	30 min
Sil-1-600		800	600	2 min		0.99	0.93	1.91	0.034	0.016	0.036	0.948	-2.470	CT18	
Sil-2-600		800	600	2 min		2.00	1.11	3.11	0.055	0.033	0.045	0.922	-2.697	CT16	
Sil-3-600		800	600	2 min		1.64	1.09	2.73	0.049	0.027	0.043	0.930	-2.583	CT16	
Sil-4-600		800	600	2 min		1.15	0.93	2.08	0.037	0.019	0.037	0.944	-2.594	CT19	
Sil-5-600		800	600	2 min		1.98	1.05	3.03	0.054	0.032	0.043	0.925	-2.793	CT19	
Sil-6-600		800	600	2 min		2.05	1.05	3.09	0.055	0.033	0.043	0.924	-2.821	CT19	bubbles
Sil-9-550		800	550	5min		2.35	1.01	3.36	0.060	0.038	0.042	0.919	-2.971	CT18	
Sil-13-550		800	550	5min		2.67	1.04	3.71	0.066	0.043	0.044	0.912	-3.007	CT16	
Sil-15-550		800	550	5min		2.27	1.04	3.31	0.059	0.037	0.043	0.920	-2.900	CT16	
Sil-16-550		800	550	5min		1.89	1.10	3.00	0.053	0.031	0.044	0.925	-2.671	CT19	
Sil-18-550		800	550	5min		1.17	0.99	2.15	0.038	0.019	0.039	0.942	-2.495	CT19	

Table 2.5: The speciation of water in pure silica glass
epsilons from Blank, Silver, and Stolper (unpublished) e5200 = 1.5 l/mol-cm; e4500 = 4.3 l/mol-cm;
experiments CT- were performed in internally-heated apparatus;
experiments Sil- were performed in rapid-quench cold-seal apparatus
see Table 1.5 for mole fraction calculations

SAMPLE	Starting material	Pressure (bars)	Temp (C)	time (hrs)	H2O Hmltn	H2O,mol	OH	H2O,tot	X(B)	X(H2O)	X(OH)	X(O)	ln(Ks)	Comments
SP-3-c	ab core	3000	1100	72	6.8	4.27	2.05	6.32	0.109	0.074	0.071	0.855	-2.53	lt pink
SP-3-e						4.05	1.92	5.97	0.104	0.070	0.067	0.863	-2.61	
SP-6-c	ab core	500	1100	48	2.7	1.19	1.63	2.82	0.050	0.021	0.058	0.921	-1.76	lt yellow; first run
SP-6-e						1.12	1.56	2.68	0.048	0.020	0.056	0.924	-1.78	at 2 kbar, 1100°C
SP-7-c	ab core	2000	1100	48	5.7	3.42	1.94	5.36	0.093	0.060	0.067	0.873	-2.44	yellow
SP-7-e						3.45	1.99	5.44	0.095	0.060	0.069	0.871	-2.39	
SP-8-c	ab powder	2000	1100	48	6.2	3.85	1.95	5.80	0.101	0.067	0.068	0.865	-2.54	not opalescent
SP-8-e						4.02	2.09	6.11	0.106	0.070	0.072	0.858	-2.43	
SP-10-c	ab core	500	1100	48	1.6	0.34	1.10	1.44	0.026	0.006	0.040	0.954	-1.30	zoned yellow;
SP-10-e						0.81	1.52	2.32	0.041	0.014	0.054	0.931	-1.52	capsule leaked to Ar
alb600-1a	SP-3 or 8	800	600	2min		3.48	2.47	5.95	0.103	0.060	0.086	0.854	-1.95	
alb600-1b		800	600	2min		3.46	2.42	5.88	0.102	0.060	0.084	0.856	-1.99	
alb600-2	SP-6	800	600	2min		0.99	1.66	2.65	0.047	0.018	0.059	0.923	-1.54	
alb600-3	SP-10	800	600	2min		0.71	1.43	2.13	0.038	0.013	0.051	0.936	-1.52	
alb600-3+		800	600	2min		0.70	1.41	2.10	0.038	0.012	0.050	0.937	-1.53	
alb600-3-		800	600	2min		0.72	1.45	2.17	0.039	0.013	0.052	0.935	-1.50	
alb600-4	SP-7	800	600	2min		2.98	2.16	5.14	0.090	0.052	0.075	0.873	-2.08	
alb-6 550	SP-6	800	550	5min		1.08	1.73	2.81	0.050	0.019	0.062	0.919	-1.54	
alb-7 550	SP-7	800	550	5min		3.32	2.50	5.82	0.101	0.058	0.087	0.856	-1.88	
alb-8 550	SP-8	800	550	5min		3.58	2.54	6.12	0.106	0.062	0.088	0.850	-1.92	
alb-10 550	SP-10	800	550	5min		0.85	1.60	2.44	0.044	0.015	0.057	0.928	-1.46	

Table 2.6: The speciation of water in albitic glasses
epsilons from Silver and Stolper (1989) e5200 = 1.67 l/mol-cm; e4500 = 1.13 l/mol-cm;
experiments SP 3-10 were performed in internally-heated apparatus with argon as pressure medium;
experiments alb- were performed in rapid-quench cold-seal apparatus with water as pressure medium;
see Table 1.5 for mole fraction calculations

Sample ID	Starting Mtl	Pressure (Kbars)	Temp (C)	Quench Rate (C/min)	H2O,mol	OH	H2O,tot	X(B)	X(H2O)	X(OH)	X(O)	ln (Ks)
QR-60	B17	9.3	1200	1	3.16	1.24	4.40	0.077	0.055	0.043	0.902	-3.28
QR-61	B17	9.3	1200	80	2.71	1.41	4.12	0.072	0.047	0.049	0.903	-2.86
QR-62	B17	9.3	1200	2400	3.07	1.73	4.80	0.083	0.053	0.060	0.887	-2.57
QR-78	B17	4.7	1200	2400	2.18	1.61	3.78	0.066	0.038	0.056	0.906	-2.39
QR-87	B16	9.3	1200	0.1667	3.77	1.48	5.26	0.091	0.065	0.051	0.883	-3.09
QR-88	B16	4.7	1200	100	2.58	1.56	4.14	0.072	0.045	0.054	0.900	-2.62
QR-92	B16	4.7	1200	0.1667	3.27	1.26	4.53	0.079	0.057	0.044	0.899	-3.28
QR-93	B16	9.3	1200	4	3.35	1.38	4.73	0.082	0.058	0.048	0.894	-3.12
QR-B16	LGM	1	850	100	2.97	1.60	4.57	0.080	0.052	0.056	0.893	-2.70
QR-B18	LGM	1	850	4	3.60	1.56	5.16	0.089	0.062	0.054	0.884	-2.94

Table 2.7: The speciation of water in rhyolitic glasses quenched at variable quench rates
experiments QR 60-93 were performed in piston cylinder apparatus;
quench rates set by ramping programmable Eurotherm temperature controller
except QR-62, 78, and B-18; determined by chart recorder measurements,
and B-16; estimated from blast quenching cold-seal vessel
all run durations were for 1 hour plus cooling time
experiments QR B16-18 were performed in slow-quench cold-seal apparatus
see Table 1.5 for mole fraction calculations

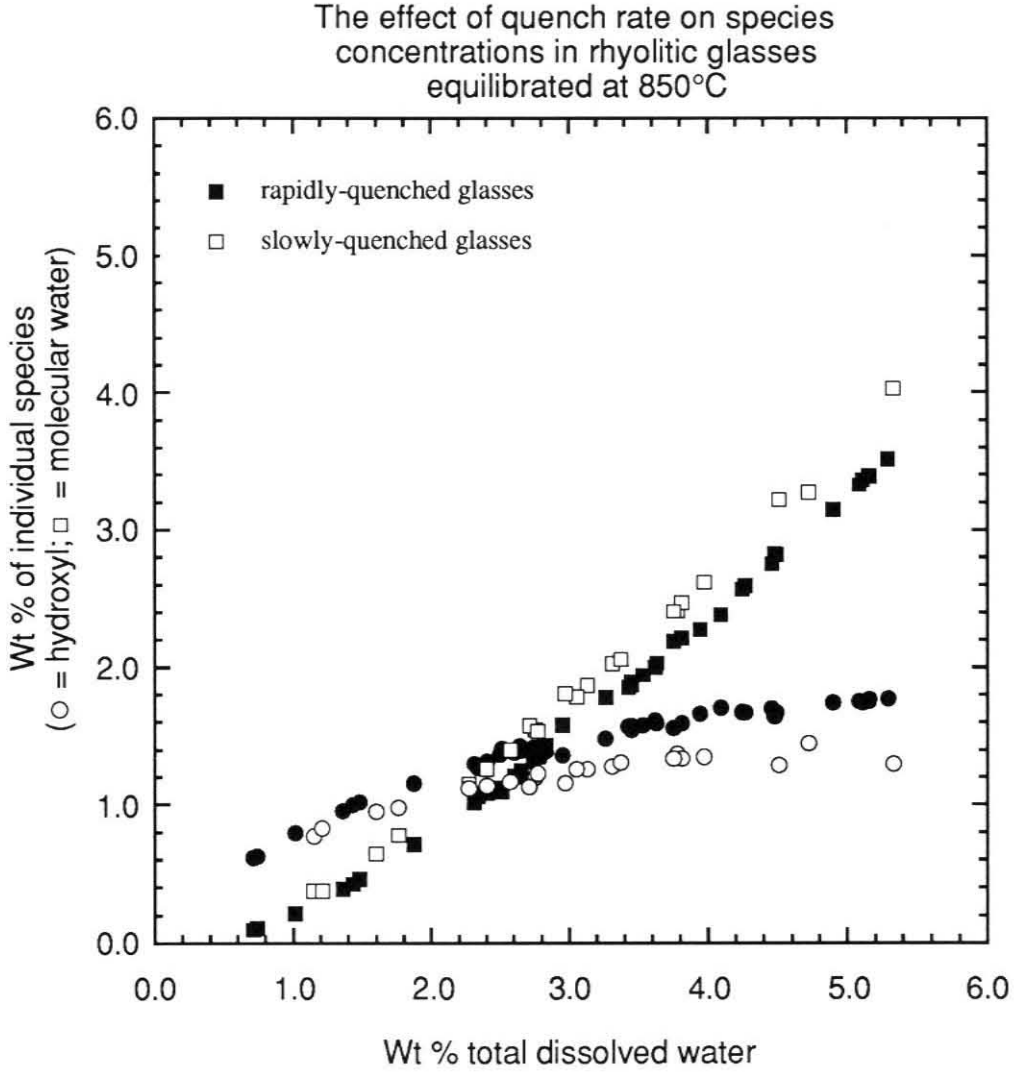

Figure 2.1: The concentration of dissolved water species in water-saturated rhyolitic glasses quenched rapidly (filled symbols) and slowly (hollow symbols) from 850°C in cold-seal pressure vessels. The squares represent the concentration of molecular water species and the circles represent the concentration of hydroxyl groups. Molar absorptivities are calibrated in Chapter 1 (ε_{5200} = 1.51 l/mol cm and ε_{4500} = 1.73 l/mol cm).

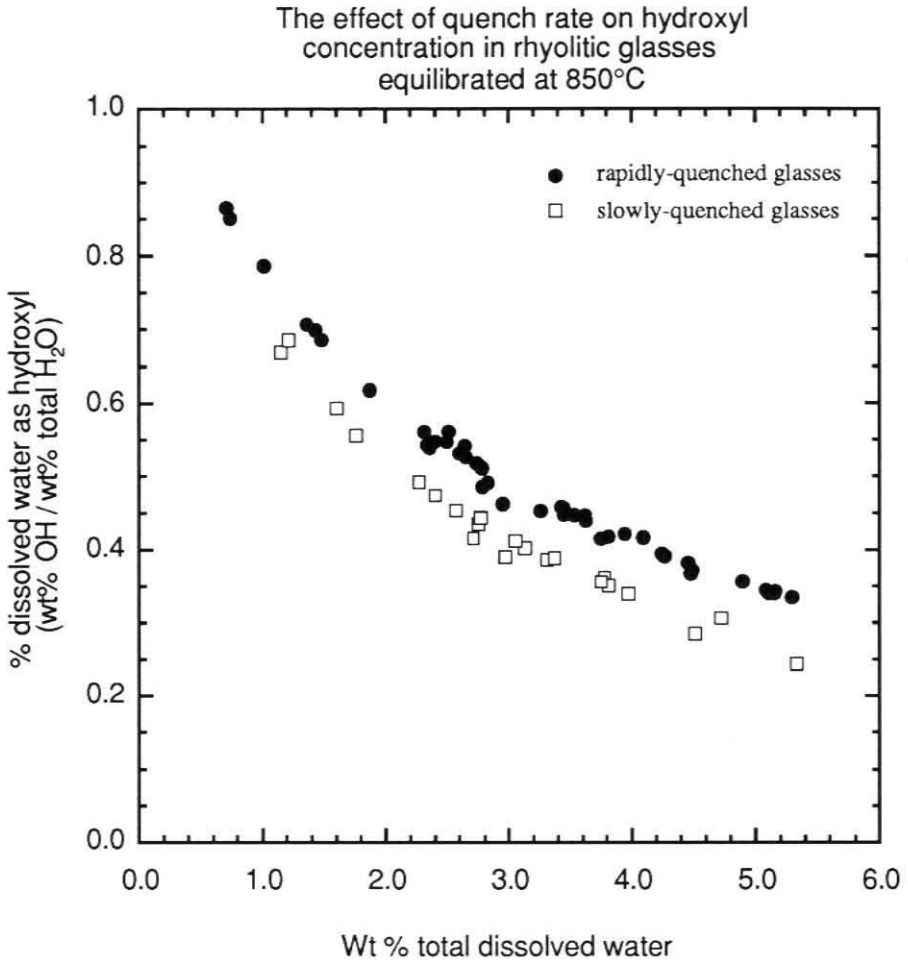

Figure 2.2: The speciation of water in water-saturated rhyolitic glasses expressed as a single parameter; the ratio of the concentration of hydroxyl groups to the concentration of the total dissolved water (wt % OH/ wt % total H2O). The filled circles represent glasses quenched from 850°C in rapid-quench cold seal apparatus, and the hollow squares represent glasses quenched from 850°C in slow-quench cold-seal apparatus. The rapidly-quenched samples have a greater proportion of hydroxyl to molecular water species than the slowly-quenched samples. Both trends indicate that initially, all water dissolves as hydroxyl species.

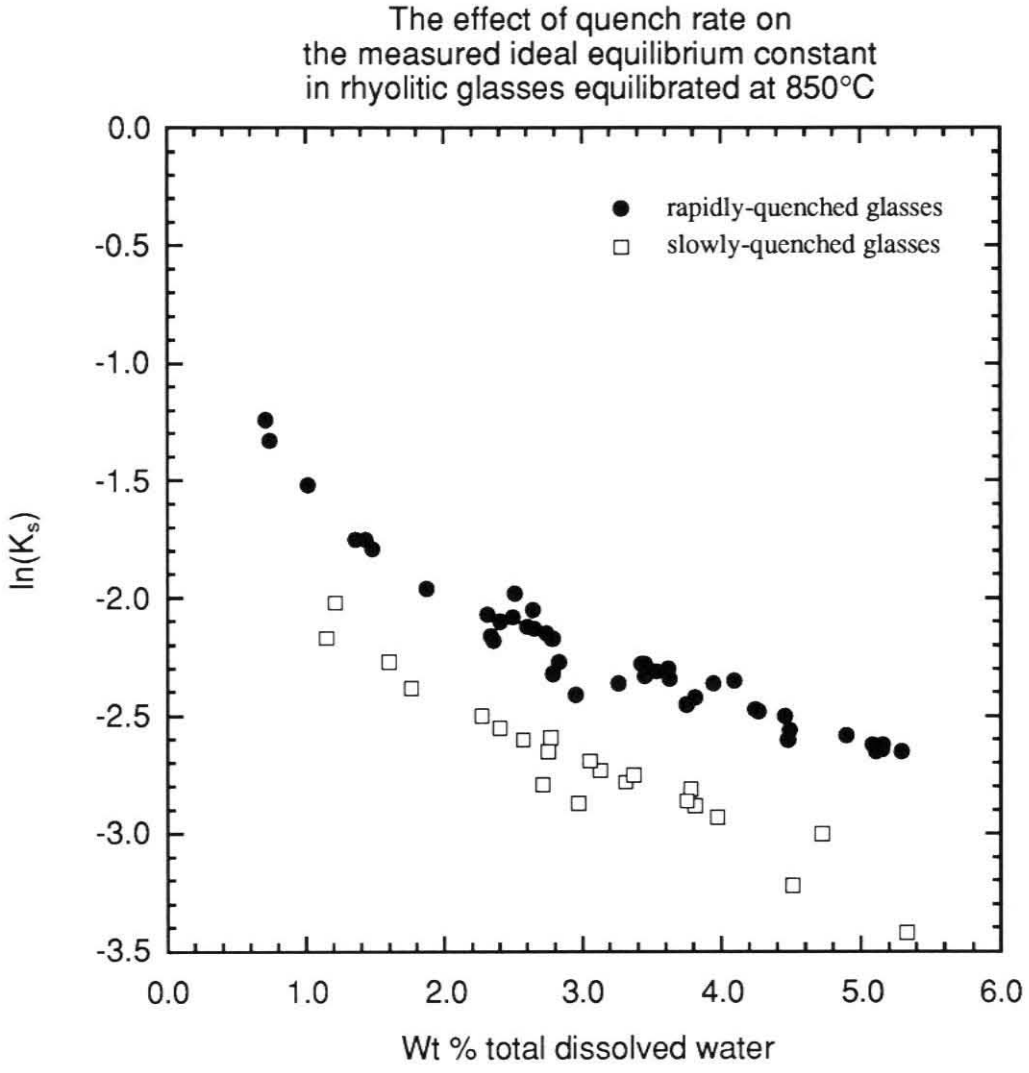

Figure 2.3: The speciation of water in rhyolitic glasses expressed as the natural logarithm of K_S, where K_S is as defined in the text. The two trends parallel one another with increasing water content.

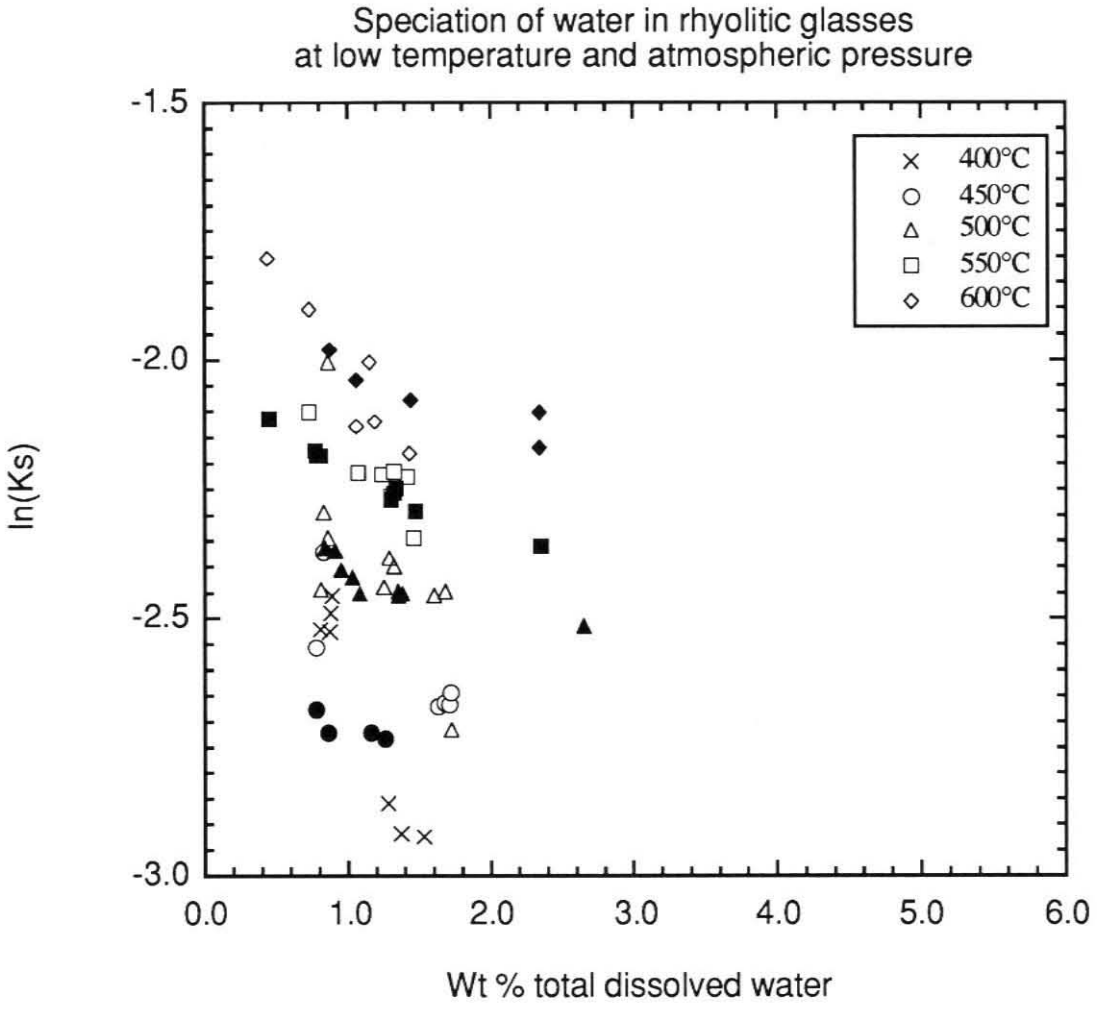

Figure 2.4: The speciation of water in rhyolitic glasses quenched rapidly from 1 atm equilibrium experiments. Hollow symbols are from Stolper (1989) and filled symbols are from Zhang et al. (1990). Both data sets have been recalculated using recalibrated εs for the 5200 cm^{-1} band (see Table 2.3). The temperature of equilibrium for each experiment is given in the legend (Stolper samples are ± 20°C of the indicated temperature). All data indicate decreasing ln (K_S) with increasing water content.

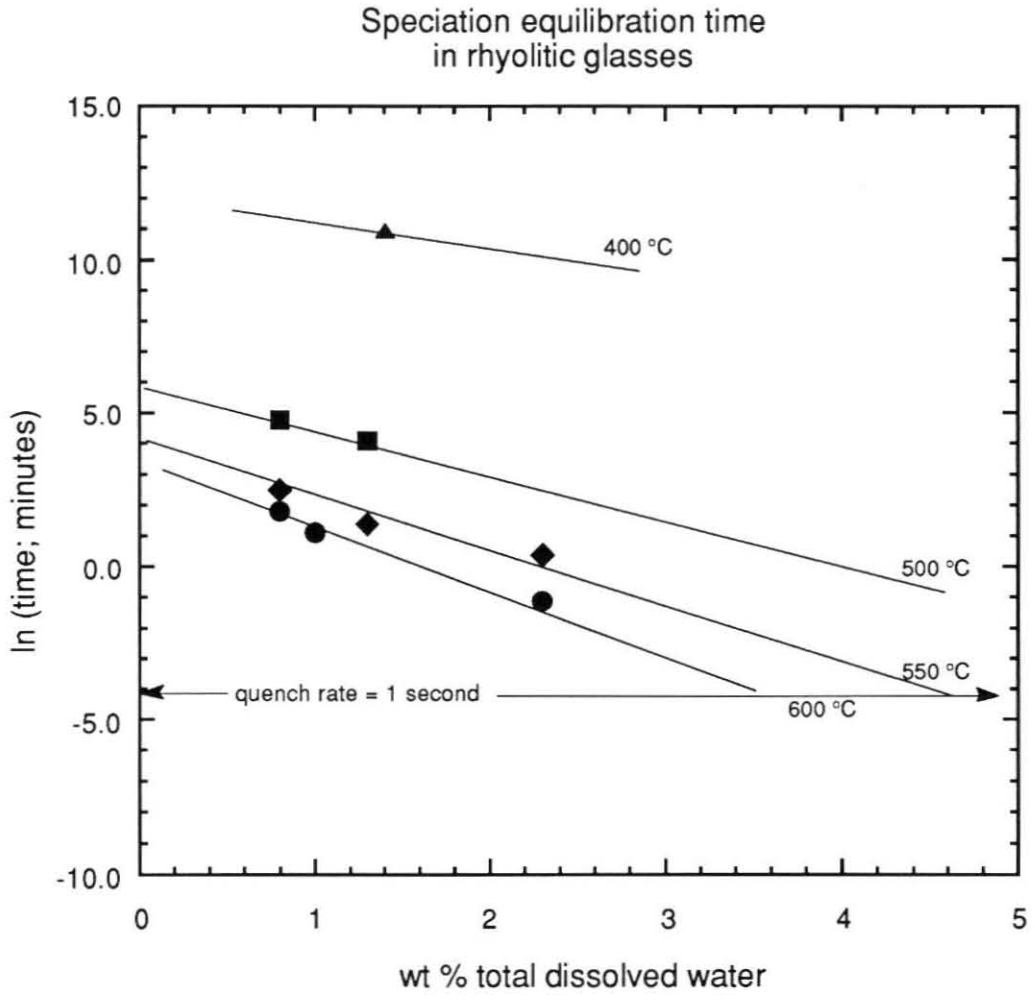

Figure 2.5: The time required for dissolved water species to reach equilibrium in rhyolitic glasses, as measured by Zhang et al. (1990; Appendix 3). Isotherms of 400, 500, 550, and 600°C have been sketched in, demonstrating the influence of temperature and water content on the reaction, $H_2O^{melt} + O^{melt} = 2OH^{melt}$. The quench rate of the rapid-quench apparatus (≈ 1 second) is also shown as a horizontal line.

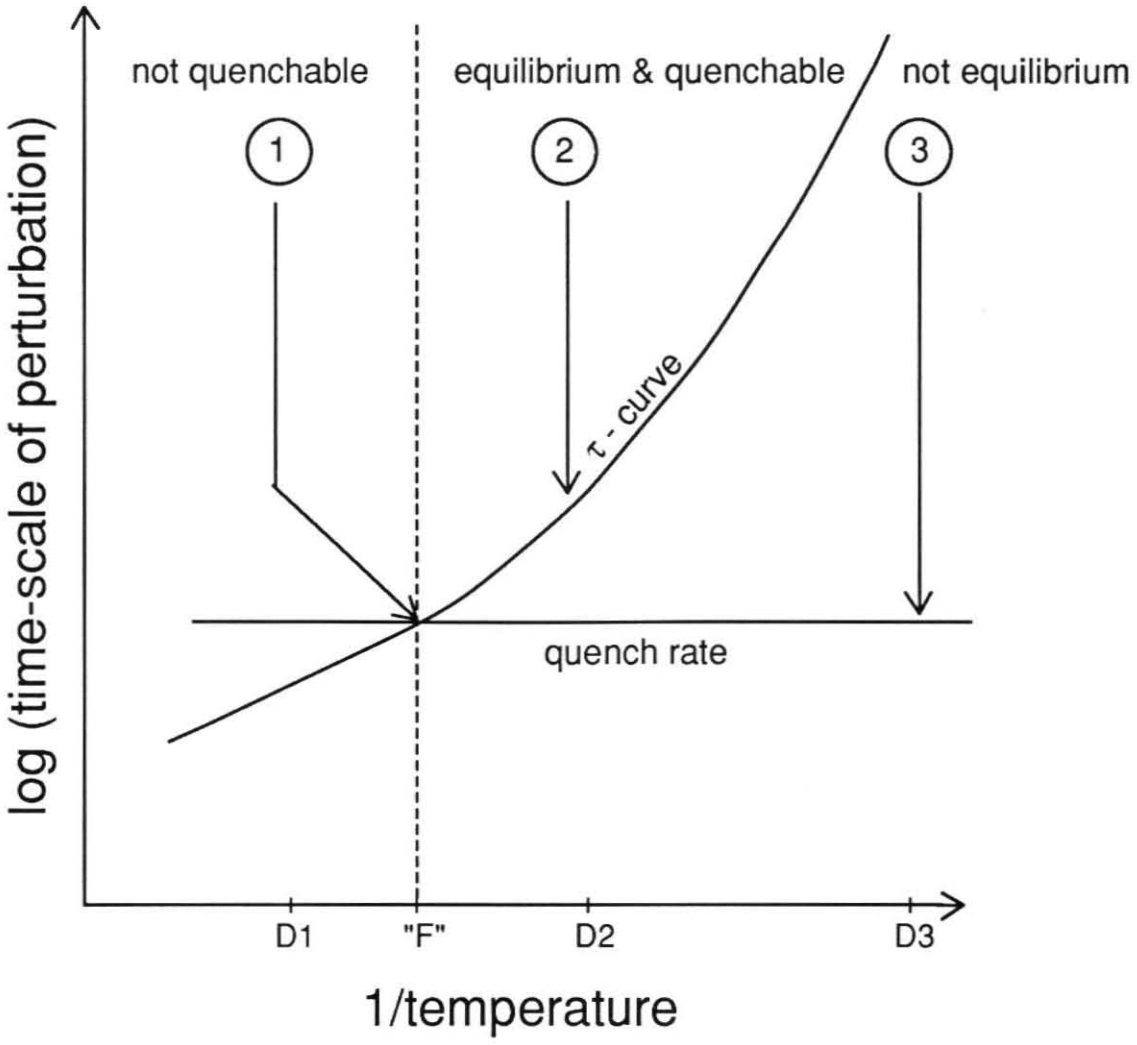

Figure 2.6: Schematic illustration of relaxation theory (after Dingwell and Webb, 1990). The fictive temperature is determined by the intersection of the quench rate curve with the relaxation curve, labeled the τ - curve. Samples above and to the left of the τ-curve (i.e., samples at higher temperatures and experiencing disturbances at shorter timescales) will respond as a liquid, and those below and to the right of the τ-curve will respond as a glass. Experiment 1 will quench in equilibrium conditions at fictive temperature "F," and fail to preserve the equilibrium conditions characteristic at the dwell temperature D1. Experiment 2 will quench in equilibrium conditions at dwell temperature D2. Experiment 3 will quench in the non-equilibrium conditions characteristic of dwell temperature D3.

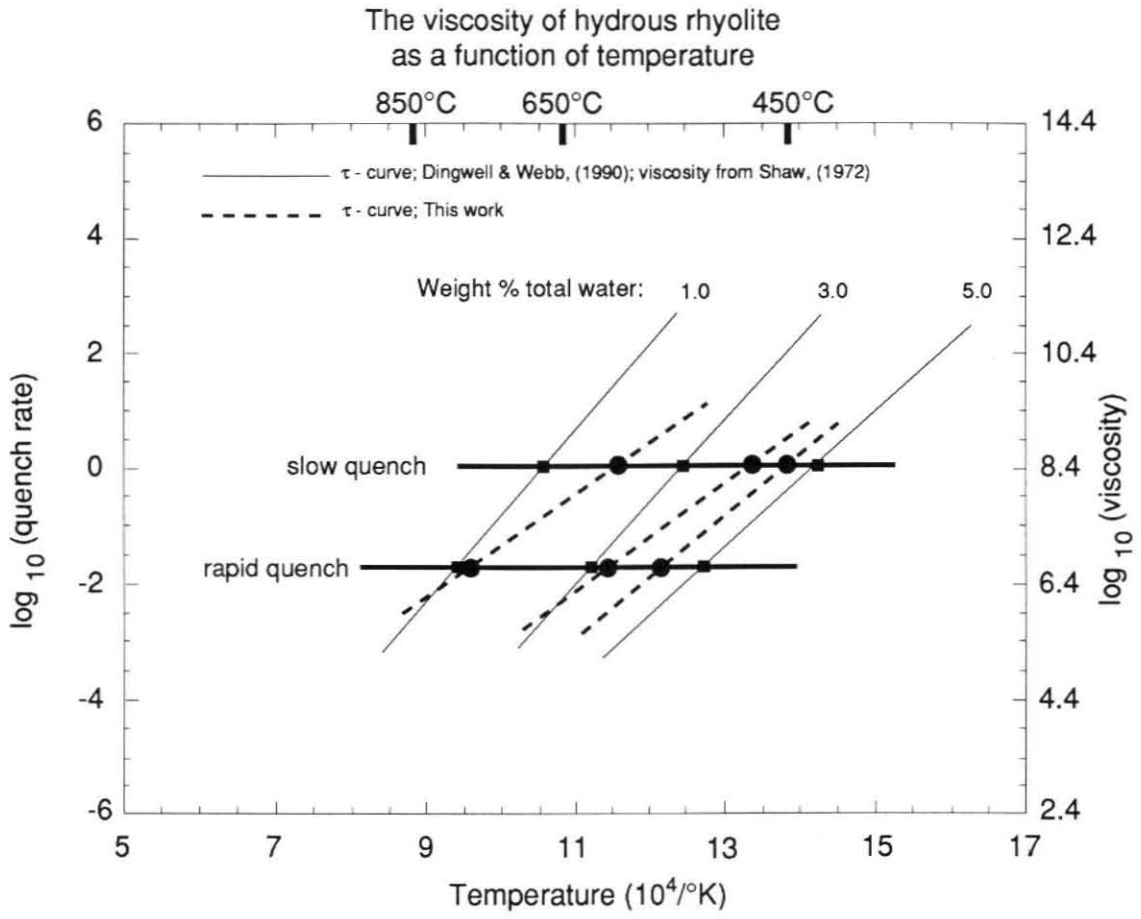

Figure 2.7: Comparison of the dependence of viscosity on temperature and water content in rhyolitic melts between the empirical method of Shaw (1972; after Dingwell and Webb, 1990, Figure 12), shown as squares and solid lines, and the experimental results of this work, shown as circles and dotted lines. Viscosity values are given on the right-hand side of the figure. Temperatures and viscosities for squares were determined using Shaw's 1972 algorithm (calculated by Dingwell and Webb, 1990). Temperatures and quench rates for circles were determined by estimating intersection of equilibrium isotherms (see Fig. 2.8) with respective fictive temperature curves (see Fig. 2.3).

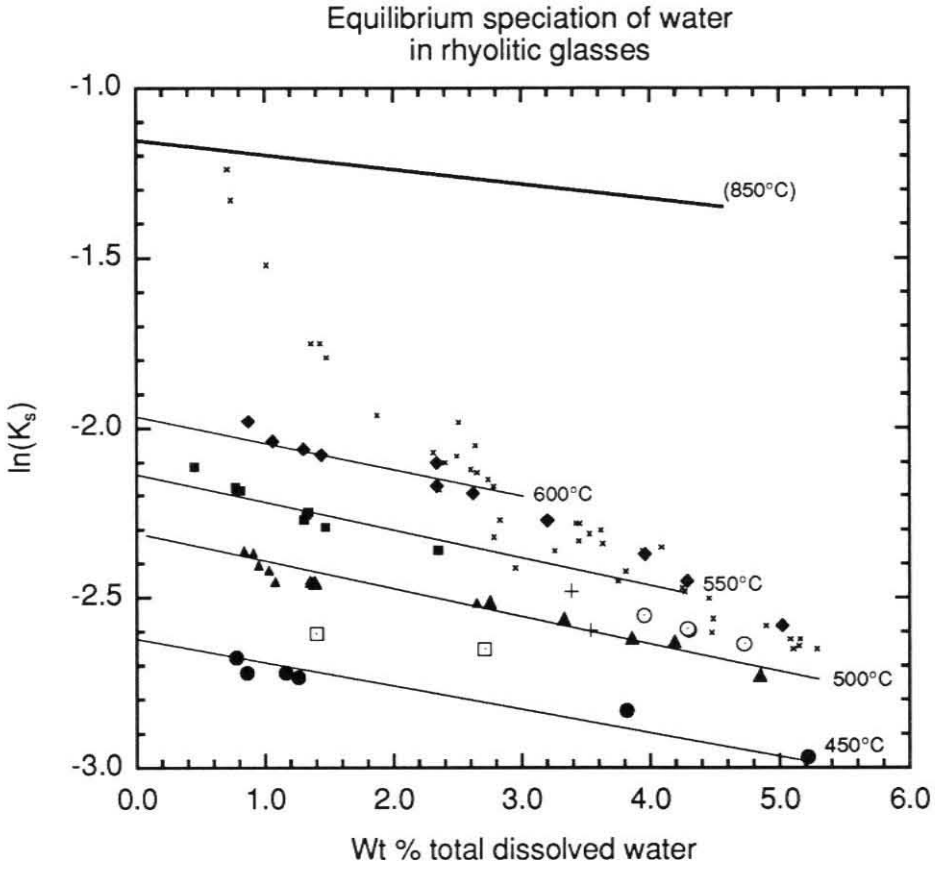

Figure 2.8: The equilibrium speciation of water in rhyolitic glasses held at temperatures below their associated closure temperatures as defined in Fig. 2.6. Samples were quenched in ≈ 2 seconds. Data from this work (Table 2.4) and Zhang et al. (1990; Table 2.3 and Appendix 3). The following symbols represent the respective temperatures of equilibration: diamonds = 600°C, squares = 550°C, hollow circles = 530°C, triangles = 500°C, hollow squares = 475°C, filled circles = 450°C, pluses = haplogranitic composition at 500°C (higher ln Ks value) and 475°C (lower ln Ks value). Isotherms indicate dependence of speciation on water content. xs show the speciation of water measured in glasses quenched rapidly from 850°C and represent the locus of fictive temperatures defined by the quench rate of the apparatus at each water content. (850°C) is the model-predicted isotherm (see text).

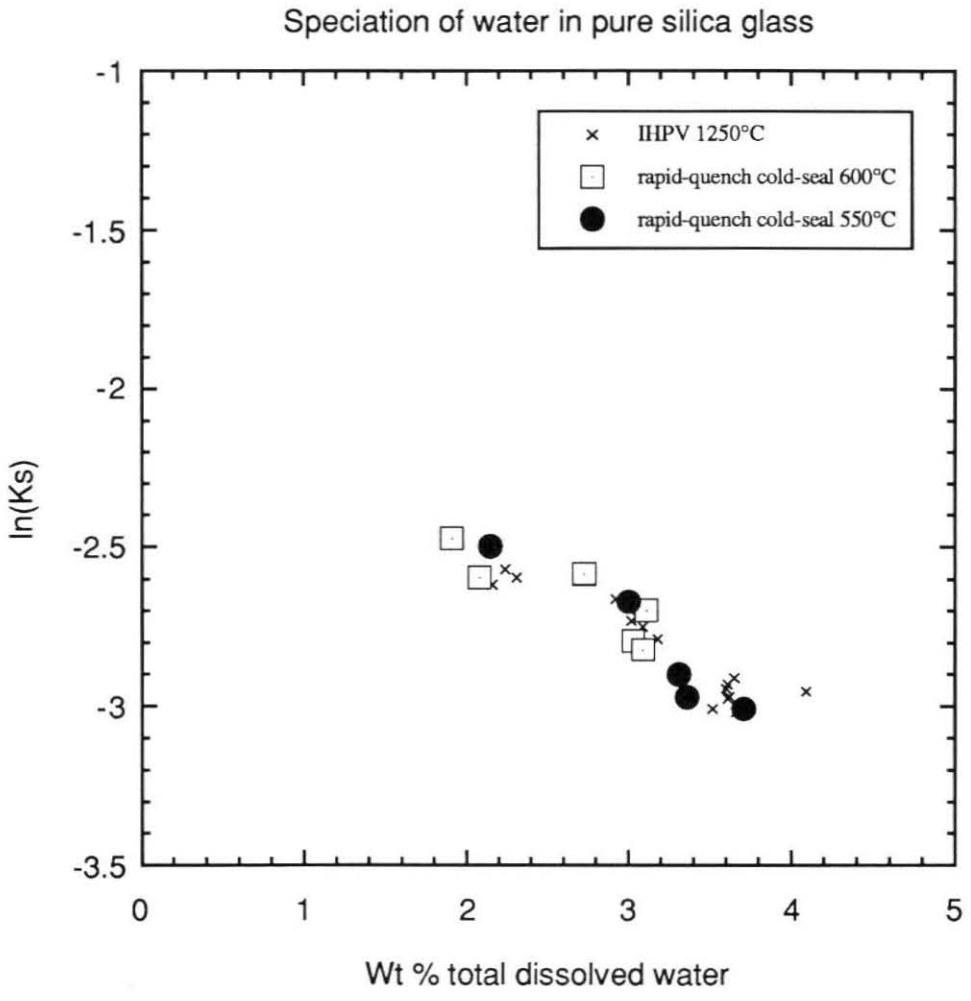

Figure 2.9: The speciation of water in pure silica glass. Xs are samples quenched from 1250°C in IHPV. Hollow boxes represent samples held at 600°C for 2 minutes and quenched rapidly in cold-seal apparatus. Filled circles represent samples held at 550°C for 5 minutes and quenched rapidly in cold-seal apparatus. Initial starting materials for cold-seal experiments were glasses synthesized in IHPV. ε values from Blank, Silver, and Stolper (unpublished data, see text). The speciation recorded in these samples probably represent unequilibrated values.

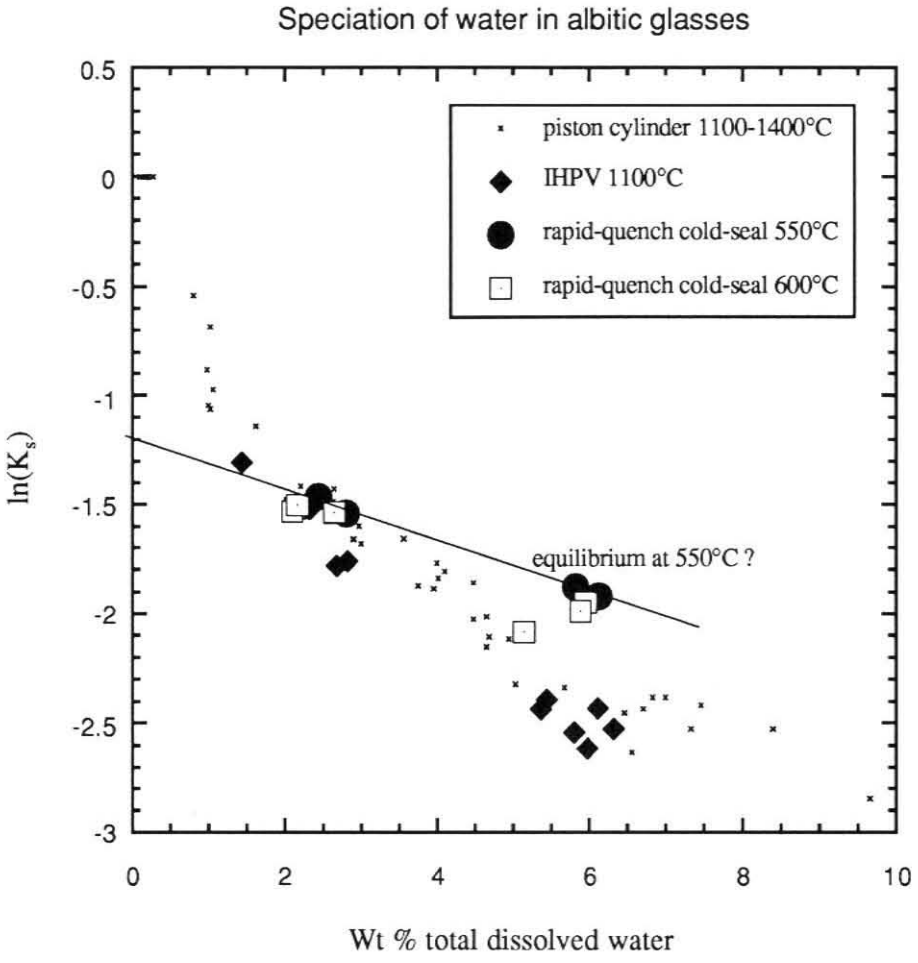

Figure 2.10: The speciation of water in albitic glasses. Xs are samples quenched from 1100-1400°C in IHPV (data from this work and Silver and Stolper, 1989). Hollow boxes represent samples held at 600°C for 2 minutes and quenched rapidly in cold-seal apparatus. Filled circles represent samples held at 550°C for 5 minutes and quenched rapidly in cold-seal apparatus. Initial starting materials for cold-seal experiments were glasses synthesized in IHPV. ε values from Silver and Stolper (1989). The speciation recorded in 600°C samples probably represent unequilibrated values. The speciation recorded in 550°C samples may represent equilibrated values, and a tentative 550°C isotherm is sketched through the data.

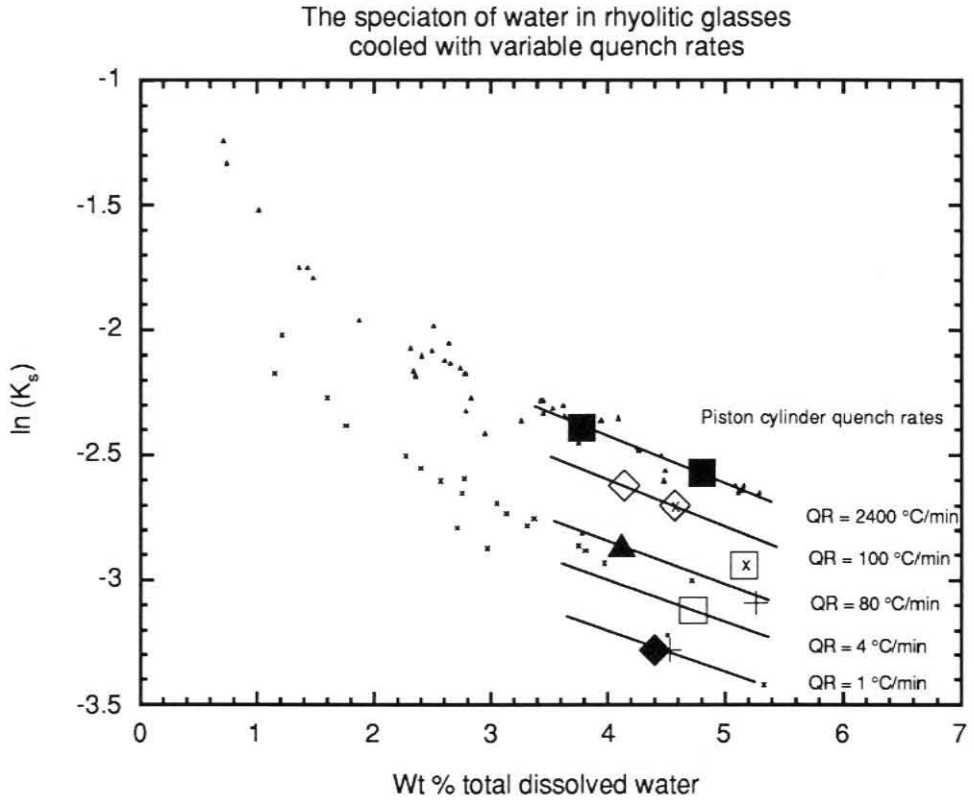

Figure 2.11: The speciation of water recorded in rhyolitic glasses quenched from 1250°C at controlled cooling rates in piston-cylinder apparatus; filled squares = 2400°C/min, hollow diamonds = 100°C/min, filled triangle = 80°C/min, hollow square = 4°C/min, filled diamond = 1°C/min, pluses = 0.17°C/min. Symbols with enclosed Xs represent samples that were quenched in cold-seal apparatus. Small triangles represent samples quenched rapidly from 850°C in modified cold-seal apparatus (Appendix 2), and small xs represent samples quenched slowly from 850°C in cold-seal apparatus.

Chapter 3:

The Fractionation of Hydrogen Isotopes in Granitic Melt

Introduction:

Understanding the behavior of hydrogen isotopes has been an important concern for geochemists since their discovery in 1932 (Urey, 1932). Knowledge of the partitioning of deuterium from protium has shed invaluable insights into many phenomena, ranging from the determination of paleo-temperatures (e.g., Epstein and Krishnamurthy, 1990) to constraining the various reservoirs involved in the condensing solar nebula (Yang and Epstein, 1982). The impressive array of major contributions provided by studying hydrogen isotopes is simply too long to list. Yet, our understanding of the hydrogen cycle within the earth and its variation through time is, at best, poor. What is the isotopic composition of "primordial" hydrogen? How much oceanic water is recycled down subduction zones back into the mantle? What is the relationship of the isotopic composition of water in a magma at the surface of the earth to the water at its source region? Not only do isotopic measurements provide information about the source of magmas, but they offer insights into the processes which control their evolution. How much fractionation of amphibole is involved in the genesis of andesite? What is the role of aqueous fluids in the formation of pegmatites? What is the nature of degassing in shallow-level eruptive centers? These are questions that we are now beginning to address using the powerful tool of hydrogen isotope mass spectrometry.

The isotopic composition of water in erupted magmas was first investigated by Friedman and Smith (1958). They examined water released from both the water-rich perlitic over-growths and the water-poor rhyolitic cores on obsidian pairs collected from all over the world. Their technique, following Shepherd (1938), also allowed for precise measurement of the water content of the two distinctive glassy regions. The hydration rinds, typically 50 microns thick, usually contained over 3 weight percent water while the low water content cores usually contained as little as 0.3 weight percent water. The isotopic analyses of the water recovered from both glassy regions proved very insightful;

the isotopic composition of the water released from the hydration rinds was consistently 40 ‰ lighter than the isotopic composition of their present-day local meteoric waters, while the water released from the core of the samples bore no such resemblance to their local waters. Friedman and Smith (1958) concluded that the water released from the water-poor cores was representative of water indigenous to the magma at the time of eruption. Though the rinds were clearly the products of interaction with surrounding ground waters, much could be said about the sample representing water emerging from depth. With such important implications, it is surprising to note the scarcity of papers published on the isotopic compositions of unaltered plutonic rocks (e.g., Godfrey, 1962; O'Neil et al., 1977; O'Neil and Chappel, 1977; Masi et al., 1981; Craig and Lupton, 1976; Nabelek et al., 1983; Brigham and O'Neil, 1985), fresh continental volcanic rocks (e.g., Taylor et al., 1983; Newman et al., 1988; Anderson and Fink, 1989), and fresh oceanic rocks (e.g., Moore, 1970; Kyser and O'Neil, 1984; Poreda, 1985; Poreda et al., 1986; Dobson and O'Neil, 1987) in the thirty-three years following the publication of this paper. This, in part, may be due to the conclusion that nearly all crustal rocks have exchanged with circulating ground waters (e.g., Taylor, 1974). Though there is much truth in this observation, the references cited above demonstrate that if care is taken to seek out uncontaminated samples, much can be learned from the study of hydrogen isotopes in the igneous environment.

In Chapters 1 and 2, I have discussed the nature of hydrogen speciation and its relationship to the solubility of water in rhyolitic melt. The demonstration that two dissolved water species are present and vary as regular functions of the total water content of the melt implies that the fractionation of hydrogen isotopes between the melt with an aqueous vapor phase will depend not only on temperature, but also on the total amount of water in the melt. Precise knowledge of the equilibrium speciation in the melt, as discussed in Chapter 2, is required for full and proper analyses of the bulk fractionation between silicate melt and vapor. Previous studies have failed to consider this additional

complication in interpreting melt-vapor fractionation (e.g., Kuroda et al., 1982; Taylor and Westrich, 1985).

This study looks at the isotopic partitioning of hydrogen isotopes between rhyolitic melt and pure water vapor. I present the results of the first experimental determination of the fractionation factors that govern the isotopic equilibrium of hydrogen isotopes in a silicate melt-aqueous vapor system. These results are then applied to natural geologic settings to shed insights on igneous processes which govern the evolution of magmatic systems.

Experimental Procedure

The experimental procedure is straightforward. Hydrogen isotopes will partition between three energetically distinguishable sites in the saturated silicate melt system, including ; (1) dissolved hydroxyl groups, (2) dissolved molecular water groups, and (3) water molecules in the vapor. We can envision isotopic equilibrium with the box model illustrated in Fig. 3.1. Two independent fractionation factors describe the partitioning of hydrogen and deuterium between the silicate melt and pure water vapor. We can express these fractionation factors in terms of their D/H ratios as follows;

$$\alpha_{\text{vapor-OH}} = \frac{\frac{D}{H}_{\text{vapor}}}{\frac{D}{H}_{\text{hydroxyl species in the melt}}} \qquad (1)$$

$$\alpha_{\text{vapor-H}_2O_{\text{molecular}}} = \frac{\frac{D}{H}_{\text{vapor}}}{\frac{D}{H}_{\text{molecular species in the melt}}} \qquad (2)$$

where $\alpha_{\text{vapor-}i}$ is the fractionation factor between vapor and melt species *i*., and $\frac{D}{H}_i$ is the ratio of deuterium to hydrogen in species *i*.

Theoretically, the two independent fractionation factors can be extracted from just one experiment. Separate analyses of the three species will yield the equilibrium partitioning in the melt-vapor system at a given temperature of equilibration. Unfortunately, as described in Chapter 1, the two dissolved water species cannot be extracted independently for separate analyses, and the bulk composition of the dissolved water must be determined as a single measurement. However, a series of experiments with variable species concentrations can be combined to constrain the respective fractionation factors. The difference in the isotopic composition between the vapor and the melt ($\Delta_{vapor-melt}$) can be measured in each experiment, and the two fractionation factors can be deconvolved in a simple regression analysis. The experiments outlined in Chapter 1 were designed for this purpose; rhyolitic melts with variable water concentration (and hence with variable species concentrations) were equilibrated with pure water vapor at 850°C. These experiments have been performed under a range of pressures, and to the degree that pressure has no effect on the fractionation behavior, this set of experiments can be used to extract the fractionation factors which govern the equilibrium of hydrogen isotopes between vapor and rhyolitic melt. The assumption that pressure has no influence on the partitioning of hydrogen isotopes has been demonstrated by many authors (e.g., O'Neil, 1986) and its effect in these experiments (all performed at less than 2 kbars) will be ignored in this discussion.

The experimental methods are described in detail in Chapter 1. Natural water-poor (0.024 % H2O) obsidian chips were loaded with triply distilled water ($\delta D = -102$) into platinum capsules and carefully weighed on an electrobalance to within 0.01 milligrams. The capsules were sealed by arc-welding with a graphite rod, heated at 110°C for ≈ 5 minutes, and re-weighed to check for leaks. Leaky capsules expose the melt to the pressure medium present throughout the apparatus and any samples that gained or lost weight during the experiment were discarded. The welded capsules were mounted on elevator rods and loaded into the rapid-quench pressure vessels described in Appendix 1.

In some experiments, an auxiliary capsule containing ≈ 120 μmoles of triply distilled water was mounted adjacent to the sample to provide a second check of the isotopic composition of the vapor phase at the conclusion of the experiment. The apparatus was brought up to run temperature and pressure before the sample was positioned in the hot spot of the vessel. Run times of several days were needed to achieve equilibrium at temperatures of 850°C, several weeks at 750°C, and several months at 650°C. Samples held at 650°C crystallized a significant quantity of plagioclase and could not be used for isotopic measurements. Quenching of the samples occurred at time-scales of ≈ 2 seconds. Although re-equilibration of the dissolved species is likely to have taken place on quench, there is good evidence to suggest that no re-distribution of hydrogen isotopes took place between vapor and melt during the quench (see Chapter 2). Thus, separate isotopic analyses of the vapor phase and the dissolved melt phase determine the partitioning of isotopes between vapor and melt for each experiment. The variation in bulk fractionation with total water content can be used to extract the individual fractionation factors between the melt and the two respective dissolved species. The extraction technique and isotopic analyses are described below.

Extraction technique: The procedure for extracting water from both the melt and vapor phase is discussed in detail in Chapter 1. A brief summary of the techniques used in extracting the vapor and dissolved components of the experiments is presented below, including a discussion of the potential complications for the determination of the isotopic composition of these components. The evolved water from both components was converted to hydrogen gas in a uranium furnace at 700°C (Bigeleisen et al., 1952) and measured manometrically with an accuracy of ≈ 1 % of the total sample. The gas was collected in tubes and transported to a hydrogen mass spectrometer. The mass spectrometer used in this work is a single-focusing, double-collecting instrument similar to that described by Nier (1947), with modifications as described by McKinney et al. (1950).

The D/H ratio of each sample is compared to that of a reference gas of known isotopic composition and converted to the standard δ notation relative to SMOW;

$$\delta D_{sample} = 1000 * \{\frac{(D/H)_{sample}}{(D/H)_{SMOW}} - 1\} \quad . \qquad (3)$$

The uncertainty in the δD measurements is about 2 ‰ based on many replicate analyses of standard waters.

The analyses of the isotopic composition of samples passed through the extraction line have several errors associated with them. As discussed at length in Chapter 1, there is a significant blank contribution added to the yields of each extraction. As observed in Table 1.4, these blanks are isotopically characterized and accounted for in the description of the high-temperature extraction procedure below. In addition to the complications associated with characterizing the blank effect, there is an observable memory effect associated with the conversion of H_2O to H_2 gas in the uranium furnace (Bigeleisen et al., 1952). Presumably, there is a finite concentration of uranium hydride, which exchange hydrogen and deuterium atoms with each passing gas sample. Table 3.1 lists a series of samples which have passed through the extraction line and their measured isotopic compositions. The initial shift of the isotopic composition is a function of the size of the sample, the length of time the sample was in contact with the furnace, and the previous history of the furnace (i.e., the isotopic composition and the size of the previous sample). The data in Table 3.1 are used to formulate a correction procedure for all samples passed through the furnace. This procedure assumes that all samples were pumped over to the manometer at the same rate and for the same length of time. An average of the shifted compositions in Table 3.1 yields a correction factor of 0.000382 ‰ shift/μmole. I have applied this memory calibration to every sample passed through the uranium furnace. To minimize the memory effect, I have standardized the "memory" exchanged in each sample by flushing the uranium with two aliquots (≈200 μmoles each) of standard waters before

converting the vapor and the evolved dissolved waters to H_2 gas in the uranium furnace. The correction procedure described above typically results in a change in the bulk partitioning of less than 1 ‰.

The isotopic composition of the vapor: The procedure for extracting the vapor from the charges is described in detail in Chapter 1. Briefly, run products were weighed at the conclusion of each experiment and leak-tight capsules were loaded in a capsule-piercing device. Capsules were pierced under vacuum without exposure to a liquid nitrogen trap to prevent the sudden formation of ice crystals before extraction. The water vapor was collected and purified cryogenically before conversion to H_2 gas in the uranium furnace. In general, recovery of the vapor was within 5 μmoles of the weight-loss determination performed after the extraction. The high-yield samples provided confidence in the isotopic value of the vapor phase. Although a fractionation is associated with the extraction procedure, the small amounts of residual vapor will not affect the final isotopic composition of the large vapor yields by more than a fraction of a permil. In several cases, a second measurement of the vapor phase was obtained by measuring the isotopic composition of the water extracted from an auxiliary capsule located next to the charge during the experiment. The diffusivity of hydrogen through the platinum walls is sufficiently rapid to homogenize the isotopic composition of the vapor in the pressure medium, the capsule loaded with silicate, and the capsule containing only water vapor within hours at 850°C (P. Ihinger, unpublished data). Measured vapor samples from the same experiment have isotopic compositions within 5 ‰.

There was an additional complication associated with the isotopic composition of the vapor phase. Richet et al. (1986) used argon for the pressure medium in a similar set of experiments performed in internally-heated pressure vessels and found that diffusive loss of hydrogen was a significant problem; the isotopic composition of the vapor continually varied during their experiments, and equilibrium was never achieved. The experiments in

this study were designed with water as a pressure medium, so that the H_2 fugacity would quickly equalize across the permeable platinum capsule.

After each experiment, the isotopic composition of the pressure medium was measured and consistently found to be around -102 ‰, identical to its initial value determined before the experiment. However, the value of the vapor was typically greater than 10 ‰ lighter than that of the pressure medium. Because the diffusivity of hydrogen through the platinum capsule is rapid compared to the time-scale of the experiment, the isotopic composition of the vapor represents the isotopic composition of the pressure medium in the hot-spot of the apparatus. Because the molar volume of water is so much greater at high temperatures, the quantity of water which resides in the hot portion of the apparatus represents a tiny fraction of the total water in the pressure vessel. At the conclusion of the experiment, the water from the upper hot portion of the apparatus is mixed into the much greater quantity of colder fluid below, and its lighter signature is not detectable in the final measurement. Some process involving fractionation must be occurring within the hotter portion of the bomb. Further, the fractionated signature is not being eliminated by convection or diffusion within the pressurizing fluid. Little convection is expected to occur within the apparatus, as the configuration of the apparatus is thermally stable; i.e., the hot less dense fluid resides above the water-chilled fluid below. Thus, any exchange of isotopes between the two regions will be controlled by diffusion. In fact, one explanation for the isotopic gradient within the bomb is via the mechanism of thermal diffusion, or Soret diffusion. A temperature gradient applied to a gravitationally stable fluid will cause small and light particles to preferentially migrate to the hotter end of the system in a predictable fashion (see, e.g., deGroot and Mazur, 1962). However, this effect should be relatively small at 850°C and does not explain the variability in the magnitude of the shifts in isotopic composition observed in several experiments (see Table 3.2).

Another possible explanation for the variable isotopic composition at the hotter end of the apparatus involves the formation of metal-hydroxides on the bomb walls. Small brown and green metallic chips are observed in the bomb-water samples recovered after each experiment. These chips were analyzed by X-ray diffraction and found to be dominantly composed of iron hydroxide and nickel oxide. The isotopic composition of these "rust" products are lighter than the fluid from which they form (e.g., see O'Neil, 1986). Thus, the light value on the walls may serve as a "memory" which is imprinted onto the fluids with which they come in contact in future experiments in some still unexplained fashion. Nevertheless, the composition of the vapor will be relatively stable during the duration of the experiment as demonstrated by the following experiment: platinum capsules containing waters with δD = -260 ‰, -102 ‰, and -60 ‰ were held adjacent to one another at 850°C for 24 hours in an apparatus with a pressure medium of δD = -102 ‰. At the conclusion of the experiment, the values had all equilibrated to δD = -117 ± 1 ‰ and the bomb water was measured at δD = -102 ‰. Though the vapors were not in equilibrium with the bulk of the pressurizing medium, they all rapidly converged on the steady-state value of the buffering fluid in the hot portion of the apparatus.

The isotopic composition of the glass: The water representative of the dissolved component in the melt was extracted from quenched glass chips on the extraction line illustrated in Fig. 1.1 using the extraction vessel illustrated in Fig. 1.2. As described in Chapter 1, unusually long extraction times were required for complete recovery of dissolved water, and a rather large blank contribution was added to the yields of each extraction. These blanks have been isotopically accounted for in Table 1.4. A reproducible blank of -120 ± 10 ‰ characterized the adsorbed component, while the isotopic composition of HF-treated capsules typically ranged between -130 and -140 ‰ (the value observed on pre-heating the HF-soaked crucibles for 1-3 hours before subsequent glass extractions). A blank of -120 ‰ was assigned to the extractions of GB 68-76, while a

value of -130 ‰ was applied to the blank corrections of samples GB 7-65. The respective blank assignment from Table 1.5 is listed for each experiment and subtracted from each yield using the mass balance equation;

$$(\mu moles_{measured} * \delta D_{measured}) = (\mu moles_{sample} * \delta D_{sample}) + (\mu moles_{blank} * \delta D_{blank}) \quad (8)$$

A series of experiments was performed with identical water contents (all saturated with pure water vapor at 500 bars) to investigate the complexities of the extraction process. The glass chips were heated to 1200°C at different rates, which resulted in a large range of bulk fractionation values (see Table 3.2; $\Delta_{(vapor\text{-}melt)}$ ranged between -35 and +22 ‰). The two experiments that were held below their melting temperature (≈ 700 - 800°C) for the longest period of time showed the greatest degree of frothiness as well as the greatest deviation from the range of values for $\Delta_{(vapor\text{-}melt)}$ determined from good extractions. Re-examination of the heating schedules for these samples revealed that they were not held between 450-550°C for any length of time. Fig. 1.3 demonstrates that molecular water is evolved from rhyolitic glasses at these lower temperatures. Thus, it may be that molecular water groups are nucleating as small bubbles within the glass at these lower temperatures and serve as traps for diffusing water molecules. At higher temperatures, the glass softens and the bubbles grow in size. The expansion of the bubbles increases their cross-section and a greater percentage of diffusing molecules will be trapped. The surface tension of the bubbles is large enough to maintain their integrity even at the 1200°C temperature step (this observation was made after all of the 500 bar glass extractions). Thus, the water molecules trapped in the bubbles are not recovered in the extraction process. Fig. 3.2 shows the observed correlation of negatively shifted $\Delta_{vapor\text{-}melt}$ with time spent at the 450 - 550°C temperature step. Thus, despite the fact that the bubbles are being *formed* by the diffusing molecular water component, it is the isotopically lighter hydroxyl component that gets

trapped in the bubbles as they diffuse (most likely as water molecules; see Zhang et al., 1991) at the higher temperatures. Dr. David Pyle (personal communication) has demonstrated with nucleation theory that the formation of bubbles, too small to be seen microscopically, is a likely process in a rapidly-heated water-rich glass at 500°C. To avoid the formation of these bubbles, the glasses must be held at temperatures lower than 400°C for long periods of time such that the molecular component is removed from the glass before their collision frequency is favorable for bubble stability. The heating schedule outlined in Table 1.3 was successful in inhibiting bubble formation in most water-rich samples, but even the long extraction times listed could not prevent small bubbles from forming in the most water-rich samples equilibrated at high pressures.

Results

The results of the isotopic measurements made on glasses and vapors equilibrated from 200 to 1600 bars are listed in Table 3.1. The isotopic composition of the samples are subtracted from the isotopic composition of the vapor to determine the bulk fractionation in the melt-vapor system. These results are presented as a function of the total dissolved water content in Fig. 3.3. The results show a distinct trend of decreasing $\Delta_{vapor\text{-}melt}$ with increasing water content; i.e., as the proportion of the molecular water species increases, the isotopic composition of the melt becomes more similar to that of the vapor.

This general trend is schematically illustrated in Fig. 3.4, in which hypothetical fractionation factors are assigned to describe the equilibrium of the vapor with the two melt species. In Fig. 3.4, $\alpha_{vapor\text{-}OH}$ is greater than $\alpha_{vapor\text{-}H_2O\ molecular}$. At low total water contents, the hydroxyl groups are the dominant species, and the partitioning of hydrogen isotopes will be controlled by the large fractionation associated with $\alpha_{vapor\text{-}OH}$. With increasing water content, the proportion of molecular species increases in the melt, and the bulk fractionation between melt and vapor will increasingly reflect the influence of the

smaller fractionation associated with $\alpha_{vapor\text{-}H_2O\ molecular}$. At very high water concentrations, the melt is dominated by molecular water groups, and $\Delta_{vapor\text{-}melt}$ will be controlled by $\alpha_{vapor\text{-}H_2O\ molecular}$. The isotopic composition of the bulk melt is shown as a grey ball in the one-dimensional diagram in Fig. 3.4. With increasing molecular water concentration, the grey-level gets darker and the bulk fractionation approaches that of the value of the molecular species. I note that it is impossible to conduct an experiment with only the molecular water species dissolved in the melt. A finite concentration of hydroxyl species will always be present in a hydrous melt (see Fig. 1.1, which shows the leveling of the concentration of hydroxyl groups with increasing dissolved water content).

Fig. 3.5 illustrates the change in $\Delta_{vapor\text{-}melt}$ with the change in the proportion of the two dissolved species in the melt; the abscissa reflects the percent of total dissolved water present as molecular species (where OH is given in terms of its H_2O equivalence). As observed in Fig. 3.3, the decrease in bulk vapor/melt fractionation with increasing molecular water content is apparent. Also shown in Fig. 3.5 are the expected trends for melt-vapor fractionation with hypothetical fractionation factors of $\alpha_{vapor\text{-}OH} = 36$ ‰, and $\alpha_{vapor\text{-}H_2O\ molecular} = +30$, 0, and -30 ‰. The data, though rather scattered, fall between the two projected trends of $\alpha_{vapor\text{-}H_2O\ molecular} = 0$ and -30 ‰, indicating that there is a small, near-zero fractionation associated with the equilibrium between water vapor and molecular species in the melt (i.e., $\alpha_{vapor\text{-}H_2O\ molecular} = 0$ ‰).

The result of a small $\alpha_{vapor\text{-}H_2O\ molecular}$ is in agreement with the results on the partial molar volume of the molecular water component in the silicate melt described in Chapter 1. Fig. 1.14 demonstrates that the partial molar volume of molecular water groups is very nearly equal to 0, as if they are filling holes in the melt structure. If the dissolution mechanism approximates this "filling of holes," we would expect the energetics of the respective atomic positions for hydrogen and deuterium to be similar to those in the free vapor state. The fractionation of hydrogen isotopes between the two positions is thus not expected to be very large. On the other hand, the bonding environments associated with

the formation of the hydroxyl groups are significantly different from both those of the vapor and dissolved molecular species. It is not surprising that a significant fractionation exists even at the high temperature of 850°C.

The results of this study are in excellent agreement with previous work on hydrogen isotope partitioning between vapor and rhyolitic melt. Fig. 3.3 illustrates the two other well-constrained experiments in the literature. The two diamond symbols represent the results of Dobson, et al. (1989), who determined the fractionation of hydrogen isotopes between rhyolitic melt and aqueous vapor at very low pressures. The $\Delta_{vapor\text{-}melt}$ measured in their experiments is a direct reflection of $\alpha_{vapor\text{-}OH}$. They performed experiments at 530, 650, 750, and 850°C and measured respective fractionation factors of 1.051, 1.045, 1.041, and 1.041 ± 2 ‰. The three lower temperature fractionation factors are linear with $1/T^2$, and are roughly parallel with the trend in 1000 ln $\alpha_{vapor\text{-}mineral}$ vs. $1/T^2$ observed by Suzuoki and Epstein (1976) on the hydrous mineral phases biotite, hornblende, and muscovite. The result of Dobson et al. (1989) at 850°C is identical to their observed fractionation at 750°C, suggesting to them that the fractionation behavior is reflecting the onset of the glass transition, which for anhydrous rhyolite occurs between these temperatures (Bacon ,1977). If experimental difficulties occur in their 850°C experiments (e.g., the reaction of water vapor with the walls of their quartz vessels becomes problematic at 850°C), we might predict the actual fractionation by extending the linear trend defined by their lower temperature data. This predicted value ($\Delta_{vapor\text{-}melt}$ = 36 ‰) is plotted as the lower of the two diamond symbols in Fig. 3.4 and agrees with my results. Also plotted in Fig. 3.4 is the result of Taylor and Westrich (1985) at 950°C on a natural rhyolitic obsidian. Their value of = 23.6 ‰ falls well within the error of the results of this study.

Multiple regression analyses of the data illustrated in Figs. 3.4 and 3.6 could be performed to extract the best-fit fractionation factors associated with the partitioning of

hydrogen isotopes between pure aqueous vapor and rhyolitic melt. Briefly, we can write the mass balance of hydrogen isotopes within the melt as;

$$(X_B * \delta D_{melt}) = (\frac{X_{OH}}{2} * \delta D_{OH}) + (X_{H_2O} * \delta D_{H_2O}) \quad (1)$$

where X_B = the mole fraction of water on an anhydrous per mole of oxygen basis, X_{OH} is the mole fraction of water dissolved as hydroxyl groups, X_{H_2O} is the mole fraction of molecular water dissolved in the melt, and δD_i is the isotopic composition of *i*. We can express the fractionation factors associated with the isotopic equilibrium between the vapor phase and the two dissolved species as:

$$\alpha_{vapor\text{-}OH} = \frac{1000 + \delta D_{vapor}}{1000 + \delta D_{OH}} \quad (2)$$

$$\alpha_{vapor\text{-}H_2O} = \frac{1000 + \delta D_{vapor}}{1000 + \delta D_{H_2O}} \quad (3)$$

By expressing equations 2 and 3 in terms of δD_{OH} and δD_{H_2O}, we can rewrite equation (1) as follows:

$$X_B \delta D_{GLASS} = \frac{X_{OH}}{2} * \frac{1000 + \delta D_{vapor}}{\alpha_{vapor\text{-}OH}} - \frac{1000 X_{OH}}{2} + X_{H_2O} * \frac{1000 + \delta D_{vapor}}{\alpha_{vapor\text{-}H_2O}} - 1000 X_{H_2O} \quad (4)$$

Equation (4) can be rewritten in terms of $\frac{1}{\alpha_{vapor\text{-}OH}}$ and $\frac{1}{\alpha_{vapor\text{-}H_2O}}$ as follows;

$$X_B \delta D_{GLASS} + \frac{1000 X_{OH}}{2} + 1000 X_{H_2O} = \frac{1}{\alpha_{vapor\text{-}OH}} * (\frac{X_{OH}}{2} * (1000 + \delta D_{vapor})) + \frac{1}{\alpha_{vapor\text{-}H_2O}} * (X_{H_2O} * (1000 + \delta D_{vapor})) \quad (5)$$

Knowledge of the true speciation in the melt at 850°C is necessary for the accurate calculation of $\alpha_{vapor\text{-}OH}$ and $\alpha_{vapor\text{-}H_2O\ molecular}$. By applying the regular solution model developed in Chapter 2, each experiment can be expressed in the form;

$$A = \frac{B}{\alpha_1} + \frac{C}{\alpha_2} \qquad (7)$$

where $\alpha_1 = \alpha_{vapor\text{-}OH}$, and $\alpha_2 = \alpha_{vapor\text{-}H_2O\ molecular}$. Again, I stress that the results illustrated in Fig. 3.3 and 3.5 are rather scattered due to the complications of bubble growth in the water-rich samples. The technique has improved tremendously over the course of the investigation, and more precise results can be expected on similar experiments to be performed in the future.

There is one experiment performed at 750°C which is described in Table 3.2. Sample GB 68 was equilibrated at 1600 bars and thus represents the most water-rich sample analyzed to date. The measured value of $\Delta_{vapor\text{-}melt} = +22$ ‰ suggests an increased fractionation at lower temperatures, in agreement with the results of Dobson et al. (1989). However, the quenched run product was observed to have small bubbles, suggesting that a slight loss of pressure may have occurred during the long duration (19 days) of the experiment. These bubbles represent a small fraction of the total volume of the sample (there was no difficulty in locating a bubble-free pathway through the 530 microns of polished glass for IR analyses. However, these bubbles may have served as traps for both the molecular and hydroxyl components during extraction and this value may not be a true representative of the equilibrium fractionation under these conditions.

Discussion

The results of the experiments described above represent the first comprehensive determination of the fractionation factors that control the equilibrium of hydrogen isotopes between the dissolved species within a silicate melt. We can apply these values to modelling a variety of magmatic processes involving the partitioning of water between water-rich melts and other hydrous phases. For instance, knowledge of the fractionation factors between vapor and hydrous mineral phases (such as hornblende or biotite) will allow for the modelling of the hydrogen isotope systematics of fractionating wet magmas. Knowledge of the isotopic composition of a suite of magmas (basaltic to rhyolitic) may shed insights into their possible genetic relationships, as well as constraining the quantity of potentially fractionated hydrous minerals. Such constraints can only be made with the additional knowledge of the fractionation involved between the dissolved melt species and the crystallizing phases. Very little experimental work has been published on the fractionation of water vapor with igneous amphiboles (e.g., see Graham et al., 1984 for a discussion of the difficulties associated with this measurement). Suzuoki and Epstein (1976) have measured the partitioning of hydrogen isotopes between water vapor and biotite, hornblende, and muscovite as a function of temperature. Knowledge of the hydrogen isotope partitioning between the two dissolved melt species with water vapor determined in this study in addition to the data of Suzuoki and Epstein provide for the calculation of the fractionation factors that control the partitioning of hydrogen isotopes between the hydrous mineral phases and the magma. These data can now be used to model the crystallization paths of plutonic rocks such as the Notch Peak granitic stock described by Nabelek et al. (1983).

Knowledge of the fractionation factors governing melt-vapor equilibrium also allow for the modelling of the degassing history of shallow-level volcanic systems. O'Neil and coworkers have observed a systematic trend in the isotopic composition of plutonic suites

of rocks around the world (e.g., O'Neil et al., 1977; O'Neil and Chappel, 1977; Masi et al., 1981; Nabelek et al., 1983; Brigham and O'Neil, 1985). They consistently observed a general decrease in the whole rock isotopic composition of these rocks with decreasing total water content (see Fig. 3.6). Taylor et al. (1983) observed the same trend of isotopic composition with water content in the volcanic glasses they analyzed from Little Glass Mountain in California; water-rich samples from tephra deposits (1-3 wt % total water; δD ranged between -60 and -80 ‰) were considerably heavier than the samples they measured from the extrusive domes (<0.2 wt % total water; $\delta D \approx -130$ ‰). They modelled this shallow level magmatic system using a single fractionation factor of 1.004 in an open system Rayleigh distillation degassing calculation. Newman et al. (1988) analyzed a series of similar samples from the Mono Craters eruptive center in California and observed the same trend of δD with water content. They also measured the CO_2 content of their glasses, and interpreted the trends of volatile contents in the glasses recovered from tephra deposits as indicating a closed system degassing history prior to eruption. With the onset of open system degassing, the δD of the magmas dropped precipitously and subsequent eruptions occurred quiescently as extrusive domes. They recognized the need for the application of two fractionation factors in the description of degassing magmas, and assigned two reasonable αs in their modelling. The results of this study further constrain these important parameters. Fig. 3.7 illustrates the effect of two fractionation factors on the degassing history of a rhyolitic magma with an initial water content of 3.0 wt % water, and a $\delta D = -45$. Using the speciation model developed in Chapter 2 and the best-fit fractionation factors of this study, the calculated closed-system degassing trend yields higher δD values at a given water content than any reasonable value of a single fractionation factor assigned to describe melt-vapor isotopic equilibrium, thus fitting the measured values found in the tephra deposits. Fig. 3.8 shows the data of Newman et al. (1988) and two calculated degassing trends. Closed-system Rayleigh distillation adequately describes the degassing trend until the water content of the magma is reduced to $\approx$ 0.8 wt %. Continued open-

system degassing fits the observed data from the glasses recovered from the extrusive domes.

Conclusions

The fractionation factors that describe the equilibrium partitioning of hydrogen isotopes between dissolved melt species and water vapor has been determined. The bulk fractionation of hydrogen isotopes in the melt-vapor system is dependent upon the water content of the melt; at low total water contents, the fractionation between melt and vapor is controlled by the fractionation factor between vapor and hydroxyl groups ($\alpha_{vapor\text{-}OH} \approx 1.036 \pm 0.010$ ‰). At high total water contents, the melt-vapor fractionation is controlled by the fractionation between vapor and the molecular water species ($\alpha_{vapor\text{-}molecular\ water} \approx 1.000 \pm 0.010$ ‰). These data can be used to describe the fractionation of hydrogen isotopes in hydrous melt systems involving other hydrous phases. The measured experimental values successfully describe the evolution of shallow-level magmatic eruptive centers in California and can be applied to other magmatic systems to determine the degree of crystallization and degassing they may have experienced in their evolution.

Sample	umoles	delta D	
HDO-92,5-bw	191.1	-76.8	
HDO-93	49.3	-56.6	<
HDO-96	41.1	-160	>
HDO-97	158.1	-186.9	
HDO-98	180.2	-189.1	
HDO-99	171.6	-180	
AH-std	272.1	-75.8	
Sed-1	282.2	-68.2	<
LWS-1	440.6	-132.1	>
LWS-2	353.7	-140.8	
LWS-3	371.2	-139	
LWS-4	409.2	-139.5	<
HDO-100,2wb1	309.6	9.2	>
HDO-100,2wb2	116.2	26.3	
HDO-100	165.8	13.1	
HDO-101	164.8	22	
HDO-102	175.7	13.7	<
M40-3.1	-	-93.6	>
M40-3.2	162.8	-99.8	
M40-3.3	157.8	-101.7	

Table 3.1 A series of isotopic analyses made on samples converted to H2 gas in the uranium furnace on the vacuum extraction line. < & > symbols indicate isotopic shifts used in the calibration of the memory effect.

Sample	Temp (°C)	P (bars)	time (hrs)	µmoles vapor	µmoles glass	blank	µmoles left	µmoles sample	IR (c) wt %	CO2 man wt %	∂D sample observed	Last (smpl)	Shift crctd ∂D smpl(obs)	∂D sample blank	∂D sample (blnk-rsd)	∂D Bomb	∂D Vapor	Last (vapor)	crrctd ∂D vapor	corrctd Big Δ	Comments
GB3-7	850	202	84	114	80	23	1.3	59	1.09	1.14	-135	-104	-136	-135	-133	-104	-107	-103	-107	26	*
GB3-8	850	409	84	142	130	29	1.2	102	2.25	2.10	-142	-180	-140	-135	-140	-103	-117	-103	-117	22	*
GB3-9	850	1206	84	165	207	8	1.2	200	4.26	4.25	-131	-180	-127	-135	-126	-104	-111	-104	-111	15	*
GB3-11	850	635	216	117	131	15	1.0	116	2.97	2.95	-148	-146	-148	-135	-148	-102					
GB3-12	850	1066	216	140	171	10	1.0	161	3.77	4.09	-129	-136	-129	-135	-128		-112	-115	-111	16	*
GB3-13	850	1362	216	160	184	17	0.9	168	4.60	4.64	-144	-163	-142	-135	-142	-105	-133	-105	-135	7	*
GB3-18	850	501	117	136	120	14	1.0	107	2.29	2.60	-141	-159	-140	-135	-140	-103	-119	-103	-119	20	*
GB3-19	850	498	117	185	111	13	1.1	99	2.34	2.25	-140	-149	-140	-135	-139	-103	-122	-103	-123	16	
GB3-20	850	795	117	127	177	14	1.2	164	3.40	3.32	-137	-148	-136	-135	-135	-104	-114	-104	-115	20	*
GB3-25.1	850	500	312	139	108	12	0.9	97	2.74	2.77	-130	-100	-131	-135	-130	-102	-115	-106	-116	14	w/ powder
GB3-25.2	850	500	312	139	113	6	0.9	108	2.74	3.14	-126	-102	-127	-135	-125	-102	-115	-106	-116	9	w/ powder
GB3-26.2	850	498	243	155	96	5	0.8	91	2.69	2.96	-133	-99	-134	-135	-133	-102	-124	-104	-126	7	>150µm
GB3-43.1	850	546	185	156	73	7	1.0	67	2.27	2.63	-83	-75	-84	-135	-77	-75	-70	-79	-69	7	fine powder
GB3-43.2	850	546	185	156	99	7	1.3	93	2.27	2.82	-87	-77	-88	-135	-83	-75	-70	-79	-69	14	large bits
GB3-44.1	850	518	185	163	105	23	0.7	83	2.85	3.18	-101	-103	-101	-135	-91	H2	-75	-103	-73	18	
GB3-44.2	850	518	185	163	84	12	0.7	73	2.85	2.96	-89	-72	-89	-135	-81	H2	-75	-103	-73	8	
GB3-45	850	486	185	161	146	14	0.5	132	2.56	2.86	-102	-77	-104	-135	-100	-77	-85	-78	-85	15	
GB4-52.1	850	1590	504	220	104	5	0.4	100	4.93	5.62	-139	-141	-139	-135	-138	-103					
GB4-52.2	850	1590	504	220	83	40	0.2	43	4.93	5.72	-121	-104	-122	-135	-109	-103					
GB4-64.1	850	501	234	122	103	43	0.7	103	2.66	3.73	-126	-108	-127	-135	-70	-103	-107	-103	-107	-37	
GB4-64.2	850	501	234	122	81	11	0.7	82	2.66	3.13	-116	-98	-117	-135	-98	-103	-107	-103	-107	-9	
GB4-65.1	850	501	234	165	96	9	0.7	97	2.70	3.24	-129	-110	-130	-135	-117	-104	-135	-104	-137	-19	
GB4-65.2	850	501	234	165	72	10	0.6	72	2.70	3.19	-120	-107	-120	-135	-100	-104	-135	-104	-137	-36	
GB4-71.1	850	1204	345	273	115	12	0.6	103	4.30	4.54	-120	-113	-120	-135	-118	-104	-109	-104	-109	9	*w/out CO2 rmvl
GB4-71.2	850	1204	345	273	94	12	0.5	82	4.30	4.51	-116	-105	-116	-135	-112	-104	-109	-104	-109	3	
GB4-73.1	850	1410	597	5	139	6	0.6	133	4.89	5.19	-131	-103	-133	-135	-132	-100	-128	-95	-128	4	vapor from side
GB4-73.2	850	1410	597	5	144	9	0.7	135	4.89	4.96	-135	-103	-136	-135	-136	-100	-128	-95	-128	8	*
GB4-74.1	850	806	596.5	137	101	14	0.6	88		3.48	-143	-114	-144	-135	-145	-114	-135	-112	-136	8	
GB4-74.2	850	806	596.5	137	131	7	0.8	125		3.74	-147	-116	-148	-135	-148	-114	-135	-112	-136	12	*
GB4-75.1	850	1207	596.5	120	144	31	0.7	114		3.94	-132	-107	-134	-135	-133	-102	-105	-102	-105	28	missing 25 µm
GB4-75.2	850	1207	596.5	120	168	18	0.8	151		4.48	-121	-130	-120	-135	-118	-102	-105	-102	-105	13	*
GB4-76.1	850	1002	596.5	148	129	22	0.7	107	4.08	3.78	-129	-102	-131	-135	-129	-102	-120	-99	-121	7	
GB4-76.2	850	1002	596.5	148	123	25	0.7	99	4.08	3.77	-136	-99	-138	-135	-138	-102	-120	-99	-121	16	*
GB4-68.1	750	1669	452.5	186	192	21	0.7	172	5.66	6.07	-149	-96	-153	-135	-154		-134	-99	-137	17	

Table 3.2: Experiments bearing on the isotopic fractionation of hydrogen isotopes between water vapor and rhyolitic melt
* = used in regression

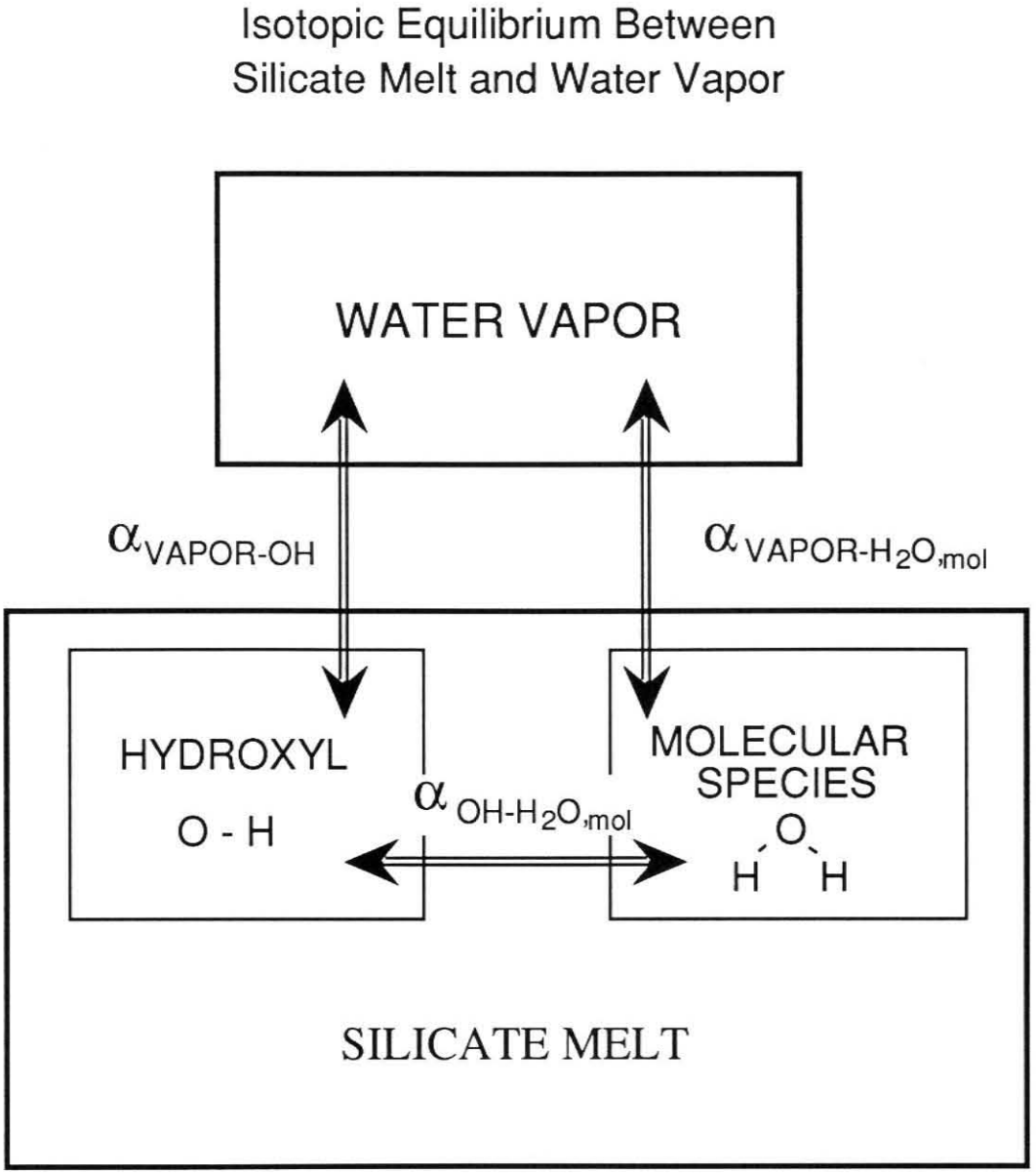

Figure 3.1: A box model illustrating the three distinguishable species involved in hydrogen isotope fractionation within a silicate melt/aqueous vapor system. Two independent fractionation factors are needed to explain the fractionation between the vapor and the melt.

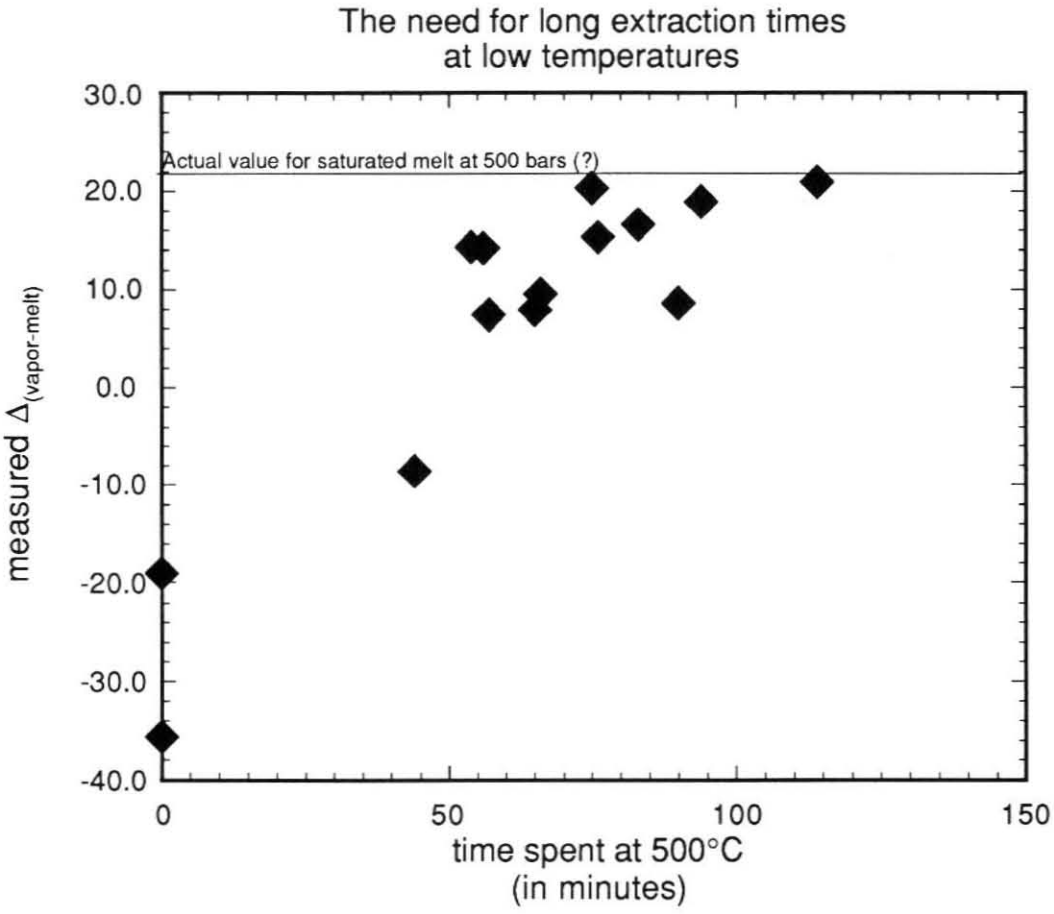

Figure 3.2: The measured hydrogen isotopic fractionation between water vapor and rhyolitic glass for a series of experiments equilibrated at 500 bars and 850°C. The figure demonstrates that the isotopic composition of water extracted from the quenched glasses is a function of the amount of time the sample was held at 500°C (the temperature at which molecular water groups rapidly diffuse out of the glass; see Fig. 1.3). Glasses held at this temperature for short periods of time will nucleate bubbles at higher temperatures. These bubbles serve as traps for subsequent diffusing water molecules and prevent the complete collection of the dissolved water component, leading to the erroneous low values of $\Delta_{vapor\text{-}melt}$.

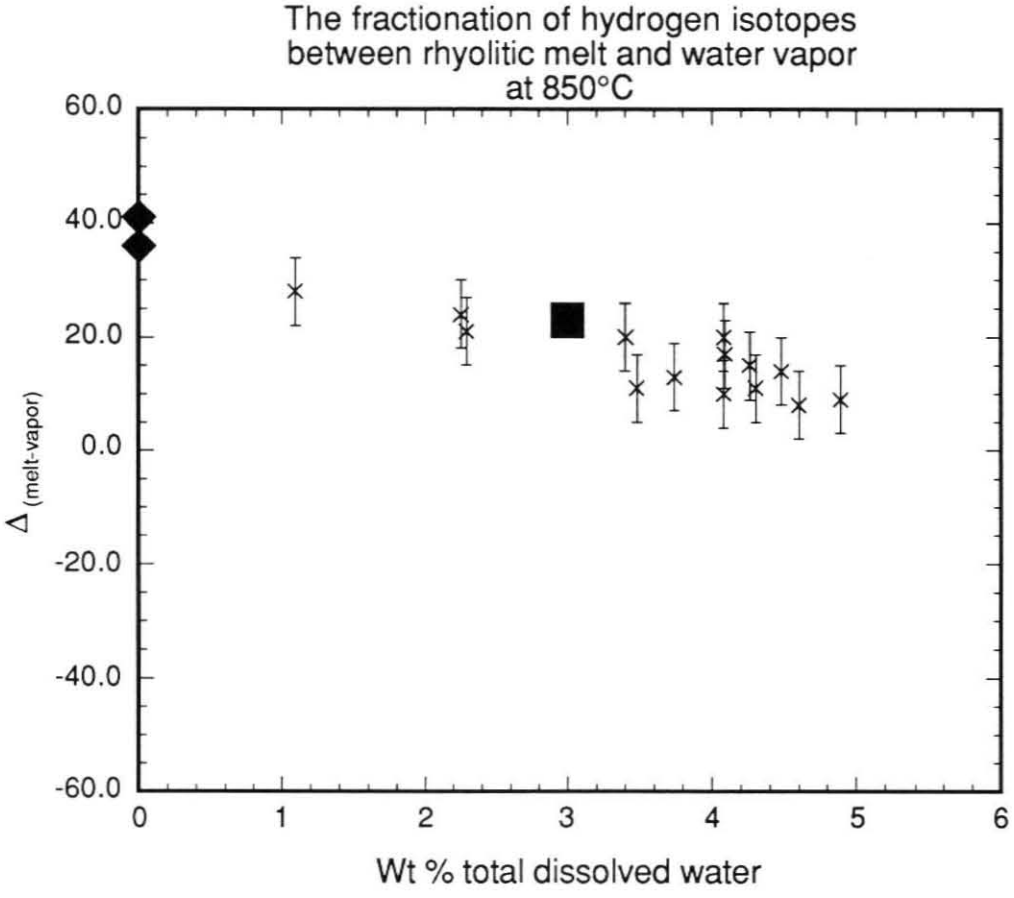

Figure 3.3: The fractionation of hydrogen isotopes between saturated rhyolitic melts and aqueous vapor as a function of the total amount of water dissolved in the glass. Xs are samples equilibrated at 850°C determined in this study. Error bars are assigned by propagating 2 ‰ uncertainties in the isotopic analyses of the vapor, the melt, and the blank measurements. The diamonds are the results of Dobson et al. (1989); the higher value is their actual measured value, and the lower value is the extrapolated value determined by extending the linear trend (vs $1/T^2$) of their lower temperature results to 850°C, (see text). The solid square is the value of Taylor and Westrich (1985) determined on melts quenched from 950°C.

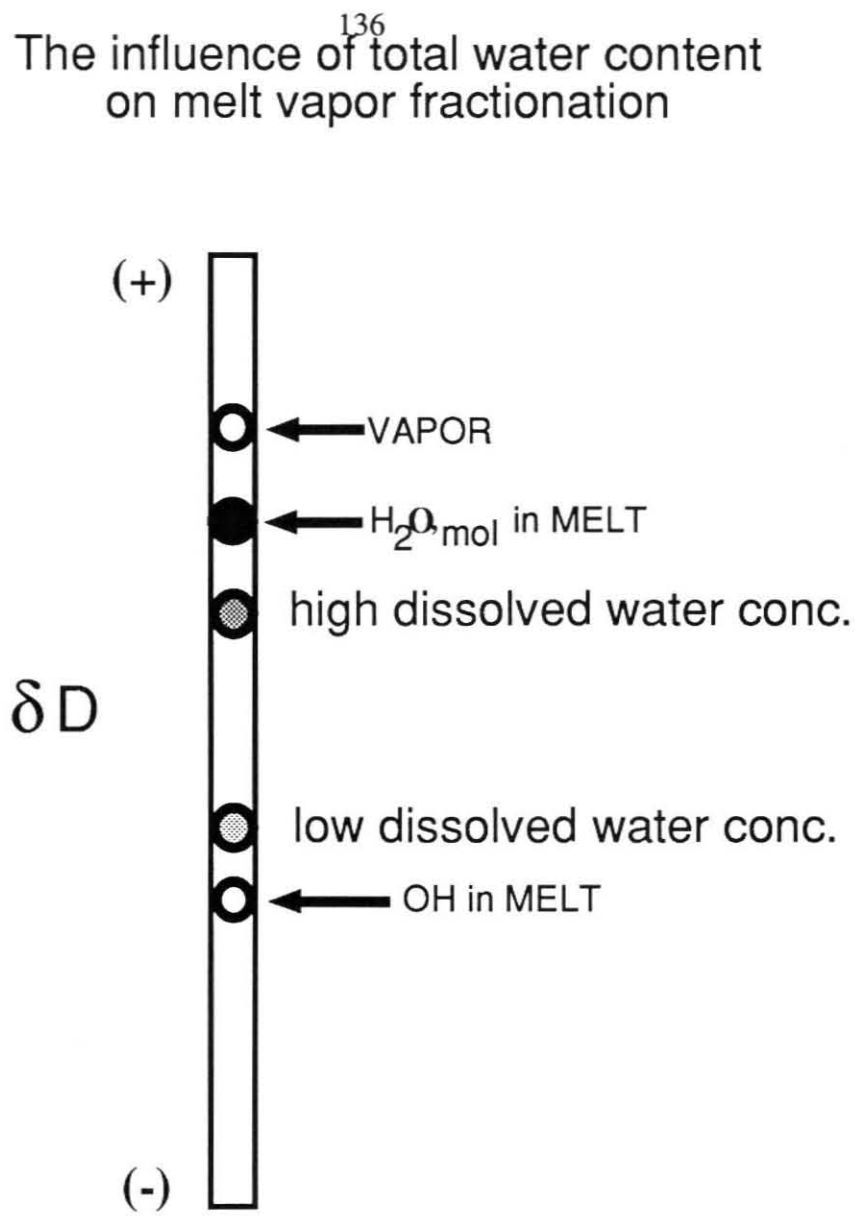

Figure 3.4: Schematic illustration showing the influence of total water content on the fractionation of hydrogen isotopes between bulk melt and vapor. Hypothetical fractionation factors: $\alpha_{\text{hydroxyl-vapor}} > \alpha_{\text{molecular species-vapor}}$

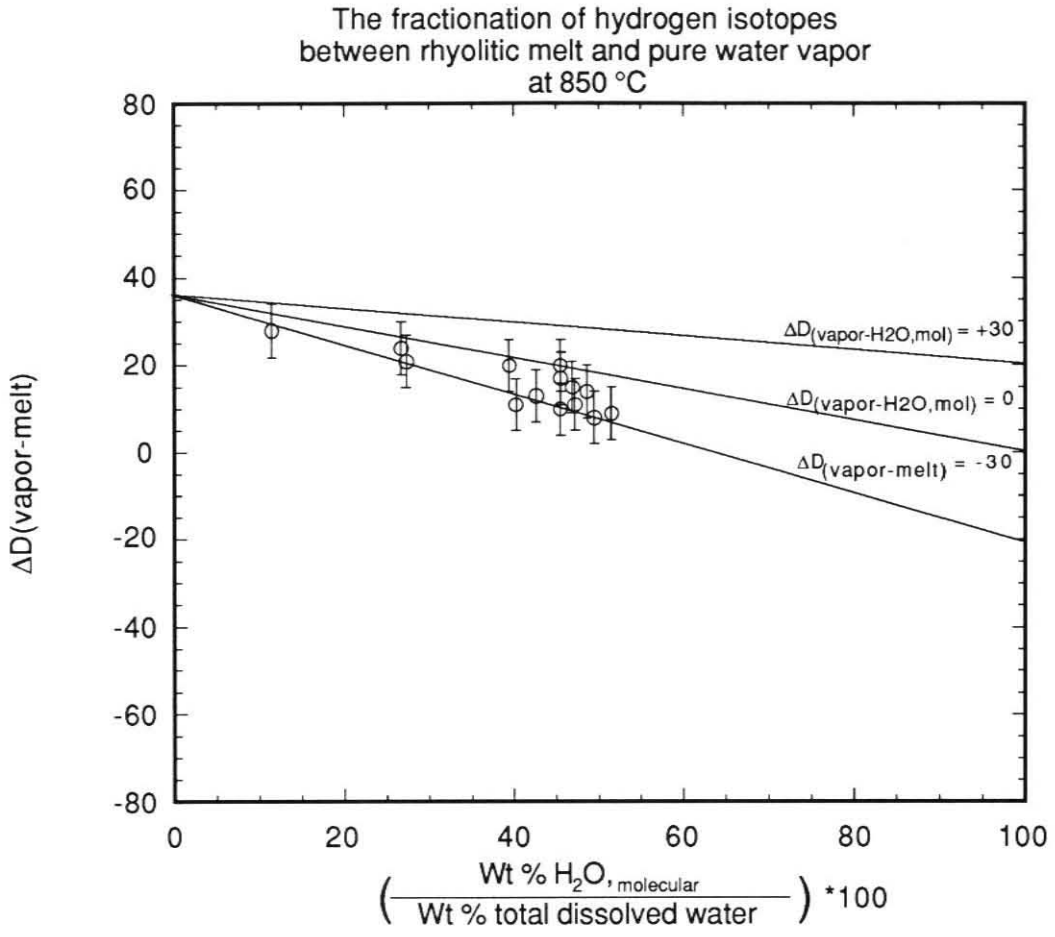

Figure 3.5: The fractionation of hydrogen isotopes as a function of the relative concentration of molecular species dissolved in the melt. Error bars assigned as in Fig. 3.3. The fractionation between vapor and hydroxyl groups is defined by the left-hand intercept of the figure, and the fractionation between vapor and the molecular water species is defined by the right-hand intercept of the figure. Three potential $\Delta_{vapor\text{-}H_2O,molecular}$ values are schematically shown for comparison to the data (the value of $\Delta_{vapor\text{-}OH}$ is fixed by the extrapolated value at 850°C of Dobson et al., 1989). The scatter in the water-rich samples may due to the formation of bubbles during the extraction process, driving bulk $\Delta_{vapor\text{-}melt}$ to lower values.

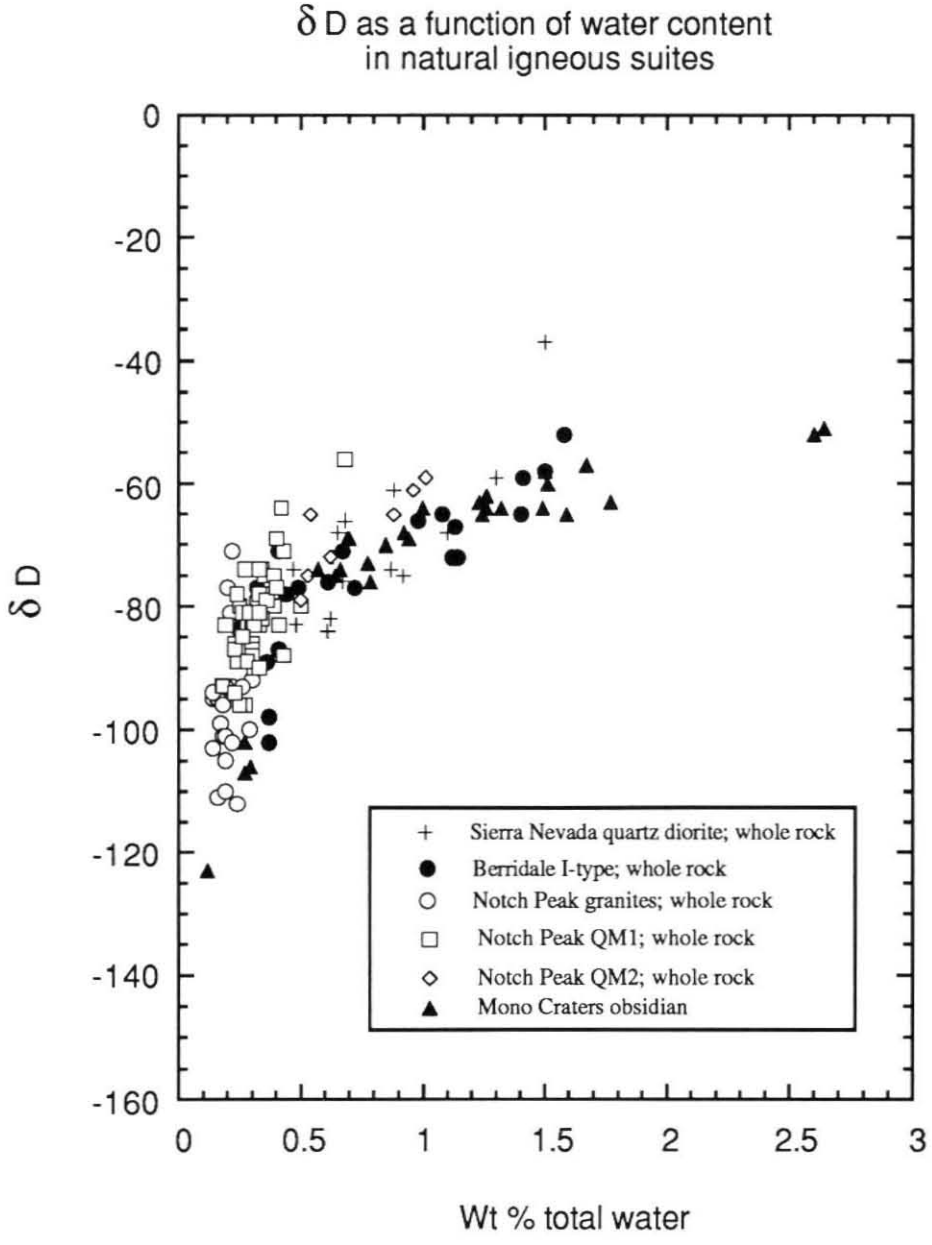

Figure 3.6: The isotopic composition of several natural igneous suites of rocks, including data on volcanic rocks (Mono Craters obsidians, Newman et al., 1988) and on plutonic rocks (Sierra Nevada quartz diorites, Masi et al., 1981; Berridale I-type granites, O'Neil and Chappell: Notch Peak granites and quartz diorites, Nabelek et al., 1983). The trend of decreasing δD with decreasing water content is observed in each of these suites.

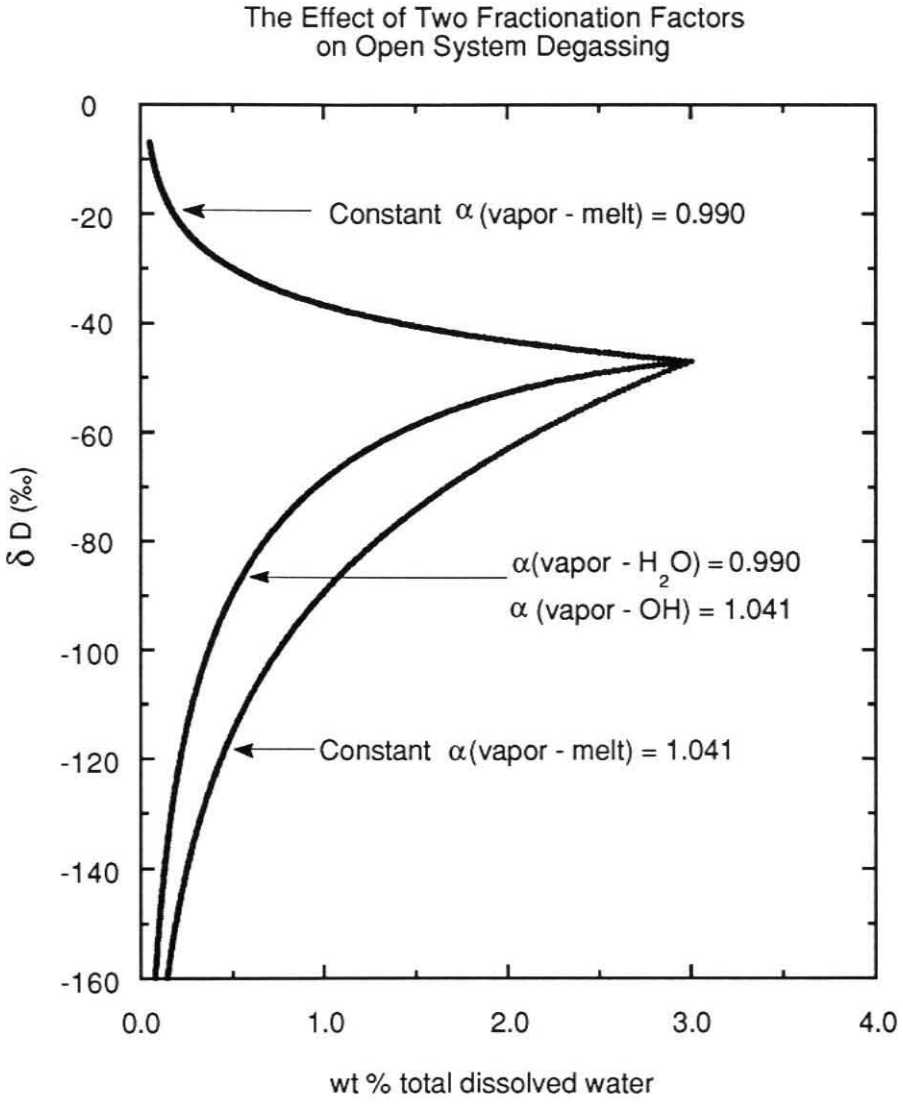

Figure 3.7: Hypothetical hydrogen isotopic fractionation paths for degassing magmas with an initial water content of 3.0 wt % total water. Individual curves describe open system Rayleigh fractionation for melt-vapor systems governed by one fractionation factor ($\alpha_{\text{vapor-bulk melt}} = 0.990$ and $\alpha_{\text{vapor-bulk melt}} = 1.041$) and melt-vapor systems governed by two fractionation factors ($\alpha_{\text{vapor-}H_2O,\text{ molecular}} = 0.990$ and $\alpha_{\text{vapor-OH}} = 1.041$).

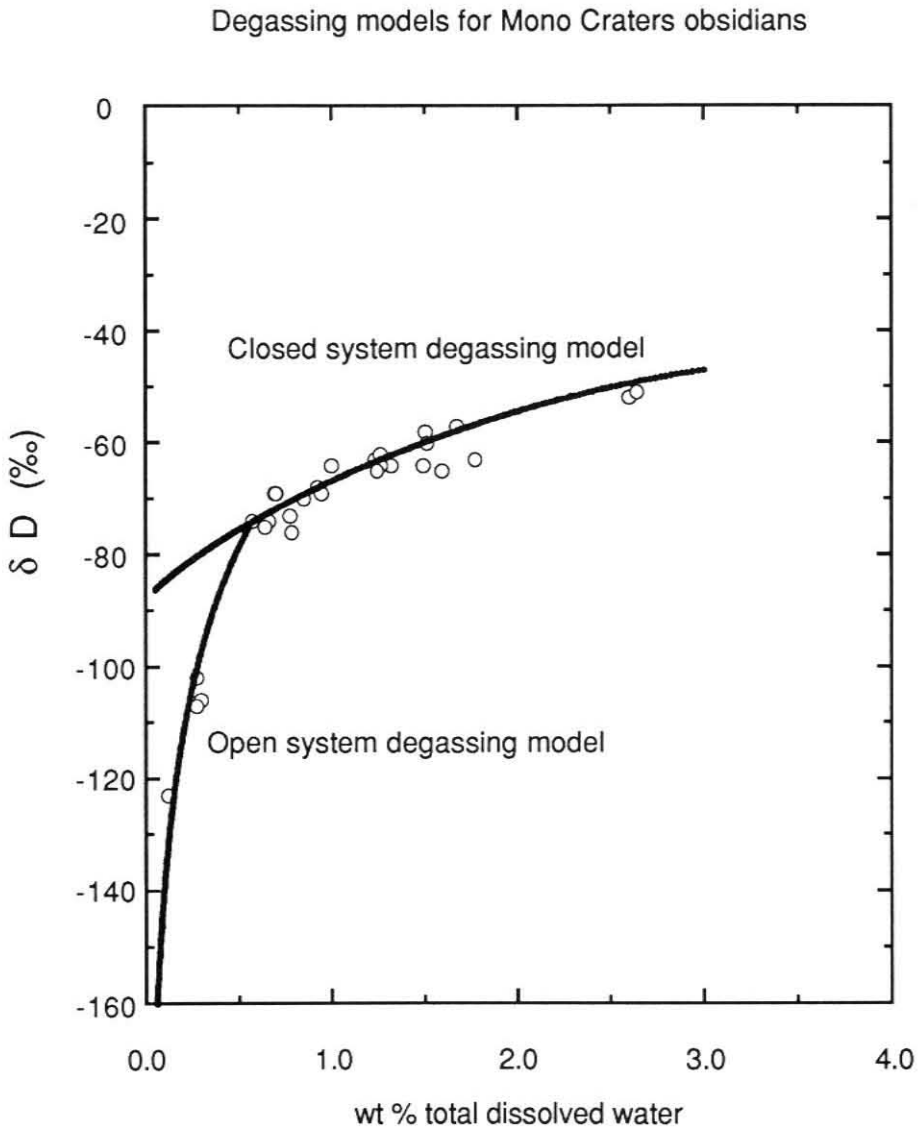

Figure 3.8: The isotopic composition of Mono Craters obsidians (from Newman et al, 1988) as a function of water content. The two curves represent the corresponding fractionation paths of a rhyolitic magma chamber with initially 3.0 wt % water undergoing closed system degassing to 0.8 wt %, and subsequent open system degassing. Vapor-melt equilibrium is governed by the two fractionation factors: $\alpha_{vapor\text{-}H_2O,molecular} = 0.990$ and $\alpha_{vapor\text{-}OH} = 1.041$.

References:

Aines, R. D., Silver, L. A., Rossman, G. R. & Stolper, E. M., 1983. Direct observation of water speciation in rhyolite at temperatures up to 850°C. *Geol. Soc. Am. Abstr. Prog.,* **15,** 512.

Albarede, F. & Provost, A., 1977. Petrological and geochemical mass-balance equations: an algorithm for least-squares fitting and general error analysis. *Computers and Geosciences,* **3,** 309-326.

Anderson, A. T., 1976. Magma mixing: petrological process and volcanological tool. *J. of Volcan. and Geotherm. Res.,* **1,** 3-33.

Anderson, S. W. & Fink, J. H., 1989. Hydrogen-isotope evidence for extrusion mechanisms of the Mount St Helens lava dome. *Nature,* **341,** 521-523.

Arndt, J. & Häberle, F., 1973. Thermal expansion and glass transition temperatures of synthetic glasses of plagioclase-like compositions. *Contrib. Mineral. Petrol.,* **39,** 175-183.

Bacon, C. R., 1977. High temperature heat content and heat capacity of silicate glasses: experimental determination and a model for calculation. *Amer. J. Sci.,* **277,** 109-135.

Bacon, C. R., 1982. Time-predictable bimodal volcanism in the Coso Range, California. *Geology,* **10,** 65-69.

Bacon, C. R., 1986. Magmatic inclusions in silicic and intermediate volcanic rocks. *Journal of Geophysical Research,* **91:B6,** 6091-6112.

Bartholomew, R. F., Butler, B. L., Hoover, H. L. & Wu, C. K., 1980. Infrared spectra of a water-containing glass. *J. Am. Ceram. Soc.,* **63,** 481-485.

Bartholomew, R. F. & Schreurs, J. W. H., 1980. Wide-line NMR study of protons in hydrosilicate glasses of different water content. *J. Non-crystalline Solids,* **38-39,** 679-684.

Bigeleisen, J., Perlman, M. L. & Prosser, H. C., 1952. Conversion of hydrogenic materials to hydrogen for isotopic analysis. *Analyt. Chem.*, **24,** 1356-1357.

Bottinga, Y. & Weill, D. F., 1970. Densities of liquid silicate systems calculated from partial molar volumes of oxide components. *Amer. J. Sci.*, **269,** 169-182.

Boulos, E. N. & Kreidl, N. J., 1972. Water in glass: a review. *J. Canad. Cer. Soc.*, **41,** 83-90.

Bowen, N. L., 1928. *The Evolution of the Igneous Rocks*. Princeton University Press, 334*pp*.

Brewster, D., 1826. On the existence of two new fluids in the cavities of minerals, which are immiscible, and possess remarkable physical properties. *Trans. Roy. Soc. Edin.*, **10,** 1-41.

Brigham, R. H. & O' Neil, J. R., 1985. Genesis and evolution of water in two-mica pluton: a hydrogen isotope study. *Chem. Geol.*, **49,** 159-177.

Burnham, C. W., 1975a. Thermodynamics of melting in experimental silicate-volatile systems. *Fortschr. Miner.*, **52,** 101-118.

Burnham, C. W., 1975b. Water and magmas; a mixing model. *Geochim. Cosmochim. Acta*, **39,** 1077-1084.

Burnham, C. W. & Davis, N. F., 1974. The role of H_2O in silicate melts: II. thermodynamic and phase relations in the system $NaAlSi_3O_8$-H_2O to 10 Kilobars, 700°C to 1300°C. *Amer. J. Sci.*, **274,** 902-940.

Burnham, C. W. & Jahns, R. H., 1962. A method for determining the solubility of water in silicate melts. *Amer. J. Sci.*, **260,** 721-745.

Chamberlin, R. T., 1908. *The gases in rocks*. The Carnegie Inst. of Wash., 80*pp*.

Clark, S. P., 1966. *Handbook of Physical Constants*. 587*pp*.

Craig, H. & Lupton, J. E., 1976. Primordial neon, helium, and hydrogen in oceanic basalts. *Earth Planet Sci. Lett.*, **31,** 369-385.

Davy, H., 1822. *Phil. Trans. Pt. II*, 367-376.

Day, H. W. & Fenn, P. M., 1982. Estimating the P-T-X H2O conditions during crystallization of low calcium granites. *J. Geology* , **90,** 485-507.

deGroot, S. R. & Mazur, P., 1962. *Non-equilibrium Thermodynamics.*

Dingwell, D. B., Harris, D. M. & Scarfe, C. M., 1984. The solubility of H_2O in melts in the system SiO_2-Al_2O_3-Na_2O-K_2O at 1 to 2 Kbars. *J. Geology,* **92,** 387-395.

Dingwell, D. B. & Webb, S. L., 1990. Relaxation in silicate melts. *Eur. J. Mineral.,* **2,** 427-449.

Dobson, P. F., Epstein, S. & Stolper, E. M., 1989. Hydrogen isotope fractionation between coexisting vapor and silicate glasses and melts at low pressure. *Geochim. Cosmochim. Acta.,* **53,** 2723-2730.

Dobson, P. F. & O'Neil, J. R., 1987. Stable isotope compositions and water contents of boninite series volcanic rocks from Chichi-jima, Bonin islands, Japan. *Earth Planet Sci. Lett.,* **82,** 75-86.

Dodd, D. M. & Fraser, D. B., 1966. Optical determinations of OH in fused silica. *J. of Applied Phys.,* **37,** 3911.

Eckert, H., Yesinowski, J. P., Silver, L. A. & Stolper, E. M., 1988. Water in silicate glasses: quantitation and structural studies by ^1H solid echo and MAS-NMR methods. *J. Phys. Chem.,* **92,** 2055-2064.

Eckert, H., Yesinowski, J. P., Stolper, E. M., Stanton, T. R. & Holloway, J., 1987. The state of water in rhyolitic glasses: a deuterium NMR study. *J. Non-crystalline Solids,* **93,** 93.

Egglar, D. H. & Burnham, C. W., 1984. Solution of H_2O in diopside melts: a thermodynamic model. *Contrib. Mineral. Petrol.,* **85,** 58-66.

Eichelberger, J. C., 1978. Andesitic volcanism and crustal evolution. *Nature,* **275,** 21-27.

Epstein, S. & Krishnamurthy, R. V., 1990. Environmental information in the isotopic record in trees. *Phil. Trans. R. Soc. Lond.,* **A 330,** 427-439.

Ernsberger, F. M., 1977. Molecular water in glass. *J. Am. Ceram. Soc.,* **60,** 91-92.

Friedman, I. & Smith, R. L., 1958. The deuterium content of water in some volcanic glasses. *Geochim. Cosmochim. Acta,* **15,** 218-228.

Gerlach, D. C. & Grove, T. L., 1982. Petrology of Medicine Lake Highland volcanics: characterization of endmembers of magma mixing. *Contrib. Mineral. Petrol.,* **80,** 147-159.

Godfrey, J. D., 1962. The deuterium content of hydrous minerals from the East-Central Sierra Nevada and Yosemite National Park. *Geochim. Cosmochim. Acta,* **26,** 1215-1245.

Goranson, R., 1931. The solubility of water in granite magmas. *Amer. J. Sci.,* **22,** 481-502.

Goranson, R. W., 1936. Silicate-water systems: the solubility of water in albite-melt. *Trans. Am. Geophys. Union,* **17,** 257-259.

Goranson, R. W., 1938. Silicate-water systems; phase equilibria in the $NaAlSi_3O_8$-H_2O and $KAlSi_3O_8$-H_2O systems at high temperatures and pressures. *Amer. J. Sci.,* **35-A,** 71-91.

Graham, T., 1876. *Chemical and Physical Researches.*

Guggenheim, E. A., 1952. *Mixtures.* Oxford University Press, 270*pp.*

Hamilton, D. L., Burnham, C. W. & Osborn, E. F., 1964. The solubility of water and effects of oxygen fugacity and water content on crystallization in mafic magmas. *J. Petrol.,* **5,** 21-39.

Hamilton, D. L. & Oxtoby, S., 1986. Solubility of water in albite-melt determined by the weight-loss method. *J. Geology,* **94,** 626-630.

Harrison, A. J., 1947. Water content and infrared transmission of simple glasses. *Am. Ceram. Soc. Jour.,* **30,** 362-366.

Hodges, F. N., 1973. Solubility of H2O in forsterite melt at 20 Kbar. *Carnegie Inst. Wash. Yearb.,* **72,** 495-497.

Hodges, F. N., 1974. The solubility of H_2O in silicate melts. *Carnegie Inst. Wash. Yearb.*, **73,** 251-255.

Holloway, J. R., 1977. *Fugacity and activity of molecular species in supercritical fliuds.* D. Reidel, 161-181.

Huppert, H. E. & Sparks, R. S. J., 1980. The fluid dynamics of a basaltic magma chamber replenished by influx of hot, dense ultrabasic magma. *Contrib. Mineral. Petrol.*, **75,** 279-289.

Karsten, J. L., Holloway, J. R. & Delaney, J. R., 1982. Ion microprobe studies of water in silicate melts: temperature-dependent water diffusion in obsidian. *Earth Planet. Sci. Lett.*, **59,** 420-428.

Keller, W. D. & Pickett, E. E., 1954. Hydroxyl and water in perlite from Superior, Arizona. *Am. J. Sci.*, **252,** 87-98.

Kennedy, G. C., 1950. A portion of the system silica-water. *Econ. Geology,* **45,** 629-653.

Kennedy, G. C., Wasserburg, G. J., Heard, H. C. & Newton, R. C., 1962. The upper three phase region in the system SiO_2-H_2O. *Amer. J. Sci.*, **260,** 501-521.

Kerrick, D. M., 1987. Cold-seal systems. In: G. C. Ulmer & H. L. Barnes (ed.) *Hydrothermal Experimental Techniques*. John Wiley & Sons, 293-323.

Khitarov, N. I., Lebedev, E. B. & Rengarten, E. V., 1959. The solubility of water in basaltic and granitic melts. *Geokhimiya,* **5,** 479-492.

Kurkjian, C. R. & Russell, L. E., 1958. Solubility of water in molten alkali silicates. *J. Soc. Glass Tech.*, **42,** 130-144.

Kuroda, Y., Suzuoki, T., Matsuo, S. & Kanisawa, S., 1974. D/H fractionation of coexisting biotite and hornblende in some granitic rock masses. *J. Japan. Assoc. Min. Petr. Econ. Geol.*, **69,** 95-102.

Kyser, T. K. & O'Neil, J. R., 1984. Hydrogen isotope systematics of submarine basalts. *Geochim. Cosmochim. Acta,* **48,** 2123-2133.

Langer, K. & Flörke, O. W., 1974. Near infrared absorption spectra (4000-9000 cm^{-1}) of opals and the role of "water" in these $SiO_2 \cdot nH_2O$ minerals. *Fortsch. Miner.*, **52,** 17-51.

Leshin, L. A., Stolper, E. M. & Eckert, H., 1990. Water in alkali silicate glasses: A MAS NMR and FTIR study. *V.M. Goldschmidt Conf. Progr. & Abstr.*, **2,** 61.

London, D., Hervig, R. L. & Morgan VI, G. B., 1988. Melt-vapor solubilities and elemental partitioning in peraluminous granite-pegmatite systems: experimental results with Macusani glass at 200 MPa. *Contrib. Mineral. Petrol.*, **99,** 360-373.

Maaløe, S. & Wyllie, P. J., 1975. Water content of a granite magma deduced from the sequence of crystallization determined experimentally with water-undersaturated conditions. *Contrib. Mineral. Petrol.*, **52,** 175-191.

Masi, U., O'Neil, J. R. & Kistler, R. W., 1981. Stable isotope systematics in Mesozoic granites of central and northern California and southwestern Oregon. *Contrib. Mineral. Petrol.*, **76,** 116-126.

McKinney, C. R., McCrea, J. M., Epstein, S., Allen, H. A. & Urey, H. C., 1950. *Rev. Sci. Instr.*, **21,** 724.

McMillan, P. F., Jakobsson, S., Holloway, J. R. & Silver, L. A., 1983. A note on the Raman spectra of water-bearing albite glasses. *Geochim. Cosmochim. Acta,* **47,** 1937-1943.

McMillan, P. W. & Chlebik, A., 1980. The effect of hydroxyl ion content on the mechanical and other properties of soda-lime-silica glass. *J. Non-cryst. Solids,* **38,** 509-514.

Mond, L., Ramsay, W. & Shields, J., 1895. On the occlusion of oxygen and hydrogen by platinum black. (Part I.).

Moore, J. G., 1970. Water content of basalt erupted on the ocean floor. *Contrib. Mineral. Petrol.*, **28,** 272-279.

Moulson, A. J. & Roberts, J. P., 1960. Water in silica glass. *Trans. Brit. Ceram. Soc.*, **59,** 388-399.

Mysen, B. O., Virgo, B., Harrison, W. J. & Scarfe, C. M., 1980. Solubility mechanisms of H_2O in silicate melts at high pressures and temperatures: A Raman spectroscopic study. *Am. Mineral.*, **65,** 900-914.

Mysen, B. O. & Virgo, D., 1980. Solubility mechanisms of water in basalt melt at high pressures and temperatures: $NaCaAlSi_2O_7$-H_20 as a model. *Am. Mineral.*, **65,** 1176-1184.

Mysen, B. O. & Virgo, D., 1986. Volatiles in silicate melts at high pressure and temperature: 1. Interaction between OH groups and Si^{4+}, Al^{3+}, Ca^{2+}, Na^{+}, and H^{+}. *Chem. Geol.*, **57,** 303-331.

Nabelek, P. I., O'Neil, J. R. & Papike, J. J., 1983. Vapor phase exsolution as a controlling factor in hydrogen isotope variation in granitic rocks: the Notch Peak granitic stock, Utah. *Earth Planet Sci. Lett.*, **66,** 137-150.

Newman, S., Epstein, S. & Stolper, E. M., 1988. Water, carbon dioxide, and hydrogen isotopes in glasses from the ca. 1340 A.D. eruption of the Mono Craters, California: Constraints on degassing phenomena and initial volatile content. *J. Volcan. Geotherm. Res.*, **35,** 75-96.

Newman, S., Stolper, E. M. & Epstein, S., 1986. Measurement of water in rhyolitic glasses: calibration of an infrared spectroscopic technique. *Am. Mineral.*, **71,** 1527-1541.

Nier, A. O., 1947. *Rev. Sci. Instr.*, **18,** 398.

O'Neil, J. R., 1986. Theoretical and experimental aspects of isotopic fractionation. In: J. W. Valley, H. P. Taylor & J. R. O'Neil (ed.) *Stable isotopes in high temperature geological processes*. 16. Min. Soc. of Amer., 1-40.

O'Neil, J. R. & Chappell, B. W., 1977. Oxygen and hydrogen isotope relations in the Berridale batholith. *J. Geol. Soc. Lond.*, **133,** 559-571.

O'Neil, J. R., Shaw, S. E. & Flood, R. H., 1977. Oxygen and hydrogen isotope compositions as indicators of granite genesis in the New England Batholith, Australia. *Contrib. Mineral. Petrol.*, **62,** 313-328.

Oldenburg, C. M., Spera, F. J., Yuen, D. A. & Sewell, G., 1989. Dynamic mixing in magma bodies: theory, simulations, and implications. *J. Geophys. Res.*, **94:B7,** 9215-9236.

Orlova, G. P., 1964. Solubility of water in albite melts-under pressure. *Internat. Geology Rev.*, **6,** 254-258.

Ostrovskiy, I. A., Orlova, G. P. & Rudnitskaya, Y. S., 1964. Stoichiometry in the solution of water in alkali-aluminosilicate melts. *Doklady Akad. Nauk SSR,* **157,** 149-151.

Oxtoby, S. & Hamilton, D. L., 1978. The discrete association of water with Na_2O and SiO_2 in NaAl silicate melts. *Contrib. Mineral. Petrol.*, **66,** 185-188.

Pichavant, M., 1981. An experimental study of the effect of boron on a water-saturated haplogranite at 1 Kbar pressure: geological applications. *Contrib. Mineral. Petrol.*, **76,** 430-439.

Poreda, R., 1985. Helium-3 and deuterium in back-arc basalts: Lau-Basin and the Mariana Trough. *Earth Planet Sci. Lett.*, **73,** 244-254.

Poreda, R., Schilling, J.-G. & Craig, H., 1986. Helium and hydrogen isotopes in ocean-ridge basalts north and south of Iceland. *Earth Planet Sci. Lett.*, **78,** 1-17.

Prestwich, J., 1885. On the agency of water in volcanic eruptions: with some observations on the thickness of the Earth's crust from a geological point of view; and on the primary cause of volcanic action. *Proc. R. Soc. London,* **38,** 253-260.

Pyle, D. M., 1991. The volume and residence time of magma beneath active volcanoes. *submitted to Earth Planet. Sci. Lett.,*

Rice, A., 1981. Convective fractionation: a mechanism to provide cryptic zoning (macrosegregation), layering, crescumulates, banded tuffs and explosive volcanism in igneous processes. *J. Geophys. Res.,* **86:B1,** 405-417.

Richet, P., Roux, J. & Pineau, F., 1986. Hydrogen isotope fractionation in the system H_2O-liquid $NaAlSi_3O_8$: New data and comments on D/H fractionation in hydrothermal experiments. *Earth Planet. Sci. Lett.,* **78,** 115-120.

Robie, R. A., Hemingway, B. S. & Fisher, J. R., 1978. Thermodynamic properties of minerals and related substances at 298.15K and 1 bar(10^5 Pascals) pressure and at higher temperatures. *U. S. Geol. Surv. Bull.,* **1452,**

Russell, J. K., 1990. Magma mixing processes: insights and constraints from thermodynamic calculations. In: (ed.) *Modelling Igneous Petrologic Processes.* 22. Reviews in Mineralogy, 153.

Russell, L. E., 1957. Solubility of water in molten glass. *J. Soc. Glass Technology,* **41,** 304-317T.

Sakuyama, M., 1981. Petrological study of the Myoko and Kurohime volcanoes, Japan: crystallization sequence and evidence for magma mixing. *J. of Petrol.,* **22,** 553-583.

Schairer, J. F. & Bowen, N. L., 1947. The system anorthite-leucite-silica. *Com. Géol. El. de Finlande Bull.,* **24,** 67-87.

Schairer, J. F. & Bowen, N. L., 1955. The system K_2O-Al_2O_3-SiO_2. *Amer. J. Sci.,* **253,** 681-746.

Scherer, G. W., 1984. Use of the Adams-Gibbs equation in the analysis of structural relaxation. *J. Amer. Ceram. Soc.,* **67,** 504-511.

Scherer, G. W., 1986. *Relaxation in glass and composites.* Wiley, 331*pp.*

Scholze, H., 1960. Zur frage der unterscheidung zwischen H_2O-moleculen und OH-Gruppen in Gläsern und Mineralen. *Naturwiss,* **47,** 226-227.

Shaw, H. R., 1963a. Obsidian-H_2O viscosities at 1000 and 2000 bars in the temperature range 700°C to 900°C. *J. Geophys. Res.*, **68,** 6337-6343.

Shaw, H. R., 1963b. Theoretical solubility of H_2O in silicate melts: quasi-crystalline models. 601-617.

Shaw, H. R., 1963c. The four-phase curve sanidine-quartz-liquid-gas between 500 and 4000 bars. *Am. Mineral.*, **48,** 883-896.

Shaw, H. R., 1972. Viscosities of magmatic silicate liquids: an empirical method of prediction. *Amer. J. Sci.*, **272,** 870-893.

Shepherd, E. S., 1938. The gases in rocks and some related problems. 311-351.

Silver, L. A., 1988. Water in silicate glasses. Ph.D., Cal. Inst. Tech.

Silver, L. A., Ihinger, P. D. & Stolper, E. M., 1990. The influence of bulk composition on the speciation of water in silicate glasses. *Contrib. Mineral. Petrol.*, **104,** 142-162.

Silver, L. A. & Stolper, E. M., 1985. A thermodynamic model for hydrous silicate melts. *J. Geology,* **93,** 161-178.

Silver, L. A. & Stolper, E. M., 1989. Water in albitic glasses. *J. Petrol.*, **30,** 667-709.

Smith, R. L., 1979. Ash-flow magmatism. *Geol. Soc. Am.*, **Special Paper 180,** 5-16.

Sorby, H. C. & Butler, P. J., 1869. On the structure of rubies, sapphires, diamonds, and some other minerals. *Pros. Roy. Soc.*, **17,** 291-303.

Sparks, R. S. J. & Marshall, L. A., 1986. Thermal and mechanical constraints on mixing between mafic and silicic magmas. *J. Volcan. Geotherm. Res.*, **29,** 99-124.

Sparks, R. S. J., Sigurdsson, H. & Wilson, L., 1977. Magma mixing: a mechanism for triggering acid explosive eruptions. *Nature,* **267,** 315-318.

Spengler, C. J. & Burnham, C. W., 1962. Compositions in the upper three-phase region of the system $KAlSi_3O_8$-H_2O at pressures up to 6 kilobars. *Geol. Soc. Amer. Spec. Paper,* **68,** 277.

Stern, C. R. & Wyllie, P. J., 1973. Water-saturated and undersaturated melting relations of a granite to 35 kilobars. *Earth Planet Sci. Lett.*, **18,** 163-167.

Stewart, D. B., 1958. The system $CaAl_2Si_2O_8$-SiO_2-H_2O. *Geol. Soc. Amer. Bull.*, **69,** 1648.

Stolper, E. M., 1982a. Water in silicate glasses: an infrared spectroscopic study. *Contrib. Mineral. Petrol.*, **81,** 1-17.

Stolper, E. M., 1982b. The speciation of water in silicate melts. *Geochim. Cosmochim. Acta.*, **46,** 2609-2620.

Stolper, E. M., 1989. Temperature dependence of the speciation of water in rhyolitic melts and glasses. *Am. Mineral.*, **74,** 1247-1257.

Stolper, E. M., Silver, L. A. & Aines, R. D., 1983. The effects of quenching rate and temperature on the speciation of water in silicate glasses. *EOS,* **64,** 339.

Suzuoki, T. & Epstein, S., 1976. Hydrogen isotope fractionation between OH-bearing minerals and water. *Geochim. Cosmochim. Acta,* **40,** 1229-1240.

Tait, S., Jaupart, C. & Vergniolle, S., 1989. Pressure, gas content and eruption periodicity of a shallow, crystallizing magma chamber. *Earth Planet. Sci. Lett.*, **92,** 107-123.

Taylor, B. E., 1988. Degassing of rhyolitic magmas: hydrogen isotope evidence and implications for magmatic-hydrothermal ore deposits. In: R. P. Taylor & D. F. Strong (ed.) *Recent Advances in the Geology of Granite-Related Mineral Deposits.* 39. Canadian Inst. Min. Metal., 33-49.

Taylor, B. E., Eichelberger, J. C. & Westrich, H. R., 1983. Hydrogen isotopic evidence of rhyolitic magma degassing during shallow intrusion and eruption. *Nature,* **306,** 541-545.

Taylor, B. E. & Westrich, H. R., 1985. Hydrogen isotope exchange and water solubility in experiments using natural rhyolite obsidian. *EOS,* **66,** 387.

Taylor, H. P., 1974. The application of oxygen and hydrogen isotope studies to problems of hydrothermal alteration and ore deposition. *Econ. Geol.*, **69,** 843-883.

Tilden, W. A., 1896. An attempt to determine the condition in which helium and the associated gases exist in minerals. *Pros. Roy. Soc.*, **59,** 218-224.

Tomlinson, J. W., 1956. A note on the solubility of water in a molten sodium silicate. *J. Soc. Glass Tech.*, **40,** 25-31T.

Tuttle, O. F. & Bowen, N. L., 1958. Origin of granite in the light of experimental studies in the system $NaAlSi_3O_8$-$KAlSi_3O_8$-SiO_2-H_2O. *Geol. Soc. Amer. Mem.*, **74,** 153.

Uys, J. M. & King, T. B., 1963. The effect of basicity on the solubility of water in silicate melts. *Trans. Met. Soc. A.I.M.E.*, **227,** 492-500.

Wadge, A., 1980. Output rate of magma from active central volcanoes. *Nature,* **288,** 253-255.

Wasserburg, G. J., 1957. The effects of H_2O in silicate systems. *J. Geol.*, **65,** 15-23.

Watson, E. B., 1979. Diffusion of cesium ions in H_2O-saturated granitic melt. *Science,* **205,** 1259-1260.

Whitney, J. A., 1975. The effects of pressure, temperature, and XH_2O on phase assemblage in four synthetic rock compositions. *J. Geology,* **83,** 1-31.

Wones, D. R., 1972. Stability of biotite: a reply. *Am. Mineral.*, **57,** 316-317.

Wones, D. R. & Eugster, H. P., 1965. Stability of biotite: experiment, theory, and application. *Am. Mineral.*, **50,** 1228-1272.

Yang, J. & Epstein, S., 1982. The concentration and isotopic composition of hydrogen and carbon in meteorites. *Lunar and Planet. Sci.*, **XIII,** (abstr).

Yoder, H. S., Stewart, D. B. & Smith, J. R., 1956. Ternary feldspars. *Carnegie Inst. Wash. Year Book,* **57,** 189-191.

Zhang, Y., Stolper, E. M. & Ihinger, P. D., 1990. Reaction kinetics of $H_2O + O = 2OH$ and its equilibrium revisited. *V.M. Goldschmidt Conf. Progr. & Abstr.*, **2,** 94.

Zhang, Y., Stolper, E. M. & Wasserburg, G. J., 1991. Diffusion of water in rhyolitic glasses. *Geochim. Cosmochim. Acta,* **55,** 441-456.

Zhang, Y., Walker, D. & Lesher, C. E., 1989. Diffusive crystal dissolution. *Contrib. Mineral. Petrol.*, **102,** 492-513.

Appendix I:

A Modified Rapid-Quench Cold-Seal Pressure Vessel

Introduction:

Experimental investigations at mid to upper crustal conditions are most easily performed in cold-seal pressure vessels (Tuttle, 1949). These apparatus are capable of maintaining steady temperatures and pressures for the long durations often necessary for attaining chemical equilibrium. There are two characteristics of the experimental apparatus that determine whether the quenched sample represents the equilibrium assemblage at run conditions; these are the temperature gradient across the sample during the run and the quench rate at the conclusion of the experiment. Steady state temperature gradients across the sample establish chemical potential gradients which lead to inhomogeneous run products. The quenching procedure relies on the assumption that no reaction occurs during the relaxation of the sample to atmospheric conditions. This assumption leads to problems with reactions that are particularly sensitive to temperature, and the need for faster quench rates has increasingly become necessary (see Chapters 1-3). This short note introduces a new design for cold-seal pressure vessels that significantly reduces temperature gradients and increases the quench rate of the apparatus. In addition, the design of this pressure vessel lengthens the life of the bombs and is considerably safer to use than conventional apparatus.

I describe a modification of the cold-seal bomb first presented by Tuttle (1949). The apparatus consists of a Ni-alloy bomb inserted into a furnace such that the pressure seal remains external to the furnace; hence the apparatus has been given the name "cold-seal" pressure vessel. Quenching is achieved by blasting the bomb with compressed air and subsequently immersing it in cold water. Thus, the experimental charge is cooled only after conducting heat through the thick bomb walls. The sample takes about five minutes to fall from 700°C to room temperature. Wellman (1970) modified the apparatus by lengthening the bomb such that much of the vessel extended outside the furnace. At the conclusion of the experiment, the horizontally-mounted apparatus is tilted such that the experimental charge is allowed to slide down the length of the vessel to the cooled external

portion of the bomb. He estimated quench times from 700°C to 100°C at three seconds or less. Rudert et al. (1976) further modified this design by dividing the one long bomb into two separate bombs connected by a double-coned pressure seal. The same procedure of opening the split horizontal furnace, tilting the apparatus to a vertical position, and jostling the vessel yields estimated quench times approaching one second. Another method for rapidly cooling experimental charges has been developed by Jacobs and Kerrick (1983). They inject cold fluid over the capsule which remains in its run position, and they observe temperature drops from 600°C to 300°C in 30 seconds. The quench procedure described in this note is similar to that described by Greenwood (Kerrick, 1987) and was developed independently in our laboratory at Caltech. The principle is modeled after Wellman's concept of capsule mobility, but quenching is achieved by rapid movement of the capsule from the hot to the cold region of the apparatus without any need of manipulating the furnace or the pressure vessel. This design simplifies the quenching procedure and provides the maximum quench rate attainable in hydrothermal apparatus.

Much discussion has been devoted to the problem of unacceptable thermal gradients in the horizontally-mounted apparatus. Boettcher and Kerrick (1971) discussed the need for the insertion of a filler rod to reduce the capacity for convection of the pressure medium. Rudert et al. (1976) also discussed the need for filler rods and found temperature gradients of less then 5°C across reasonable sample lengths (3 cm) only when using particularly long (30.5 cm) pressure vessels with argon as a pressure medium. Ludington (1978) measured the temperature gradients in cold-seal apparatus equipped with water jackets around the extruding cold end of the vessel and observed unacceptable gradients of 60 degrees across 3 cm long experimental charges. He noted that tilting the horizontal apparatus by as much as 10 degrees may reduce these gradients to 20 degrees or less. These modifications strive to minimize the powerful effect of an unstable thermal configuration. One approach to minimizing temperature gradients across the sample is to position the experimental charge in a thermally stable environment. I present and

characterize a new vessel design in which the hot spot sits above the cooler portion of a vertically-oriented apparatus.

The design of the apparatus:

The apparatus is schematically shown in Fig. A1. The principle of the apparatus is to magnetically suspend the sample in the hot portion of the bomb. The vessel consists of a hot bomb connected to a cold bomb using a double-coned coupling to make two pressure seals. A cooling nut is used to apply pressure on the coupling to ensure pressure-tight seals. The hollow space between the cooling nut and the coupling is filled with flowing chilled water. At the conclusion of the experiment, quenching is achieved by dropping the sample into the coupling whose exterior is bathed in cold water.

A doughnut-shaped permanent magnet wraps around the cold bomb such that it easily slides up and down the length of the bomb. The sample is attached to the top of an elevator rod which is capable of sliding through the internal length of the bomb. The only magnetic materials present in the system are the 1 inch base of the elevator rod (made of simple tool steel) and the magnet itself. The length of the elevator rod is designed such that the sample resides at the highest (and hottest) region of the bomb when the magnet is positioned immediately below the cooling nut. Placement of the hot sample into the cold bomb during the quench will heat the surrounding pressure medium and may prevent the sample from rapidly reaching room temperature. To combat this effect, the bomb coupling was made of a material with a high thermal conductivity. A beryllium copper alloy was chosen for the coupling because of its high thermal conductivity (1.3 Watts/cm·sec), and because its coefficient of thermal expansion is similar to that of the René alloy hot bomb ($20.6*10^{-6}$ per °C). Heat transferred from the sample to the pressure medium is efficiently carried away through the coupling and into the recirculating water system. To ensure placement of the sample within the Be-Cu coupling on quench, a pedestal of appropriate length rests at the bottom of the cold bomb.

Isobaric quenching is not possible in this apparatus. Rather, on lowering the elevator rod into the colder portion of the bomb, the heated volume previously occupied by the rod is replaced by the more expandable pressure medium. A pressure increase then results in the fixed-volume system. Some elevator rod designs can minimize this effect. I have chosen to use a hollow silver palladium tube (.090" OD) for three reasons; its shape is conducive for securely mounting the sample, it is easily attached to the tool steel base, and its behavior is inert in any conventional pressure medium. A typical pressure increase observed in quenching a platinum capsule 0.75" in length is about 60 bars.

Vessel characterization:

Temperatures are monitored using chromel-alumel Type K thermocouples inserted into an external bore adjacent to the sample in the hot bomb. A continuous internal thermal profile has been determined using a 50 inch long flexible (.010" OD) inconel-sheathed Type K thermocouple. The thermocouple is welded through the pressure medium input port located at the bottom of the cold bomb. The bulk of the sheath is coiled around the pedestal before firmly attaching it through the full length of the elevator rod. The thermocouple sheath then acts as an expandable spring as the elevator rod is raised and lowered within the hot bomb. The thermocouple junction (next to the sample) monitors the temperature inside the vessel. This position is easily determined by the location of the magnet relative to the cooling nut. Table A1 presents the results of several internal thermal profiles of the rapid-quench apparatus using the coiled thermocouple. Included are profiles for apparatus under a range of pressures and control temperatures. Water is used as a pressure medium in these experiments, as it has been shown to display the most pronounced thermal gradient effects (Rudert et al., 1976).

Figure A2 shows the temperature profiles extending from the hot spot to within an inch of the bomb coupling for vessels held at three different temperatures. Temperature profiles from 850°C, 750°C, and 650°C hot spots are all similar. The important feature to

note is the flat shape at the high end of all these profiles. The temperatures fall less than 15 degrees over the first inch of the apparatus, ensuring acceptable gradients across typical experimental charges. It should be noted that these temperature gradients may be reduced simply by flushing the cooling water further below the bottom of the furnace. The design in Fig. A1 is intended to minimize the length of the hot bomb by fully inserting it into the furnace. This is advantageous in that it minimizes the length required for the elevator rod to extend into the hot spot (and hence minimizing the length of the cold bomb to ensure quenching within the bomb coupling). Thus, this design is intended to minimize cost and may easily be modified to satisfy thermal gradient constraints for longer experimental charges if necessary.

Increasing bomb pressure will compress the fluid and change the viscosity and heat conductivity of the pressure medium. Varying the total pressure inside the bomb will thus change the internal thermal profile of the pressure vessel. Figure A3 shows two internal thermal profiles for apparatus with hot spot temperatures at 650°C and water pressure at 300 and 1000 bars. The profiles are virtually identical in the vicinity of the sample. The largest differential occurs midway down the bomb and is smaller than 20°C. The design of the modified rapid-quench pressure vessel is effective at minimizing temperature gradients over the full range of operating pressures in the cold-seal apparatus.

The configuration of the apparatus within the furnace will also affect the temperature profile within a pressure vessel. Each furnace and bomb configuration will have its own temperature profile and should be independently determined. Figure A4 shows the dependence of internal temperature on the volume of air that exists between the top of the bomb and the bottom of a plug inserted into the top of the furnace. The profile labeled "short plug" has an open space of 2 1/2" above the bomb, whereas the "long plug" has an open space of less than 1/2". The length of the plug has a noticeable effect on the temperature gradient within the vessel; filling the two inches of space above the bomb with solid material reduces the temperature gradients by several degrees over the typical length

of a sample in the hot spot. This data suggests care in positioning the bomb within the furnace is required to achieve the smallest possible temperature gradient across an experimental sample.

Discussion:

The modified rapid-quench pressure vessel presented in this note has several useful capabilities new to the cold-seal apparatus. It has been adapted to higher strength alloys capable of achieving higher temperatures and pressures. Williams (1966, 1968) introduced an alloy consisting of 99.42 wt% molybdenum, 0.50 wt% titanium, and 0.08 wt% zirconium which is capable of maintaining temperatures of 1200°C at several kilobars pressure. This alloy easily oxidizes in air at high temperatures and must be bathed in argon to prevent metal embrittlement and subsequent explosive rupture. Figure A1 illustrates the adaptations necessary for such a TZM cold-seal vessel. An inconel sheath is tightened into the cooling nut with an additional input port through which argon flows at a steady rate. It should be noted that argon must be used as the pressure medium in this apparatus. The modified design presented in this paper dramatically increases the quench rate of experiments performed at temperatures higher than 900°C.

The design has another useful characteristic for experimentalists. The pressure vessel can be brought to the run temperature of interest while holding the sample at room temperature. This allows precisely measuring run times to within a few seconds. This feature is particularly useful when performing experiments that determine the kinetic behavior of reactions; for example, crystal nucleation, bubble growth, and dissolved species' reaction rates can be accurately determined using precise run times at pressure and temperature in this apparatus (see Chapter 1). In addition, diffusion studies at high temperatures and pressures are ideally suited for this apparatus. Appendix 2 presents one such example in determining the relative permeability of hydrogen through precious metals

with important implications for the stability of oxygen, hydrogen, and water fugacities in experimental charges.

There are practical advantages to the design presented in this note. The quench procedure does not require removal of the vessel from the furnace; thus the hot bomb is never thermally "shocked" and can cool down as slowly as desired. This reduces radial stresses created by differential temperatures between the hot interior and the chilled exterior of the bomb. The gentle bomb quench has resulted in noticeably longer-lived vessels. Additionally, the design can be configured such that the magnet can be lowered remotely, either with an electrical switch or a manual pulley set-up. Thus, the operator is never exposed to the hot apparatus. The modified cold-seal pressure-vessel presented in this note can thus be considerably safer to use than conventional apparatus currently in use.

Summary:

I introduce a modified rapid-quench cold-seal pressure vessel which provides faster quench rates, smaller thermal gradients, and longer-lived vessels. It is safer and easier to use than conventional cold-seal apparatus. Existing conventional apparatus can easily be converted to the modified design with the construction of just a few relatively inexpensive pieces.

TABLE A1: Internal thermal profiles for the modified rapid-quench cold-seal pressure vessel

Internal : Long plug 850°C : 300 bars		Internal : Long plug 750°C : 300 bars		Internal : Long plug 650°C : 300 bars		Internal : Long plug 650°C : 1000 bars		Internal : Long plug 850°C : 500 bars		Internal : Short plug 850°C : 500 bars	
distance from top (inches)	Temperature (°C)	distance from top (inches)	Temperature (°C)	distance from top (inches)	Temperature (°C)	distance from top (inches)	Temperature (°C)	distance from top (inches)	Temperature (°C)	distance from top (inches)	Temperature (°C)
0	833	0	733	0	634	0	636	0	842	0	839
0.27	832	0.28	731	0.57	627	0.15	634	0.35	837	0.3	833
0.43	831	0.41	730	0.43	630	0.33	632	0.72	826	0.82	817
0.56	829	0.56	728	0.23	631	0.48	630	1.2	808	1.24	796
0.73	827	0.72	725	1.05	615	0.64	628	1.7	780	1.77	770
0.91	823	0.91	720	1.21	612	0.75	625	2.31	748	2.25	736
1.07	818	1.56	699	1.35	607	1.02	619	2.72	709	2.77	693
1.24	813	1.4	705	1.56	599	1.06	615	3.2	659	3.2	643
1.4	808	1.23	710	2.2	571	1.29	611	3.78	591	3.74	574
1.56	802	1.07	715	2.06	579	1.45	606	4.27	517	4.22	502
1.76	794	1.76	690	1.9	586	1.58	601	4.78	433	4.75	409
1.89	786	1.91	683	3.06	519	1.81	593	5.29	339	5.27	314
2.05	778	2.05	675	2.88	530	1.95	587	5.78	232	5.74	197
2.21	769	2.21	667	2.72	540	2.1	580	6.34	115	6.27	94
2.44	756	2.45	655	2.58	549	2.22	573	7	65	6.74	57
2.63	743	2.61	643	2.42	559	2.54	558	7.4	35	7.24	28
2.81	733	2.75	633	3.08	517	2.66	550	8	33	7.6	27
2.94	721	2.89	621	3.25	504	2.85	540				
3.09	707	3.08	608	3.39	491	2.97	530				
3.29	690	3.26	593	3.54	481	3.07	521				
3.45	675	3.4	579	3.71	465	3.34	504				
3.59	660	3.57	565	4.55	383	3.5	493				
3.73	641	3.72	548	4.38	400	3.63	481				
3.95	618	4.1	508	4.22	414	3.75	469				
4.11	600	4.25	490	4.06	431	3.97	450				
4.26	581	4.41	471	3.92	446	4.14	435				
4.4	561	4.57	449	4.71	357	4.31	418				
4.56	535	4.74	431	4.9	338	4.43	406				
4.75	502	4.89	402	5.04	317	4.58	390				
4.9	486	5.04	379	5.22	302	4.78	368				
5.05	462	5.21	360	5.44	255	4.92	350				
5.2	426	5.42	323	5.57	238	5.07	333				
5.47	382	5.57	286	5.76	213	5.21	311				
5.63	345	5.75	273	5.92	201	5.48	297				
5.8	316	5.93	244	6.03	175	5.61	264				
5.93	300	6.06	220	6.25	162	5.82	233				
6.03	264	6.25	149	6.41	117	5.98	207				
6.25	221	6.41	127	6.53	94	6.03	164				
6.44	186	6.56	124	6.72	83	6.19	154				
6.56	149	6.72	100	7.16	52	6.39	127				
6.72	119	6.91	80	7.59	48	6.56	102				
6.75	97	7.31	55			6.67	91				
7.06	79					6.75	75				
7.13	63					7.16	48				

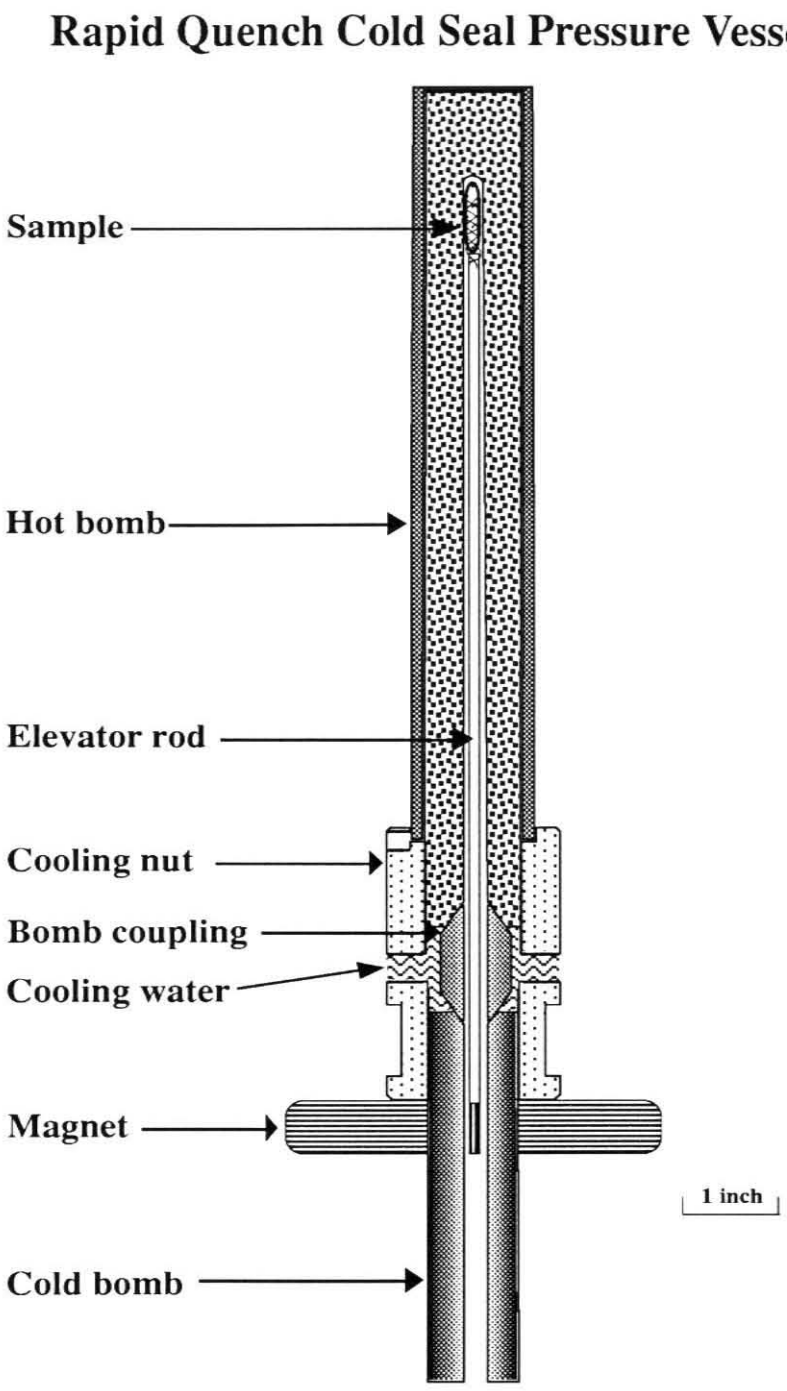

Figure A.1: Schematic cross-section of rapid-quench cold-seal apparatus. Drawing is to scale.

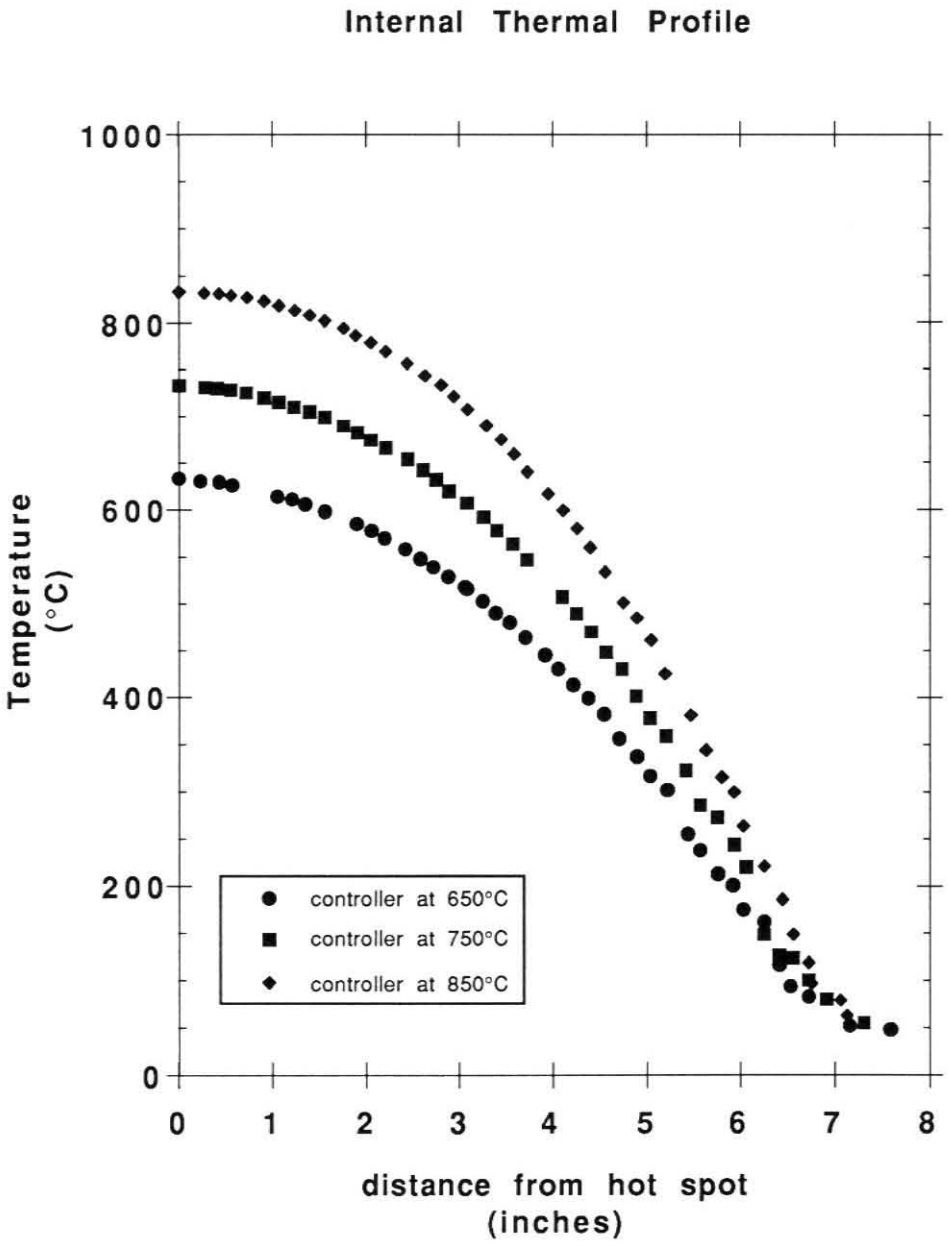

Fig. A.2: Thermal profile within rapid-quench cold-seal apparatus as a function of hot spot temperature.

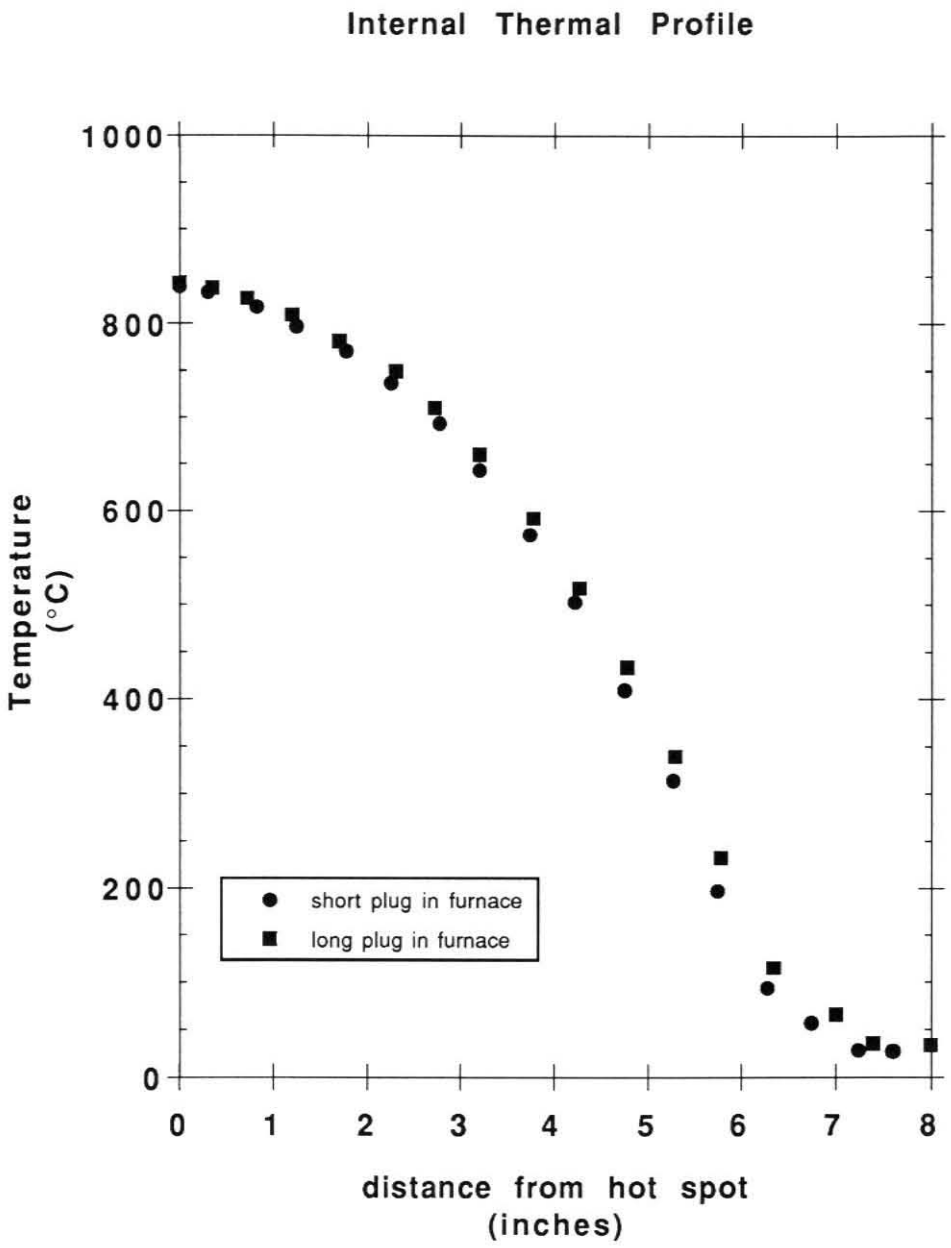

Fig. A.3: Thermal profile within rapid-quench cold-seal apparatus as a function of pressure.

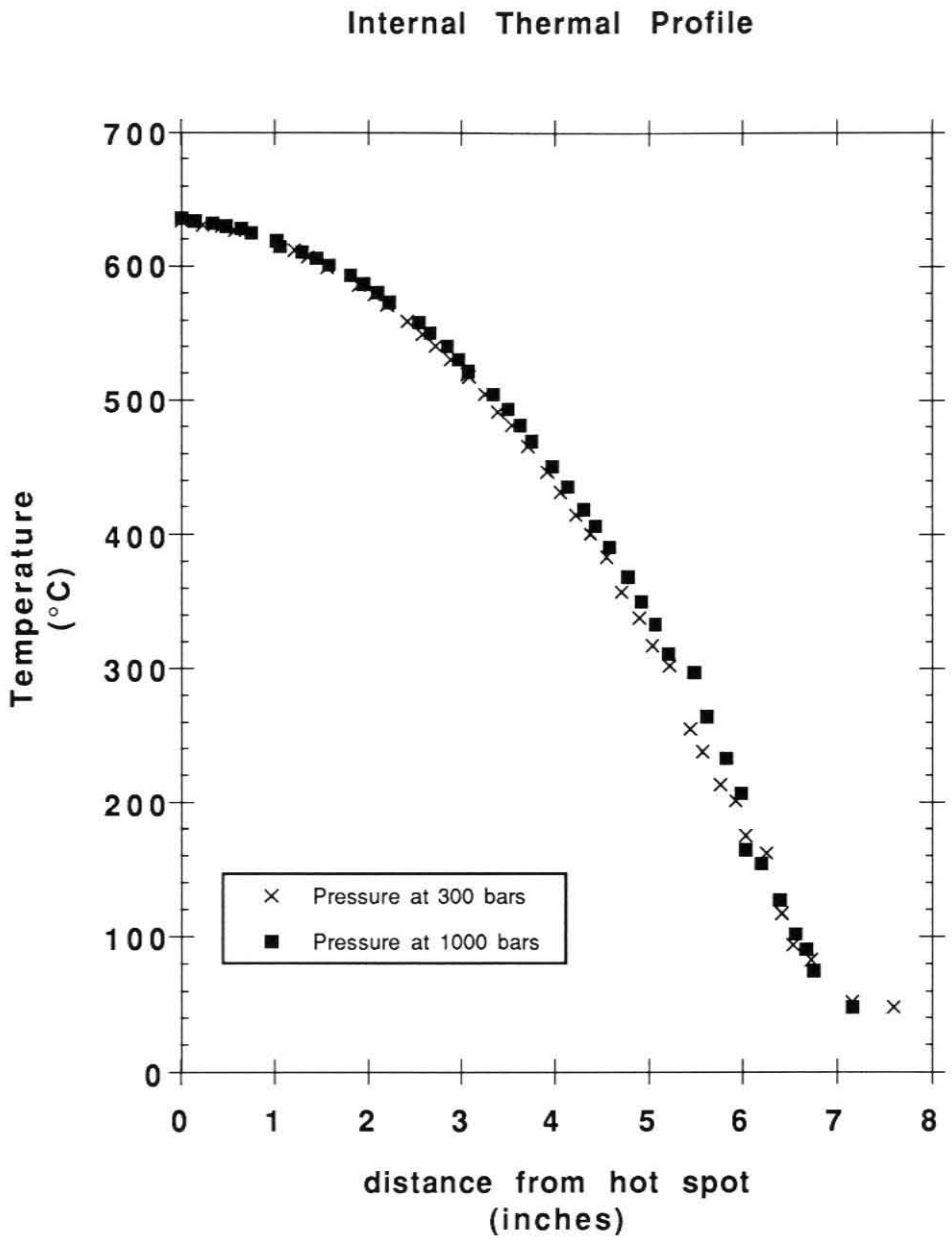

Fig. A.4: Thermal profile within rapid-quench cold-seal apparatus as a function of furnace configuration.

Appendix 2:

The Influence of Bulk Composition on the Speciation of Water in Silicate Glasses

Contrib Mineral Petrol (1990) 104:142–162

Contributions to Mineralogy and Petrology

The influence of bulk composition on the speciation of water in silicate glasses

Lynn A. Silver*, Phillip D. Ihinger, and Edward Stolper
Division of Geological and Planetary Sciences, California Institute of Technology, Pasadena, CA 91125, USA

Abstract. Infrared spectroscopy was used to determine the concentrations of molecular water and hydroxyl groups in hydrous rhyolitic, orthoclasic, jadeitic, and Ca–Al-silicate glasses synthesized by quenching of melts from elevated pressure and temperature. The rhyolitic glasses and some of the Ca–Al-silicate glasses were quenched from water-vapor-saturated melts and used to determine the solubility of water in melts of these compositions. For all compositions studied, hydroxyl groups are the dominant hydrous species at low total water contents, whereas molecular water dominates at elevated water contents. Although the trends in species concentrations in all these compositions are similar, the proportions of the two hydrous species are influenced by silicate chemistry: increasing silica content and K relative to Na both favor molecular water over hydroxyl. Results on rhyolitic glass demonstrate that molecular water is also favored by decreasing temperature at $T<850°$ C. For rhyolitic glasses quenched from vapor-saturated melts, the mole fraction of molecular water is proportional to water fugacity for $P(H_2O) \leq 1500$ bars, demonstrating that the behavior of molecular water is approximately Henrian at total water contents up to at least several weight percent. Data on water solubility for albitic, orthoclasic, and Ca–Al-silicate melts to higher pressures can also be fit by assuming Henrian behavior for molecular water and can be used to set constraints on the partial molar volume of water in these melts. The demonstration of Henry's law for molecular water in these liquids provides a link between spectroscopic measurements of microscopic species concentrations and macroscopic thermodynamic properties.

Introduction

It is well established from spectroscopic investigations of hydrous silicate glasses that water dissolves in them in at least two forms (Orlova 1962; Ostrovskiy et al. 1964; Persikov 1972; Ernsberger 1977; Takata et al. 1981; Wu 1980; Bartholomew et al. 1980; Bartholomew and Schreurs 1980; Stolper 1982a; McMillan et al. 1983; Acocella et al. 1984; Epel'baum 1985; Mysen and Virgo 1986a, b; Newman et al. 1986, 1988; Eckert et al. 1987, 1988; Silver and Stolper 1989). Quantitative infrared and nuclear magnetic resonance (NMR) spectroscopic studies have illustrated a common pattern for all glass compositions: At low total water contents, hydroxyl groups formed by reaction between water and the silicate matrix are the dominant hydrous species. At total water contents of a few tenths of a weight percent, dissolved molecules of water can also be detected; when the total water content exceeds a few weight percent, most of the water is dissolved as molecular water. An important additional feature of these quantitative studies is that once the total dissolved water content exceeds a few weight percent, essentially all additional water dissolves in molecular form; that is, the hydroxyl group concentration initially increases with total water content but reaches an approximately constant maximum value once the total water content exceeds a few weight percent. The limited available data suggest that the saturation level of hydroxyl groups in glasses depends on the chemical composition of the glass, though no pattern has yet been recognized.

Quantitative measurement of the concentrations of hydrous species in glasses using infrared spectroscopy requires that a calibration be carried out for each composition. The molar absorption coefficient (i.e., the constant of proportionality between band intensity and concentration) for each absorption band of interest must first be determined for each composition from the spectra of glasses with known water contents. The water contents of these standards must be precisely known and should ideally range from a few tenths of a weight percent up to several weight percent total dissolved water. To date, such a calibration has been carried out on only two glass compositions of direct petrological interest: rhyolite (Newmann et al. 1986) and albite (Silver and Stolper 1989). Thus, although the general trends in the speciation of water in silicate glasses are known, the details of the influence of bulk composition have not yet been established. These details can set constraints on the nature of the reactions between water and silicate melt and can be used for developing a framework to understand the behavior of water in magmas covering a range in composition.

In the first sections of this paper, we use infrared spectroscopy to determine the speciation of water in a range of silicate glasses of geological interest and to examine the influence of bulk composition on water speciation in silicate glasses. The compositions studied are rhyolitic, orthoclasic, jadeitic, and from the system silica-anorthite-wollastonite. Anhydrous melts of these compositions are highly polymer-

* Now at: Xerox Microelectronics Center, 701 South Aviation Boulevard, M 3-58 El Segundo, CA 90245, USA

Offprint requests to: E. Stolper

ized; i.e., nearly every oxygen atom acts as a bridge between two tetrahedrally coordinated cations. The ratio of bridging oxygens to total oxygens in these anhydrous melts is approximately 1.0, except for one composition for which this ratio is about 0.9 in the silica-anorthite-wollastonite system.

In the final sections of this paper, we examine the extent to which the concentrations of hydrous species in glasses provide a basis for thermodynamic modelling of hydrous silicate liquids. In our previous work on this topic (Stolper 1982a, b; Silver and Stolper 1985, 1989), we have pursued the idea that the activity of molecular water in melts is proportional to the mole fraction of molecular water determined from spectroscopic measurements; that is, that Henry's law applies. In this paper, we use our determinations of molecular water concentration as a function of total water content in conjunction with new and previously published data on water solubility in silicate melts to evaluate explicitly the validity of this Henrian approximation.

Experimental methods

The hydrous glasses included in this study were synthesized by quenching melts generated at elevated pressures and temperatures. Most of glasses were synthesized at Caltech; others were prepared elsewhere and made available for this study. Details of sample preparation and synthesis techniques for each composition are described below and in Silver and Stolper (1989). Major element compositions of selected glasses were analyzed by electron microprobe and are listed in Table 1.

Glass synthesis

Anorthite-silica-wollastonite eutectic (CAS) and E2. Starting material of CAS composition was prepared by grinding appropriate amounts of SiO_2, Al_2O_3, and $CaCO_3$ powders (Johnson-Matthey SpecPure reagents) for 5 h in agate under ethanol; this mixture was melted at 1300° C and 1 atm and quenched to a glass; the glass was then finely ground, dried at 800° C for 24 h and stored over desiccant.

Anhydrous glass was sealed in Pt capsules with known amounts of triply distilled water by arc-welding. These capsules were then held at 15–20 kbar and 1400°–1450° C in piston cylinder apparatus for 2–6 h. Run conditions of the individual samples are listed in Table 2. Many CAS glasses were synthesized at Caltech in a 0.5 inch piston cylinder apparatus using a talc cell with a pyrex sleeve. Glasses were also synthesized at the University of California, Los Angeles, in Professor A. Montana's laboratory, in a one inch piston cylinder using a NaCl + pyrex cell with either a boron nitride (BN)-bearing assembly (samples CAS-11, CAS-12, CAS-13, CAS-14) or a BN-free fired pyrophyllite assembly (samples CAS-15, CAS-16). Details of these experimental procedures are described in Silver and Stolper (1989).

A series of hydrous glasses with an anhydrous composition similar to that of the CAS glasses and with total water contents up to 9.25 wt % was provided by Professor P. McMillan of Arizona State University. These samples were synthesized in an internally heated pressure vessel (IHPV) at pressures between 103 and 5130 bars and temperatues between 1175° and 1191° C. The details of the synthesis of these glasses are reported by McMillan et al. (1986). Run conditions are listed in Table 2.

Orthoclase (KAS). Starting material of orthoclasic composition was prepared by grinding appropriate amounts of oxide and carbonate reagents in agate under ethanol for 5 h; the resulting mixture was dried at 800° C for 24 h and stored over desiccant. Hydrous glasses were synthesized in piston cylinder apparatus as described above for the CAS composition by quenching from melts held at 1450° C and 15–20 kbar for 2 h. The run conditions are given in Table 3. The syntheses were done either at Caltech using a 0.5 inch talc cell with a pyrex sleeve, or at UCLA using a one inch NaCl + pyrex cell with either a BN-bearing assembly (sampes KAS-2, KAS-3) or a BN-free fired pyrophyllite assembly (samples KAS-5, KAS-6, KAS-7, KAS-8, KAS-9).

Jadeite (JD). Starting material of jadeitic composition was prepared by grinding Burma jadeite (sample provided by Professor W. Johannes; see Johannes et al. 1971) in agate under ethanol for 5 h; the powder was then dried and stored as described above for the KAS composition. Two hydrous JD glasses were synthesized as described above for the CAS composition at 1450° C and 15 kbar at Caltech in a 0.5 inch piston cylinder apparatus using a talc cell with a pyrex sleeve. Two other JD glasses were synthesized in IHPVs at the Johnson Space Center after sealing powdered starting materials with known amounts of triply distilled water into Pt capsules by arc-welding. Details of the experimental procedures are described in Silver and Stolper (1989). One hydrous JD glass (JD + 5) was obtained from Dr. B.O. Mysen; details of the synthesis techniques are reported in Mysen and Virgo (1986b). The run conditions for the JD samples are listed in Table 4.

Anorthite-silica (ANS). A series of hydrous glasses with bulk compositions along the join anorthite-silica (An30Si70 to An51Si49) and total water contents between 8.8 and 12.5 wt % were provided by Dr. D. Stewart of the U.S.G.S. (sample numbers are from Stewart 1967). These glasses were synthesized in IHPVs at 5 to 10 kbar and temperatures between 850° and 1050° C. Details of the syntheses are given by Stewart (1967). Run conditions for these samples are listed in Table 5.

Table 1. Anhydrous glass compositions (wt %)

Composition	CAS[a]	E2[a]	Orthoclase[a]	Rhyolite[a]	An(30-51)Si(70-49)[b]	Jadeite[c]	Na, Zn-rich silicate[d]
Sample	CAS-7	E2-7	KAS-9	KS	ANS	Burma	
SiO_2	62.8	63.7	65.2	77.5	83.0–71.0	57.8	72.9
Al_2O_3	14.3	14.3	17.8	12.5	11.0–18.7	25.3	2.1
CaO	22.9	22.0	–	0.5	6.0–10.3	0.6	–
FeO	–	–	–	1.0	–	0.5	–
Na_2O	–	–	–	3.6	–	14.0	10.6
K_2O	–	–	17.0	4.8	–	0.04	4.5
ZnO	–	–	–	–	–	–	10.0

[a] For CAS, E2, orthoclase, and rhyolite: Reported analyses are electron microprobe analyses based on an average of 10 individual points per sample. Sample # refers to specific sample analyzed. Analyses normalized to 100% to reflect anhydrous composition
[b] ANS compositions are nominal starting materials calculated on an anhydrous basis (Stewart 1967)
[c] Jadeite from Burma analyzed by H.D. Zimmermann (1969 Diss., Göttingen)
[d] Na, Zn-rich silicate starting composition of Bartholomew et al. (1980)

Table 2. Hydrous CAS and E2 glasses: experimental data

Sample #	Starting material	P (kb)	T (C)	Time (min)	Amt H_2O added	Density[a] (g/l)	H_2O, mol (wt %)	OH (wt %)	H_2O, tot[c] (wt %)	H_2O (total)[b] (wt %)		Remarks[d,e]	Mole fractions		
													$X(B)$	$X(H_2O)$	$X(OH)^f$
CAS-2	Syn. oxide	15	1450	150	5.3	2620 e	3.03	2.37	5.40 (0.11)	5.11* (0.11)		c, f, p	0.098	0.055	0.086
CAS-3	Syn. oxide	15	1450	130	12.2	2425 h	7.71	2.46	10.17 (0.15)	10.17* (0.26)		c, f, p	0.177	0.134	0.086
CAS-4	Syn. oxide	15	1450	150	4.0	2670 e	1.77	2.11	3.89 (0.03)			c, f, p	0.072	0.033	0.078
CAS-6	Syn. oxide	20	1450	210	5.7	2650 e	2.35	2.11	4.46 (0.15)			c, f, p	0.082	0.043	0.077
CAS-7	Syn. oxide	20	1450	195	2.0	2718 e	0.08	0.81	0.89 (0.02)	0.88* (0.03)		c, f, p	0.017	0.002	0.031
CAS-8	Syn. oxide	20	1450	185	3.9	2500 e	1.64	2.01	3.66 (0.20)			c, f, p	0.067	0.030	0.074
CAS-11	Syn. oxide	15	1450	120	9.5	2507 d	6.18	2.45	8.63 (0.29)	8.82* (0.10),	8.76** (0.44)	b, c, f, u, p	0.152	0.109	0.087
CAS-12	Syn. oxide	15	1450	120	8.9	2554 d	4.61	2.46	7.07 (0.14)	7.93* (0.11),	7.87** (0.39)	b, c, f, u, p	0.127	0.083	0.088
CAS-13	Syn. oxide	20	1450	120	2.2	2700 e	0.30	1.26	1.56 (0.10)	1.76* (0.04),	1.73** (0.09)	b, c, f, u, p	0.029	0.006	0.047
CAS-14	Syn. oxide	20	1450	120	0.9	2727 d	0.03	0.58	0.61 (0.04)	0.67* (0.02),	0.73** (0.04)	b, c, f, u, p	0.012	0.001	0.022
CAS-15	Syn. oxide	20	1450	90	0.9	2719 d	0.14	0.95	1.09 (0.14)	0.99* (0.02),	1.06** (0.05)	c, f, p, u	0.021	0.003	0.036
CAS-16	Syn. oxide	20	1450	120	9.0	2575 e	4.43	2.68	7.11 (0.22)		6.96** (0.35)	c, f, p, u	0.127	0.079	0.096
E2-34	Syn. oxide	0.103	1180			2535 e	0.07	0.64	0.72 {0.10}	0.93***		f, x, i, s	0.014	0.001	0.024
E2-31	Syn. oxide	0.258	1180			2515 g	0.36	1.28	1.64 {0.30}	1.88****		f, i, s	0.031	0.007	0.048
E2-25	Syn. oxide	0.445	1170			2505 g	0.87	1.77	2.64 {0.11}	2.57***		f, i, s	0.049	0.016	0.066
E2-26	Syn. oxide	0.600	1191			2500 g	1.09	1.89	2.98 {0.05}	2.90***		f, i, s	0.055	0.020	0.070
E2-32	Syn. oxide	0.752	1181			2495 e	1.30	2.05	3.35 {0.12}	3.25***		f, i, s	0.062	0.024	0.076
E2-7	Syn. oxide	1.004	1175			2485 g	1.64	2.07	3.71 {0.12}			f, i, s	0.068	0.030	0.076
E2-27	Syn. oxide	1.025	1179			2485 g	1.70	2.11	3.81 {0.08}	3.89***		f, x, i, s	0.070	0.031	0.078
E2-30	Syn. oxide	1.514	1175			2425 g	2.69	2.19	4.88 {0.31}	4.55***		f, i, s	0.089	0.049	0.080
E2-36	Syn. oxide	5.130	1177			2405 g	6.56	2.45	9.00 {0.17}	9.25***		f, bb, i, s	0.159	0.116	0.086

[a] Density measured using: d = Berman balance; h = heavy liquids; e = density estimated based on comparison with glasses with similar total water contents; g = density calculated from refractive index measured by P. Lambert (P. McMillan, personal comm.); refractive indices: E2(dry) = 1.546, E2-31 = 1.550, E2-25 = 1.547, E2-26 = 1.547, E2-7 = 1.545, E2-27 = 1.545, E2-30 = 1.542, E2-36 = 1.538

[b] * Total water contents determined by H2 manometry, ( ) indicates estimated error; ** Total water contents determined by NMR, ( ) = error estimated 5%; *** Total water contents determined by TGA (McMillan et al. 1986)

[c] Total water contents determined from sum of molecular H_2O and OH; ( ) indicates analytical error based on several analyses; { } indicates estimated analytical error based on one analysis

[d] Samples synthesized in: p = piston cylinder apparatus; b = used boron-nitride assemblies; i = samples synthesized in IHPV; u = samples synthesized at UCLA

[e] Infrared spectra taken using: c = Cary 17 spectrometer; f = Nicolet FTIR spectrometer; bb = bubbles; x = crystals; s = saturation experiments

[f] Mole fraction calculation: $X(B) = (\text{wt\% } H_2O, \text{tot}/18.015)/((\text{wt\% } H_2O, \text{tot}/18.015) + (100 - \text{wt\% } H_2O, \text{tot})/34.32)$;
$X(H_2O, \text{molecular}) = (\text{wt\% } H_2O, \text{mol}/18.015)/(\text{wt\% } H_2O, \text{tot}/18.015 + (100 - \text{wt\% } H_2O, \text{tot})/34.32)$; $X(OH) = 2*(X(B) - X(H_2O, \text{molecular}))$ where 34.32 = molecular weight of anhydrous silicate on a one oxygen basis in gm/mol O

[g] This value supercedes the value of 0.89 wt % reported in McMillan et al. (1986); P. McMillan, personal communication

Table 3. Orthoclasic glasses: experimental data

Sample #	Starting material	P (kb)	T (C)	Time (min)	Amt H_2O added	Density[a] (g/l)	H_2O, mol (wt%)	OH (wt%)	H_2O, tot[c] (wt%)	H_2O (total)[b] (wt%)	Remarks[d]	Mole fractions[e]		
												$X(H)$	$X(H_2O)$	$X(OH)$
KAS-2	Syn. oxide	15	1450	140	5.9	2380 e	1.74	1.55	3.29 (0.57)	3.32** (0.17)	b, f, u	0.062	0.033	0.058
KAS-3	Syn. oxide	15	1400	120	7.5	2335 e	3.46	1.84	5.30 (0.16)	5.95** (0.30)	b, f, u	0.098	0.064	0.068
KAS-5	Syn. oxide	20	1450	5	0.7	2438 d	0.39	0.96	1.36 (0.11)	1.50** (0.08)	f, u	0.026	0.007	0.037
KAS-6	Syn. oxide	20	1450	90	1.7	2425 d	0.80	1.32	2.12 (0.12)	1.93* (0.04), 1.92** (0.10)	f, u	0.040	0.015	0.050
KAS-7	Syn. oxide	20	1450	90	1.9	2408 d	1.06	1.38	2.44 (0.08)	2.53* (0.03), 2.62** (0.13)	f, u	0.046	0.020	0.052
KAS-8	Syn. oxide	20	1450	90	3.7	2487 d	0.13	0.73	0.86 (0.05)	0.96* (0.03), 1.01** (0.05)	f, u	0.016	0.003	0.028
KAS-9	Syn. oxide	20	1450	90	1.5	2425 h	0.71	1.23	1.94 (0.35)	1.87** (0.10)	f, u	0.037	0.013	0.047
KAS-10	Syn. oxide	20	1450	120	7.9	2365 h	2.67	1.77	4.44 (0.21)	4.71* (0.10), 4.66** (0.20)	f	0.082	0.049	0.066
KAS-11	Syn. oxide	20	1450	120	12.3	2290 h	5.07	1.98	7.04 (0.30)	7.09* (0.23)	f	0.128	0.092	0.072
KAS-12	Syn. oxide	20	1450	120	9.4	2350 h	4.36	2.13	6.49 (0.17)	6.20* (0.10), 6.33** (0.32)	f	0.118	0.079	0.078

[a] Density measurements: *h* = made with heavy liquids (error: 25 g/l); *d* = density measured with Berman balance (error: 10–20 g/l); *e* = density estimated based on comparison with glasses of similar water contents (error: 30 g/l)

[b] * Total H_2O content measured by H_2 manometry, ( ) indicates estimates analytical error; ** Total H_2O contents measured by NMR spectroscopy, ( ) estimated 5% error

[c] Total H_2O contents determined from sum of molecular H_2O and OH, ( ) represents analytical uncertainty based on several analyses

[d] All samples synthesized in piston cylinder apparatus: *u* = samples synthesized at UCLA; *b* = used boron-nitride assemblies. Infrared spectra taken with: *f* = Nicolet FTIR spectrometer

[e] Mole fraction calculation, see footnote f, Table 2

Rhyolite. A naturally occurring rhyolitic glass (KS) from the ca. 1340 A.D. eruption of the Mono Craters, California was used as a starting material. The rhyolitic glass is bubble-free with minor amounts of crystallites and has a water content of 0.78 wt% (Newman et al. 1986). Cores of this glass were drilled with a 3.5 mm diamond drill core using water as a lubricant. These cores were weighed with known amounts of triply distilled water into Au capsules that were then sealed by arc-welding. The amounts of water loaded into the capsules were sufficient to ensure that the melt was vapor-saturated at the pressure and temperature of the experiment.

Hydrous rhyolitic glasses were synthesized in two types of cold seal pressure vessels: (1) an "air-quench" apparatus in which the bombs are removed from the furnace after the power is turned off and cooled by blasting with a flow of compressed air (cooling rates ~3° C/s), and (2) a "rapid-quench" apparatus in which the sample is quenched under pressure by dropping into a cooled part of the pressure vessel (cooling rates ≥400° C/s; P.D. Ihinger, unpublished results); details of our rapid-quench apparatus will be presented elsewhere. The capsules were held at constant temperature (850° C) and pressures between 49 and 1500 bars. The pressure medium was triply distilled water, and the pressure was monitored using Bourdon tube gauges. For the air-quench cold seal pressure vessels, the temperature was controlled via an internal Chromel–Alumel (Cr–Al) thermocouple and was verified with an external Cr–Al thermocouple. For the rapid quench apparatus, the temperature was controlled via an external Cr–Al thermocouple. The run times were usually longer than 48 h, which, based on the diffusion coefficients for water in rhyolitic glasses given by Karsten et al. (1982), would be sufficient for the water to be homogeneously distributed in the samples. Sample homogeneity was verified after quenching by measuring by infrared spectroscopy the water contents at the center, at the edge, and at various lengths along our experimental charges; typical variations in total water content were no more than a few tenths of a weight percent at several weight percent total dissolved water. Some of the experiments in the air-quench cold seal bombs were reversal experiments in which the sample was held at a pressure about 200 bars above the final pressure for about 48 h and then dropped to the final pressure and held for another 48 h to allow the melt to reequilibrate with vapor. The run conditions of the samples synthesized in air-quench cold seal pressure vessels (samples KS-) and those synthesized in the rapid-quench bombs (samples PDI-) are listed in Table 6.

Infrared spectroscopy

Doubly polished plates were made of each sample for the infrared spectroscopic work. Sample thicknesses were measured with a digital dial indicator. Infrared spectra were obtained using a Cary 17 spectrometer or a Nicolet Instruments 60SX Fourier transform infrared spectrometer. Details of the infrared techniques and procedures for measuring absorption band intensities are given in Newman et al. (1986) and Silver and Stolper (1989). Densities of most of the glasses were measured either by weighing in air and in toluene with a Berman balance or by the float-sink method using heavy liquids of known densities. For samples that contained bubbles or for which small sample size precluded density measurements, the densities were estimated by comparison with glasses of similar water contents or calculated from the Gladstone-Dale rule (see Appendix 1). Precisions of measurements of absorption band intensity, density, and sample thickness are discussed in Newman et al. (1986) and Silver and Stolper (1989).

Water analyses

Total water contents of many of the samples were determined by a hydrogen manometric technique (Newman et al. 1986). Total water contents of selected glasses were also determined by NMR spectroscopy (Eckert et al. 1988). Water contents determined by these methods are listed in Tables 2–4.

Table 4. Hydrous Jadeitic glasses: experimental data

Sample #	Starting material	P (kb)	T (C)	Time (min)	Amt H_2O added	Density[a] (g/l)	H_2O, mol (wt%)	OH (wt%)	H_2O, tot[c] (wt%)	H_2O (total)[b] (wt%)	Remarks[d]	Mole fractions[e] $X(B)$	$X(H_2O)$	$X(OH)$
CJD-1	Burma jd	20	1450	360	3.9	2400 e	1.42	1.49	2.91 (0.1)	2.91 (0.14)*	f, p	0.053	0.026	0.054
CJD-3	Burma jd	20	1450	330	4.9	2370 e	2.50	1.58	4.08 (0.1)	4.08 (0.12)*	f, p	0.074	0.045	0.057
JD+5		15	1550	240	5.0	2367 e	3.22	1.60	4.82 {0.14}	5.0**	c, p	0.087	0.058	0.057
J1	Burma jd	5	1000	240	1.2	2400 e	1.88	1.59	3.47 (0.3)		c, i	0.063	0.034	0.058
J7	Burma jd	2	1150	8640	10.5	2325 e	5.35	1.62	6.97 (0.3)		c, i	0.123	0.094	0.057

[a] e = Densities estimated
[b] * Total water contents determined by H_2 manometry; ** Total water content based on amount of water weighed into capsule
[c] Total H_2O contents determined from sum of molecular H_2O and OH; reported H_2O content is average of several samples, except JD+5 (one analysis); ( ) represents analytical uncertainty based on several analyses; { } represents estimated analytical uncertainty based on one analysis
[d] Infrared spectra obtained using: c = Cary 17 spectrometer, f = FTIR spectrometer; samples synthesized in: i = IHPV, p = piston cylinder apparatus
[e] Mole fraction calculation, see footnote f, Table 2

Table 5. Hydrous Anorthite-Silica glasses: experimental data

Sample #	Starting composition	P (kb)	T (C)	Amt H_2O added	Density[a] (g/l)	H_2O, mol (wt%)	OH (wt%)	H_2O, tot[c] (wt%)	H_2O (total)[b] (wt%)	Remarks[d]	Mole fractions $X(B)$	$X(H_2O)$	$X(OH)$
ANS-162	An30Si70	5	1010	15.2	2250	7.46	2.13	9.59 {0.20}	9.9	c, i	0.156	0.121	0.069
ANS-167	An35Si65	5	950	16.1	2260	8.61	1.97	10.58 {0.19}	10.6	c, i	0.172	0.140	0.064
ANS-329	An40Si60	10	900	17.8	2200	10.41	1.84	12.25 {0.25}	12.3	c, i	0.198	0.168	0.059
ANS-156	An40Si60	5	875	16.2	2285	8.36	2.00	10.36 {0.17}		c, i	0.169	0.137	0.065
ANS-161	An45Si55	5	1010	15.0	2294	7.16	2.15	9.31 {0.14}	8.8	c, i	0.154	0.119	0.071
ANS-367	An45Si55	10	1050	18.0	2224	10.40	1.77	12.17 {0.19}	11.3	c, i	0.198	0.169	0.058
ANS-166	An45Si55	5	950	16.2	2286	7.79	2.01	9.80 {0.15}	9.6	c, i	0.162	0.129	0.066
ANS-328	An45Si55	10	900	25.3	2207	9.87	1.95	11.82 {0.27}	12.5	c, i	0.192	0.161	0.064
ANS-357	An45Si55	10	850	18.1	2232	9.86	1.84	11.70 {0.22}	11.2	c, i	0.191	0.161	0.060
ANS-358	An50Si50	10	850	19.6	2245	9.38	1.76	11.14 {0.16}	12.0	c, i	0.183	0.154	0.058
ANS-359	An51Si49	10	850	12.1	2232	10.36	1.85	12.22 {0.22}	12.1	c, i	0.200	0.169	0.061

[a] Densities determined by Stewart (1967)
[b] Total water contents determined by a weight-loss method (Stewart 1967)
[c] Total water contents determined from sum of molecular H_2O and OH; { } represents estimated analytical uncertainty based on one analysis
[d] Samples synthesized in: i = IHPV; Infrared spectra taken with: c = Cary 17
[e] Mole fraction calculation, see footnote f, Table 2

Infrared spectroscopy

Figure 1 shows the near-infrared absorption spectra of hydrous jadeitic, orthoclasic, albitic and E2 glasses, all with similar total water contents (2.5–3.5 wt% H_2O).[1] Figure 2 shows the spectra of hydrous CAS and anorthite-silica glasses with much higher total water contents (8.6–9.8 wt% H_2O). The locations of the bands near 4500, 5200 and 7100 cm^{-1} for each composition are listed in Table 7. As reviewed by Newman et al. (1986), these bands are assigned to combination modes for molecular water (5200 cm^{-1}) and OH groups (4500 cm^{-1}) and the first overtone modes due to both species (7100 cm^{-1}).

For the range of compositions studied, the frequency of each band shifts to higher energy (i.e., higher wavenumber) with increasing silica content (Table 7). Despite the small differences in the positions of the four bands in this region, the overall lineshapes are similar for all these compositions and for hydrous albitic glasses (Silver and Stolper 1989). All spectra shown in Figure 2 show a well-developed shoulder at 6850 cm^{-1}, similar to the feature seen in the spectra of hydrous albitic glasses with total water contents greater than 3 wt% (Silver and Stolper 1989); this shoulder may reflect clustering of water molecules by analogy with a similar feature that has been observed in the infrared spectra of opals (Langer and Flörke 1974).

Determination of molar absorption coefficients

In order to use the intensities of infrared absorption bands to determine species concentrations, the molar absorption coefficient (ε) for each band must be determined for each silicate glass composition. In this study, the 5200 and 4500 cm^{-1} bands were used for measuring the concentrations of molecular water and OH groups. The molar absorption coefficients for these bands were determined following the method of Newman et al. (1986), who have shown this technique to be precise. Briefly, infrared spectra of hydrous glasses spanning a range of total water contents were obtained, and the peak heights of the 5200 and 4500 cm^{-1} bands were measured. The total water contents of these same glasses were determined by hydrogen manometry (Newman et al. 1986) and/or by NMR spectroscopy (Eckert et al. 1988). For samples analyzed by both techniques, we

[1] The water contents referred to in this section were determined by infrared spectroscopy.

Table 6. Hydrous rhyolitic glasses: experimental data[d]

Sample #	P[a] (bars)	T (C)	Time (h)	Density[a] (g/l)	H_2O, mol (wt%)	OH (wt%)	H_2O, tot[b] (wt%)	Remarks[c]	Mole fractions[f]		
									X(B)	$X(H_2O)$	X(OH)
KS-100	118	850	20	2319	0.36	0.77	1.12 (0.12)	c, f, aq	0.020	0.006	0.027
KS-200	223	850	50	2317	0.61	0.95	1.56 (0.04)	c, f, aq	0.028	0.011	0.034
KS-300	357	850	51	2325	1.08	1.12	2.20 (0.05)	c, f, aq	0.039	0.019	0.040
KS-400	482	850	52	2312	1.31	1.17	2.48 (0.07)	c, f, aq	0.044	0.023	0.041
KS-500	522	846	50	2325	1.45	1.20	2.66 (0.06)	c, f, aq	0.047	0.026	0.042
KS-500X	500	850	72	2325	1.48	1.13	2.61 (0.20)	bb, c, f	0.046	0.026	0.040
KS-600	717	850	49	2315	1.90	1.28	3.18 (0.07)	c, f, aq	0.056	0.033	0.045
KS-800	793	850	22	2315	1.93	1.31	3.24 (0.15)	c, f, aq	0.057	0.034	0.046
KS-900	1044	850	4	2310	1.75	1.26	3.01 (0.25)	c, f, aq	0.053	0.031	0.044
KS-310	370/232	850	54	2350	0.73	1.98	1.70 (0.02)	c, f, aq	0.030	0.013	0.035
KS-311	310/113	850	48	2350	0.36	0.83	1.19 (0.05)	c, aq	0.021	0.006	0.030
KS-530	540/366	850	72	2340	1.18	1.14	1.32 (0.02)	c, f, aq	0.041	0.021	0.040
KS-640	625/452	850	48	2340	1.44	1.23	2.67 (0.05)	c, f, aq	0.047	0.025	0.043
KS-650	680/548	850	114	2340	1.68	1.26	2.95 (0.10)	c, f, aq	0.052	0.030	0.044
KS-800.2	800	850	94	2310	2.26	1.37	3.63 (0.06)	c, f, aq	0.064	0.040	0.048
KSR-800	1000/800	850	116	2310	2.32	1.34	3.67 {0.08}	f, aq	0.064	0.041	0.047
KS-950	945	850	67	2300	2.46	1.35	2.80 (0.08)	c, f, aq	0.067	0.043	0.047
KS-960	960	850	25	2300	2.26	1.34	3.60 {0.04}	c, f, aq	0.063	0.040	0.047
KS-1000	1000	850	29	2300	3.07	1.45	4.53 (0.19)	bb, c, aq	0.079	0.053	0.051
DOBS-152	500	850	151	2340	1.70	1.16	2.86 {0.05}	aq, f, **	0.050	0.030	0.041
DOBS-153	1000	850	151	2316	3.02	1.29	4.31 {0.05}	aq, c, f, **	0.075	0.053	0.045
DOBS-154	2000	850	151	2294	3.78	1.30	5.08 {0.06}	aq, c, f, **	0.088	0.065	0.045
PDIKS107	49	850	59	2341	0.16	0.61	0.76 {0.04}	rq, f	0.014	0.003	0.022
PDIKS108	156	850	94	2334	0.37	0.96	1.33 {0.05}	rq, f	0.024	0.007	0.034
PDIKS110	190	850	67	2333	0.44	1.02	1.46 {0.02}	rq, f	0.026	0.008	0.036
PDIKS105	299	850	57	2329	0.67	1.16	1.83 {0.07}	rq, f	0.032	0.012	0.041
PDIKS101	500	850	45	2320	1.19	1.38	2.57 {0.05}	rq, f	0.045	0.021	0.049
PDIKS102	500	850	64	2321	1.17	1.34	2.51 {0.05}	rq, f	0.044	0.021	0.047
PDIKS104	699	850	50	2314	1.67	1.48	3.15 {0.05}	rq, f	0.055	0.029	0.052
PDIKS114	799	850	46	2310	1.90	1.59	3.50 {0.05}	rq, f	0.061	0.033	0.056
PDIKS103	917	850	49	2307	2.13	1.62	3.75 {0.06}	rq, f	0.066	0.037	0.057
PDIKS115	980	850	56	2305	2.23	1.70	3.94 {0.07}	rq, f	0.069	0.039	0.060
PDIKS111	1470	850	48	2292	3.29	1.77	5.06 {0.06}	rq, f	0.088	0.057	0.061
PDIKS113	1260	850	96	2299	2.68	1.74	4.43 {0.04}	rq, f	0.077	0.047	0.061
PDIKS109	98	850	47	2342	0.09	0.62	0.71 {0.07}	rq, f	0.013	0.002	0.022
PDIKS106	1080	850	49	2308	2.07	1.58	3.65 {0.05}	rq, f	0.064	0.036	0.055

[a] Densities estimated based on comparison with rhyolites with similar water contents
[b] Total water contents based on sum of molecular H_2O and OH; ( ) represents analytical uncertainty based on several analyses; { } represents estimated analytical uncertainty based on a single measurement
[c] Infrared spectra taken with: *c* = Cary 17 spectrometer, *f* = Nicolet FTIR spectrometer, *bb* = bubbles; samples synthesized in cold seal apparatus: rq = rapid quench, aq = air-quench apparatus; ** samples from Shaw (1974)
[d] All experiments were saturated with pure water vapor
[e] Reversal runs indicated by P(start)/P(final)
[f] Mole fraction calculation, see footnote f, Table 2

used only the manometric measurements for calibration purposes. The molar absorption coefficients were determined separately for each composition by linear regression of Eq. (2) in Newman et al. (1986). This procedure is based on the assumptions that the molar absorption coefficients are constant over the range of water contents studied and that there are only two dissolved hydrous species.

CAS and E2. The compositions of the E2 and CAS glasses are similar, so they have been treated as a single data set. Five glasses of the CAS composition with water contents between 0.9 and 10.2 wt% were used in the regressioon to determine the molar absorption coefficients. Total water contents for these glasses were determined by H_2 manometry and/or NMR spectroscopy. For the E2 composition, we used eight glasses; total water contents were determined by a weight loss method by McMillan et al. (1986) and are between 0.9 and 9.3 wt% H_2O. The best fit ε values for these two bands are given in Table 7. The ε values are similar whether the data on the CAS and E2 glasses are fitted separately or as a single data set. Figure 3 shows that the total water contents determined from the sum of the molecular water (from the 5200 cm^{-1} band) and hydroxyl group (from the 4500 cm^{-1} band) contents determined by infrared spectroscopy are similar to the total water contents determined by hydrogen manometry, NMR spectroscopy, and weight loss.

Four CAS glasses were synthesized in BN-bearing assemblies and the infrared spectra of the two low water contents samples (CAS-13, CAS-14) show extra absorption bands at 4125 and 5030 cm^{-1}. These four samples were not included in the calibration because of the possible ex-

148

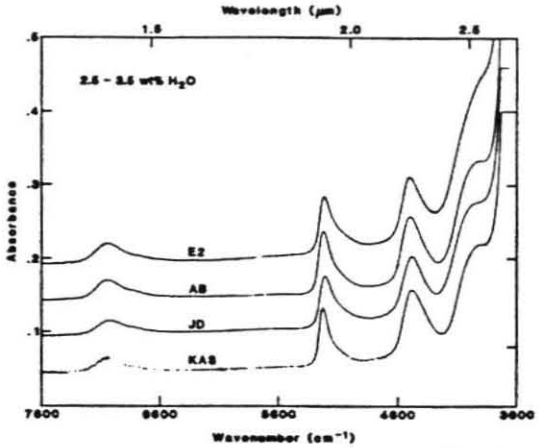

Fig. 1. Near-infrared absorption spectra of hydrous jadeitic, orthoclasic, albitic, and E2 glasses with total water contents between 2.5 and 3.5 wt%, scaled to a thickness of 300 μ. Spectra have been offset by 0.05 absorbance units for clarity. Samples shown are KAS-7 (2.5 wt% H_2O), CJD-1 (2.9 wt% H_2O), A1010 (3.0 wt% H_2O), and E2-27 (3.5 wt% H_2O)

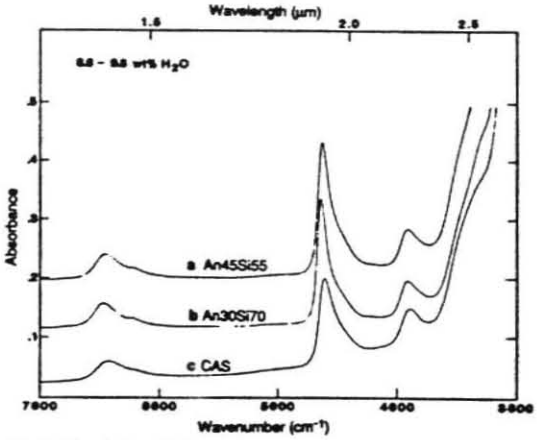

Fig. 2. Near-infrared absorption spectra of hydrous CAS and anorthite-silica (An45Si55 and An30Si70) glasses with total water contents between 8.6 and 9.8 wt%, scaled to a thickness of 150 μ. Spectra have been offset by 0.05 absorbance units for clarity. Samples shown are *a*: ANS-166 (9.4 wt% H_2O), *b*: ANS-162 (9.8 wt% H_2O), and *c*: CAS-11 (8.6 wt% H_2O)

Table 7. Band assignments and extinction coefficients

Composition	SiO_2 (mol%)	Molecular water		Hydroxyl		OH-overtone
		Peak position (cm^{-1})	ε (l/mole-cm)	Peak position (cm^{-1})	ε (l/mole-cm)	Peak position (cm^{-1})
CAS-E2	66	5204	1.07±0.04	4485	0.85±0.03	7028
JD	66	5207	1.13	4476	1.12	7010
Albite	75	5218	1.67±0.06	4485	1.13±0.04	7030
KAS	75	5222	1.87±0.07	4472	1.43±0.05	7030
Rhyolite	83	5225	1.61±0.05	4503	1.73±0.02	7086
Combined ANS	76–87	5220–5232	1.50±0.15	4515–4503	1.20±0.59	7054–7055

Errors reported on epsilon values were determined by a least squares regression method similar to Albarede and Provost (1977)

istence of additional H-bearing species (see Silver and Stolper 1989); however, the molar absorption coefficients are similar whether or not these samples are included in the regression.

Orthoclase. Eight orthoclasic glasses with water contents between 0.9 and 7.0 wt% were used in the regression to determine molar absorption coefficients. Total water contents of these KAS glasses were determined by H_2 manometry and/or NMR spectroscopy. The best fit ε values for the 4500 and 5200 cm^{-1} bands are listed in Table 7. As illustrated in Fig. 4, the total water contents (molecular water + hydroxyl groups) determined by infrared spectroscopy using these ε values are similar to the total water contents determined by NMR spectroscopy and/or H_2 manometry. Two of the KAS samples were synthesized in BN-bearing assemblies and were not included in the regression for reasons discussed above, although the molar absorption coefficients are similar whether or not these samples are included.

Jadeite. Two jadeitic glasses with water contents of 2.9 and 4.1 wt% were used to solve for the molar absorption coefficients for this composition. Total water contents were measured by hydrogen manometry, and the molar absorption coefficients are listed in Table 7. As a test of these values, the total water content was determined by infrared spectroscopy for a hydrous jadeitic glass (JD + 5) provided by Dr. B. Mysen, for which Mysen and Virgo (1986b) report a water content of 5 wt% based on the amount of H_2O weighed into the capsule. The total water content based on the best fit ε values (4.8 wt%) is similar to the amount loaded into this sample. Despite this good agreement, additional samples with a wider range of water contents, particularly low-water samples, will be needed to confirm the calibration.

Anorthite-silica. The samples provided by Dr. D. Stewart vary in bulk composition (excluding the water content) from An30Si70 to An51Si49, with total water contents (determined by a weight loss technique) between 8.8 and 12.5 wt%. Because molar absorption coefficients depend on composition, the same molar absorption coefficients probably do not apply over this range of silicate composition. However, because of the limited number of samples, the

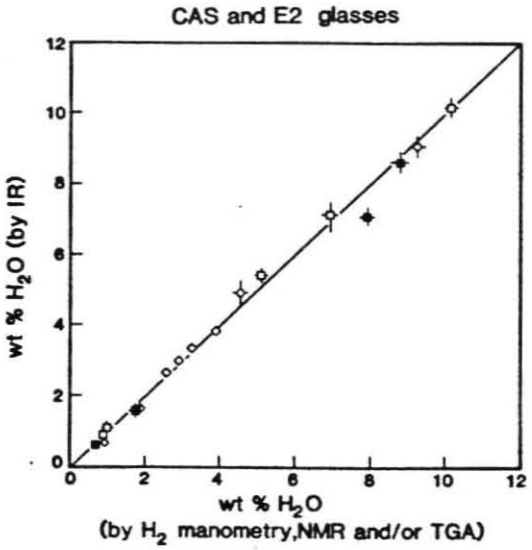

Fig. 3. Total water contents determined by infrared spectroscopy (from the sum of molecular water (5200 cm^{-1} band) and water dissolved as OH groups (4500 cm^{-1} band)) vs total water contents (determined by H_2 manometry, NMR spectroscopy, or TGA) in CAS (*squares*) and E2 (*diamonds*) glasses. *Open symbols* show samples synthesized in BN-free assemblies; *filled symbols* show samples synthesized in BN-bearing assemblies. Estimated errors due to analytical uncertainty are indicated by error bars. Samples shown are CAS-2, CAS-3, CAS-7, CAS-11, CAS-12, CAS-13, CAS-14, CAS-15, CAS-16, E2-25, E2-26, E2-27, E2-30, E2-31, E2-32,E2-34, and E2-36

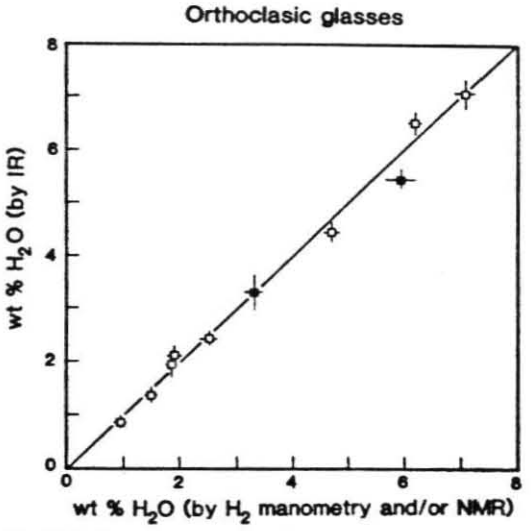

Fig. 4. Total water contents in orthoclasic glasses determined by infrared spectroscopy (from the sum of molecular water (5200 cm^{-1} band) and water dissolved as OH groups (4500 cm^{-1} band)) vs total water contents measured by H_2 manometry and/or NMR spectroscopy. *Open symbols* show samples synthesized in BN-free assemblies; *filled symbols* show samples synthesized in BN-bearing assemblies. Estimated errors due to analytical uncertainty are indicated by error bars. Samples shown are KAS-2, KAS-3, KAS-5, KAS-6, KAS-7, KAS-8, KAS-9, KAS-10, KAS-11, and KAS-12

entire data set was used to determine one pair of best fit molar absorption coefficients. Similar values are obtained if molar absorption coefficients are determined separately from the data on samples with compositions An(30–40)Si(70–60) and from the data on samples with composition An45Si55.

The molar absorption coefficients for the ANS glasses are at best approximate values. In particular, the coefficient for the OH band is poorly constrained because the glasses cover a narrow range in total water contents over which the OH content is low and approximately constant. Figure 5 compares the total water contents determined by infrared spectroscopy with the total water contents determined by Stewart (1967). Given the uncertainties in the molar absorption coefficients and the fact that the almost thirty years separated the synthesis and infrared analysis of these water-rich glasses, the agreement between these two methods is good.

Rhyolite. The molar absorption coefficients for the 5200 and 4500 cm^{-1} bands for rhyolitic glasses have been previously determined by Newman et al. (1986) for samples with total water contents up to about 2 wt%. Based on unpublished data on rhyolitic glasses, we have confirmed the validity of these molar absorption coefficients for glasses with up to at least 4 wt% total water.

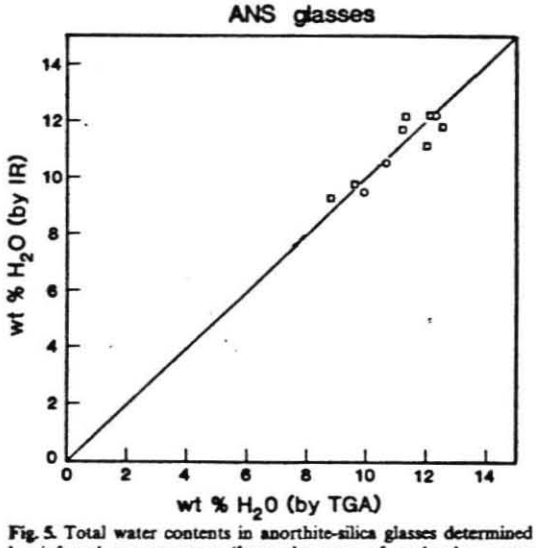

Fig. 5. Total water contents in anorthite-silica glasses determined by infrared spectroscopy (from the sum of molecular water (5200 cm^{-1} band) and water dissolved as OH groups (4500 cm^{-1} band)) vs total water contents determined by a weight loss method (TGA) (Stewart 1967). *Open squares* show samples with compositions An(45-51)Si(55-49); *open circles* show samples with compositions An(30-40)Si(70-60). Estimated errors based on analytical uncertainty are indicated by error bars. Samples shown are: ANS-162, ANS-167, ANS-329, ANS-161, ANS-166, ANS-367, ANS-328, ANS-357, ANS-358, and ANS-359

Summary of calibrations

The molar absorption coefficients determined in this study, Newman et al. (1986), and Silver and Stolper (1989) vary with silicate composition: 1.1–1.9 l/mole-cm for the 5200 cm^{-1} band and 0.9–1.7 l/mole-cm for the 4500 cm^{-1} band. This variation demonstrates the importance of carrying out a calibration for each composition if quantitative results are desired. Improvements in the calibrations presented here would result if additional samples of each composition with low total water contents (i.e., in the range where nearly all the water is dissolved as hydroxyl) were available. This would help especially in constraining the molar absorption coefficient for the 4500 cm^{-1} band. Nevertheless, our results confirm that infrared spectroscopy does provide a precise method for determining total water contents and species concentrations in hydrous silicate glasses.

The speciation of water in silicate glasses

Using the molar absorption coefficients given in Table 7 and in Newman et al. (1986), the molecular water, hydroxyl group, and total water contents were determined by infrared spectroscopy for the glasses included in this study. The hydrous species concentrations are given in Tables 2–6 and summarized below.

CAS-E2 and orthoclase. Figures 6 and 7 show the concentrations of molecular water and hydroxyl groups as functions of total water for the CAS-E2 and orthoclasic glasses. Also shown in Figs. 6 and 7 are fits to the measured molecular water and OH group contents (see Appendix 2 for fitting procedure). The general trends in species concentrations are similar to those determined for hydrous albitic glasses (see Fig. 6 in Silver and Stolper 1989), though the hydroxyl content does not quite level off in the orthoclasic glasses for this range of total water contents. At low total water contents, most of the water is dissolved as hydroxyl groups. At a total water content of about 3 wt% (for orthoclase) and 4 wt% (for CAS), equal amounts of water are dissolved as molecular water and OH groups. At higher total water contents, most of the water is dissolved as molecular water and the OH concentration remains approximately constant or increases very little.

The similarity in the ratio of molecular water to hydroxyl groups at a given total water content for the CAS and E2 glasses suggests a weak dependence of the speciation of water on the pressure and temperature of equilibration. Silver and Stolper (1989) found a similar result for albitic glasses, though a small temperature dependence was detected. In addition, the E2 glasses were synthesized in IHPV and the CAS glasses in piston-cylinder apparatus; this suggests, as discussed in Silver and Stolper (1989), that quenching rates in IHPVs, although slower than in piston cylinder apparatus, may under some circumstances be rapid enough to preserve high temperature species concentrations.

Jadeite and anorthite-silica. Figures 8 and 9 show the concentrations of molecular water and hydroxyl groups as functions of total water content for hydrous JD and ANS glasses quenched from melts synthesized over a range of experimental conditions. Although the molar absorption coefficients are not well constrained for these compositions, it is clear

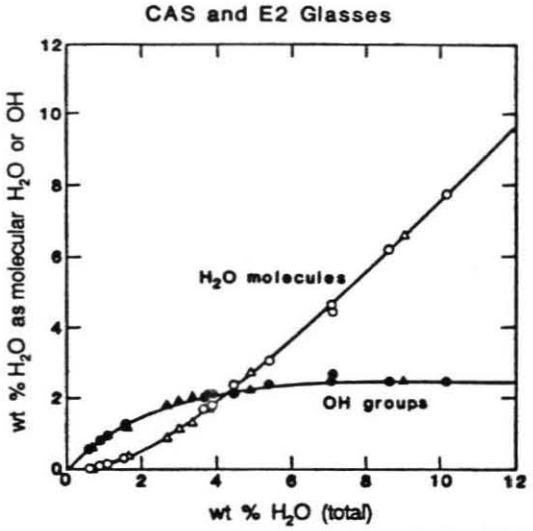

Fig. 6. The concentrations of water dissolved as molecules of H_2O (*open symbols*) and as OH (*filled symbols*) as functions of total water content in CAS (*circles*) and E2 (*triangles*) glasses, together with a fit to the data (see Appendix 2). The run conditions for all the samples are listed in Table 2. Typical analytical uncertainty is ±0.1–0.2 wt% for each species

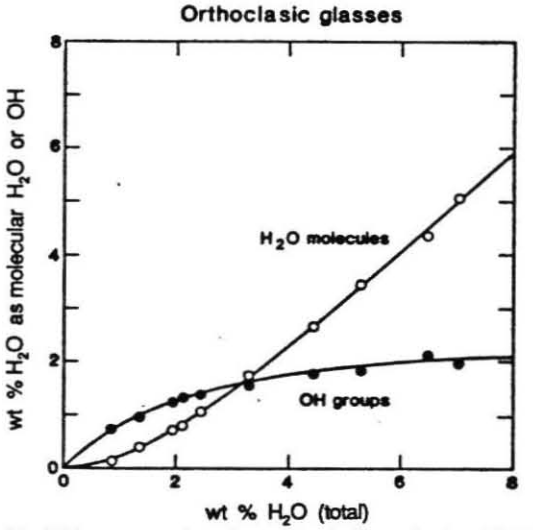

Fig. 7. The concentrations of water dissolved as molecules of H_2O (*open symbols*) and as OH (*filled symbols*) as functions of total water content in orthoclasic glasses, together with a fit to the data (see Appendix 2). The run conditions for all the samples are listed in Table 3. Typical analytical uncertainty is ±0.1–0.2 wt% for each species

that the trends in the speciation of water for hydrous JD and ANS glasses are similar to those observed for other compositions. As in the case of the CAS-E2 glasses, the jadeitic glasses synthesized in an IHPV are not distinguishable in terms of their species concentrations from those syn-

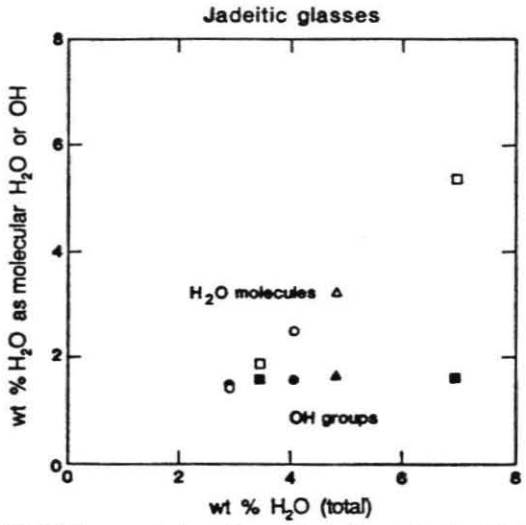

Fig. 8. The concentrations of water dissolved as molecules of H_2O (*open symbols*) and as OH (*filled symbols*) as functions of total water content in jadeitic glasses synthesized in piston cylinder apparatus and IHPVs over a range of experimental conditions. The *circles* show samples synthesized by us in piston cylinder apparatus; the *squares* show samples synthesized by us in IHPVs; the *triangles* represent one sample synthesized in a piston cylinder apparatus by Mysen and Virgo (1986b). The run conditions for all the samples are listed in Table 4. Typical analytical uncertainty is ±0.1–0.2 wt% for each species

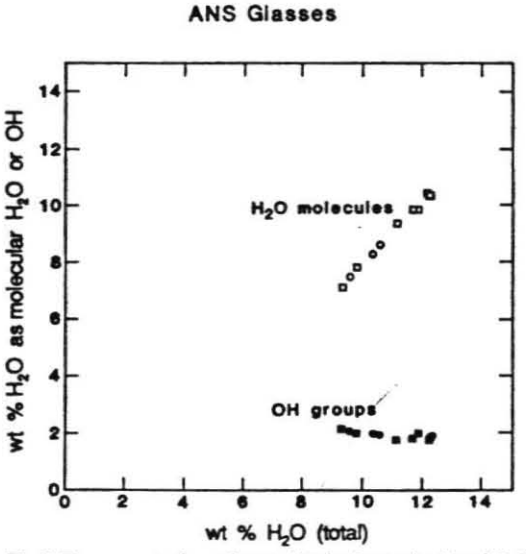

Fig. 9. The concentrations of water dissolved as molecules of H_2O (*open symbols*) and as OH (*filled symbols*) as functions of total water content in anorthite-silica glasses. The *squares* show samples with bulk compositions An(45-51)Si(55–49); the *circles* show samples with bulk compositions An(30-40)Si(70-60). The run conditions for all the samples are listed in Table 5. Typical analytical uncertainty is ±0.1–0.2 wt% for each species

thesized in piston cylinder apparatus at higher temperatures and pressures.

The concentration of OH groups in the ANS glasses decreases slightly with increasing total water contents (Fig. 9). Bartholomew et al. (1980) observed a similar trend for OH groups in a Na, Zn-rich silicate glass (composition listed in Table 1) at total water contents greater than about 4 wt%. The decrease observed in the ANS glasses may be a quenching effect (possibly more pronounced in these very water-rich glasses synthesized in an IHPV) or due to "aging" of the glasses in the many years that intervened between synthesis and the infrared measurements. However, such a decrease in the OH content at high water contents is expected based on extrapolation of the regular solution model discussed by Silver and Stolper (1989) and Stolper (1989), particularly at low temperatures.

Rhyolite. Figure 10a shows the concentrations of molecular water and OH groups as functions of total water content for hydrous rhyolitic glasses synthesized in rapid quench cold seal pressure vessels at 850° C and pressures up to 1500 bars, together with a fit to the data (see Appendix 2 for fitting procedure; this fitting procedure assumes that variations in pressure have a negligible influence on the speciation of water over the small range of pressures covered by these samples; see Silver and Stolper 1989). At low total water contents, most of the water is dissolved as OH groups. At ~3 wt% total water, there are equal amounts of water dissolved as molecular water and hydroxyl groups; this cross-over point is the lowest of the compositions included in this study. At higher total water contents, most of the water is dissolved as molecular water and its concentration increases rapidly with increasing total water, whereas the OH content increases slightly, but does not completely level off over this range of water contents, similar to orthoclasic glasses but in contrast to the behavior observed in albitic and CAS glasses. The overall trends in the hydrous species concentrations, however, are similar to those observed for all the silicate glasses previously described.

Figure 10b compares the concentrations of molecular water and hydroxyl groups in rhyolitic glasses synthesized in air-quench cold seal pressure vessels at 850° C and pressures up to 1000 bars with the fit to the rapid-quench cold seal data. Also shown in Fig. 10b are the concentrations of molecular water and OH groups in a series of naturally occurring hydrous rhyolitic glasses from the Mono Craters, California (Newman et al. 1988). Figure 10b shows that at a given total water content the ratio of molecular water to OH groups for the glasses synthesized in air-quench cold seal apparatus is higher than for the rhyolites synthesized in rapid-quench apparatus. The difference in the relative proportions of the two hydrous species must be related to differences in cooling rates because the two sets of glasses were quenched from melts equilibrated at the same temperature and over the same pressure interval. It is known that the ratio of molecular water to hydroxyl increases with decreasing temperature (Aines et al. 1984; Pickett and Stolper 1984; Silver and Stolper 1989; Stolper 1989). Thus, the species concentrations of glasses cooled at sufficiently slow rates will reflect conversion of OH to molecular water as the melt/glass cooled.

The trends illustrated in Fig. 10b demonstrate the necessity of rapid quenches for preserving in rhyolitic glasses the high temperature characteristics of melts. We must em-

152

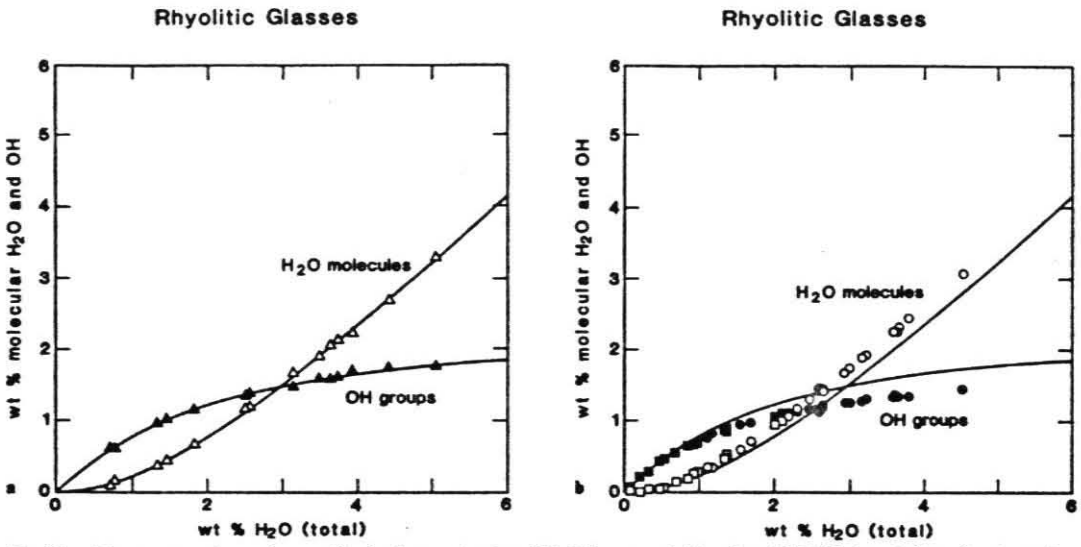

Fig. 10. **a** The concentrations of water dissolved as molecules of H_2O (*open symbols*) and as OH (*filled symbols*) as functions of total water content in rhyolitic glasses synthesized in rapid quench cold seal bombs, together with a fit to the data (see Appendix 2). The run conditions for all the samples are listed in Table 6. Typical analytical uncertainty is ±0.1–0.2 wt % for each species. **b** The concentrations of water dissolved as molecules of H_2O (*open symbols*) and as OH (*filled symbols*) as functions of total water content in rhyolitic glasses synthesized in air-quench cold seal apparatus (*circles*) and in natural rhyolitic glasses from the Mono Craters, California (*squares*), together with the fit to the data for the rapid quench rhyolites shown in **a**. The run conditions for the synthetic glasses are listed in Table 6; the rhyolitic glasses from the Mono Craters are described by Newman et al. (1988)

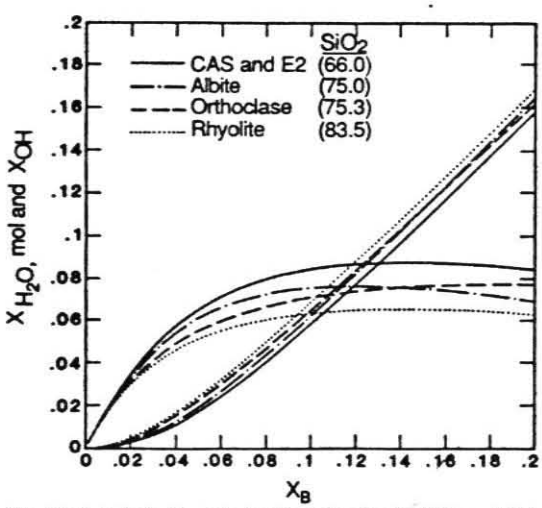

Fig. 11. Best fits to the mole fractions of molecular H_2O and OH groups as functions of X_B for CAS-E2 (1170°–1450° C), orthoclasic (1450° C), rhyolitic (850° C), and albitic (1400° C) glasses. See Appendix 2 for best fit parameters. Errors due to analytical uncertainty are sufficiently small to make the fits distinguishable

phasize, however, that the hydrous species may reequilibrate at rates much faster than quenching rates obtainable in high pressure experiments and that difficulties in preserving high temperature species concentration on quenching are likely to be most pronounced at high total water contents. It is thus possible that none of the rhyolitic glasses on which we report in this paper preserve high temperature species concentrations. Despite the uncertainty introduced by the possible effects of quenching on even our most rapidly quenched samples, the effects of temperature on speciation in rhyolitic glasses are believed to be comparatively small (Stolper 1989), so the overall trends we observe are unlikely to have been strongly affected. In addition, we note that among the glasses we have studied, only rhyolitic glasses have displayed a dependence of speciation on quench rate, yet the speciation trends are very similar for all glasses. We suggest, however, that detailed study of the kinetics of reactions among hydrous species in silicate glasses and melts would be of considerable value, as would in situ infrared spectra on hydrous melts and glasses at elevated temperatures and pressures (e.g., Aines et al. 1984).

The low temperatures recorded by the speciation of water in the natural samples shown in Fig. 10b place constraints on eruption temperatures and/or cooling rates for natural volcanic glasses. This has been discussed by Newman et al. (1988); they suggest that these glasses came from glassy margins of the conduit system of the volcano and were held at 500–600° C for a prolonged period and then cooled rapidly on eruption.

The influence of bulk composition on the speciation of water

Figure 11 summarizes our data for CAS-E2, orthoclasic, rhyolitic, and albitic glasses on the variations in mole fractions of molecular water and hydroxyl groups with total water content (X_B is the mole fraction of total water expressed on a single oxygen basis; see footnote f of Table 2,

and Appendix 2). The various curves are fits to the data shown in Figs. 6 and 7, and 10a and in Silver and Stolper (1989). The JD and ANS glasses have been excluded because the molar absorption coefficients are not well constrained for these compositions.

For all compositions studied, the OH content increases rapidly at low total water contents and then levels off or even begins to decrease at high water contents. The exact concentration at which the OH content begins to level off varies from one composition to another, as does the point at which equal amounts of water are dissolved as molecular water and hydroxyl. At a given total water content, the molecular water to OH ratio increases with increasing silica content from CAS, to albite, to KAS, to rhyolite. Based on these results, we predict that silica glass will have even higher ratios of molecular water to hydroxyl groups and that its "saturation" level of hydroxyl groups will be lower than in these more complex compositions. Preliminary results confirm this (Stolper and Silver 1985). We note, however, that the rhyolite glasses were synthesized at 850° C, whereas the other fits shown in Fig. 11 are based on glasses synthesized at near 1400° C; increasing temperature would increase the hydroxyl concentration at a given total water content and bring the rhyolites closer to the other compositions shown in Fig. 11, although the magnitude of this effect at these high temperatures is at present unknown.

Comparison with other studies

The speciation of water in hydrous silicate glasses determined in this study is similar to that observed in other silicate glasses using infrared spectroscopy (Bartholomew et al. 1980; Acocella et al. 1984; Silver and Stolper 1989). Although the decline in the hydroxyl group content with increasing total water in Na, Zn-rich silicate glasses observed by Bartholomew et al. (1980) is more pronounced than in the ANS composition, the general trends in the species concentrations are still similar.

The concentrations of molecular water and hydroxyl groups as functions of total water content determined in this study by infrared spectroscopy have been verified by NMR spectroscopic studies on many of the same samples (Eckert et al. 1988). Similar results were also obtained when both NMR and infrared techniques were used to determine the speciation of water in hydrous Na, Zn-rich silicate glasses (Bartholomew and Schreurs 1980; Bartholomew et al. 1980).

The trends presented in Fig. 11 are similar but not identical to those obtained for hydrous silica glass by Farnan et al. (1987) using cross-polarization NMR techniques, and in a preliminary study by us using infrared spectroscopy. All these results contrast with those presented by Mysen and Virgo (1986a) based on Raman studies of hydrous silica glass. Although further study is necessary to constrain the details for hydrous silica glass, no infrared or NMR investigations have yielded results similar to those obtained by Raman spectroscopy.

Solution mechanisms for water in silicate melts and glasses

The concentrations of molecular water and hydroxyl groups observed in every composition studied to date by either NMR or infrared spectroscopy exhibit similar trends over a wide range of total water contents. Although it is tempting to suggest that the leveling off of hydroxyl group contents at high water concentrations reflects the exhaustion of a particular type of cation or oxygen anion in the melt that is essential to the generation of hydroxyl groups (and indeed the model described by Silver and Stolper 1989, based on the exchange reaction between H and Na proposed by Burnham 1975, 1979, can account quantitatively for the saturation of OH contents in albitic melts), the similarity in the speciation of water over the range of compositions studied suggests that this is probably not the only factor. The fact that the hydroxyl group content "saturates", though at slightly different levels, in all these compositions (including silica, based on our preliminary results) suggests that this is a fundamental feature of the interaction between highly polymerized silicate melts and water. The non-ideal and polymer models presented by Silver and Stolper (1989) are examples of solution models that could account for the similarity of speciation patterns in most highly polymerized melts.

We note that although the presence of charge-balancing cations does not appear to be essential to generate the levelling off of the hydroxyl concentration at high water contents, the actual amount of OH at a given total water content does seem to depend on the charge-balancing cations. If the charge-balancing cation had no influence on the speciation of water, then we would expect albitic and orthoclasic glasses to have identical OH and molecular water contents given their similar melt chemistries. The small difference in the species concentrations at a given total water content for these two compositions demonstrates that charge-balancing cations do play a role in the dissolution mechanisms for water.

Our measurements may be useful for rationalizing certain variations in macroscopic properties of melt-water systems in terms of their molecular level interactions. For example, at a given total water content, there are more OH groups in albitic glasses than in orthoclasic glasses, suggesting that water may be more reactive with Na-bearing units to produce hydroxyls than with K-bearing ones. Precisely this explanation was offered by Pichavant and Ramboz (1985) to explain phase relations in the system albite-orthoclase-silica-water, in which the phase boundaries move toward more albitic compositions with the addition of water. Likewise, preliminary results on silica glass indicate a lower level of hydroxyl groups in hydrous silica glasses than in albitic or orthoclasic glasses at a given total water content. This may help to explain the expansion of the quartz liquidus volume relative to the Na- and K-feldspar fields in the albite-orthoclase-silica-water system with increasing water pressure (Tuttle and Bowen 1958) and the lower solubility of water in silica melt than in feldspar melts (Stolper 1982a, b). McMillan and Holloway (1987) also suggested that the preferential affinity of water for certain cations may explain the variations in water solubility as a function of silicate composition. Our results support these suggestions and may ultimately be used to rationalize quantitatively the variations in water solubility and solid-liquid phase equilibria in these and other systems using the approach outlined by Silver and Stolper (1989) for the albite-H_2O system.

The solubility of water in silicate melts

One of the goals of our studies of the speciation of water in silicate glasses is to use them as constraints on descrip-

tions of the thermodynamics of hydrous silicate melts. The simplest approach to linking our measurements with the thermodynamic properties of silicate liquids is to assume Henry's law is valid over the range of water concentrations we have studied; i.e., we assume that $a^m_{H_2O} \propto X^m_{H_2O,mol}$ where $X^m_{H_2O,mol}$ is the mole fraction of molecular water in the melt. As discussed in detail by Silver and Stolper (1989), this approximation accounts well for phase equilibrium data in the system $NaAlSi_3O_8-H_2O$. In this section, we use both new and previously published data on the solubility of water in silicate melts in conjunction with our spectroscopic measurements of species concentrations to evaluate explicitly the utility of this approximation.

The activity of water in vapor-saturated melt as a function of pressure and temperature is given by

$$a^m_{H_2O}(P_2, T_2) = a^m_{H_2O}(P_1, T_1)\frac{f^0_{H_2O}(P_2, T_2)}{f^0_{H_2O}(P_1, T_1)} \cdot \exp\left\{-\int_{P_1}^{P_2}\frac{V^{0,m}_{H_2O}(P, T_2)}{RT_2}dP + \int_{T_1}^{T_2}\frac{\Delta H^0_{H_2O}(P_1, T)}{RT^2}dT\right\} \quad (1)$$

where P_1, T_1 and P_2, T_2 refer to two sets of vapor-saturated conditions; $a^m_{H_2O}(P_2, T_2)$ and $a^m_{H_2O}(P_1, T_1)$ are the activities of water in the melt at P_2, T_2 and P_1, T_1; $f^0_{H_2O}(P_2, T_2)$ and $f^0_{H_2O}(P_1, T_1)$ are the fugacities of pure water vapor at P_2, T_2 and P_1, T_1; $V^{0,m}_{H_2O}(P, T)$ is the molar volume of water in the melt in its standard state; and $\Delta H^0_{H_2O}$ is the standard state enthalpy change for the dissolution of water vapor in the melt. If the activity of water in vapor-saturated melt at any P and T (i.e., P_1, T_1) is known along with expressions for $V^{0,m}_{H_2O}$ and $\Delta H^{0,m}_{H_2O}$, then the activity of water in vapor-saturated melts can be calculated at any other P and T (i.e., P_2, T_2) from Eq. (1) given an expression for $f^0_{H_2O}(P, T)$. Use of Eq. (1) assumes that the vapor in equilibrium with the melt is pure water.

As $P_2 \rightarrow P_1$, the integral containing the volume term in Eq. (1) approaches zero, so in the low pressure limit at constant temperature the activity of water in water vapor-saturated melts will be approximately proportional to water fugacity. Thus, the validity of the particular description of the relationship between water activity and composition can be tested by determining whether the water activity in a series of melts equilibrated with water vapor over a range of low total pressures is proportional to water fugacity[2]; i.e., if the Henrian approximation is valid, the mole fraction of molecular water in melts equilibrated with water vapor at low pressure should be proportional to water fugacity. This approach to constraining the activity-composition relation for hydrous melts has been taken previously: by noting there is a linear relationship between the square of the mole fraction of water and water pressure (or fugacity) at very low pressures, glass scientists long ago concluded that the activity of water is proportional to the square of the mole fraction of water in the melt under these conditions (e.g., Tomlinson et al. 1956; Kurkjian and Russell 1958; Moulson and Roberts 1960; Uys and King 1963). When the difference between P_2 and P_1 is large, the integral containing the volume term in Eq. (1) becomes significant and, given the validity of a particular activity-composition relation, $V^{0,m}_{H_2O}$ can be determined from the activity-fugacity relationship.

[2] Note that the volume term could be completely eliminated by comparing solubility at constant temperature and pressure but varying f_{H_2O} (i.e., variable vapor composition).

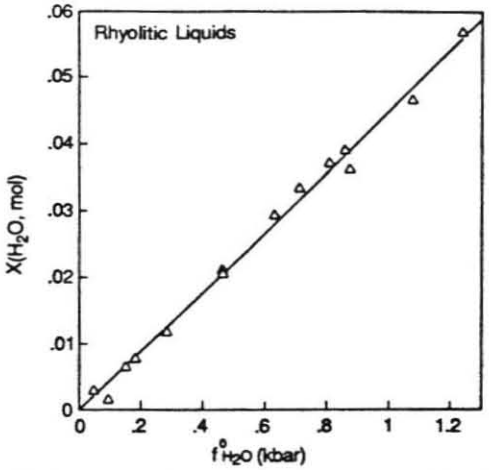

Fig. 12. Mole fraction of molecular water (based on infrared spectroscopic data) vs water fugacity for rhyolitic glasses quenched from water-saturated melts in rapid-quench cold seal apparatus at 850° C. The *solid curve* shows the best fit to these data based on Eq. (1). Best fit parameters are given in Table 8. The maximum error is on the order of the size of the symbols

There are four compositions for which both speciation and water solubility measurements are available: rhyolite, CAS-E2, albite, and orthoclase. In the following sections, we evaluate the Henrian approximation for each of these compositions by comparing $X^m_{H_2O,mol}$ to $f^0_{H_2O}$ at low pressures. In each case, the composition of the vapor has been assumed to be pure water vapor, $f^0_{H_2O}$ values are based on a modified Redlich-Kwong equation of state (Holloway 1977), and the species concentrations measured in glasses are assumed to be representative of the melts from which they were quenched. For most of these compositions, data are also available at higher pressure, allowing constraints to be placed on $V^{0,m}_{H_2O}$ given the assumption of Henrian behavior.

Rhyolitic melts. The solubility and speciation of water in hydrous rhyolitic glasses quenched from water-saturated melts held at pressures up to 1500 bars at 850° C have been determined by infrared spectroscopy. Details of the experimental techniques are described above. Total water contents and the concentrations of molecular water and hydroxyl groups are listed in Table 6. Figure 12 shows the mole fraction of molecular water from our infrared measurements as a function of water fugacity for the rhyolitic glasses hydrated in the rapid quench apparatus. Also shown is a curve based on a least-squares fit of these data to Eq. (1), given the assumption that $a^m_{H_2O} \propto X^m_{H_2O,mol}$. The best fit parameters are listed in Table 8. The essentially linear relationship between $X^m_{H_2O,mol}$ and fugacity clearly demonstrates that water activity can be described by the mole fraction of molecular water in the melt over this pressure range.

The best fit value of $V^{0,m}_{H_2O}$ is approximately zero for the rhyolitic melts (Table 8). This value is lower than expected based on the determinations of volumes of hydrous albitic melts by Burnham and Davis (1971). However, the measurements by Burnham and Davis (1971) were all at higher

Table 8. Results of fit of solubility data to Eq. (1)

$$\ln \frac{X^{m}_{H_2O,mol}(P_2, T_2)}{f^{0}_{H_2O}(P_2, T_2)} = \ln \frac{X^{m}_{H_2O,mol}(P_1, T_1)}{f^{0}_{H_2O}(P_1, T_1)} - \int_{P_1}^{P_2} \frac{V^{0,m}_{H_2O}(P, T_2)}{RT_2} dP + \int_{T_1}^{T_2} \frac{\Delta H^{0}_{H_2O}(P_1, T)}{RT^2} dT$$

	P_1 (bars)	T_1 (°C)	$\ln \frac{X^{m}_{H_2O,mol}(P_1, T_1)}{f^{0}_{H_2O}(P_1, T_1)}$	$V^{0,m}_{H_2O}(P, T_2)$ (cc/mole)	$\Delta H^{0}_{H_2O}(P_1, T)$ (cal/mole)
Rhyolite	1	850	−10.05 (0.04)	−3.3 (2.8)	–
E2	1	1180	−10.21 (0.06)	16.2 (1.7)	–
Albite	1	850	−9.36 (0.06)	20.9 (0.6) + 0.010 (0.004) • $(T_2 - T_1)$	−4420 (490)
Orthoclase	1	850	−9.71 (0.09)	25.1 (1.4)	−6310 (680)

Numbers in parentheses indicate standard errors on best fit values
Water fugacity calculated using modified Redlich-Kwong equation of state (Holloway 1977)
All fits based on the assumption that $a^{m}_{H_2O} \propto X^{m}_{H_2O,mol}$

pressures (3–8.5 kbar) and higher water contents (8–11 wt% water) than the solubility experiments reported here, and it is possible that the partial molar volume of water in felsic melts initially increases with water content. A low partial molar volume for water in silicate melts at low water contents is consistent with the results of McMillan and Chlebik (1980), who found that density increases with initial incorporation of water (up to several hundred ppm) as hydroxyl into sodium silicate glass, indicating a partial molar volume of water that is close to zero, or even negative. In addition, Boulos and Kriedel (1972) postulated that the dissolution of water as hydroxyl in glasses may result in an increase in density as the network structure collapses and due to hydrogen bonding. A small partial molar volume of water would also result if molecular water enters the melt by filling holes. Further work will be required to determine if the partial molar volume of water is indeed low at low pressures and water contents, or if it is an artifact of (1) the approximation that $a^{m}_{H_2O} \propto X^{m}_{H_2O,mol}$; (2) the difficulty in resolving values of volume from Eq. (1) over small pressure intervals; or (3) our assumption in this analysis that the speciation of water in our rapidly quenched samples was completely unaltered on quenching.

Figure 13a compares the calculated water solubility in rhyolitic melts at 850° C (based on the best fit parameters listed in Table 8 and the fit to the speciation data shown in Fig. 10a and listed in Table A.2) with experimental determinations from this study; the agreement between the calculated and measured solubilities is excellent. The right- and left-pointing arrows indicate the direction from which equilibrium was approached for glasses synthesized in air-quench cold seal pressure vessels (see Experimental Methods section). The circles are results for the experiments conducted in rapid quench bombs. The total water contents determined for both sets of cold seal experiments are similar, even though the relative proportions of molecular water and OH groups at a given total water content are different due to the differences in cooling rates (Fig. 10a, b). The agreement between the reversed and unreversed runs demonstrates that equilibrium was closely approached in these experiments. We also note that the agreement between the solubility measurements from this study and previous determinations is good (Fig. 13b).

The results presented in Figs. 12 and 13 substantiate a Henrian ($a^{m}_{H_2O} \propto X^{m}_{H_2O,mol}$) activity-composition relation based on spectroscopic measurements. An alternative and popular approach is the approximation that $a^{m}_{H_2O} \propto (X^{m}_{w})^2$ for total water contents ≤ 6.5 wt%, where X^{m}_{w} is defined as in Burnham (1979). Figure 14 shows $X^{m}_{H_2O,mol}$ vs $(X^{m}_{w})^2$ for the rhyolitic glasses synthesized in rapid quench bombs. The approximate proportionality between $X^{m}_{H_2O,mol}$ and $(X^{m}_{w})^2$ demonstrates that the activity of water in the melt according to Burnham's model is basically equivalent to our approximation. However, the validity of Burnham's activity-composition relationship does not imply that his structural model for water dissolution is correct; in fact, our measurements demonstrate that his conclusion that nearly all of the water dissolves as hydroxyl groups is incorrect. As discussed by Stolper (1982b) and McMillan and Holloway (1987), if water dissolves exclusively as hydroxyl groups, $a^{m}_{H_2O}$ is not expected to be proportional to $(X^{m}_{w})^2$ except at very low total water contents.

Calcium aluminosilicate (E2) melts. The E2 glasses included in this study provide an opportunity to extend this thermodynamic analysis to another hydrous melt composition. These glasses were synthesized in IHPVs by quenching from melts equilibrated with water vapor at pressures up to 5130 bars at ~1180° C. The solubility and speciation of water were determined for each glass sample by infrared spectroscopy. Figure 15 shows the mole fraction of molecular water from our infrared spectroscopic measurements versus the fugacity of water for the E2 glasses along with a curve based on a least squares fit of these data to Eq. (1) given the assumption that $a^{m}_{H_2O} \propto X^{m}_{H_2O,mol}$. The best fit parameters are listed in Table 8. The measured mole fraction of molecular water is approximately linear with water fugacity up to $P = 1500$ bars, demonstrating the applicability of the Henrian activity-composition relation.

Note the downward curvature of the best fit curve shown in Fig. 15, reflecting the non-zero value of $V^{0,m}_{H_2O}$ in the fit to Eq. (1). The best fit value of $V^{0,m}_{H_2O}$ is about 16 cc/mole; this value is highly sensitive to the single data point at a pressure of about 5 kbar.

Albitic melts. Although we do not have measurements of hydrous species concentrations in albitic glasses quenched from melts saturated with water vapor, the speciation of water in undersaturated glasses quenched from albitic melts has been studied in detail (Silver and Stolper 1989) and varies little with pressure and temperature. Combining these speciation data with the data of Hamilton and Oxtoby (1986) on the solubility of water in albitic melts up to 8 kbar at temperatures between 750 and 1375° C, we can compare

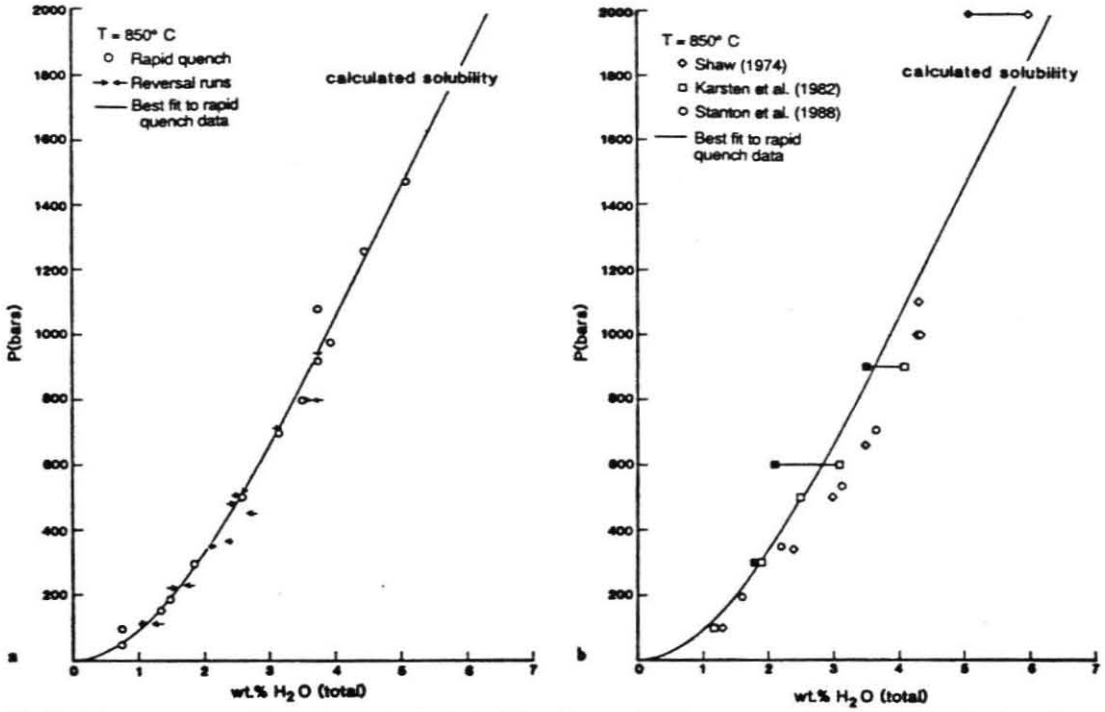

Fig. 13. **a** The pressure dependence of water solubility in rhyolitic melts up to 2000 bars at 850° C. The curve was calculated as follows: for each P, $X^m_{H_2O,mol}$ was calculated using Eq. (1) and the best fit parameters listed in Table 8; the total water content was then calculated using the relationship between $X^m_{H_2O,mol}$ and X_g given by the fit to our speciation given in Appendix 2. The *circles* show water solubility measurements from this study for rhyolitic glasses synthesized in rapid-quench apparatus; the *arrows* show rhyolitic glasses synthesized in air-quench cold-seal apparatus, where the direction of the arrow signifies the direction from which equilibrium was approached. **b** Comparison between calculated solubility of water in rhyolitic melts at 850° C as shown in **a** based on our data (*solid curve*) and data from the literature. The *squares* are results from Karsten et al. (1982), the *diamonds* are data from Shaw (1974), and the *circles* are results from Stanton et al. (1988). Note that at some pressures two measurements were obtained, one reported in the literature (*open symbols*) and a second value determined by infrared spectroscopy on the same samples (*filled symbols*)

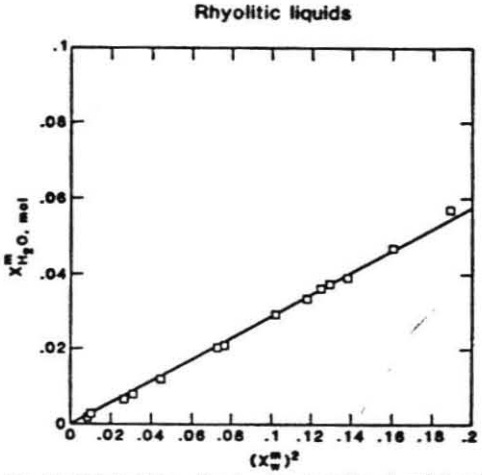

Fig. 14. Mole fractions of molecular water (based on infrared spectroscopic data) in hydrous rhyolitic glasses synthesized in rapid-quench apparatus vs the square of the mole fraction of total water, $(X^m_w)^2$, where X^m_w is given by Burnham (1979). The line is a fit to the data constrained to pass through the origin. The maximum error is on the order of the size of the symbols

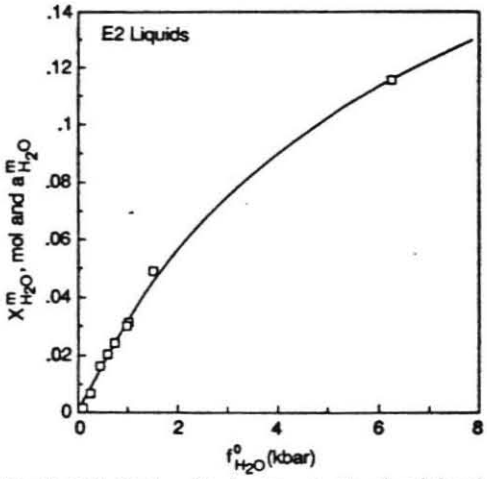

Fig. 15. Mole fraction of molecular water (based on infrared spectroscopic data) vs water fugacity for E2 glasses quenched from water-saturated melts in IHPVs at ~1180° C. The *solid curve* shows the best fit to the data based on Eq. (1). Best fit parameters are given in Table 8

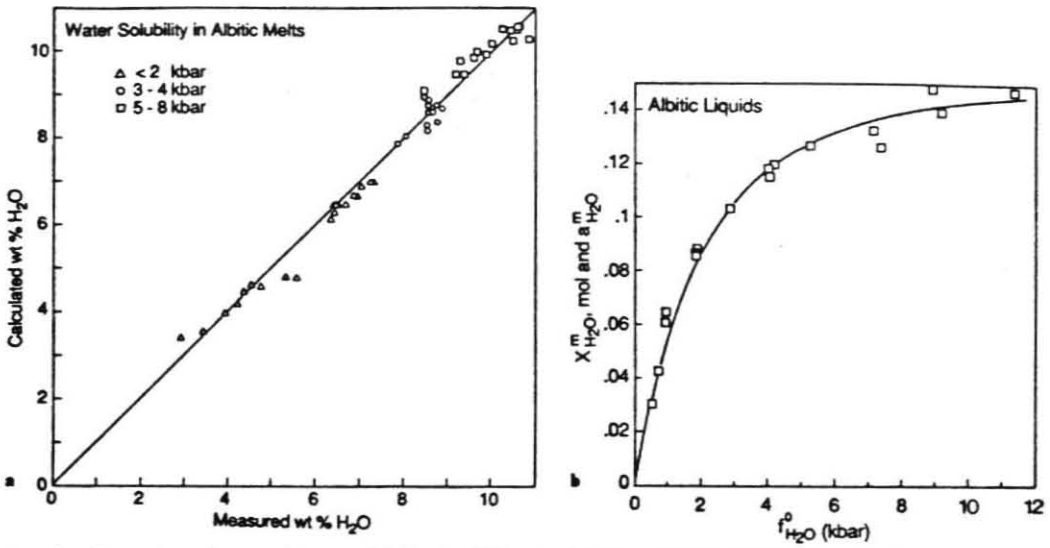

Fig. 16. a Comparison of measured water solubility in albitic melts (750°–1375° C, 0.56–8.0 kbar) from Hamilton and Oxtoby (1986) with values calculated based on best fit to Eq. (1) as described in the text. Water solubilities were calculated at the P and T of each of Hamilton and Oxtoby's experiments as follows: $X^m_{H_2O,mol}$ was calculated using Eq. (1) and the best fit parameters given in Table 8. The total water content was then calculated using the temperature-dependent relationship between $X^m_{H_2O,mol}$ and X_g given in Silver and Stolper (1989); b Mole fraction of molecular water vs water fugacity for water-saturated albitic melts. Water solubility data from Hamilton and Oxtoby (1986) at 950°–1050° C; mole fractions of molecular water are from the spectroscopically determined relationship between total water and molecular water content in undersaturated albitic glasses given by Silver and Stolper (1989). The *solid curve* shows the calculated trend at 1000° C using the best fit parameters given in Table 8

$X^m_{H_2O,mol}$ and $f^0_{H_2O}$ for albitic melts as we have done above for rhyolitic and E2 glasses. For each solubility measurement reported by Hamilton and Oxtoby (1986) the mole fraction of molecular water was computed using the fit to the data on water speciation given in Silver and Stolper (1989). We then assumed that Henry's law holds and fit these values of $X^m_{H_2O,mol}$ to a function of the form of Eq. (1). Hamilton and Oxtoby (1986) present solubility data over a large enough range of experimental conditions to constrain both $V^{0,m}_{H_2O}$ and $\Delta H^*_{H_2O}$ in Eq. (1). The best fit parameters are listed in Table 8.

Figure 16a compares the measured solubility of water in albitic melts from Hamilton and Oxtoby (1986) with our calculated values. For the conditions of each of their experiments, the fit to Eq. (1) was used to calculate $X^m_{H_2O,mol}$; this was then converted to a total dissolved water content using the fit to the speciation data of Silver and Stolper (1989). It is clear from Fig. 16a that the data of Hamilton and Oxtoby (1986) are fit well by this procedure, which is based on the assumption that $a^m_{H_2O} \propto X^m_{H_2O,mol}$. This is also illustrated in Fig. 16b, which compares $X^m_{H_2O,mol}$ vs $f^0_{H_2O}$ for the data of Hamilton and Oxtoby (1986) at $1000 \pm 50°$ C with a curve calculated using the best fit to Eq. (1). As expected, $X^m_{H_2O,mol}$ is approximately proportional to $f^0_{H_2O}$ at low pressures; the downward curvature at higher pressures is reflected in the non-zero best fit value of $V^{0,m}_{H_2O}$.

In the fit of the Hamilton and Oxtoby (1986) data to Eq. (1), we took $V^{0,m}_{H_2O}$ to be independent of pressure and a linear function of temperature. At 1000° C, the best fit volume is 22.4 cc/mole, and the coefficient of thermal expansion for this component is about $45(10^{-5})\,K^{-1}$. Over the 3–8 kbar pressure range at about 1000° C, Burnham and Davis (1971) found that the partial molar volume of water in albitic melts decreased from about 22 to 17 cc/mole, in reasonable agreement with our best fit value. Moreover, they measured a high value (compared to typical anhydrous silicate melts) for the coefficient of thermal expansion of this component of $70–80(10^{-5})\,K^{-1}$, similar to our value. We note that in principle, Eq. (1) could be used to fit solubility data using *any* assumed relationship between $a^m_{H_2O}$ and composition; however, inaccuracies in the activity-composition relationship would be absorbed into the volume and enthalpy functions. Thus, grossly incorrect formulations of activity versus composition would not be expected to yield values of $V^{0,m}_{H_2O}$ similar to the actual partial molar volume. Thus, the agreement of our best fit volume function with the volume measurements of Burnham and Davis (1971) further supports the Henrian approximation.

As pointed out by Silver and Stolper (1989), in which Eq. (1) was used in conjunction with the assumption of Henry's law and the volumetric data of Burnham and Davis (1971) to model the solubility of water in albitic melt (in contrast to the approach taken here, in which the solubility data is used to obtain a best fit to the volume function), the solubility data of Hamilton and Oxtoby (1986) are not perfectly compatible with the volumetric data of Burnham and Davis (1971). According to Hamilton and Oxtoby (1986), the derivative of the solubility of water with respect to pressure approaches zero at about 8 kbar, implying that the partial molar volume of water in albitic melt at 8 kbar approaches the molar volume of water vapor under the same conditions (~22–25 cc/mole at 800°–1000° C). The partial molar volume of water in albitic melt at 8 kbar, 1000° C, as determined by Burnham and Davis (1971), is

158

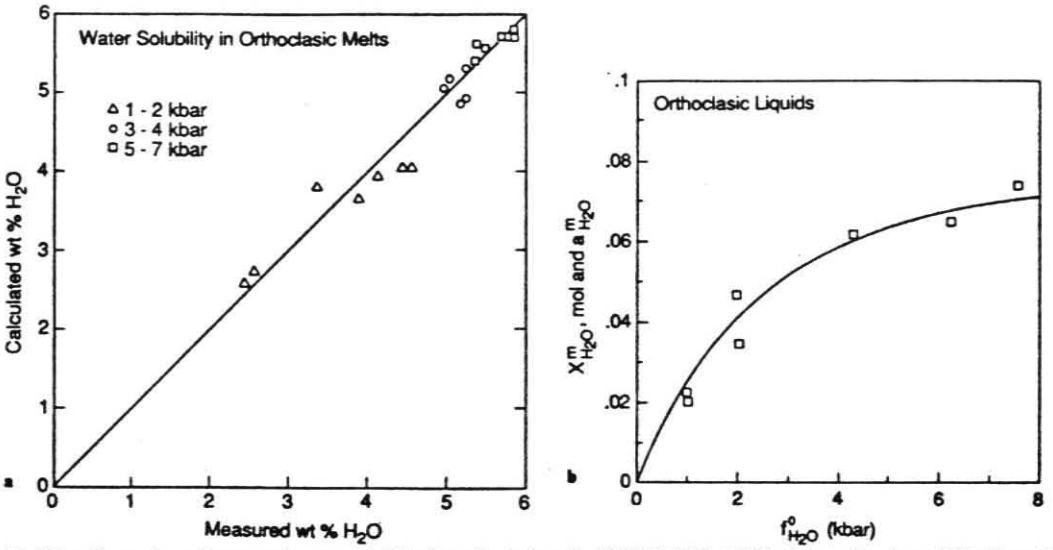

Fig. 17. a Comparison of measured water solubility in orthoclasic melts (900°–1340° C, 1–7 kbar) from Oxtoby and Hamilton (1978; personal communication, 1988) with values calculated based on best fit to Eq. (1) as described in the text. Water solubilities were calculated at the P and T of each of Hamilton and Oxtoby's experiments as described in the caption of Fig. 16a, except the relationship between $X^m_{H_2O,mol}$ and X_g used is given in Appendix 2 (T dependence assumed to be as in albitic melts; Silver and Stolper 1989); b Mole fraction of molecular water vs water fugacity for water-saturated orthoclasic melts. Water solubility data from Oxtoby and Hamilton (1978; personal communication, 1988) at 1100°–1300° C; mole fractions of molecular water are from the spectroscopically determined relationship between water and molecular water content given in Appendix 2 (T dependence as in albitic melts; Silver and Stolper 1989). The *solid curve* shows the calculated trend at 1200° C using the best fit parameters given in Table 8

~17 cc/mole, and thus it is difficult to reconcile the levelling off of water solubility at ~8 kbar as observed by Hamilton and Oxtoby (1986) with the data of Burnham and Davis (1971). The earlier determination of the solubility of water in albitic melt at elevated pressure by Burnham and Jahns (1962) did not show the levelling off reported by Hamilton and Oxtoby (1986) and appears to be more consistent with the volumetric data of Burnham and Davis (1971). Additional solubility and/or volumetric measurements will be needed to resolve these discrepancies. We emphasize, however, that regardless of their resolution, the approximation that $a^m_{H_2O} \propto X^m_{H_2O,mol}$ appears to be an excellent one for hydrous albitic melts.

Orthoclasic melts. The solubility of water in orthoclasic melts has been experimentally determined at 1–7 kbar, 900°–1340° C by Oxtoby and Hamilton (1978), and the speciation of water in orthoclasic glasses has been determined in this study. These two data sets can be combined as described above for albitic melts to test the approximation that $a^m_{H_2O} \propto X^m_{H_2O}$ for this system. For each solubility experiment, the mole fraction of molecular water was computed using the fit to the data on water speciation given in Appendix 2 (the temperature dependence of the speciation of water in albitic melts given in Silver and Stolper, 1989, was adopted for these calculations on orthoclasic melts). We then assumed that Henry's law holds and fit these values of $X^m_{H_2O,mol}$ to a function of the form of Eq. (1); the resulting best fit parameters are listed in Table 8. Figure 17a compares the measured solubility of water in orthoclasic melts from Oxtoby and Hamilton (1978 and personal communication, 1988) with our calculated values. Figure 17b compares $X^m_{H_2O,mol}$ vs $f^0_{H_2O}$ at 1100°–1300° C for the data points given by Oxtoby and Hamilton with a curve calculated using the best fit to Eq. (1). It is clear from Fig. 17 that the solubility data for orthoclasic melts are well fit by Eq. (1) given the assumption that $a^m_{H_2O} \propto X^m_{H_2O,mol}$. At low pressures, $X^m_{H_2O,mol}$ is approximately proportional to water fugacity; at high pressures, the data deviate from linearity in a fashion consistent with a single, relatively high value (~25 cc/mole) of $V^{0,m}_{H_2O}$. The high value of $V^{0,m}_{H_2O}$ reflects the fact that according to Oxtoby and Hamilton (1978 and personal communication, 1988), water solubility levels off at $P > 3000$ bars.

Summary

1. We determined the concentrations of molecular water and hydroxyl groups in hydrous silicate glasses quenched from melts equilibrated over a range of experimental conditions. Anhydrous glass compositions include jadeite, rhyolite, orthoclase, and compositions in the system anorthite-silica-wollastonite.

2. For all the compositions studied, the trends in the concentrations of molecular water and hydroxyl groups as functions of total water content are similar to those observed for albitic glass and for other silicate compositions using infrared and NMR spectroscopies. The proportions of molecular water and hydroxyl groups at a given total water content vary with silicate chemistry, but for each silicate composition the hydroxyl group content is approximately constant for total water contents greater than 4–5 wt%. Increasing silica content appears to increase the ratio of molecular water to hydroxyl groups at a constant total water content.

3. The consistently higher ratio of molecular water to OH groups at a given total water content in rhyolitic glasses synthesized in air-quench apparatus compared to those synthesized in rapid-quench apparatus demonstrates that the speciation of water in rhyolitic melts is temperature dependent at $T<850°$ C.

4. The similarity in the speciation of water in the studied compositions, all of which are highly polymerized melt compositions when anhydrous, suggests that the dissolution mechanisms for water are similar over this composition range. The fact that hydroxyl group contents saturate with increasing total water content in all these compositions suggests that hydroxyl group saturation is not caused solely by the exhaustion of available charge-balancing cations in the melt. These cations do, however, appear to influence the saturation hydroxyl group concentration.

5. For hydrous rhyolitic glasses quenched from melts equilibrated with water vapor at 850° C, $P=100$–1500 bars, the mole fraction molecular water ($X^m_{H_2O,mol}$) is proportional to $f^0_{H_2O}$. These results demonstrate that Henry's Law ($a^m_{H_2O} \propto X^m_{H_2O,mol}$) is a good approximation for these melts with total water contents up to at least several wt% and provides a basis for linking spectroscopic measurements of species concentrations with macroscopic thermodynamic properties. Data on water solubility for albitic, orthoclasic, and Ca–Al-silicate melts to higher pressures can also be fit based on a Henrian relationship between $X^m_{H_2O,mol}$ and $a^m_{H_2O}$, and can be used to set constraints on the partial molar volume of water in these melts.

Appendix 1

Densities of hydrous silicate glasses

Determination of water concentrations in weight percent from infrared measurements requires knowledge of glass densities. In this Appendix, we describe the procedures we used for measuring and estimating densities of hydrous glasses.

For samples from which individual glass fragments weighing 10–40 mg could be obtained, densities were measured using a Berman balance by weighing in air and in toluene at a known temperature. The density of a 30 mg quartz fragment was measured each time glass densities were measured. The quartz standard has a density of 2.659 ± 0.005 g/cc (1σ) based on 45 repeated analyses made over several years using this technique. Based on these results for the quartz standard, density measurements made with a Berman balance on 20–40 mg samples typically have errors of about 0.2%. For samples weighing less than 10–15 mg, densities were determined with a float-sink method using heavy liquids of known densities in the range 2.2–2.5 g/cc, with tolerances of ± 0.005 g/cc. To assess changes in density due to evaporation or other aging effects, the densities of these liquids were checked using density standards (with tolerances of ± 0.0005 g/cc) each time the liquids were used. The density measurements made by this technique have errors of about 0.5–1%.

Glass density is plotted in Fig. 18a versus total water content for bubble-free albitic, orthoclasic, and CAS glasses quenched from melts equilibrated at 1200°–1450° C and 15–20 kbar. Also shown is density versus total water content for a series of bubble-free rhyolitic glasses quenched from melts equilibrated at 1–7 kbar and 800–1150° C in IHPV or cold-seal pressure vessels (L.A. Silver and E. Stolper, unpublished results). For each composition there is a roughly linear relationship between density and water content, with density decreasing as water content increases. Figure 18b shows the relationship between density and total water content determined for hydrous glasses of other compositions, including $Na_2Si_3O_7-H_2O$ (Acocella et al. 1984), albite–H_2O (Orlova 1962), and hydrous Na, Zn-rich silicates (Bartholomew et al. 1980); these results are similar to those shown in Fig. 18a.

Densities were converted to volumes (per mole of oxygen) from the following relation:

$$V=\frac{100}{\rho(\text{wt\% } H_2O/18.015+(100\text{-wt\% } H_2O)/M_O)} \quad \text{(A.1)}$$

where V is the molar volume of the glass, ρ is the density in g/cc, 18.015 is the molecular weight of water, and M_O is the molecular weight of the anhydrous silicate on a single oxygen basis as follows: for albite, $M_O=32.78$ g/mole; for CAS, $M_O=34.32$ g/mole; for orthoclase, $M_O=34.79$ g/mole; for rhyolite, $M_O=32.49$ g/mole; for $Na_2Si_3O_7$, $M_O=34.57$ g/mole; for the Na, Zn-rich silicate, $M_O=35.36$ g/mole. Figure 19a shows V as a function of the mole fraction of total water, X_B, for albitic, orthoclasic, and CAS glasses synthesized at high P and T in this study. Figure 19b shows the volumes derived from the density measurements shown in Fig. 19 for albitic, $Na_2Si_3O_7$, rhyolitic, and Na, Zn-rich silicate glasses at lower pressures.

For the glasses synthesized at 15–20 kbar (Fig. 19a), the molar volume increases slightly with increasing total water content, whereas the molar volume decreases with increasing total water content for the glasses synthesized at pressures up to 7 kbar (Fig. 19b), even though for all the glasses the density decreases with increasing total water content (Fig. 18). This difference probably reflects the higher densities of the anhydrous glass components synthesized at elevated pressure (e.g., Kushiro 1978). The effect of synthesis pressure on the densities of glasses can be seen by comparing Fig. 18a and b: the high pressure albitic glasses from this study have densities about 0.05 g/cc higher than glasses with similar total water contents synthesized by Orlova (1962) at lower pressures (though it is difficult to assess the effects of trapped bubbles on her reported densities).

The data shown in Fig. 19 have been fitted to the relation

$$V=X_B \bar{V}_{H_2O}+(1-X_B)\bar{V}_O \quad \text{(A.2)}$$

where $\bar{V}_{H_2O}$ and $\bar{V}_O$ are the partial molar volumes of the bulk water and anhydrous silicate (on a single oxygen basis) components in the glasses. The partial molar volumes of the anhydrous and water components were derived from a least squares regression of Eq. (A.2) based on the density measurements and the known total water contents for each composition. The results are shown in Fig. 19 as the best fit lines and are also listed in the figure captions. These fits provide a basis for estimating the densities of hydrous glasses with known total water contents. The values of $\bar{V}_{H_2O}$ and $\bar{V}_O$ vary both with bulk composition and with the pressure from which the glasses were quenched. For albitic glasses, the low pressure value for $\bar{V}_O$ of 13.8 cc/mole from Orlova (1962) is similar to the values determined on anhydrous albitic glass by Arndt and Haberle (1973) and Kushiro (1978) at 1 atm and 25° C; our data on albitic glasses synthesized at high P indicate a value for $\bar{V}_O$ of about 13.1 cc/mole, similar to the value based on density measurements of anhydrous albitic glasses synthesized at similar pressures (Kushiro 1978). The partial molar volume of water for the albitic glasses studied by Silver and Stolper (1988) and the value derived from Orlova's data also differ, though we have no simple explanation for why the volume of the component is higher in the high-pressure glasses.

In a few cases, glass densities were estimated using the Gladstone-Dale rule (Gladstone and Dale 1864; Larsen 1909). This is an empirical relationship between the specific refractive energy (K), the mean refractive index ($\bar{n}$), and the density (ρ) given by

$$K=\frac{\bar{n}-1}{\rho}=\Sigma k_i w_i \quad \text{(A.3)}$$

where w_i are the weight fractions and k_i are the specific refractive energies of the oxide components in the glass. Using the data given by Morey (1954) on the densities and refractive indices of about 400 simple oxide glasses at 1 atm and using hydrous samples from

160

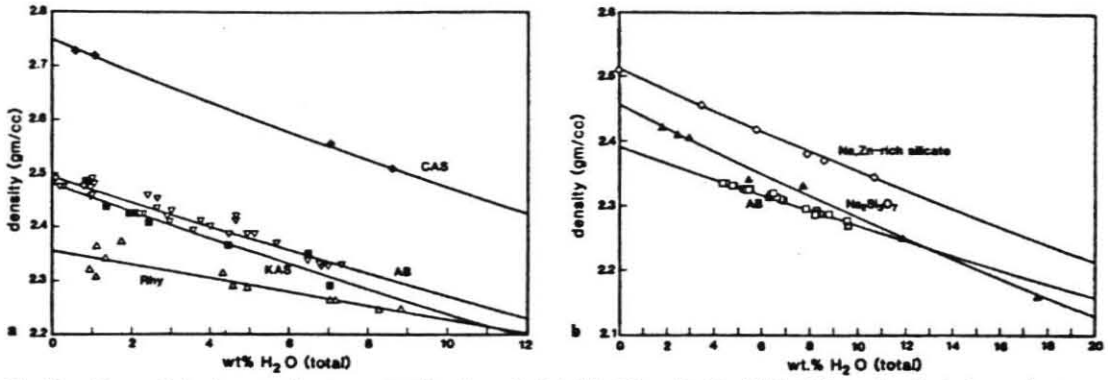

Fig. 18. **a** Measured density vs total water content for glasses included in this study. The CAS, albitic, and orthoclasic samples were synthesized at 15–20 kbar and 1200°–1450° C. The rhyolitic glasses were synthesized in IHPVs at 1–7 kbar and 600°–1150° C at the Johnson Space Center (L.A. Silver and E. Stolper, unpublished data). The total water contents are based on the sum of the molecular H_2O and OH group contents obtained from IR measurements, using best fit molar absorption coefficients. The *filled diamonds* show CAS glasses, the *inverted triangles* show albitic glasses, the *filled squares* show orthoclasic glasses, and the *triangles* show rhyolitic glasses. Typical errors for the Berman balance measurements are ≤ the size of the symbols; for heavy liquids measurements, typical errors are ±0.02 g/cc. *Solid curves* were calculated based on fits to Eq. (A.2) as described in the text; **b** Measured density vs total water content for synthetic silicate glasses reported in the literature. These glasses were all synthesized at pressures up to 4 kbar. The *diamonds* show Na, Zn-rich silicate glasses from Bartholomew et al. (1980); the *filled triangles* show $Na_2Si_2O_7$ glasses from Acocella et al. (1984); and the *squares* show albitic glasses from Orlova (1962). The errors (as reported by the authors) are ≤ the size of the symbols. *Solid curves* were calculated based on fits to Eq. (A.2) as described in the text

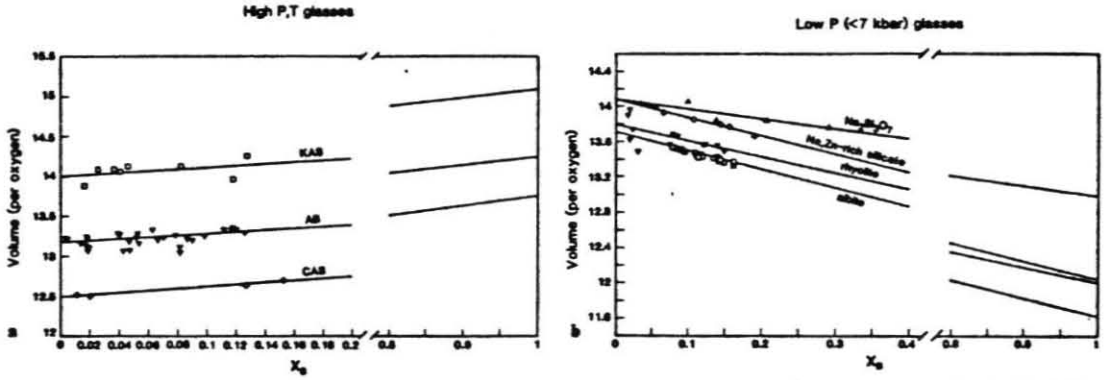

Fig. 19. **a** Volume of hydrous glass (per mole of oxygen) vs total water content (mole fraction of total water, X_w) for the CAS-E2, orthoclasic, and albitic glasses included in this study, all synthesized at 15–20 kbar and 1200°–1450° C. The volumes were calculated from the measured densities using Eq. (A.1). The *diamonds* are CAS glasses; the *filled inverted triangles* are albitic glasses; and the *squares* are KAS glasses. The best fit lines were calculated from Eq. (A.2). Best fit partial molar volumes of anhydrous silicate and water for each composition in cc/mole: CAS-E2: $\bar{V}_O = 12.5$, $\bar{V}_{H_2O} = 13.8$; Orthoclase: $\bar{V}_O = 14.0$, $\bar{V}_{H_2O} = 15.1$; Albite: $\bar{V}_O = 13.1$, $\bar{V}_{H_2O} = 14.3$. **b** Volume (per mole of oxygen) of hydrous glass vs total water content for glasses synthesized at P up to 7 kbar. Volumes were calculated from the measured densities using Eq. (A.1). The *filled inverted triangles* are rhyolitic glasses (L.A. Silver, unpublished data), the *squares* are albitic glasses from Orlova (1962), the *diamonds* are Na, Zn-rich silicate glasses from Bartholomew et al. (1980), and the *filled triangles* are $Na_2Si_2O_7$ glasses from Acocella et al. (1984). The best fit lines were calculated as described in the caption to **a**. Best fit partial molar volumes in cc/mole: Rhyolite: $\bar{V}_O = 13.8$, $\bar{V}_{H_2O} = 12.0$; Albite: $\bar{V}_O = 13.7$, $\bar{V}_{H_2O} = 11.6$; Na, Zn-rich silicate: $\bar{V}_O = 14.1$, $\bar{V}_{H_2O} = 12.0$; $Na_2Si_2O_7$: $\bar{V}_O = 14.1$, $\bar{V}_{H_2O} = 13.0$

the anorthite-silica system (Stewart 1967), we solved for values for k_i for 7 oxide components (including H_2O) by a multiple least squares regression of Eq. (A.3). The coefficients are given in Table A.1.

This method can be used to calculate densities of glasses for which the refractive indices have been measured. Comparison of the measured densities with those calculated using Eq. (A.3) indicates that this method can retrieve the measured values to within 0.05 g/cc, but the agreement is generally much better for glasses that do not contain FeO or MgO (typically within 0.01 g/cc of the measured values).

This method was used to calculate the densities for the *E*2 glasses from McMillan et al. (1986) for which the refractive indices (Table 2) had been determined by P. Lambert (P. McMillan, personal communication, 1986). The calculated densities are given in Table 8 and approximately 0.05 g/cc lower than those measured for the CAS glasses using a Berman balance. This difference is not unexpected because the E2 glasses were synthesized at pressures

Table A.1. Coefficients for the Gladstone-Dale rule

Oxide	$k_i^{(1,2)}$
SiO_2	0.208
Al_2O_3	0.225
MgO	0.215
CaO	0.227
Na_2O	0.194
K_2O	0.204
H_2O	0.313

[1] Values are based on fit to data using hydrous samples from the anorthite-silica system (Stewart 1967) and on data in Morey (1954) on glasses in the following systems: $SiO_2-CaO-Na_2O$, SiO_2-Na_2O, $K_2O-MgO-SiO_2$, SiO_2-Na_2O-CaO, SiO_2-K_2O-CaO, $SiO_2-MgO-CaO$, $K_2O-CaO-SiO_2$, SiO_2-MgO, and $SiO_2-Na_2O-K_2O-CaO$

[2] Typical errors based on regression are less than 0.004

less than 5200 bars and the CAS glasses were quenched from melts equilibrated at pressures greater than 15 kbar. Based on comparison of our results and those of Orlova (1962) on albitic glasses, the difference in synthesis pressure could easily account for variations of this magnitude.

Appendix 2

Best fit parameters to speciation measurements

In order to use spectroscopic data for calculating phase equilibria or for other applications, the relationship between the measurements of species concentrations and total water content must be described in a mathematical form. Silver and Stolper (1989) fit the speciation measurements for hydrous albitic glasses to a regular solution model. This same procedure has been applied to the speciation data for CAS, orthoclasic, and rhyolitic glasses and the method is outlined here.

The data for each composition are fit to an equation of the form

$$-\ln\left(\frac{(X^m_{OH})^2}{(X^m_{H_2O,mol})(1-X^m_{H_2O,mol})}\right)=A'+B'X^m_{OH}+C'X^m_{H_2O,mol} \qquad (A.4)$$

where A', B', and C' are functions of an equilibrium constant and the binary interaction parameters of the regular solution formalism, and $X^m_{H_2O,mol}$, X^m_{OH}, and $X^m_O(=1-X^m_{H_2O,mol}-X^m_{OH})$, the mole fractions of the three species, are based on the spectroscopic measurments as described in note f in Table 2. For each composition, A', B', and C' were determined by least squares using the infrared measurements of the concentrations of molecular water and hydroxyl groups in a series of glasses covering a range of total water contents. These best fit parameters are given in Table A.2 along with those determined for albitic glasses at 1400° C by Silver and Stolper (1989).

Equation (A.4) can be rewritten in terms of X^m_{OH} and the bulk composition of the system (given by X_B):

$$-\ln\left(\frac{(X^m_{OH})^2}{(X_B-0.5\,X^m_{OH})(1-X_B-0.5\,X^m_{OH})}\right)$$
$$=A'+(B'-0.5\,C')X^m_{OH}+C'X_B \qquad (A.5)$$

where X_B is the fraction of oxygens contributed by water divided by the total number of oxygens in the glass (Shaw 1964).

Equation (A.5) can be solved iteratively for X_{OH} at a given bulk composition (i.e., given a value of X_B). The mole fractions of molecular water and anhydrous oxygen atoms can then be obtained as follows:

$$X^m_{H_2O,mol}=X_B-0.5\,X^m_{OH} \qquad (A.6)$$

Table A.2. Constants in fits to speciation data

Composition	A'	B'	C'
CAS-E2	0.215	14.662	8.753
Orthoclase	0.878	16.720	5.395
Rhyolite	1.093	16.858	7.892
Albite	0.403	15.333	10.894

$$X^m_O=1-X_B-0.5\,X^m_{OH} \qquad (A.7)$$

If needed, these mole fractions can be recast in terms of weight percent water as follows:

$$\text{wt\% } H_2O,\text{mol}=\frac{18.015\,X^m_{H_2O,mol}}{18.015\,X_B+(1-X_B)M_O}\times 100 \qquad (A.8)$$

$$\text{wt\% } H_2O,\text{total}=\frac{18.015\,X_B}{18.015\,X_B+(1-X_B)M_O}\times 100 \qquad (A.9)$$

$$\text{wt\% OH(as } H_2O)=\text{wt\% } H_2O,\text{total}-\text{wt\% } H_2O,\text{mol} \qquad (A.10)$$

where M_O is the molecular weight of the anhydrous component on a single oxygen basis (see Appendix 1).

Acknowledgements. We thank Dr. H. Eckert for the NMR spectroscopic analyses; Drs. P. Dobson and S. Newman for assistance with the hydrogen extraction procedure; Dr. D.L. Hamilton for unpublished data on the solubility of water in orthoclasic melts; Dr. G. Lofgren and Profs. S. Epstein, A.L. Montana, G. Rossman, and P.J. Wyllie for opening their laboratories to us; Mr. T. Stanton, Profs. W. Johannes and P. McMillan, and Drs. B. Mysen, H.R. Shaw, and D. Stewart for providing us with samples; and Dr. K. Burke of the Lunar and Planetary Institute for financial assistance to support work done at the Johnson Space Center by L.A.S. We also acknowledge suggestions from an anonymous reviewer. This work was supported by NSF Grants EAR-8212765, EAR-8417434, and EAR-8618229 and by the donors of the Petroleum Research Fund, administered by the American Chemical Society (Grant 17737-AC2). Caltech Division of Geological and Planetary Sciences Contribution 4540.

References

Acocella J, Tomozawa M, Watson EB (1984) The nature of dissolved water in sodium silicate glasses and its effect on various properties. J Non-Cryst Solids 65:175–183

Aines RD, Silver LA, Rossman BR, Stolper EM, Holloway JR (1984) Direct observation of water speciation in rhyolite at temperatures up to 850° C (abs). In: Geol Soc Am 96th Ann Mtg 15(6):512

Albarede F, Provost A (1977) Petrological and geochemical mass-balance equations: an algorithm for least-squares fitting and general error analysis. Comput Geosci 3:309–326

Arndt J, Haberle F (1973) Thermal expansion and glass transition temperatures of synthetic glasses of plagioclase-like compositions. Contrib Mineral Petrol 39:175–183

Bartholomew RF, Schreurs IWH (1980) Wide-line NMR study of the protons in hydrosilicate glasses of different water content. J Non-Cryst Solids 38/39:679–684

Bartholomew RF, Butler BL, Hoover HL, Wu CK (1980) Infrared spectra of a water-containing glass. J Am Ceram Soc 63:481–485

Boulos EN, Kreidl NJ (1972) Water in glass: a review. J Canad Ceram Soc 41:83–90

Burnham CW (1975) Water and magmas: a mixing model. Geochim Cosmochim Acta 39:1077–1084

Burnham CW (1979) The importance of volatile constituents. In: Yoder HS Jr (ed) The evolution of the igneous rocks. Princeton Univ Press, Princeton, pp 439–482

Burnham CW, Davis NF (1971) The role of H_2O in silicate melts: I. P-V-T relations in the system $NaAlSi_3O_8-H_2O$ to 1 kilobars and 1000° C. Am J Sci 270:54–79

Burnham CW, Jahns RH (1962) A method for determining the solubility of water in silicate melts. Am J Sci 260:721–745

Eckert H, Yesinowski JP, Stolper EM, Stanton TR, Holloway J (1987) The state of water in rhyolitic glasses: a deuterium NMR study. J Non-Cryst Solids 93:93–114

Eckert H, Yesinowski JP, Silver LA, Stolper EM (1988) Water in silicate glasses: quantitation and structural studies by ^1H solid echo and MAS-NMR methods. J Chem Phys 92:2055–2064

Epel'baum MB (1985) The structure and properties of hydrous granitic melts. Geol Carpath 36:491–498

Ernsberger FM (1977) Molecular water in glass. J Am Ceram Soc 60:91

Farnan I, Kohn SC, Dupree R (1987) A study of the structural role of water in hydrous silica glass using cross-polarization magic angle spinning NMR. Geochim Cosmochim Acta 51:2869–2873

Gladstone JH, Dale TP (1864) Researches on the refraction, dispersion, and sensitiveness of liquids. Philos Trans R Soc London 153:317–343

Hamilton DL, Oxtoby S (1986) Solubility of water in albite-melt determined by the weight-loss method. J Geol 94:626–630

Holloway JR (1977) Fugacity and activity of molecular species in supercritical fluids. In: Fraser D (ed) Thermodynamics in geology. Reidel, Boston, pp 161–181

Johannes W, Bell PM, Mao HK, Boettcher AL, Chipman DW, Hays JF, Newton RC, Seifert F (1971) An interlaboratory comparison of piston-cylinder calibration using the albite-breakdown reaction. Contrib Mineral Petrol 32:24–38

Karsten JL, Holloway JR, Delaney JR (1982) Ion microprobe studies of water in silicate melts: temperature-dependent water diffusion in obsidian. Earth Planet Sci Lett 59:420–428

Kurkjian CR, Russell LE (1958) Solubility of water in molten alkali silicates. J Soc Glass Techn 42:130T–144T

Kushiro I (1978) Viscosity and structural changes of albite ($NaAlSi_3O_8$) melt at high pressures. Earth Planet Sci Lett 41:87–90

Langer K, Flörke OW (1974) Near infrared absorption spectra (4000–9000 cm^{-1}) of opals and the role of "water" in these $SiO_2 \cdot nH_2O$ minerals. Fortsch Mineral 52:17–51

Larsen ES (1909) The relationship between refractive index and density of some crystallized silicates and their glasses. Am J Sci 28:263–274

McMillan PF, Holloway JR (1987) Water solubility in aluminosilicate melts. Contrib Mineral Petrol 97:320–332

McMillan PF, Jakobsson S, Holloway JR, Silver LA (1983) A note on the Raman spectra of water-bearing albite glass. Geochim Cosmochim Acta 47:1937–1943

McMillan PF, Peraudeau G, Holloway J, Coutures J-P (1986) Water solubility in a calcium aluminosilicate melt. Contrib Mineral Petrol 94:178–182

McMillan PW, Chlebik A (1980) The effect of hydroxyl ion content on the mechanical and other properties of soda-lime-silica glass. J Non-Cryst Solids 38/39:509–514

Morey GW (1954) The properties of glass (2nd ed). ACS Monograph 124. Reinhold, New York, p 591

Moulson AJ, Roberts JP (1960) Water in silica glass. Trans Brit Ceram Soc 59:388–399

Mysen BO, Virgo D (1986a) Volatiles in silicate melts at high pressure and temperature. 1. Interaction between OH groups and Si^{4+}, Al^{3+}, Ca^{2+}, Na^+ and H^+. Chem Geol 57:303–331

Mysen BO, Virgo D (1986b) Volatiles in silicate melts at high pressure and temperature. 2. Water in melts along the join $NaAlO_2-SiO_2$ and a comparison of solubility mechanisms of water and fluorine. Chem Geol 57:333–358

Newman S, Stolper EM, Epstein S (1986) Measurement of water in rhyolitic glasses: Calibration of an infrared spectroscopic technique. Am Mineral 71:1527–1541

Newman S, Epstein S, Stolper EM (1988) Water, carbon dioxide, and hydrogen isotopes in glasses from the ca. 1340 A.D. eruption of the Mono Craters, California: constraints on degassing phenomena and initial volatile content. J Volcanol Geotherm Res 35:75–96

Orlova GP (1962) The solubility of water in albite melts. Int Geol Rev 6:254–258

Ostrovskiy IA, Orlova GP, Rudnitskaya YS (1964) Stoichiometry in the solution of water in alkali-aluminosilicate melts. Doklady Akad Nauk SSR 157:149–151

Oxtoby S, Hamilton DL (1978) Solubility of water in melts of the $Na_2O-Al_2O_3-SiO_2$ and $K_2O-Al_2O_3-SiO_2$ systems. In: Mackenzie WS (ed) Progress in experimental petrology. Natl Environ Res Council Pub Ser D No 11, Dept Geology, Manchester Univ

Persikov ES (1972) Experimental studies of solubility of water in granitic melt and kinetics of the melt-water equilibria at high pressures. Int Geol Rev 16:1062–1067

Pichavant M, Ramboz C (1985) Première détermination expérimentale des relations de phases dans le système haplogranitique en conditions de sous-saturation en H_2O. CR Acad Sci Paris 301, Ser II:607–610

Pickett DA, Stolper EM (1984) Thermometry of rhyolitic obsidians based on water speciation (abs). EOS Trans Am Geophys Un 65:1128

Shaw HR (1964) Theoretical solubility of H_2O in silicate melts: quasicrystalline models. J Geol 72:601–617

Shaw HR (1974) Diffusion of H_2O in granitic liquid. I. Experimental data. II. Mass transfer in magma chambers. In: Hoffmann AW, Giletti BJ, Yoder HS Jr, Yund RA (eds) Geochemical transport and kinetics. Carnegie Inst Washington Publ 634:139–170

Silver LA, Stolper E (1985) A thermodynamic model for hydrous silicate melts. J Geol 93:161–178

Silver LA, Stolper E (1989) Water in albitic glasses. J Petrol 30:667–709

Stanton TR, Holloway JR, Hervig RL, Stolper EM (1988) Isotopic investigations of water diffusion mechanism in silicate melts. I: D_2O diffusion in rhyolitic melts (in preparation)

Stewart DB (1967) Four-phase curve in the system $CaAl_2Si_2O_8-SiO_2-H_2O$ between 1 and 10 kilobars. Schweiz Mineral Petrogr Mitt 47/1:35–59

Stolper EM (1982a) Water in silicate glasses: An infrared spectroscopic study. Contrib Mineral Petrol 94:178–182

Stolper EM (1982b) The speciation of water in silicate melts. Geochim Cosmochim Acta 46:2609–2620

Stolper EM (1989) The temperature dependence of the speciation of water in rhyolitic melts and glasses. Am Mineral (in press)

Stolper EM, Silver LA (1985) The speciation of water in silicate glasses: The influence of bulk composition. EOS 66:1140

Takata M, Acocella J, Tomozawa M, Watson EB (1981) Effect of water content on the electrical conductivity of $Na_2O \cdot 3\,SiO_2$ glass. J Am Ceram Soc 64:719–724

Tomlinson JW (1956) A note on the solubility of water in molten sodium silicate. J Soc Glass Technol 40:25–31

Tuttle OF, Bowen NL (1958) Origin of granite in the light of experimental studies in the system $NaSlSi_3O_8$–$KAlSi_3O_8-SiO_2-H_2O$. Geol Soc Am Mem 74

Uys JM, King TB (1963) The effect of basicity on the solubility of water in silicate melts. Trans Met Soc AIME 227:492–500

Wu CK (1980) Nature of incorporated water in hydrated silicate glasses. J Amer Ceram Soc 63:453–457

Received August 30, 1988 / Accepted July 24, 1989
Editorial responsibility: I.S.E. Carmichael

Appendix 3:

Reaction Kinetics of $H_2O + O = 2OH$ and Its Equilibrium Revisited

REACTION KINETICS OF $H_2O+O=2OH$ AND ITS EQUILIBRIUM, REVISITED

ZHANG, Y., STOLPER, E.M., and IHINGER, P.D., Division of Geological and Planetary Sciences, California Institute of Technology, Pasadena, CA 91125

We have studied the reaction kinetics of $H_2O+O=2OH$ in rhyolitic and albitic glasses at various temperatures and total water concentrations. Doubly-polished glass chips are held at 400, 500, and 600°C for different duration and then quenched quickly in water. The changes in OH and molecular H_2O concentrations are measured. Some preliminary results are as follows: (1) Changes in speciation with time are best explained by the presence of at least two different types of OH groups that are generated or consumed at different rates by reaction of molecular H_2O with anhydrous melt species. (2) The rate of reaction increases with the concentrations of OH and H_2O species. (3) The reaction rate depends strongly on temperature. For example, in rhyolitic glass with 1 wt % total water, at 600°C, equilibrium for the overall reaction is reached in about 3 minutes; at 500°C, the equilibrium is reached in about 2 hours; at 400°C, the equilibrium is not reached in 40 days. Hence care must be taken to quench quantitatively water speciation from high temperatures, and indeed, above a certain temperature it may not be possible.

We have also obtained new data on the equilibrium distribution of water between OH and H_2O species in rhyolitic glasses, with particular attention to demonstrating that the results are unaffected by quenching. There is a clear dependence of the equilibrium constant K [$=X_{OH}^2/(X_{H_2O} \cdot X_O)$] on temperature and on total water concentration. A plot of $\ln K$ vs. $1/T$ for samples with 0.7 to 1.4 wt % total water gives a $\Delta H^0 = 5.5 \pm 1$ kcal/mol for the overall reaction. The dependence on water concentration can be modelled by a simple regular solution model. The speciation and reaction kinetics data can be applied to study the thermal history of natural water-bearing rhyolites, and some of the samples we studied appear to have experienced complicated cooling histories. We are continuing to investigate the nature of the various OH species (which cannot be directly measured but can be inferred from reaction kinetics) and to study water in glasses of other chemical compositions.